

# Pair Correlations from Symmetry-Broken States in Strongly Correlated Electronic Systems

Von der Fakultät für Mathematik, Naturwissenschaften und Informatik  
der Brandenburgischen Technischen Universität Cottbus

zur Erlangung des akademischen Grades

Doktor der Naturwissenschaften  
(Dr. rer. nat.)

genehmigte Dissertation

vorgelegt von

Diplom-Physiker

FALK GÜNTHER

geboren am 13. Februar 1980 in Großenhain

Gutachter: Prof. Dr. Götz Seibold, BTU

Gutachter: Prof. Dr. Marco Grilli, Univ. La Sapienza, Rom

Gutachter: Prof. Dr. Vladimir Hizhnyakov, Univ. Tartu

Tag der mündlichen Prüfung: 15. Oktober 2010



Pair Correlations from Symmetry-Broken States in  
Strongly Correlated Electronic Systems

Falk Günther

October 2010



Non quia difficilia sunt, non audemus,  
sed quia non audemus, difficilia sunt.

LUCIUS ANNAEUS SENECA



# Contents

|   |            |
|---|------------|
| <b>Kurzfassung</b>  | <b>x</b>   |
| <b>Abstract</b>   | <b>xii</b> |
| <b>1 Introduction</b>   | <b>1</b>   |
| 1.1 Crystal Structure and Electronic Configuration . . . . .        | 9          |
| <b>2 Hubbard Model -<br/>Limits and Approximations</b>              | <b>15</b>  |
| 2.1 The Hubbard Model - Exact and Approximative Solutions . . . . . | 15         |
| 2.2 Hartree Fock Approximation of the<br>Hubbard Model . . . . .    | 17         |
| 2.3 Bogoliubov Transformation . . . . .                             | 18         |
| 2.4 Attraction Repulsion Transformation . . . . .                   | 21         |
| <b>3 Gutzwiller Approach<br/>and Model Specifications</b>           | <b>23</b>  |
| 3.1 Gutzwiller's Wave-function and Approximation . . . . .          | 24         |
| 3.2 Charge-Rotationally-Invariant Gutzwiller Approach . . . . .     | 26         |
| 3.3 Extended Hubbard Model with Local On-Site Attraction . . . . .  | 32         |
| 3.4 Unified Slave Boson Representation . . . . .                    | 35         |

|          |  |            |
|----------|--|------------|
| 3.5      | Gutzwiller Energy Functional and<br>Lagrangian Multipliers . . . . .   | 43         |
| 3.6      | Numerical Method . . . . .   | 44         |
| 3.7      | Characterization of the Solution . . . . .                             | 48         |
| <b>4</b> | <b>Homogeneous SC and CDW Solutions</b>                                | <b>53</b>  |
| 4.1      | Stability Analysis in Infinite Dimensions . . . . .                    | 54         |
| 4.2      | Solutions in the HFA and GA . . . . .                                  | 58         |
| 4.3      | Transformation to an Effective GA-BCS Hamiltonian . . . . .            | 62         |
| 4.4      | $d$ -Wave Superconductivity . . . . .                                  | 66         |
| <b>5</b> | <b>Inhomogeneous Solutions</b>   | <b>73</b>  |
| 5.1      | Homogeneous Charged Stripes . . . . .                                  | 75         |
| 5.2      | Stripe-less Solution for $V > 0$ . . . . .                             | 81         |
| 5.3      | Stripes with $V > 0$ . . . . .   | 85         |
| 5.4      | Vortices and Point-Like Inhomogeneities . . . . .                      | 91         |
| <b>6</b> | <b>Gutzwiller Analysis of the Superfluid Stiffness</b>                 | <b>105</b> |
| 6.1      | Definition and Interpretation of the<br>Superfluid Stiffness . . . . . | 106        |
| 6.2      | Superfluid Stiffness of the Gutzwiller Solution . . . . .              | 109        |
| 6.3      | Superfluid Stiffness and Sum Rules . . . . .                           | 114        |
|          | <b>Summary and Conclusion</b>  | <b>119</b> |
| <b>A</b> |  | <b>123</b> |
| A.1      | Notation and Conventions . . . . .                                     | 123        |
| <b>B</b> |  | <b>127</b> |



|          |   |            |
|----------|---|------------|
| B.1      | Effective Mean Field Hubbard Hamiltonian . . . . .  | 127        |
| B.2      | Fourier Transformation of the $d$ -wave Interaction Term . . . . .                                  | 128        |
| B.3      | Interaction Kernel of the ph-Channel in the<br>Free Energy Expansion of the GA Functional . . . . . | 129        |
| B.4      | The Constrained GA Energy Functional . . . . .  | 130        |
| B.5      | Derivatives of the GA-functional . . . . .  | 131        |
| B.6      | Derivatives of the $z$ -Factors . . . . .   | 140        |
| B.7      | Derivatives of the MFA Matrix $\mathbf{A}^i$ . . . . .  | 144        |
| B.8      | Derivatives of the Inter Site Repulsion Term . . . . .  | 150        |
| <b>C</b> |   | <b>153</b> |
| C.1      | The Bardeen-Cooper-Schrieffer Theory . . . . .  | 153        |
| C.2      | Attraction-Repulsion Transformation . . . . .   | 155        |
| C.3      | Second Order Perturbation Theory . . . . .  | 156        |
| C.4      | Green's Function and Sum Rule . . . . .   | 157        |

## List of Abbreviations

|                  |   |
|------------------|---|
| BCS              | Bardeen-Cooper-Schrieffer               |
| BZ               | Brillouin zone                          |
| CDW              | Charge density wave                     |
| DOS, $N(\omega)$ | Density of states                       |
| GA               | Gutzwiller Approximation                |
| HFA              | Hartree-Fock approximation              |
| HTSC             | High temperature superconductor         |
| Im               | Imaginary part                          |
| KR               | Kotliar-Ruckenstein                     |
| MFA              | Mean field approximation                |
| PDW              | Pair density wave                       |
| QMC              | Quantum-Monte-Carlo                     |
| Re               | Real part                               |
| RPA              | Random phase approximation              |
| SC               | Superconductor                          |
| SDW              | Spin density wave                       |
| $\sigma$         | Spin index                              |
| TDGA             | Time dependent Gutzwiller approximation |
| VAV              | Vortex-anti-vortex                      |

|                               |  |
|-------------------------------|--|
| $ \dots\rangle$               | Vector in Hilbert space                  |
| $\hat{c}, \hat{c}^\dagger$    | Operator and complex conjugate           |
| $a = \langle \hat{a} \rangle$ | Expectation value of observable $a$      |
| $i = (i_x, i_y)$              | Site index with $x$ - and $y$ -component |
| $\rho_{ij}^{\sigma\sigma'}$   | Elements of the density matrix           |
| $\mathbf{J}_i$                | Charge vector lattice site $i$           |
| $\mathbf{M}, M_{ij}$          | Matrix and matrix entries                |

## Kurzfassung

Das Ergebnis der letzten 20 Jahre experimenteller und theoretischer Untersuchungen zu Hochtemperatursupraleitern (HTSL) ist ein hoch komplexes, reichhaltiges Phasendiagramm, welches noch immer nicht vollständig beschrieben werden kann. Zahlreiche experimentelle Ergebnisse geben starke Hinweise auf eine inhomogene Verteilung von Spin- und Ladungskorrelationen in HTSL. Motiviert durch die experimentellen Ergebnisse versuchen wir die Frage zu beantworten, ob Paarkorrelationen in Zuständen mit Symmetriebrechung im Rahmen der Gutzwillernäherung des Hubbardmodells gefunden werden können.

Nach einer einleitenden Diskussion ausgewählter experimenteller Arbeiten und theoretischer Modelle leiten wir das ladungsrotationsinvariante Gutzwiller-Energiefunktional im Rahmen des Ein-Band-Hubbard-Modells her. Auf dieser Basis berechnen wir vielfältige Zustände am Sattelpunkt des Funktionals im attraktiven Bereich ( $U < 0$ ). Beginnend mit einer Entwicklung der Energie bis zur zweiten Ordnung untersuchen wir zunächst die Instabilität eines normalen Systems hinsichtlich Supraleitung im Rahmen der zeitabhängigen Gutzwillerapproximation (TDGA). Wir leiten ein Kriterium für den Übergang von der normalen zur supraleitenden Phase im paramagnetischen Bereich her. Unsere Ergebnisse für ein unendlich-dimensionales Gitter zeigen gute Übereinstimmung mit den Daten der Quantum-Monte-Carlo-Methode (QMC).

Im nächsten Abschnitt dieser Arbeit präsentieren wir Ergebnisse für zweidimensionale Systeme. Wir vergleichen hierbei numerische Ergebnisse der Gutzwillernäherung mit der konventionellen Hartree-Fock-Näherung. Am Beispiel eines homogen supraleitenden und eines ladungsgeordneten Zustandes zeigen wir, dass die Unterschiede vor allem im Übergang von schwacher zu starker Kopplung zu finden sind, wobei die Ordnungsparameter von der Renormierung beeinflusst sind. Als eine weitere Anwendung leiten wir ausgehend von der Sattelpunktlösung einen effektiven Hamiltonoperator

her. Wir vergleichen unseren Formalismus analytisch mit den Schlussfolgerungen der Bardeen-Cooper-Schrieffer-Theorie (BCS).

Motiviert durch verschiedene experimentelle Arbeiten zu  $d$ -wellensymmetrischen,  $k$ -abhängigen 'supraleitenden Gaps' konzentrieren wir uns auf die Frage, ob Zustände mit nicht-lokalen Paarkorrelationen eine Lösung der Gutzwillernäherung sind und ob diese Korrelationen die Energie erniedrigen. Wir diskutieren formale Anforderungen an eine mögliche Lösung im Hinblick auf eine koexistierende Spinordnung und das Zusammenspiel mit den nicht-lokalen Paarordnungen.

Als nächste Anwendung präparieren wir Lösungen im normalen und im erweiterten Hubbardmodell, wobei wir eine zusätzliche Zwischen-Gitterplatz-Wechselwirkung durch den Parameter  $V > 0$  einführen. Wir zeigen inhomogene Lösungen, welche durch streifenförmige Bereiche charakterisiert sind, in welchen sich die Parameter für Ladungs- und Paarordnung in Phase und Amplitude ändern. Wir stellen Ergebnisse für das normale und das erweiterte Hubbardmodell vor und diskutieren den Einfluss des Parameters  $V$ . Wir zeigen, dass für den Fall  $V > 0$  eine Paardichte-Welle ohne Streifenordnung der Grundzustand ist.

Ein weiterer Schwerpunkt dieser Arbeit liegt auf einfachen punktförmigen Inhomogenitäten wie Polaronen und (Anti)-Vortices in finiten Clustern. Wir präsentieren Ergebnisse in guter Übereinstimmung mit der logarithmischen Abhängigkeit der Energie vom Radius des Vortex sowie einer möglichen Anziehung zwischen Vortex und Antivortex. Schließlich führen wir im letzten Kapitel die superfluide Dichte ein und diskutieren in diesem Zusammenhang die Stabilität unserer Lösung in endlich-dimensionalen Systemen. Wir folgen einer Herleitung, welche auf einer Entwicklung der Energie bezüglich einer Verdrehung des Ladungsvektorfeldes beruht. Wir diskutieren diesen Zugang im Vergleich mit exakten QMC-Daten wobei die Ergebnisse unsere Herleitung gute qualitative Übereinstimmung zeigen.

## Abstract

As a result of 20 years of experimental and theoretical investigations of high temperature superconductors (HTSC) one can draw a very complex and rich phase diagram that cannot be described completely yet. Numerous experimental findings give strong hints for an inhomogeneous distribution of spin and charge correlations in HTSC. Motivated by the experimental findings we try to answer the question whether pair correlations from broken symmetry states can be found in the framework of the Gutzwiller approximation of the Hubbard model. After an introductory discussion of selected experimental works and theoretical models we derive the charge-rotationally invariant Gutzwiller functional for the one-band Hubbard model. On this basis we calculate various states from the saddle point solution of functional in the attractive ( $U < 0$ ) regime.

Starting with a second order expansion we investigate the instability of a normal system towards SC in the framework of the time dependent Gutzwiller approximation (TDGA). We derive criteria for a phase transition from the normal to the superconducting phase in the paramagnetic regime. We show results for an infinite dimensional lattice that are in good agreement with QMC data.

In the next section of this work we present results for finite dimensional systems. We compare numerical results from the GA with the conventional Hartree-Fock approximation. As an example we discuss a homogeneously superconducting and a charge-ordered state. We show that the difference is mainly in the crossover from weak to strong coupling which is due to the renormalization in the Gutzwiller formalism. In a next step we derive an effective Hamiltonian on top of the saddle point solution. We compare the formalism analytically with the findings from the well known BCS theory. We verify our conclusions by numerical calculations.

Motivated by different experimental works on  $d$ -wave symmetric  $k$ -dependent SC gaps

we focus on the question whether states including non-local pair correlations can be a solution of the GA and how does this correlation lower the energy. We restrict to the repulsive regime ( $U > 0$ ) and discuss the formal requirements for a possible solution in view of a coexisting spin order and the interplay of local and non-local pair order.

As a next application we prepare inhomogeneous solutions in the normal and in the extended Hubbard model where we include an additional inter-site interaction by the parameter  $V > 0$ . We present inhomogeneous solutions that are characterized by stripe-shaped domains where the parameters for charge- and pair- ordering change their phases or their amplitude. We obtain results for the normal and the extended Hubbard model and we discuss the influence of the parameter  $V$ . We show that in case of  $V > 0$  a pair density wave (PDW) without stripes is the ground state.

Another focus of the work is on point-like inhomogeneities namely polarons and (anti-)vortices in finite clusters. We present results that show a good agreement with the logarithmic dependence of the energy of the vortex state with respect to the vortex radius as well as possible attraction between vortex and anti-vortices. Finally in the last chapter we introduce the superfluid density in order to discuss the stability of our solutions in finite dimensional systems. We give a short overview on different analytical approaches to this quantity. We present an approach that is based on an energy expansion view of an angular distortion of the charge vector field. We discuss this approach by comparing the numerical GA results with exact QMC results where our approach turned out to be in good qualitative agreement.





# Chapter 1

## Introduction

Even more than 20 years after the discovery of high temperature superconductivity in ceramic compounds containing copper oxide planes the physics behind is widely non understood. Since the experimental finding of the phenomenon in 1986 [1] these materials show new physical anomalous characteristics beyond the tremendous high critical temperature as for example unconventional electronic transport properties.

All of the high- $T_c$ -materials contain copper oxide ( $Cu - O$ ) planes and can be classified as complex cuprate compounds. Based on parent compounds that are believed to be Mott insulators these substances become conductors by electron or hole doping and show a number of phase transitions depending on doping rate and the temperature. This can be summarized in a simplified phase diagram in Fig.(1.1) for hole doped HTSC showing the different phases of these materials as a function of doping.

The parent compounds such as  $La_2CuO_4$  (LCO) or  $YBa_2Cu_3O_6$  (YBCO) are anti-ferromagnetic insulators if the temperature is below the Néel temperature  $T_N$ . If one increases the number of holes in the cuprates by replacing  $La$  by  $Sr$  in LCO or by increasing the part of oxygen in YBCO the antiferromagnetic order rapidly vanishes at a doping of  $x_a \approx 0.02$  in Fig. (1.1).

Above a critical concentration around  $x = 0.05$  the doped materials become superconducting if the sample is cooled below the critical temperature  $T_c$ . The transition temperature increases with doping until an optimal doping around  $x_{opt} = 0.15$  and the SC breaks down above a certain doping rate. Even above the critical temperature in the normal conducting phase the doped SC's show an anomalous metallic behavior with a linear temperature-dependence of the resistance [2]. In the over-doped region  $x > x_{opt}$  the cuprates show the normal Fermi liquid behavior. Below a certain temperature one finds the so called pseudogap region [3] inducing a loss in entropy and magnetic susceptibility. The physics in the pseudogap region makes the phase diagram even more complex. The two most prominent scenarios for this region are based on (a) incoherent pairing fluctuations [4, 5] and (b) ordered states with broken symmetry which are presented in this thesis.

## Neutron Scattering Studies

One of the early models for the ordered state in the HTSC's in the under-doped regime ( $x < x_{opt}$ ) is based on the assumption that charge carriers are concentrated in striped domain walls separating domains with opposite sign in the antiferromagnetic order parameter that can be observed by a modulated spin and charge density.

Neutron scattering studies have provided important information about the momentum and energy dependence of magnetic excitations in cuprate superconductors. The motivation to search for stripe-like charge and spin modulation in HTSC came from experimental results for nickelates ( $La_{2-x}SrNiO_{4+\delta}$ ) that are insulating and isostructural with *Sr* doped *LCO*. Above a certain doping limit the antiferromagnetic order in  $La_{2-x}SrNiO_{4+\delta}$  is replaced by stripe order [6–8]. Neutron scattering results for the position and intensity of the superlattice peaks in  $La_{2-x}SrNiO_{4+\delta}$  showed an incommensurability  $\epsilon$  in the characteristic wave vectors for the spin ( $\mathbf{Q}_{AF} \pm \frac{1}{\sqrt{2}}(\epsilon, \epsilon, 0)$ ) [9, 10] and for the charge order ( $\frac{1}{\sqrt{2}}(2\epsilon, 2\epsilon, 0)$ ) that increases steadily with doping.

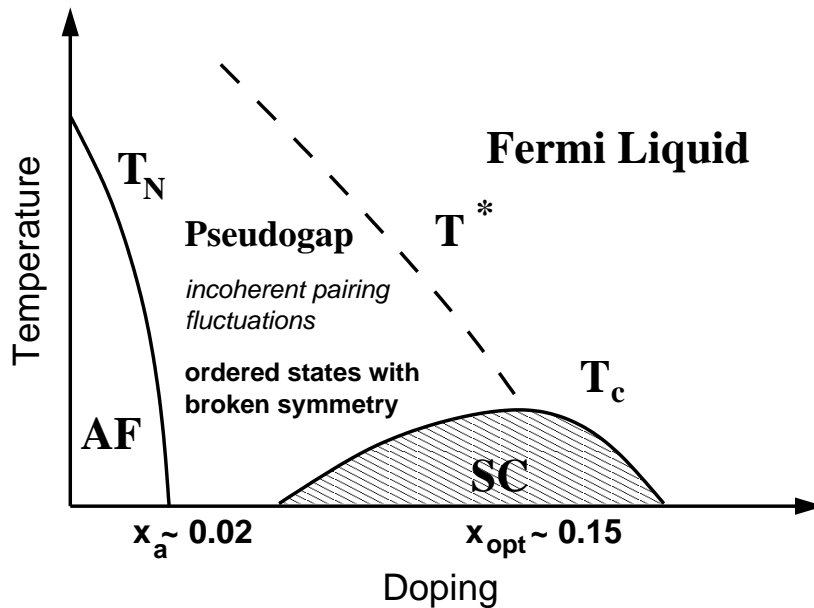


Figure 1.1: Sketch of the typical phase diagram for high- $T_c$ -superconductors.  $T_c$ : critical temperature,  $T_N$ : Néel temperature, AF (SC): antiferromagnetic (superconducting) phase,  $x_{opt}$ : optimal doping.

For HTSC cuprates experimental evidences for an incommensurability in both the spin and charge response that give hints for charge and spin stripes are only found in a couple of substances e.g.  $La_{1.875}Ba_{0.125}CuO_4$  [11] and  $La_{1.6-x}Nd_{0.4}Sr_xCuO_4$  [12, 13]. It is discussed whether the stripe formation is associated with the anomalous suppression of SC observed in  $La_{2-x}Ba_xCuO_4$  and related compounds [14] near a hole concentration of  $x = 1/8$ . The manifestation of incommensurate charge and spin order is only evidenced in compounds where the low temperature orthorhombic (LTO) structure is replaced by a low temperature tetragonal structure (LTT) by partial substitution of  $La$  with  $Nd$ . Similar experimental evidences for the charge and spin distribution are also found for  $Ba$ - $Sr$ -co-doped LCO compounds [6, 15] and further works showed that striped states could be induced by  $Eu$ -co-doping [16]. In  $Nd$  or  $Ba$  co-doped

systems the incommensurate spin response is observed by elastic neutron scattering. The co-doping causes 'pinning' of the spin and charge modulation and leads to a static ordered state. In samples without co-doping the scattering is completely inelastic. Since the incommensurability shows an equivalent doping dependence evidenced for low energies [17] this suggests the formation of dynamic stripes in  $La_{2-x}Sr_xCO_4$ .

The incommensurability in hole doped  $La$  cuprates grows linearly with the doping and survives an insulator SC transition as shown in [18] (without co-doping at finite energies). It grows in the SC phase up to doping of  $x = 1/8$  where it seems to saturate as shown in the Yamada plot in Fig. (1.2) [13, 17].

If the instability in view of stripe formation can be transferred to YBCO is still in discussion. Neutron scattering studies for highly under-doped YBCO give results for an incommensurate static charge ordering and an incommensurate magnetic resonance [19] being consistent with stripe formation. The magnetic spectrum of hole doped YBCO shows an 'hourglass' shape analogous to what is observed for hole doped LCO [20, 21] but for higher energies. Doped YBCO has a much larger spin gap ( $\Delta_s \sim 30meV$ ) than in the LCO compounds what makes it difficult to resolve any incommensurate features from neutron scattering for small energies. However the incommensurability depends linearly on the hole concentration [21] analogous to results in the doped LCO compounds. But because of the difference in the energies it is difficult to compare the results directly.

## Nuclear Magnetic Resonance

Nuclear spin resonance is an experimental method to investigate the local electronic surrounding and magnetic moments of atoms by exciting the atoms with an external electro-magnetic field. Nuclear spin studies of  $^{63,65}Cu$  using nuclear quadrupole resonance (NQR) in oxygen doped YBCO in the SC phase showed a line broadening in the  $^{63,65}Cu$  resonance spectra and new additional features in the transverse relaxation be-

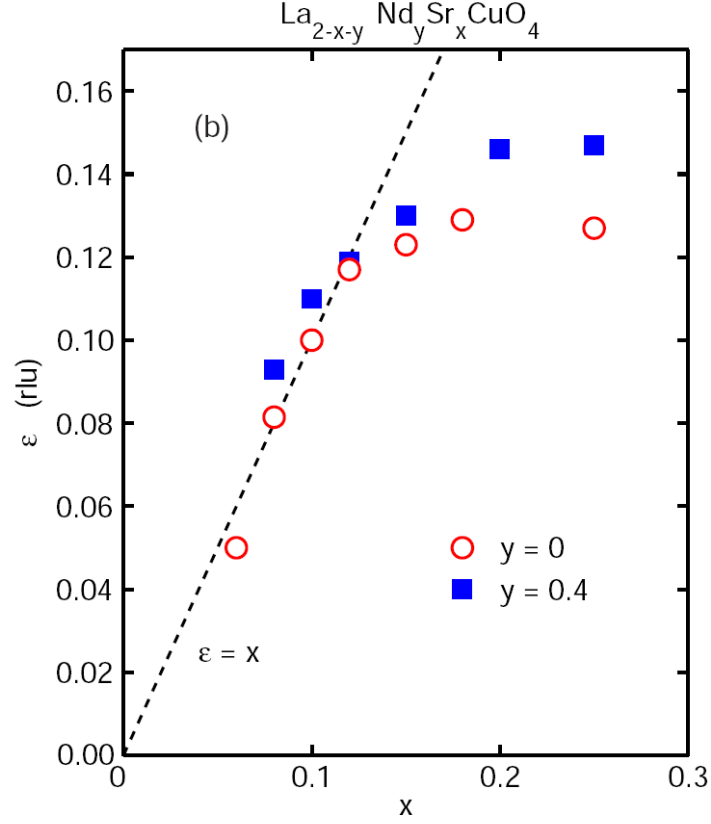


Figure 1.2: Variation of the magnetic incommensurability  $\epsilon$  in  $\text{La}_{2-x}\text{Sr}_x\text{CuO}_4$  with and without  $\text{Nd}$ -co-doping [22]. Data for excitation measurements at  $3\text{meV}$  and  $T \approx T_c$  in  $\text{La}_{2-x}\text{Sr}_x\text{CuO}_4$  from [17]. Data for elastic scattering results for  $\text{Nd}$  doped samples from [13].

low a temperature of  $35\text{K}$  which is of quadrupolar origin and which is possibly connected with a redistribution of the charge [23]. It is proposed that the order parameter-like behavior of the broadening of the line width is caused by a charge density wave state (CDW) in  $\text{YBCO}_{7-\delta}$  that couples to the nuclear position in the  $\text{CuO}$  planes and other parts of the unit cell.

Later NQR investigations of the spin-lattice-relaxation rate  $1/T_1$  of  $^{63}\text{Cu}$  in  $\text{La}_{2-x}\text{Sr}_x\text{CuO}_4$  that measures the local frequency-dependent  $\text{Cu}$ -spin fluctuation [24]

allow to deduce the spatial variation of the local hole concentration  $\Delta x_{hole}$ . The results show that the holes are not distributed equally and the variation  $\Delta x_{hole}$  increases with decreasing temperature. Basing on the NQR data a detailed analysis of the electric field gradient surrounding the  $Cu$  atoms lead also to a variation of the local hole concentration that coincide with the results from the relaxation rate investigations. Excluding possible other reasons for the inhomogeneous hole distribution such as  $Sr^{2+}$ -clustering it is discussed if there exists an electronic mechanism causing the segregation of holes that could be connected with a phase separation.

The line shape analysis of the electric field gradient of  $Cu$  and  $O$  in the  $La_{2-x}Sr_xCuO_4$  based on NMR studies [25] confirmed the increase of the line width in the spectra upon doping. The experiments showed an abrupt broadening by a factor of 50 above a hole concentration of  $x = 0.05$ , which cannot be explained with the simple impurity picture where  $Sr$  induces local changes in the hole density. In fact, it can be interpreted as a charge density variation appearing above a concentration of  $x \approx 0.05$  and varying weakly above this value with doping. The magnetic field distribution of  $^{17}O$  showed an anomalous magnetic shift in the spectrum depending on doping and temperature, that is assumed to be induced by a spin moment polarization at the  $Cu$  atoms in the external field. The observed line broadening is proportional to the external field and is also found in the  $Cu$ -spectrum where the line width increases with decreasing temperature. These facts are interpreted as short range modulation of the spin susceptibility. Based on these results it is assumed that the charge variation is somehow 'pinned' and comes along with the spin density variation with a wave length of a few lattice constants.

## Surface Sensitive Methods

Beyond the LCO and YBCO related compounds experimental results for bismuthates and oxychloride superconductors that possibly indicate the existence of modulated charge ordering come from surface sensitive probes like scanning tunneling microscopy

(STM). STM investigations are based on the analysis of the local density of states (LDOS). If sources of disorder are present in the material elastic scattering mixes eigenstates with different  $\mathbf{k}$ -values at the contour of constant energy (CCE) which can be observed by the modulation of the LDOS.

At low temperatures the HTSC  $Bi_2Sr_2CaCu_2O_{8+\delta}$  (Bi-2212) show a d-wave symmetric Fermi surface with  $\mathbf{k}$ -dependent energy gap  $\Delta(\mathbf{k})$  where the CCE forms banana shaped surfaces (for a review: [26]). High resolution STM measurements of the differential tunneling conductance  $G = dI/dV$  for the Bi-2212 surface at  $T = 4.2K$  allow a derivation of the spatial distribution of the local density of states  $LDOS(E) \sim G(V)$  [27]. Later works [28] approve the observation in under-doped  $Bi_2Sr_2CaCu_2O_{8+\delta}$ . The observed interference pattern can be explained as scattering of Bogoliubov quasiparticles. The quasiparticle scattering takes place between the ends of the banana shaped CCE's where the LDOS is high. This can be seen from the peaks in the Fourier transformed differential tunneling conductance as shown in Fig. (1.3). The regions of high density make up the tips of an octet in the first Brillouin zone. Similar observations of quasi particle interference were also made for  $Ca_{2-x}Na_xCuO_2Cl_2$  (Na-CCOC) at nearly optimal doping [29].

Another possible origin of the peaks in the Fourier transformed LDOS in Bi-2212 can be an incommensurate, spatial modulation of the electronic structure as suggested in [30]. An analysis of the topographic variation of the differential conductance approves a four-period-modulation in the LDOS which suggests a static electronic inhomogeneity. It is still under discussion whether these peaks are nondispersive in energy or follow a bias-dependent dispersion so that the observation can be understood in the framework of the octet model [27, 31]. Measurements in  $Bi_2Sr_2CaCu_2O_{8+\delta}$  [32] show a bias dependent, dispersive behavior of the quasiparticle interference below a certain energy scale whereas above this energy only scattering vectors in antinodal regions are left over suggesting the nondispersive charge order.



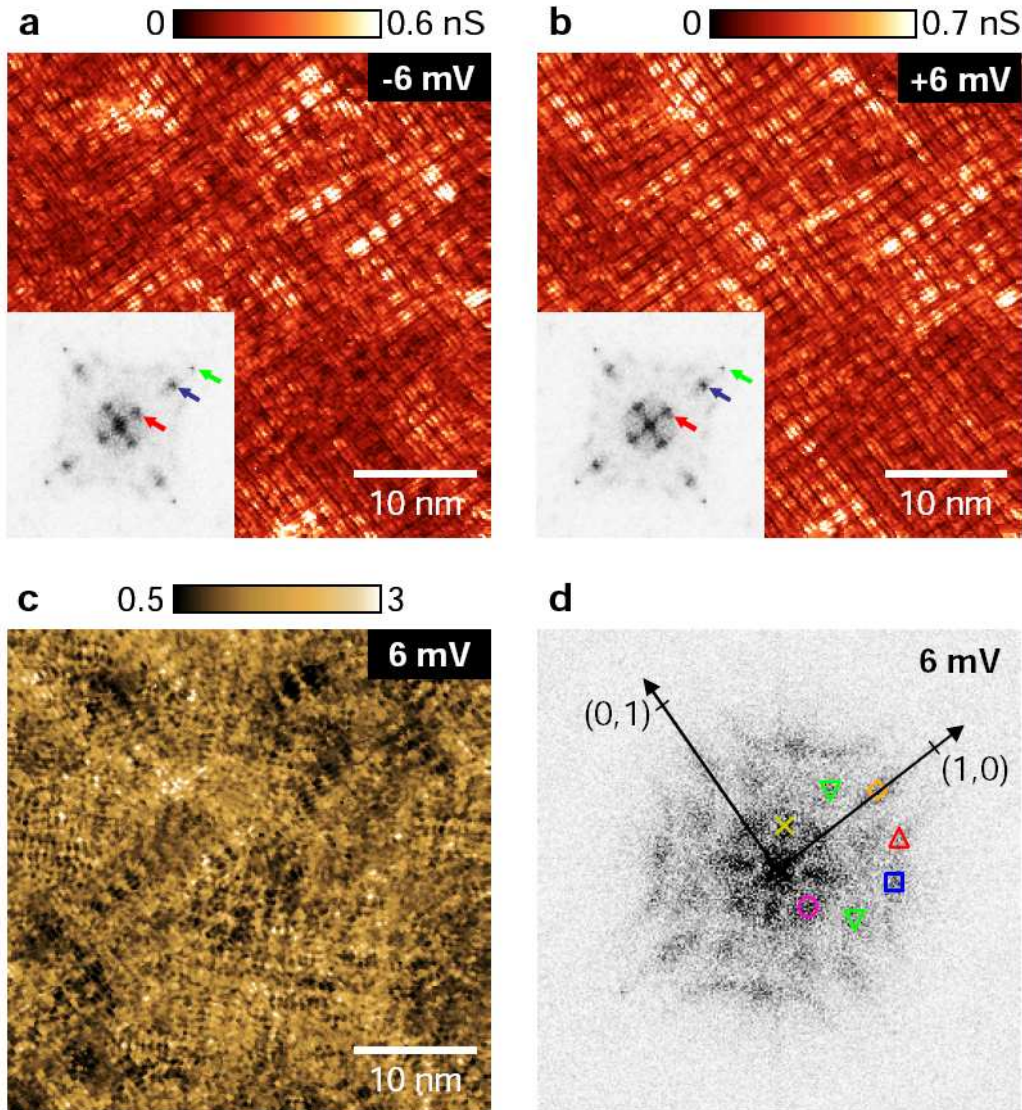


Figure 1.3: Fourier transformed STM results on Na-COOC ( $T_c \sim 28K$ ,  $x \sim 0.14$ ) demonstrating the method of analysis. (a) Topography of the differential conductance  $G(\mathbf{r}, V = -6mV)$  and (b)  $G(\mathbf{r}, V = +6mV)$ . The inset shows the Fourier transformed conductance  $|G(\mathbf{q}, V)|$  (c) Conductance ratio map  $Z(\mathbf{r}, V) = G(\mathbf{r}, V = +6mV)/G(\mathbf{r}, V = -6mV)$  (d) Fourier transformed conductance ratio  $|Z(\mathbf{q}, E)|$ . The dark spots are the regions of high intensity indicating the  $\mathbf{q}$ -vectors expected from the octet model. Images are taken from [33].



## 1.1 Crystal Structure and Electronic Configuration

From the chemical point of view all HTSC belong to the class of perovskites. Generally spoken a perovskite compound has a  $AMO_3$ -structure (e.g.  $CaTiO_3$ ) where a large cation  $A$  is surrounded by an oxidic bounded transition metal  $M$ . In all HTSC compounds the transition metal is  $Cu$  where the central atom can either be  $La$ ,  $Y$ ,  $Ba$  or  $Sr$ . The complex unit cell contains one or two  $CuO$ -planes and it shows a octahedral or orthorombic symmetry for lower temperatures.

The doping with holes (or electrons) can be reached by the exchange of the central cation. In  $La_2CuO_4$  the  $La^{3+}$  ion is replaced by  $Sr^{2+}$ . In the case of  $YBCO$  the doping works differently. One changes the amount of oxygen so that the region between the planes serves as the charge reservoir. As mentioned earlier the doping has strong influence on the physical properties and on the critical temperature.

The geometry of the unit cell of these compounds is characterized by the  $CuO$  planes which are separated by the central atoms. It is supposed that the  $CuO$  planes dominate the physics in the SC phase. In particular the critical temperature seems to depend on the number of  $CuO$  planes per unit cell.

For completeness we mention at this point that there exist compounds based on a cuprate free structure showing SC at relatively high critical temperature (e.g.  $BaBiO_3$ -systems [34] or iron-arsenide-compounds [35]) but it is still under discussion if these compounds can be counted to the class of HTSC. In this work we focus on the class of HTSC containing the typical  $CuO$  planes.

### Three-band-models

In  $La_{2-x}Sr_xCuO_4$  the  $Cu$  ion is surrounded by six  $O$  ions forming an elongated octahedral  $CuO_6$  geometry while in  $YBa_2Cu_3O_{6+x}$  the  $Cu$  ions are surrounded by five  $O$  ions. The degeneracy between the  $d$ -orbitals originating from the rotational invariance

of the isolated ions is removed by the lattice structure. Because the covalent  $CuO$  bonds are strong and charge transport in  $c$ -direction is very small we restrict to the electrons moving only on the  $CuO$  planes.

A microscopic model is two dimensional and has to respect the structure of the electronic orbitals. The copper ions  $Cu^{2+}$  have nine electrons in the five 3d-orbitals, while the  $O^{2-}$  has the three 2p orbitals occupied. The d-orbitals of the  $Cu$ -atoms and the p-orbitals of oxygen hybridize. The three orbitals that are relevant for the hybridization are the  $3d_{x^2-y^2}$  orbital of  $Cu$  and the  $2p_x$  and  $2p_y$  orbital from the in plane  $O$ . The orbital configuration is shown in Fig. (1.4).

The state with highest energy has mainly a  $d_{x^2-y^2}$ -character from the copper. In the undoped case this orbital carries one electron (hole). In this case the system can be described by a model of localized spin- $\frac{1}{2}$  states causing the antiferromagnetic, insulating character of the undoped parent compounds. This means that the electrons must be strongly correlated and the  $3d_{x^2-y^2}$  orbitals must exhibit a strong interaction so that double occupancy becomes unfavored. Based on this line of reasoning it is possible to construct a Hamiltonian for electrons in the copper oxide planes [36, 37]. In the hole notation the Hamiltonian reads as:

$$\begin{aligned} \hat{H} = & - t_{pd} \sum_{\langle ij \rangle} \sum_{\sigma=\uparrow,\downarrow} s_{ij} (\hat{d}_{i\sigma}^\dagger \hat{p}_{j\sigma} + h.c.) - t_{pp} \sum_{\langle jj' \rangle} \sum_{\sigma=\uparrow,\downarrow} s_{ij} (\hat{p}_{j\sigma}^\dagger \hat{p}_{j'\sigma} + h.c.) \quad (1.1) \\ & + U_p \sum_j \hat{n}_{j\uparrow}^p \hat{n}_{j\downarrow}^p + U_d \sum_i \hat{n}_{i\uparrow}^d \hat{n}_{i\downarrow}^d + U_{pd} \sum_{\langle ij \rangle} \hat{n}_i^d \hat{n}_j^p + \epsilon_p \sum_j \hat{n}_j^p + \epsilon_d \sum_i \hat{n}_i^d. \end{aligned}$$

$\hat{p}_{j\sigma}$  ( $\hat{d}_{j\sigma}$ ) are fermionic operators that destroy holes at the oxygen (copper) ions labeled  $j$  ( $i$ ).  $\langle ij \rangle$  refers to pairs of nearest neighbors labeled  $i$  (copper) and  $j$  (oxygen).

In Fig. (1.4) we illustrate the included interactions. The first and the second terms of Eq. (1.1) include the kinetic part. Transition processes are allowed between neighboring oxygen and copper sites ( $pd$ ) and between two neighboring oxygen orbitals ( $pp$ ). The hopping terms  $t_{pd}$  and  $t_{pp}$  correspond to the hybridization between nearest neighbors

of  $Cu$  and  $O$  atoms and are proportional to the overlap between the orbitals. The  $s_{ij}$  take values  $+1$  for symmetric or  $-1$  for antisymmetric overlap. The next three terms include the Coulomb repulsion between two holes on the same  $p$ -orbital ( $U_p$ ), on the same  $d$ -orbital ( $U_d$ ) and holes occupying adjacent  $p/d$ -orbitals. The on-site

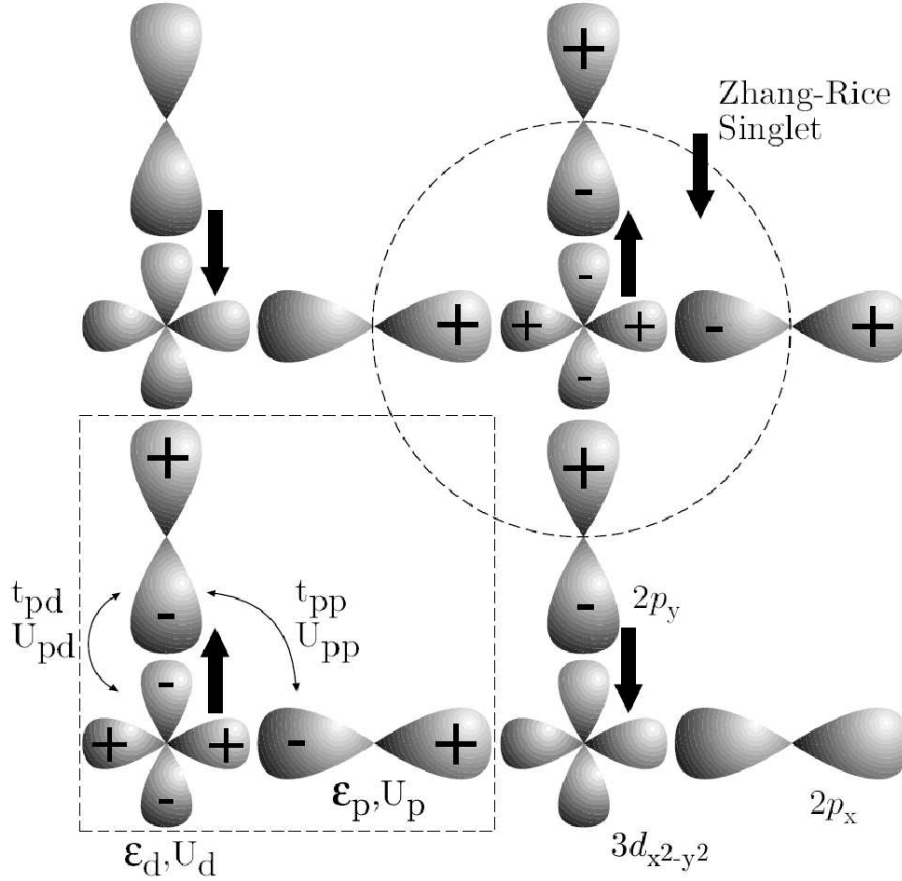


Figure 1.4: Spatial orientation of the dominating orbitals of the hybridization of  $Cu$  and  $O$ . Also shown: The local transition and repulsion parameters included in the three-band model and the Zhang-Rice-singlet. (the figure is taken from [38])

energies  $\epsilon_p$  and  $\epsilon_d$  represent the energy for creating a hole in the  $p$ - or  $d$ -orbital. From

band structure calculations [39] one can estimate the values of the parameters in the Hamiltonian (1.1) in  $eV$ :

| $\Delta$ | $t_{pp}$ | $t_{pd}$ | $U_d$ | $U_p$ | $U_{pd}$   | $U_{pp}$    |
|----------|----------|----------|-------|-------|------------|-------------|
| 3.6      | 0.65     | 1.3      | 10.5  | 4     | $\leq 1.2$ | $\approx 0$ |

We used  $\Delta = \epsilon_p - \epsilon_d$ . In the table we also included the Coulomb repulsion for two holes occupying adjacent  $p/p$ -orbitals ( $U_{pp}$  in Fig. (1.4)). Compared with other on-site repulsions summarized in the table it is very small and can be neglected. Because of  $U_d \gg \Delta$  and  $U_d \gg t_{pp,pd}$  we work in the strong coupling limit. In the undoped system there exists one hole per unit cell. We see from the Hamiltonian (1.1) that an additional hole will be placed in the  $p$ -orbital in the case of strong coupling.

## One-band-models

In order to simplify the three band model Zhang and Rice have suggested a method to reduce the complexity of the model in the strong coupling limit [40]. Because of the hybridization of the  $CuO$  orbitals a hole which is created in the oxygen  $p$ -orbital is bound to the copper ion. The hole at the oxygen can be in a symmetric (parallel) or antisymmetric (anti parallel) spin state with respect to the central hole spin at the  $Cu$ . That means the spins can either be combined in form of singlet or triplet states. To second order perturbation theory about the atomic limit (strong coupling) Zhang and Rice showed that the spin singlet state has the lowest energy (*Zhang-Rice-Singlet*).

The singlet wavefunctions between adjacent  $CuO$  plaquettes overlap and thus give rise to an effective hopping between these plaquettes. As a consequence one can replace the three band model by an effective low energy model ( $t$ - $J$  model) that was earlier suggested in [41]. The overlap of the plaquettes is proportional to  $t$  and the effective exchange between adjacent  $Cu$ -spins is the parameter  $J$ . This model includes only three states per site: either empty or single occupied by an electron with spin up or down (or

a hole respectively). It is important to mention that the reduction of the three band model is still controversial.

The  $t$ - $J$  model is more commonly obtained as the strong coupling limit of the one-band Hubbard model which we will discuss in the next section. In the context of the electronic structure of the cuprate SC the one-band Hubbard model mimics the charge transfer gap  $\Delta$  by an effective Coulomb repulsion  $U_{eff}$ . At half filling and if the on-site interaction is strong the model reduces to the Heisenberg model which well describes the spin dynamics in undoped cuprates close to  $T = 0$ .



# Chapter 2

## Hubbard Model -

## Limits and Approximations

Although the Hubbard model provides a very simple form it can be solved exactly only in one dimension [42] while for higher dimensions one has to rely on approximative methods. In this section we introduce the one-band version of the Hubbard model and we will briefly discuss exact solution and basic techniques. Before we discuss in detail the Gutzwiller variational method we explain briefly the Hartree Fock (HF) method since we will compare the results of our calculations with this method. Furthermore we need the HF method to derive the one particle Slater determinant as in input for our later computation.

### 2.1 The Hubbard Model - Exact and Approximative Solutions

The Hubbard model was independently introduced by Gutzwiller, Hubbard and Kanamori in 1963 [43–46]. The Hubbard model is one of the simplest models to describe

correlated particles on a lattice. The Hubbard Hamiltonian reads as:

$$\hat{H} = - \sum_{ij\sigma} t_{ij} \hat{c}_{i\sigma}^\dagger \hat{c}_{j\sigma} + U \sum_i \hat{n}_{i\uparrow} \hat{n}_{i\downarrow}, \quad (2.1)$$

where the kinetic term describes the motion between the sites  $i$  and  $j$ . The operator  $\hat{c}_{i\sigma}$  ( $\hat{c}_{i\sigma}^\dagger$ ) destroys (creates) a spin- $\sigma$ -electron at the lattice site  $i$ . Usually the 'hopping' integral  $t_{ij}$  is restricted to nearest neighbor transitions and it is taken as translationally invariant:  $\{t_{ij} = t \mid i, j \text{ are nearest neighbors}, t_{ij} = 0 \text{ elsewhere}\}$ .

The second term in Eq.(2.1) approximates the Coulomb interaction among the electrons which is only on-site. The operator  $\hat{n}_{i\sigma} = \hat{c}_{i\sigma}^\dagger \hat{c}_{i\sigma}$  is the particle number operator. In the repulsive Hubbard model ( $U > 0$ ) the on-site interaction approximates the Coulomb repulsion, whereas in the attractive Hubbard model ( $U < 0$ ) it describes an effective, short range attractive interaction between the electrons. The focus of this work will be mainly on the attractive on-site interaction. We will explain the nature of  $U < 0$  systems later.

Even for this reduced version (2.1) no exact solution has been found. The exact ground state can only be calculated for one dimensional systems using the Bethe Ansatz [42]. In higher dimensions one has to rely on approximative methods of which we will briefly introduce the HF-technique in the next section.

In the limit of  $U = 0$  the Hamiltonian (2.1) reduces to the free electron system. In the case of  $t = 0$ , electrons cannot move and the Hubbard Hamiltonian approaches the atomic (insulating) limit with all electrons to be localized.

The  $t$ - $J$ -model is the low energy limit of the strong coupling Hubbard model. In the case of positive  $U$  and  $\frac{U}{t} \gg 0$  doubly occupied sites become energetically unpropitious. Applying perturbation theory up to second order one can eliminate the double occupancies [47]. Via a canonical transformation  $\hat{S}$  ( $\hat{S} = \mathcal{O}(t/U)$ ) the Hamiltonian (2.1) transforms to:

$$\tilde{H} = e^{-\hat{S}} \hat{H} e^{\hat{S}}, \quad (2.2)$$



leading to the  $t$ - $J$ -model:

$$\hat{H} = -\mathcal{P}t \sum_{\langle ij \rangle \sigma} \hat{c}_{i\sigma}^\dagger \hat{c}_{j\sigma} \mathcal{P} + J \sum_{\langle ij \rangle} (\hat{\mathbf{S}}_i \hat{\mathbf{S}}_j - n_i n_j), \quad (2.3)$$

where  $J = \frac{4t^2}{U}$ . The operator  $\mathcal{P}$  projects the Hamiltonian onto the subspace where double occupancy is excluded.

In the case of half filling ( $n = 1$ ) the electrons localize and Eq.(2.3) reduces to the Heisenberg Hamiltonian:

$$\hat{H} = J \sum_{\langle ij \rangle} \hat{\mathbf{S}}_i \hat{\mathbf{S}}_j. \quad (2.4)$$

The Heisenberg Hamiltonian is a model of localized spins on a lattice and it is used in the study of critical points and phase transitions of magnetic systems. Although it has a simple form it can be solved exactly in one dimension only.

## 2.2 Hartree Fock Approximation of the Hubbard Model

We start with the Hubbard Hamiltonian (2.1) and include an extra term with the Fermi energy  $\mu$  in order to conserve the particle number:

$$\hat{H} = \sum_{i \neq j, \sigma} t_{ij} \hat{c}_{i\sigma}^\dagger \hat{c}_{j\sigma} + U \sum_i \hat{c}_{i\uparrow}^\dagger \hat{c}_{i\uparrow} \hat{c}_{i\downarrow}^\dagger \hat{c}_{i\downarrow} - \mu \left( \sum_{i\sigma} \hat{c}_{i\sigma}^\dagger \hat{c}_{i\sigma} - N_{el} \right). \quad (2.5)$$

The four operator product in (2.5) decomposes as follows:

$$\begin{aligned} \hat{c}_{i\uparrow}^\dagger \hat{c}_{i\uparrow} \hat{c}_{i\downarrow}^\dagger \hat{c}_{i\downarrow} &\approx \langle \hat{c}_{i\downarrow}^\dagger \hat{c}_{i\downarrow} \rangle \hat{c}_{i\uparrow}^\dagger \hat{c}_{i\uparrow} + \langle \hat{c}_{i\uparrow}^\dagger \hat{c}_{i\uparrow} \rangle \hat{c}_{i\downarrow}^\dagger \hat{c}_{i\downarrow} - \langle \hat{c}_{i\uparrow}^\dagger \hat{c}_{i\uparrow} \rangle \langle \hat{c}_{i\downarrow}^\dagger \hat{c}_{i\downarrow} \rangle \\ &+ \langle \hat{c}_{i\uparrow}^\dagger \hat{c}_{i\downarrow}^\dagger \rangle \hat{c}_{i\downarrow} \hat{c}_{i\uparrow} + \langle \hat{c}_{i\downarrow} \hat{c}_{i\uparrow} \rangle \hat{c}_{i\uparrow}^\dagger \hat{c}_{i\downarrow}^\dagger - \langle \hat{c}_{i\uparrow}^\dagger \hat{c}_{i\downarrow}^\dagger \rangle \langle \hat{c}_{i\downarrow} \hat{c}_{i\uparrow} \rangle. \end{aligned} \quad (2.6)$$

We ignored all terms that include spin flips.

Introducing the local charge density  $n_{i\sigma} = \langle \hat{c}_{i\sigma}^\dagger \hat{c}_{i\sigma} \rangle$  and the local pair density  $\Delta_i = \langle \hat{c}_{i\uparrow}^\dagger \hat{c}_{i\downarrow}^\dagger \rangle$  ( $\Delta_i^* = \langle \hat{c}_{i\downarrow} \hat{c}_{i\uparrow} \rangle$ ) the HF Hamiltonian reduces to:

$$\begin{aligned} \hat{H}^{HF} = & \sum_{i \neq j, \sigma} t_{ij} \hat{c}_{i\sigma}^\dagger \hat{c}_{j\sigma} + U \sum_i (n_{i\downarrow} \hat{c}_{i\uparrow}^\dagger \hat{c}_{i\uparrow} + n_{i\uparrow} \hat{c}_{i\downarrow}^\dagger \hat{c}_{i\downarrow}) + U \sum_i (\Delta_i \hat{c}_{i\uparrow}^\dagger \hat{c}_{i\downarrow}^\dagger + \Delta_i^* \hat{c}_{i\downarrow} \hat{c}_{i\uparrow}) \\ & - U \sum_i n_{i\uparrow} n_{i\downarrow} - U \sum_i \Delta_i \Delta_i^* - \mu \left( \sum_{i\sigma} \hat{c}_{i\sigma}^\dagger \hat{c}_{i\sigma} - N_{el} \right). \end{aligned} \quad (2.7)$$

The HF method decomposes the Hamiltonian (2.1) into two decoupled single particle Hamiltonians with spin  $\sigma$ :

$$\hat{H}^{HF} = \sum_{m n \sigma}^{2N} H_{mn}^\sigma \hat{\psi}_m^\sigma \hat{\psi}_n^{-\sigma} \quad (2.8)$$

with the vectors:

$$\psi^+ = (\hat{c}_{1\uparrow}^\dagger, \dots, \hat{c}_{N\uparrow}^\dagger, \hat{c}_{1\downarrow}, \dots, \hat{c}_{N\downarrow}) \quad \text{and} \quad \psi^- = (\hat{c}_{1\uparrow}, \dots, \hat{c}_{N\uparrow}, \hat{c}_{1\downarrow}^\dagger, \dots, \hat{c}_{N\downarrow}^\dagger). \quad (2.9)$$

The HF matrices are of dimension  $2N$  with the explicit elements:

$$\mathbf{H}^\sigma = \sigma \left( \begin{array}{c|c} t_{ij} & 0 \\ \hline 0 & -t_{ij} \end{array} \right) + \sigma U \left( \begin{array}{c|c} \text{diag} \{ n_{i\downarrow} - \frac{\mu}{U} \} & \text{diag} \{ \Delta_i^\sigma \} \\ \hline \text{diag} \{ \Delta_i^{-\sigma} \} & \text{diag} \{ -n_{i\uparrow} + \frac{\mu}{U} \} \end{array} \right), \quad (2.10)$$

where  $i, j \in \{1, \dots, N\}$  and  $m, n \in \{1, \dots, 2N\}$ . We defined  $\Delta_i^\pm$  as above and of course  $t_{ii} = 0$ .

The HF approximated Hubbard Hamiltonian has a single particle form that can be diagonalized.

## 2.3 Bogoliubov Transformation

The effective Hamiltonian (2.8) includes terms with combinations of two creation or two destruction operators. In order to calculate the eigenvalues of the Hartree Fock approximated Hamiltonian (2.8) we introduce a Bogoliubov transformation. If the

system consists of  $N$  lattice sites the one-particle operator  $H^\sigma$  (2.10) has a set of  $2N$  real eigenvalues. Because of the symmetric structure of (2.10) it consists of  $N$  positive and  $N$  negative eigenvalues:

$$\{-\omega_N, -\omega_{N-1}, \dots, -\omega_2, -\omega_1, \omega_1, \omega_2, \dots, \omega_{N-1}, \omega_N\}. \quad (2.11)$$

The corresponding normalized eigenvectors are written as:

$$V^k = \begin{pmatrix} X^\alpha(k) \\ Y^\alpha(k) \end{pmatrix}, \quad W^k = \begin{pmatrix} Y^\beta(k) \\ X^\beta(k) \end{pmatrix} \in \text{Vec}(2N), \quad k = 1, 2, \dots, N, \quad (2.12)$$

corresponding to the negative and positive set of eigenvalues. From the eigenvectors we construct unitary transformation matrices:

$$\mathbf{T} = \begin{pmatrix} X^\alpha & Y^\beta \\ Y^\alpha & X^\beta \end{pmatrix} \quad \text{and} \quad \mathbf{T}^\dagger = \begin{pmatrix} X^{\alpha*} & Y^{\alpha*} \\ Y^{\beta*} & X^{\beta*} \end{pmatrix}, \quad (2.13)$$

with  $\mathbf{T}^\dagger \mathbf{T} = \mathbf{1}$  that diagonalizes the HFA Hamiltonian:

$$\mathbf{T}^\dagger \mathbf{H} \mathbf{T} = \text{diag}(-\omega_N, -\omega_{N-1}, \dots, -\omega_2, -\omega_1, \omega_1, \omega_2, \dots, \omega_{N-1}, \omega_N). \quad (2.14)$$

With the help of the identity  $\hat{H}^{\sigma HF} = \hat{\psi}^\sigma \mathbf{H}^\sigma \hat{\psi}^{-\sigma} = \hat{\psi}^\sigma \mathbf{T} \mathbf{T}^\dagger \mathbf{H}^\sigma \mathbf{T} \mathbf{T}^\dagger \hat{\psi}^{-\sigma}$  respecting the unitary condition of the transformation one derives for the operators:

$$\hat{\phi}^\sigma = \hat{\psi}^\sigma \mathbf{T} \quad \text{and} \quad \hat{\phi}^{-\sigma} = \mathbf{T}^\dagger \hat{\psi}^{-\sigma}, \quad (2.15)$$

and for the back transformation:

$$\hat{\psi}^\sigma = \hat{\phi}^\sigma \mathbf{T}^\dagger \quad \text{and} \quad \hat{\psi}^{-\sigma} = \mathbf{T} \hat{\phi}^{-\sigma}. \quad (2.16)$$

We have introduced the transformed vectors  $\phi^\sigma$  consisting of the transformed single particle operators  $f_{i\sigma}$ :

$$\begin{aligned} \phi^+ &= (\hat{f}_{1\uparrow}^\dagger, \dots, \hat{f}_{N\uparrow}^\dagger, \hat{f}_{1\downarrow}, \dots, \hat{f}_{N\downarrow}) \\ \phi^- &= (\hat{f}_{1\uparrow}, \dots, \hat{f}_{N\uparrow}, \hat{f}_{1\downarrow}^\dagger, \dots, \hat{f}_{N\downarrow}^\dagger). \end{aligned} \quad (2.17)$$

The transformations for the single particle ladder operators read explicitly:

$$\begin{aligned}
\hat{c}_{j\uparrow} &= \sum_k X_j^\alpha(k) \hat{f}_{k\uparrow} + \sum_k Y_j^\beta(k) \hat{f}_{k\downarrow} \\
\hat{c}_{j\downarrow}^\dagger &= \sum_k Y_j^\alpha(k) \hat{f}_{k\uparrow} + \sum_k X_j^\beta(k) \hat{f}_{k\downarrow}^\dagger \\
\hat{c}_{i\uparrow}^\dagger &= \sum_k X_i^{\alpha*}(k) \hat{f}_{k\uparrow}^\dagger + \sum_k Y_i^{\beta*}(k) \hat{f}_{k\downarrow} \\
\hat{c}_{i\downarrow} &= \sum_k Y_i^{\alpha*}(k) \hat{f}_{k\uparrow}^\dagger + \sum_k X_i^{\beta*}(k) \hat{f}_{k\downarrow}.
\end{aligned} \tag{2.18}$$

In terms of the new transformed operators the expectation values of the single particle densities read:

$$\begin{aligned}
\langle \hat{c}_{i\uparrow}^\dagger \hat{c}_{j\uparrow} \rangle &= \sum_k X_i^{\alpha*}(k) X_j^\alpha(k) \langle \hat{f}_{k\uparrow}^\dagger \hat{f}_{k\uparrow} \rangle + \sum_k Y_i^{\beta*}(k) Y_j^\beta(k) \langle \hat{f}_{k\downarrow} \hat{f}_{k\downarrow}^\dagger \rangle \\
\langle \hat{c}_{i\downarrow}^\dagger \hat{c}_{j\downarrow} \rangle &= \sum_k X_i^\beta(k) X_j^{\beta*}(k) \langle \hat{f}_{k\downarrow}^\dagger \hat{f}_{k\downarrow} \rangle + \sum_k Y_i^\alpha(k) Y_j^{\alpha*}(k) \langle \hat{f}_{k\uparrow} \hat{f}_{k\uparrow}^\dagger \rangle \\
\langle \hat{c}_{i\uparrow}^\dagger \hat{c}_{j\downarrow} \rangle &= \sum_k X_i^{\alpha*}(k) Y_j^\alpha(k) \langle \hat{f}_{k\uparrow}^\dagger \hat{f}_{k\uparrow} \rangle + \sum_k Y_i^{\beta*}(k) X_j^\beta(k) \langle \hat{f}_{k\downarrow} \hat{f}_{k\downarrow}^\dagger \rangle \\
\langle \hat{c}_{i\downarrow} \hat{c}_{j\uparrow} \rangle &= \sum_k Y_i^{\alpha*}(k) X_j^\alpha(k) \langle \hat{f}_{k\uparrow}^\dagger \hat{f}_{k\uparrow} \rangle + \sum_k X_i^{\beta*}(k) Y_j^\beta(k) \langle \hat{f}_{k\downarrow} \hat{f}_{k\downarrow}^\dagger \rangle.
\end{aligned} \tag{2.19}$$

We used in (2.19):

$$\langle \hat{f}_{k\sigma}^\dagger \hat{f}_{k'\sigma'} \rangle = \delta_{\sigma\sigma'} \delta_{kk'} \langle \hat{f}_{k\sigma}^\dagger \hat{f}_{k\sigma} \rangle \quad \text{and} \quad \langle \hat{f}_{k\sigma}^\dagger \hat{f}_{k'\sigma'} \rangle = \langle \hat{f}_{k\sigma} \hat{f}_{k'\sigma'} \rangle = 0. \tag{2.20}$$

The new single particle operators fulfill the anti-commutator relation  $[\hat{f}_{k\sigma}^\dagger, \hat{f}_{k'\sigma'}]_+ = \delta_{kk'} \delta_{\sigma\sigma'}$  and we can replace:

$$\hat{f}_{k\sigma} \hat{f}_{k\sigma}^\dagger = 1 - \hat{f}_{k\sigma}^\dagger \hat{f}_{k\sigma}. \tag{2.21}$$

In general the expectation values of the transformed particle number operators  $\langle \hat{f}_{k\sigma}^\dagger \hat{f}_{k\sigma} \rangle$  depend on energy and temperature and obey the Fermi function  $\langle \hat{f}_{k\sigma}^\dagger \hat{f}_{k\sigma} \rangle = f(\mu, E_k, kT)$ .

In our calculation we consider the zero temperature limit  $T = 0$  and the Fermi function reduces to the Heaviside function:

$$\langle \hat{f}_{k\sigma}^\dagger \hat{f}_{k\sigma} \rangle = \Theta(\mu - E_k) = \begin{cases} 1 & \text{for } E_k \leq \mu \\ 0 & \text{for } E_k > \mu \end{cases}. \quad (2.22)$$

We rewrite the formulae (2.19):

$$\begin{aligned} \langle \hat{c}_{i\uparrow}^\dagger \hat{c}_{j\uparrow} \rangle &= \sum_{k=1}^N X_i^{\alpha*}(k) X_j^\alpha(k), & \langle \hat{c}_{i\downarrow}^\dagger \hat{c}_{j\downarrow} \rangle &= \sum_{k=1}^N X_i^\beta(k) X_j^{\beta*}(k), \\ \langle \hat{c}_{i\uparrow}^\dagger \hat{c}_{j\downarrow}^\dagger \rangle &= \sum_{k=1}^N X_i^{\alpha*}(k) Y_j^\alpha(k), & \langle \hat{c}_{i\downarrow} \hat{c}_{j\uparrow} \rangle &= \sum_{k=1}^N Y_i^{\alpha*}(k) X_j^\alpha(k). \end{aligned} \quad (2.23)$$

In our calculation the Fermi energy is a parameter which is unknown at the beginning. The eigenvectors depend on the Fermi energy and have to be calculated self-consistently in order to conserve the particle number  $N_\sigma$  which is given by:

$$N_\sigma = \sum_k \langle \hat{c}_{k\sigma}^\dagger \hat{c}_{k\sigma} \rangle. \quad (2.24)$$

The Fermi energy has to be adjusted correspondingly in each iteration cycle.

## 2.4 Attraction Repulsion Transformation

This work is focussed on the attractive Hubbard model where the Hubbard- $U$  mediates an effective attractive interaction ( $U < 0$ ).

We mentioned that exact solutions of the Hubbard model depend on the lattice dimension and on the band filling. For a qualitative analysis one can compare the attractive Hubbard model with the well known results for the repulsive case ( $U > 0$ ). There exists a canonical transformation ( $\hat{c}_{i\sigma} \rightarrow \hat{b}_{i\sigma}$ ) namely:

$$\hat{c}_{i\downarrow}^\dagger = \exp(i\mathbf{Q}\mathbf{R}_i) \hat{b}_{i\downarrow} \quad \text{and} \quad \hat{c}_{i\uparrow}^\dagger = \hat{b}_{i\uparrow}, \quad (2.25)$$

where  $\mathbf{Q}$  is the antiferromagnetic wave vector. The transformation maps the Hubbard model with on-site attraction and arbitrary band filling ( $0 \leq n \leq 2$ ) onto the half filled Hubbard model (so called normal Hubbard model) with an on-site repulsion and with an inter-site exchange interaction [48, 49] which is of the form of the Ising exchange with an external magnetic field [48, 50]. A mathematical overview is given in appendix C.2.

In case of  $U < 0$  the CDW and singlet SC order are equivalent to the magnetic ordered structures in the positive  $U$  transformed system. For half filling the CDW and SC state are strictly degenerate. Beyond half filling the degeneracy disappears. It also disappears if one assumes an additional interaction such as an inter-site repulsion mediated by the  $V > 0$  that we will discuss in the next chapter.

# Chapter 3

## Gutzwiller Approach and Model Specifications

The difficulties to find an exact quantum mechanics solution to the Hubbard model in dimensions greater than one have stimulated the growth of several approximative methods. The latter are intended to describe correctly the physics in the framework of the model in special limits.

As discussed before the strong coupling limit is appropriate when dealing with strongly correlated electron systems. Within this framework, standard many-body techniques such as Hartree-Fock cannot be applied because it covers the weak coupling limits only. In the strong coupling limit two analytical approaches turned out to be particularly successful. The Gutzwiller variational approach [51] corresponds to a variational trial wave function for the ground state and by the use of the so called Gutzwiller approximation extrapolates weak coupling results to the strong coupling region. The Gutzwiller approximation becomes exact in the limit of infinite spatial dimension ( $d \rightarrow \infty$ ) [52].

The auxiliary field or slave boson approach enlarges the Fock space at each site by adding a set of virtual bosons. The essence of this method has been applied early

in the framework of the Anderson model [53, 54]. Including additional constraints to the model the virtual bosons act as a projection operator onto electronic states as the doubly occupied states are forbidden in the  $U = \infty$  limit. A reformulation of the slave boson approach was suggested by Kotliar and Ruckenstein (KR) [55] in order to describe the finite  $U$  regime of the Hubbard model. The method reproduces some results originally derived by the Gutzwiller approximation scheme as well as other types of mean field solutions [56].

In this section we will shortly discuss the Gutzwiller variational approach and the Gutzwiller approximation and the resulting energy functional. Further we derive the energy functional again in the charge-rotational invariant formulation. We follow the concept of Kotliar and Ruckenstein but we also refer to the mean field approach suggested by Frésard and Wölfle [56] to explain the physical constraints of the mean field solution. Finally we will shortly discuss the extended and the attractive Hubbard model.

### 3.1 Gutzwiller's Wave-function and Approximation

The Gutzwiller method is an approximation to the ground state wave function  $|\Psi_0\rangle$  of the Hubbard Hamiltonian (2.5) based on a trial wave function [43]. The crucial term is the four operator product in the potential term counting the number of doubly occupied lattice sites. In its basic version the so called Gutzwiller wave function reads:

$$|\Psi_G\rangle = \prod_i (1 - (1 - \eta)\hat{n}_{i\uparrow}\hat{n}_{i\downarrow})|\Phi_0\rangle, \quad (3.1)$$

where  $|\Phi_0\rangle$  is the Slater determinant describing the ground state of uncorrelated electrons and  $\eta$  is the variational parameter. The associated density matrix usually contains only the normal part:

$$\rho_{ij}^{\sigma\sigma'} = \langle\Phi_0|\hat{c}_{i\sigma}^\dagger\hat{c}_{j\sigma'}|\Phi_0\rangle. \quad (3.2)$$



In the case of  $\eta = 0$  the ground state is projected to a subspace without double occupancies. For finite  $\eta$  the Gutzwiller projection operator reduces the weight of configurations with doubly occupied sites in the wave function. The variational parameter is determined by minimizing the expectation value of the energy:

$$E(\eta) = \frac{\langle \Psi_G | \hat{H} | \Psi_G \rangle}{\langle \Psi_G | \Psi_G \rangle} \stackrel{!}{=} \min. \quad (3.3)$$

In the limit of large values of  $|U|/|t|$  ( $U < 0$ ) doubly occupied sites become unfavorable because they cost a large amount of repulsion energy. This implies  $\eta \rightarrow 0$  to minimize doubly occupied lattice sites. One can apply similar arguments for empty sites for more than half filling. This reflects the particle-hole symmetry.

For general values of  $U$  an analytic expression for the expectation value with respect to  $|\Psi_G\rangle$  is only possible in one [57] or infinite dimensions [58]. For finite dimensions one has to apply the so called Gutzwiller approximation (GA) [59] in order to obtain quantitative results from (3.3). The GA in its original variant [51, 59] uses arguments from combinatorial theory and approximation for large numbers (Stirling approximation). In its basic version the ground state energy functional reads:

$$E^{GA} = \sum_{i,j,\sigma} t_{ij} z_{i\sigma} z_{j\sigma} \rho_{ij}^{\sigma\sigma} + U \sum_i D_i, \quad (3.4)$$

where the  $z$ -factors are given by:

$$z_{i\sigma} = \frac{\sqrt{(\rho_{ii}^{\sigma\sigma} - D_i)(1 - \rho_{ii}^{\sigma\sigma} - \rho_{ii}^{-\sigma-\sigma} + D_i)} + \sqrt{D_i(\rho_{ii}^{-\sigma-\sigma} - D_i)}}{\sqrt{(1 - \rho_{ii}^{\sigma\sigma})\rho_{ii}^{\sigma\sigma}}}. \quad (3.5)$$

The  $\rho_{ii}^{\sigma\sigma}$  refer to the elements of the density matrix and  $D_i$  is the double occupation density at the lattice site  $i$ . The energy functional (3.4) has to be minimized with respect to  $D_i$  and  $\rho$ . The potential term contains only the double occupancy.

Within the GA a strong on-site repulsion  $U$  leads to a decrease in the double occupancies  $D_i$ . This restricts the transition processes of the fermions and thus reduces the kinetic energy. This is because the  $z$ -factors depend on the variational parameter

$D_i$  and renormalize the kinetic energy which leads to a band diminution. In contrast within the HF method the potential part is decoupled while the kinetic part is not involved. Since the influence of a growing ratio  $|U|/|t|$  is not respected it covers only the weak coupling regime.

The approximated energy functional (3.4) can also be recovered by the slave boson approach [55]. An alternative method to approximate the energy functional in finite dimensions  $d$  was suggested in [60] where the Gutzwiller wave function was expanded in terms of  $1/d$  around the limit of high dimensions ( $d \rightarrow \infty$ ). In the limit of infinite dimensions the Gutzwiller approximation recovers the exact result for (3.3) with respect to  $|\Psi_G\rangle$  [52]. In this case at half-filling a transition to a localization takes place at a finite interaction strength (Brinkman Rice transition [61]). In addition it can be shown that the Gutzwiller wave function does not predict a metal-insulator transition for the Hubbard model for finite interaction strength in all finite dimensions [62] which is an artefact of the Gutzwiller approximation. Moreover in the large  $U$  regime the GA describes rather a metal Mott-insulator transition.

The GA is a 'semi-classical' technique for the calculation of expectation values and it is derived in its original version using large number arguments. For this reason it is suited for large fermion systems and it is useful for solid state models in the metallic state and in the Mott regime but it is probably too simple for small systems and for molecules.

## 3.2 Charge-Rotationally-Invariant Gutzwiller Approach

We will now derive the variational energy functional for the GA following the slave boson approach originally introduced by Kotliar and Ruckenstein [55]. We present a

general formulation by keeping the charge-rotational invariance.

Essentially, we map the superconducting system into a purely normal conducting state without superconductivity by performing a local unitary rotation in the charge space represented by a spin 1/2-algebra [63]. At this point different methods can be used to derive the Gutzwiller approximation for example counting arguments from combinatorial theory [64, 65] or one can derive the GA from the infinite dimension limit as discussed above. Alternatively, one can use a Gutzwiller projection  $\hat{P}$  directly acting on the Hartree-Fock-Bogoliubov-wave function  $|\Phi_0\rangle$  [64, 66]. In our method we use the well known equivalence between the slave boson method and the Gutzwiller approach [56, 67–70]. The procedure implemented in the following consists of three steps essentially. We assume that in our initial reference frame we have non-vanishing superconducting order which can be described by a vector field. First we rotate the system locally to a new frame where the expectation values of the superconducting order vanish. This allows, as a second step, to introduce of slave bosons within the Kotliar-Ruckenstein scheme. For the bosons we apply the saddle point (mean field) approximations. Finally, in the third step we rotate the system back to the original reference frame.

It is convenient to introduce the Nambu-vectors:

$$\Psi_i^\dagger = (\hat{c}_{i\uparrow}^\dagger, \hat{c}_{i\downarrow}) \quad \text{and} \quad \Psi_i = \begin{pmatrix} \hat{c}_{i\uparrow} \\ \hat{c}_{i\downarrow}^\dagger \end{pmatrix}. \quad (3.6)$$

We introduce the pseudo charge vectors with the components  $\hat{J}_i^m = \frac{1}{2}\Psi_i^\dagger \tau^m \Psi_i$ , ( $m = x, y, z$ ), where we used the Pauli matrices to define the  $x$ ,  $y$  and  $z$ -component. The components read explicitly:

$$\begin{aligned} J_i^x &= \frac{1}{2}(\hat{c}_{i\uparrow}^\dagger \hat{c}_{i\downarrow}^\dagger + \hat{c}_{i\downarrow} \hat{c}_{i\uparrow}), \\ J_i^y &= -\frac{i}{2}(\hat{c}_{i\uparrow}^\dagger \hat{c}_{i\downarrow}^\dagger - \hat{c}_{i\downarrow} \hat{c}_{i\uparrow}), \\ J_i^z &= \frac{1}{2}(\hat{c}_{i\uparrow}^\dagger \hat{c}_{i\uparrow} + \hat{c}_{i\downarrow}^\dagger \hat{c}_{i\downarrow} - 1). \end{aligned} \quad (3.7)$$

The components of the charge vector form a spin-1/2-algebra. The charge state of a lattice site  $i$  is now represented by the vector  $\mathbf{J}_i$  which has three degrees of freedom. The  $z$ -component is proportional to the (local) normal charge or doping rate respectively ( $\delta_i = 1 - n_i$ ). For a homogeneous half filled system then  $\langle J_i^z \rangle = 0$ . The  $x$ - and  $y$ -components consist of the electron pair creation and destruction operators.

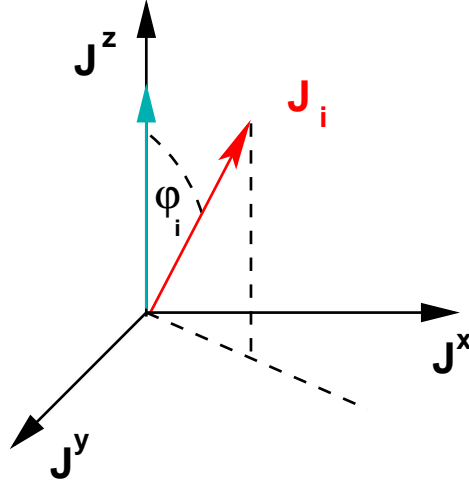


Figure 3.1: Charge vector for an arbitrary lattice site  $i$ . A charge state is a composition of normal conducting parts along  $z$  and the superconducting parts in the  $x$ - $y$ -plane.

We define the ladder operators:

$$J_i^+ = \hat{c}_{i\uparrow}^\dagger \hat{c}_{i\downarrow}^\dagger \quad \text{and} \quad J_i^- = \hat{c}_{i\downarrow} \hat{c}_{i\uparrow}, \quad (3.8)$$

which create (destroy) a SC electron pair at the lattice site  $i$  (total spin 0). If the expectation values  $\langle J_i^+ \rangle$  and  $\langle J_i^- \rangle$  are non-zero we have (local) SC order. A charge state is represented in Fig. (3.1) by the expectation values of the three components  $\hat{\mathbf{J}}_i$  where the normal charge is real and the SC order is equivalent to a projection into the  $x$ - $y$ -plane.

We now transform a general charge state into a pure normal state. We require that the SC order vanishes locally so that the expectation values  $\langle J_i^x \rangle$  and  $\langle J_i^y \rangle$  become zero.

We define the local rotations in charge space by the following transformations:

$$\tilde{\Psi}_i = \mathbf{U}_i^\dagger \Psi_i \quad \text{and} \quad \tilde{\Psi}_i^\dagger = \Psi_i^\dagger \mathbf{U}_i, \quad (3.9)$$

where we used the general definition of a unitary rotation by the angle  $\varphi_i$ :

$$\mathbf{U}_i(\varphi_i) = \mathbf{1} \cos\left(\frac{\varphi_i}{2}\right) + i \sin\left(\frac{\varphi_i}{2}\right) \tau \eta. \quad (3.10)$$

The vector  $\eta = (\eta_x, \eta_y, \eta_z)$  is the rotation axis of unity length and  $\tau = (\tau_x, \tau_y, \tau_z)$  is a vector of the Pauli matrices. The rotation axis is in the  $x$ - $y$ -plane ( $\eta_z = 0$ ) and the resulting charge vector  $\langle \tilde{\mathbf{J}}_i \rangle$  is parallel to the  $z$ -axis. Since by definition the off-diagonal

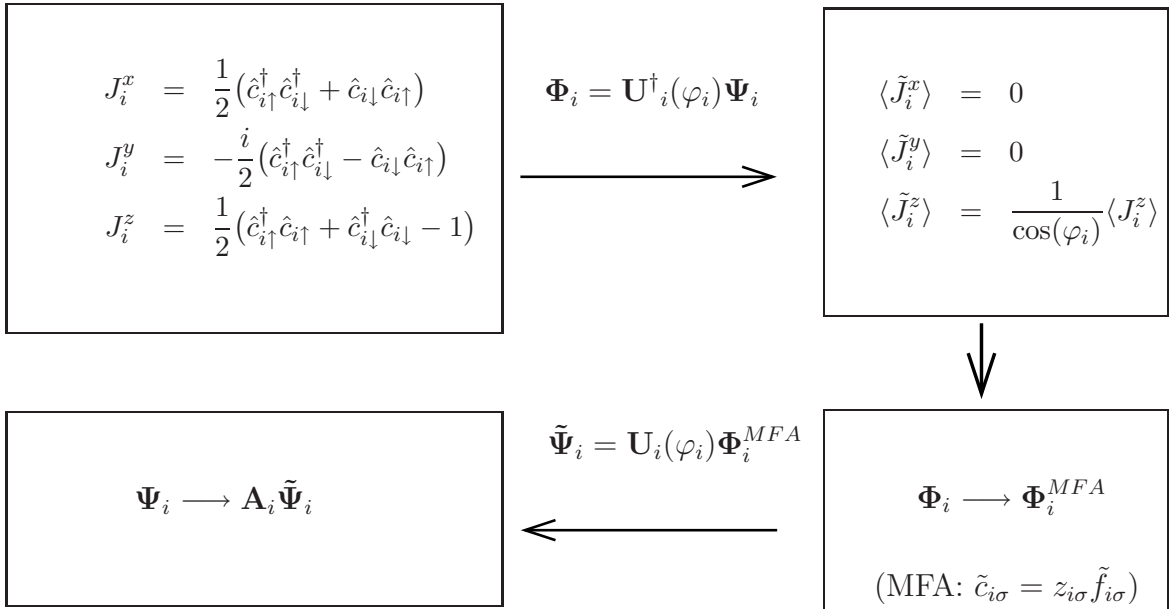


Figure 3.2: Schematic summary of the charge rotational invariant derivation of the Gutzwiller approximation using the slave bosons and the mean field approximation (MFA).

order vanishes in the rotated frame we now come to the second step where we apply the KR slave boson scheme to the associated fermions  $\tilde{f}_{i\sigma}$ :

$$\tilde{c}_{i\sigma} = z_{i\sigma} \tilde{f}_{i\sigma} \quad \text{and} \quad \tilde{c}_{i\sigma}^\dagger = z_{i\sigma}^\dagger \tilde{f}_{i\sigma}^\dagger, \quad (3.11)$$

where the tilde refers to the rotated frame. The renormalization factors read:

$$z_{i\sigma} = \frac{1}{\sqrt{\hat{e}_i^\dagger \hat{e}_i + \hat{p}_{i-\sigma}^\dagger \hat{p}_{i-\sigma}}} (\hat{e}_i^\dagger \hat{p}_{i\sigma} + \hat{p}_{i-\sigma}^\dagger \hat{d}_i) \frac{1}{\sqrt{\hat{d}_i^\dagger \hat{d}_i + \hat{p}_{i\sigma}^\dagger \hat{p}_{i\sigma}}}. \quad (3.12)$$

The boson operators refer to the empty ( $\hat{e}_i$ ), double ( $\hat{d}_i$ ) and single ( $\hat{p}_{i-\sigma}$ ) occupied lattice sites ( $i$ ) and obey the following constraints:

$$\begin{aligned} \sum_{\sigma} \hat{p}_{i\sigma}^\dagger \hat{p}_{i\sigma} + 2\hat{d}_i^\dagger \hat{d}_i &= 2\tilde{J}_i^z + 1 \\ \hat{p}_{i\uparrow}^\dagger \hat{p}_{i\uparrow} - \hat{p}_{i\downarrow}^\dagger \hat{p}_{i\downarrow} &= 2\tilde{S}_i^z \\ \hat{e}_i^\dagger \hat{e}_i + \sum_{\sigma} \hat{p}_{i\sigma}^\dagger \hat{p}_{i\sigma} + \hat{d}_i^\dagger \hat{d}_i &= 1 \end{aligned} \quad (3.13)$$

where we defined  $\tilde{S}_i^z = \frac{1}{2}(\Psi_i^\dagger \mathbf{1} \Psi_i - 1)$ . Since we follow essentially a Gutzwiller-type approach we now apply the mean field approximation (MFA) for the bosons. The Bose operators are replaced by their classical values which can be taken to be real. With the help of the equations (3.13) we are able to eliminate all bosons except of  $d_i^2$ . In the third step the system is transformed back to the original frame. All steps are summarized in Fig. (3.2).

We end up with the charge-rotational invariant GA energy functional:

$$E^{GA} = \sum_{i,j} t_{ij} \langle \Psi_i^\dagger \mathbf{A}_i \tau_z \mathbf{A}_j \Psi_j \rangle + U \sum_i \left[ D_i - J_i^z \left( \sqrt{1 + \tan^2(\varphi_i)} - 1 \right) \right]. \quad (3.14)$$

The four operator product in the potential term in (2.5) is now replaced by an expression depending on the normal charge  $J_i^z$ , the rotation angles  $\varphi_i$  and the parameter  $D_i = d_i^2$ . The functional depends on the normal and anomalous parts of the density matrix. The complete transformation matrix in Eq. (3.14) reads as:

$$\mathbf{A}_i = \begin{pmatrix} z_{i\uparrow} \cos^2 \frac{\varphi_i}{2} + z_{i\downarrow} \sin^2 \frac{\varphi_i}{2} & \frac{(J_i^x - iJ_i^y)}{2J_i^z} [z_{i\uparrow} - z_{i\downarrow}] \cos \varphi_i \\ \frac{(J_i^x + iJ_i^y)}{2J_i^z} [z_{i\uparrow} - z_{i\downarrow}] \cos \varphi_i & z_{i\uparrow} \sin^2 \frac{\varphi_i}{2} + z_{i\downarrow} \cos^2 \frac{\varphi_i}{2} \end{pmatrix}, \quad (3.15)$$

with

$$\tan^2 \varphi_i = \frac{(J_i^x)^2 + (J_i^y)^2}{(J_i^z)^2}, \quad (3.16)$$

where we skipped the  $\langle \dots \rangle$  in Eqs. (3.15) and (3.16). All expectation values refer to the state  $|\Phi_0\rangle$ . The matrix  $\mathbf{A}_i$  includes the local rotation in charge space, the  $z$ -factors for renormalization and the backward transformation to the original frame. It conserves all degrees of freedom in charge space. The off-diagonal elements in (3.15) induce pair hopping processes in the effective functional Eq. (3.14).

The  $z$ -factors depend on the mean field values of the boson fields and renormalize the kinetic energy. The Gutzwiller renormalization factors read explicitly:

$$z_{i\sigma} = \frac{e_i p_{i\sigma} + d_i p_{i-\sigma}}{\sqrt{(e_i^2 + p_{i-\sigma}^2)(d_i^2 + p_{i\sigma}^2)}}, \quad (3.17)$$

where we refer to the mean field values before the backward rotation is applied.

Because of  $(A^i)_{11}^* = A_{11}^i$ ,  $(A^i)_{22}^* = A_{22}^i$  and  $(A^i)_{12}^* = A_{21}^i$  and  $(\rho_{ij}^{\uparrow\downarrow})^* = \rho_{ji}^{\downarrow\uparrow}$  the kinetic energy term can be summarized as:

$$\begin{aligned} \sum_{ij} t_{ij} \langle \Psi_i^\dagger \mathbf{A}_i \tau_z \mathbf{A}_j \Psi_j \rangle = & \quad (3.18) \\ \sum_{ij} t_{ij} \left[ (A_{11}^i A_{11}^j - A_{12}^i A_{21}^j) \rho_{ij}^{\uparrow\uparrow} + (A_{22}^i A_{22}^j - A_{21}^i A_{12}^j) \rho_{ij}^{\downarrow\downarrow} \right. \\ & \left. + 2\text{Re}\{(A_{11}^i A_{12}^j - A_{12}^i A_{22}^j) \rho_{ij}^{\uparrow\downarrow}\} \right] \end{aligned}$$

The variational functional (3.14) is the basic functional that is used in this work. Later we will discuss the nature of the constraints that restrict (3.14). Moreover we will discuss the energy functional in the framework of the extended Hubbard model.

In the limit of vanishing SC ( $\langle \hat{J}_i^x \rangle = \langle \hat{J}_i^y \rangle = 0$ ) it follows from Eq. (3.16)  $\varphi_i = 0$ . In this case  $\mathbf{A}_i$  is diagonal and only the  $z$ -factors remain in the matrix. One recovers the standard Gutzwiller energy functional (3.4) as derived in [55, 60].

In case of the homogeneous paramagnet ( $n_{i\uparrow} = n_{i\downarrow}$ ) with arbitrary filling we obtain  $z_{i\uparrow} = z_{i\downarrow} = z_0$  and the matrix (3.15) reduces to:

$$\mathbf{A}_i = \begin{pmatrix} z_0 & 0 \\ 0 & z_0 \end{pmatrix}, \quad (3.19)$$

and the energy functional reads:

$$E^{GA} = z_0^2 \sum_{i,j,\sigma} t_{ij} \rho_{ij}^{\sigma\sigma} + U \sum_i \left[ D_i - J_i^z \left( \sqrt{1 + \tan^2(\varphi_i)} - 1 \right) \right]. \quad (3.20)$$

The kinetic energy part does not include explicit transitive pair correlations but those are included via the angle  $\varphi_i$  in the potential term and via the dependency of the  $z$ -factors on the bosons.

### 3.3 Extended Hubbard Model with Local On-Site Attraction

The Hubbard model in its basic version includes the on-site repulsion ( $U > 0$ ) that corresponds to the Coulomb interactions between the electrons in the same orbital. On the other hand one can motivate an analogous model where  $U < 0$  thus describing a local attraction between electrons. Based on the observation that the coherence length in HTSC is rather short this so-called attractive Hubbard model can account for the formation of Cooper pairs on short length scales.

The microscopic mechanism leading to an effective short-range attraction of electrons (holes) can be of various origins. The most obvious one is a strong electron lattice coupling which gives rise to the formation of small polarons. Two polarons attract each other via the induced lattice deformation, and they can form small bipolarons provided that the attraction overcomes the Coulomb repulsion. This mechanism was



initially suggested to study electric, magnetic and optical properties of amorphous materials [71, 72].

Another mechanism for short range attraction can result from a coupling between electrons and quasibosonic excitations of electronic origin such as excitons or plasmons [73–76].

Yet another possibility is a purely electronic mechanism resulting from coupling between electrons and other electronic subsystems in solids or chemical complexes. There can be considered several electronic mechanisms that lead to a non-retarded, static attraction [77–80] and thus cause a strong polarizability of anions.

These mechanisms give rise to an attraction between charge carriers that have to compete with the Coulomb repulsion. If the induced attractive potential partially overcomes the Coulomb repulsion and if the attraction is strong enough, local pair formation can take place. The concept of electron pairing basing on an attractive potential is of interest for several areas in solid state physics. The local attraction could probably provide an explanation for superconductivity of the non-BCS type especially in the field of HTSC [78, 80–83]. The concept of local attraction is also used to describe charge density wave formation in narrow band systems [78, 84, 85].

The theoretical models of local pairing either start with a microscopic derivation of the local attractive interaction or postulate some effective Hamiltonian. In the following we consider the properties of the extended Hubbard model with on-site attraction and inter-site repulsion, which can be described by the following Hamiltonian:

$$\hat{H} = - \sum_{ij\sigma} t_{ij} \hat{c}_{i\sigma}^\dagger \hat{c}_{j\sigma} + U \sum_i \hat{n}_{i\uparrow} \hat{n}_{i\downarrow} + \underbrace{\sum_{\langle ij \rangle} V_{ij} (\hat{n}_{i\uparrow} + \hat{n}_{i\downarrow}) (\hat{n}_{j\uparrow} + \hat{n}_{j\downarrow})}_{\hat{W}}, \quad (3.21)$$

where we have added the term  $\hat{W}$  to the Hamiltonian (2.1). Again  $t_{ij}$  denotes the transfer integral but the parameter  $U$  is now an effective on-site attraction ( $U < 0$ ). The new term  $\hat{W}$  is a sum over the nearest neighbors and includes the inter-site repulsion

$V_{ij} > 0$  acting between two electrons (holes) on adjacent sites.

The model (3.21) can be considered as a general result from a system of narrow-band electrons strongly coupled to a bosonic field, which they polarize and which in turn acts upon the electrons, thereby forming entirely new entities. These new entities are described by the correlated motion of the electrons and their surrounding polarization field and by an induced short range attraction which competes with the Coulomb repulsion. The bosonic modes can be phonons, excitons or acoustic plasmons that we have discussed above.

As discussed earlier for the normal Hubbard model the solution crucially depends on the lattice dimension  $d$  and the number of electrons per site ( $n = \frac{1}{N} \sum_i \langle n_i \rangle$ ,  $n \in [0, 2]$ ). Exact results for the ground state are known for half filling ( $n = 1$ ) in one dimension [86]. For arbitrary filling in one dimension the attractive Hubbard model has been solved with the Bethe ansatz [87–89]. Krivnov and Ovchinnikov have shown [87] that the single-electron excitation spectrum has a gap for arbitrary  $n$ , in contrast to the case of the repulsive Hubbard model ( $U > 0$ ) where such a gap exists only for  $n = 1$  [42]. For dimensions greater than one approximative methods have to be applied for the limits of strong or weak attraction.

In the case of  $d = 2$  the Quantum-Monte-Carlo (QMC) method can be used [90] to derive the phase diagram for the transition from the normal state into one with SC ordering. For  $n = 1$  the results are consistent with a ground state having both SC and CDW long range order at zero transition temperature and a power law decay of the pairing correlations away from half filling at a finite temperature.

Using a slave boson mean field approach the ground state energy for the negative- $U$  Hubbard model can be calculated on a saddle point level for any coupling  $U$  [67, 69]. Several SC characteristics can be calculated for arbitrary filling ( $0 \leq n \leq 2$ ) - so for example the crossover from the BCS type SC to local pair SC with increasing  $|U|$ .

For the first part of the Hamiltonian (3.21) we follow in this work the charge rotation-

ally invariant Gutzwiller approach that we have already discussed in the last section. In order to decouple the inter-site repulsion term  $\hat{W}$  we use the HF approximation. We take the repulsion to be site-independent ( $V_{ij} = V$ ) and so the operator product decomposes as follows:

$$\begin{aligned}
\hat{W} &= V \sum_{\substack{\langle ij \rangle \\ \sigma \sigma'}} \hat{c}_{i\sigma}^\dagger \hat{c}_{i\sigma} \hat{c}_{j\sigma'}^\dagger \hat{c}_{j\sigma'} & (3.22) \\
&\stackrel{\text{HF}}{=} V \sum_{\substack{\langle ij \rangle \\ \sigma \sigma'}} [\hat{c}_{i\sigma}^\dagger \hat{c}_{i\sigma} \langle \hat{c}_{j\sigma'}^\dagger \hat{c}_{j\sigma'} \rangle + \langle \hat{c}_{i\sigma}^\dagger \hat{c}_{i\sigma} \rangle \hat{c}_{j\sigma'}^\dagger \hat{c}_{j\sigma'} - \langle \hat{c}_{i\sigma}^\dagger \hat{c}_{i\sigma} \rangle \langle \hat{c}_{j\sigma'}^\dagger \hat{c}_{j\sigma'} \rangle] \\
&- V \sum_{\substack{\langle ij \rangle \\ \sigma \sigma'}} [\hat{c}_{i\sigma}^\dagger \hat{c}_{j\sigma'} \langle \hat{c}_{j\sigma'}^\dagger \hat{c}_{i\sigma} \rangle + \langle \hat{c}_{i\sigma}^\dagger \hat{c}_{j\sigma'} \rangle \hat{c}_{j\sigma'}^\dagger \hat{c}_{i\sigma} - \langle \hat{c}_{i\sigma}^\dagger \hat{c}_{j\sigma'} \rangle \langle \hat{c}_{j\sigma'}^\dagger \hat{c}_{i\sigma} \rangle] \\
&+ V \sum_{\substack{\langle ij \rangle \\ \sigma \sigma'}} [\hat{c}_{i\sigma}^\dagger \hat{c}_{j\sigma'}^\dagger \langle \hat{c}_{j\sigma'} \hat{c}_{i\sigma} \rangle + \langle \hat{c}_{i\sigma}^\dagger \hat{c}_{j\sigma'}^\dagger \rangle \hat{c}_{j\sigma'} \hat{c}_{i\sigma} - \langle \hat{c}_{i\sigma}^\dagger \hat{c}_{j\sigma'}^\dagger \rangle \langle \hat{c}_{j\sigma'} \hat{c}_{i\sigma} \rangle].
\end{aligned}$$

Now we neglect terms that include spin flips and after rearrangement of the terms we make use of the anti-commutator relations. We add the expectation value of the decoupled interaction term to the variational functional (3.14). Finally we obtain the extended version of the Gutzwiller variational energy functional:

$$\begin{aligned}
\hat{E}^{GA} &= \sum_{i \neq j} t_{ij} \langle \hat{\Psi}_i^\dagger \mathbf{A}_i \tau^z \mathbf{A}_j \hat{\Psi}_j \rangle + U \sum_i \left[ D_i - J_i^z (\sqrt{1 + \tan^2 \varphi_i} - 1) \right] & (3.23) \\
&+ V \sum_{\langle ij \rangle} \left[ n_i n_j + \sum_{\sigma} (\langle \hat{c}_{i\sigma}^\dagger \hat{c}_{j-\sigma}^\dagger \rangle \langle \hat{c}_{j-\sigma} \hat{c}_{i\sigma} \rangle - \langle \hat{c}_{i\sigma}^\dagger \hat{c}_{j\sigma} \rangle \langle \hat{c}_{j\sigma}^\dagger \hat{c}_{i\sigma} \rangle) \right],
\end{aligned}$$

which has to be minimized with respect to  $D_i$  and  $\rho$  to derive the saddle point solution.

### 3.4 Unified Slave Boson Representation

The charge rotationally invariant energy functional (3.14) allows the calculation of the GA ground state energy on a saddle point level where all degrees of freedom in charge space are conserved. The slave boson formulation ensures by the implementation of

the constraints (3.13) the solutions to be kept in the physical part of the Hilbert space. The charge rotationally invariant functional (3.14) includes the angle  $\varphi_i$  as variational parameter. The numerical implementation of this formulation including derivatives with respect to  $\varphi_i$  turned out to be too slow in the process of convergence. These problems can be avoided by a reformulation of the functional (3.14). Therefore we consider the GA variational functional in the framework of a unified slave boson representation [56,69] conserving all charge and spin degrees of freedom. The emphasis in the following is on a detailed derivation and discussion of the formal aspects and on the reformulation of the Lagrangian constraints .

We follow the method presented in [56] that is also based on the idea of a complete mapping of the electron operator representation onto slave bosons as discussed above. A lattice site  $i$  can either be empty, doubly- or  $\sigma$ -occupied. Each possible state is connected to an auxiliary slave boson.

The state at the site  $i$  is described by a product of fermionic and bosonic wave function. In order to conserve the two degrees of freedom associated with the quantization axis, the operator product is interpreted as a composite particle whose spin should be  $1/2$ . The subsequent derivation is based on the rules for combining quantum mechanical angular momenta.

We define the two (doublet) vectors representing the four possible states a lattice site can take:

$$\hat{\mathbf{f}}_i^\dagger = \begin{pmatrix} \hat{f}_{i\uparrow}^\dagger \\ \hat{f}_{i\downarrow}^\dagger \end{pmatrix} \quad \text{and} \quad \hat{\Phi}_i^\dagger = \begin{pmatrix} \hat{f}_{i\uparrow}^\dagger \hat{f}_{i\downarrow}^\dagger \\ 1 \end{pmatrix}.$$

The pseudo fermion vector  $\hat{\mathbf{f}}_i$  represents the single occupied state that makes up a spin doublet with  $S = \pm\frac{1}{2}$ . In view of the definition of the vector  $\hat{\Phi}_i$  we introduce the pseudo spin vector  $\hat{\mathbf{J}}_i$  (3.7) with  $J_i^z = \pm\frac{1}{2}$ . The vector  $\hat{\Phi}_i$  takes the form of a pseudo-spin-doublet with respect to  $\hat{\mathbf{J}}_i$ . A doubly occupied state leads to  $J_i^z = \frac{1}{2}$  and an empty state has the eigenvalue  $J_i^z = -\frac{1}{2}$ .

For each lattice site we introduce a set of auxiliary bosons that couple to the vector  $\hat{\mathbf{f}}_i$  for single occupied and to  $\hat{\Phi}_i$  for empty or doubly occupied sites.

A single occupied site denoted as  $|\sigma\rangle$  is expressed as a coupled state of Bose operators  $\hat{p}_{\sigma\sigma'}^\dagger$  and the Fermi operators  $f_\sigma$ :

$$|\sigma\rangle = \sum_{\sigma'} p_{\sigma\sigma'}^\dagger f_{\sigma'}^\dagger |\text{vac}\rangle, \quad (3.24)$$

where we dropped the site index  $i$  for simplicity. The coupled state  $|\sigma\rangle$  should have spin 1/2. Since the spin of the pseudo fermion field ( $f$ ) is 1/2 as well, possible spin values for the  $p$ -bosons are  $J_B = 0$  or  $J_B = 1$ .

For the doubly occupied and empty states ( $|2\rangle$  and  $|0\rangle$ ) we introduce the boson field  $\hat{b}_{\rho\rho'}^\dagger$ :

$$|\rho\rangle = \sum_{\rho'} \hat{b}_{\rho\rho'}^\dagger \hat{\Phi}_{\rho'}^\dagger |\text{vac}\rangle. \quad (3.25)$$

The resulting state must have a pseudo spin of either 0 for empty or 1 for doubly occupied sites. Note that the atomic states  $|\sigma\rangle$ ,  $|0\rangle$  and  $|1\rangle$  are also eigenstates of  $\hat{\mathbf{J}}_i^2$  and  $\hat{J}_i^z$ .

In order to keep all degrees of freedom we have to apply consequently the quantum mechanical rules of combining states with different angular momenta. The total pseudo spin of the fermion wave function in (3.24) and (3.25) is well defined. Therefore we have to include a scalar boson with total pseudo spin  $\mathbf{J}_B = 0$  and a boson field with total pseudo spin  $\mathbf{J}_B = 1$ . For spin and pseudo spin doublets we summarize the operators in the matrices:

$$\hat{\mathbf{P}}_{\sigma\sigma'}^\dagger = \frac{1}{\sqrt{2}} \begin{pmatrix} \hat{p}^{\dagger 0} + \hat{p}^{z\dagger} & (\hat{p}^{x\dagger} - i\hat{p}^{y\dagger}) \\ (\hat{p}^{x\dagger} + i\hat{p}^{y\dagger}) & \hat{p}^{\dagger 0} - \hat{p}^{z\dagger} \end{pmatrix}, \quad \hat{\mathbf{b}}_{\rho\rho'}^\dagger = \frac{1}{\sqrt{2}} \begin{pmatrix} \hat{b}^{\dagger 0} + \hat{b}^{z\dagger} & (\hat{b}^{x\dagger} - i\hat{b}^{y\dagger}) \\ (\hat{b}^{x\dagger} + i\hat{b}^{y\dagger}) & \hat{b}^{\dagger 0} - \hat{b}^{z\dagger} \end{pmatrix}, \quad (3.26)$$

where we defined the scalar fields  $\hat{p}_0^\dagger$  and  $\hat{b}_0^\dagger$  with respect to the pseudo spin  $\mathbf{J}_B = 0$  and the vector field  $\hat{\mathbf{p}}^\dagger = (\hat{p}_x^\dagger, \hat{p}_y^\dagger, \hat{p}_z^\dagger)$  and  $\hat{\mathbf{b}}^\dagger = (\hat{b}_x^\dagger, \hat{b}_y^\dagger, \hat{b}_z^\dagger)$  with respect to the (pseudo)

spin  $\mathbf{J}_B = 1$ . The factor  $1/\sqrt{2}$  is a result from the Clebsch Gordon coefficients and orthonormalization of the states  $|\sigma\rangle$  and  $|\rho\rangle$ . The components of the expressions (3.26) can be expressed by:

$$\hat{p}_{\sigma\sigma'}^\dagger = \frac{1}{2} \sum_{\mu=0}^3 \hat{p}_\mu^\dagger(\tau_\mu)_{\sigma\sigma'} \quad \text{and} \quad \hat{b}_{\rho\rho'}^\dagger = \frac{1}{2} \sum_{\mu=0}^3 \hat{b}_\mu^\dagger(\tau_\mu)_{\rho\rho'}, \quad (3.27)$$

where we used the Pauli matrices and  $\tau_0 = \mathbf{1}$ . The operators  $\hat{p}_{\sigma\sigma'}^\dagger$  and  $\hat{b}_{\rho\rho'}^\dagger$  obey the commutation relations:

$$[\hat{p}_{\sigma_1\sigma_2}, \hat{p}_{\sigma_3\sigma_4}^\dagger] = \frac{1}{2} \delta_{\sigma_1\sigma_4} \delta_{\sigma_2\sigma_3} \quad \text{and} \quad [\hat{b}_{\rho_1\rho_2}, \hat{b}_{\rho_3\rho_4}^\dagger] = \frac{1}{2} \delta_{\rho_1\rho_4} \delta_{\rho_2\rho_3}. \quad (3.28)$$

The electron creation operator is now a linear combination of combined fermion and boson field operators:

$$\hat{c}_{i\sigma}^\dagger = \sum_{\sigma'} (\hat{z}_{i+\sigma,+\sigma'}^\dagger \hat{f}_\sigma^\dagger + \sigma' \hat{z}_{i+\sigma,-\sigma'}^\dagger \hat{f}_{\sigma'}^\dagger), \quad (3.29)$$

where the  $\hat{f}_\sigma^\dagger$  are the fermion ladder operators and the linearly combined boson fields are included in the generalized  $z$ -factors:

$$\hat{z}_{i\rho\sigma\rho'}^\dagger = \hat{p}_{i\sigma'\sigma}^\dagger \tilde{b}_{i\rho'\rho} + \hat{b}_{i\rho'\rho}^\dagger \tilde{p}_{i\sigma'\sigma}, \quad (3.30)$$

where  $\tilde{p}_{i\sigma'\sigma}$  and  $\tilde{b}_{i\sigma'\sigma}$  are the time reversed operators:  $\tilde{p}_0 = \hat{T} \hat{p}_0 \hat{T}^{-1} = \hat{p}_0$  and  $\tilde{\mathbf{p}} = \hat{T} \hat{\mathbf{p}} \hat{T}^{-1} = -\hat{\mathbf{p}}$ .

The operator  $\hat{z}_{i\sigma,\sigma'}^\dagger$  in (3.29) describes the change in the slave boson occupation when an electron is annihilated in a two-channel process. The classical probability for these processes to happen is not simply given by taking the Bose fields in (3.29) by their classical values. This may be corrected by introducing a renormalization. It can be derived from the correct result in the non interacting limit ( $U \rightarrow 0$ ) [55,56,68]. In our case we obtain:

$$\hat{z}_i^\dagger = \hat{\mathbf{p}}_i^\dagger \mathbf{R}_i \mathbf{L}_i \tilde{\mathbf{b}}_i + \hat{\mathbf{b}}_i^\dagger \mathbf{R}_i \mathbf{L}_i \tilde{\mathbf{p}}_i, \quad (3.31)$$

where the factors  $\mathbf{L}_i = (\mathbf{1} - 2\hat{\mathbf{b}}_i^\dagger \hat{\mathbf{b}}_i - 2\hat{\mathbf{p}}_i^\dagger \hat{\mathbf{p}}_i)^{-1/2}$  and  $\mathbf{R}_i = (\mathbf{1} - 2\tilde{\mathbf{b}}_i^\dagger \tilde{\mathbf{b}}_i - 2\tilde{\mathbf{p}}_i^\dagger \tilde{\mathbf{p}}_i)^{-1/2}$  enter Eq. (3.31). The eigenvalues of  $\mathbf{L}_i$  and  $\mathbf{R}_i$  are unity, so that these operators can be added without changing the content. But the presence of  $\mathbf{L}_i$  and  $\mathbf{R}_i$  will make a difference in the framework of approximative methods.

We simplify the notation by re-writing the slave boson matrices (3.26):

$$\hat{\mathbf{B}}_i = \frac{1}{\sqrt{2}} \begin{pmatrix} \hat{D}_i & \hat{b}_{xi} + \hat{b}_{yi} \\ \hat{b}_{xi} - \hat{b}_{yi} & \hat{E}_i \end{pmatrix}, \quad (3.32)$$

with  $\hat{D}_i = \hat{b}^{\dagger 0} + \hat{b}^{z\dagger}$  and  $\hat{E}_i = \hat{b}^{\dagger 0} - \hat{b}^{z\dagger}$  representing the bosons for the doubly occupied and empty lattice sites. We apply the mean field approximation (MFA) by replacing all Bose operators by their thermodynamical expectation values (Bose condensation). The components of the Bose field are treated as variational parameters. We drop the hat in order to refer to mean field values.

In the non rotationally invariant case the  $z$ -axis in the Bose sub-space is taken as quantization axis ( $b_{xi} = 0$  and  $b_{yi} = 0$ ) and the matrix (3.32) is diagonal:

$$\mathbf{B} = \frac{1}{\sqrt{2}} \begin{pmatrix} d_i & 0 \\ 0 & e_i \end{pmatrix}. \quad (3.33)$$

In this case  $d_i$  and  $e_i$  are the scalar boson fields derived by Kotliar and Ruckenstein [55]. In our investigation we focus on the properties that follow from the charge rotationally invariant treatment of the slave boson formalism. We keep the degrees of freedom in charge space but in spin channel we restrict to the non rotational invariant case. For single occupied states we rewrite the spin boson matrix (3.26) in the diagonal form:

$$\mathbf{p}_i = \frac{1}{\sqrt{2}} \begin{pmatrix} p_{i\uparrow} & 0 \\ 0 & p_{i\downarrow} \end{pmatrix}, \quad (3.34)$$

where we have used  $p_0 \pm p_z^\dagger = p_{\uparrow/\downarrow}$ .

This point of view allows a straightforward implementation of the constraints. The well defined mapping of the fermion field to the Bose fields allows to combine the mean field values of the Bose field with the entries of the density matrix.

## Constraints of the Extended Hilbert Space

If we use the commutation relations (3.28) and the canonical (anti) commutation relations for the pseudo fermions  $\mathbf{f}$  and  $\Phi$  the correct anti-commutation relation for the  $\hat{c}$ -operators are recovered, provided the following constraints are satisfied [69]. The completeness condition  $\text{tr}(\hat{\mathbf{p}}_i^\dagger \hat{\mathbf{p}}_i) + \text{tr}(\hat{\mathbf{B}}_i^\dagger \hat{\mathbf{B}}_i) = 1$  leads to:

$$D_i^2 + E_i^2 + 2(b_{xi}^2 + b_{yi}^2) + p_\uparrow^2 + p_\downarrow^2 = 1. \quad (3.35)$$

This relation ensures that each lattice is occupied by exactly one slave boson.

A second set of constraints follows from the fact that the matrix elements of  $\hat{c}_{i\sigma}^\dagger \hat{c}_{j\sigma'}$  are related to those of  $\hat{p}_\sigma^\dagger \hat{p}_\sigma$  and  $\hat{d}_i^\dagger \hat{d}_i$  in the physical subspace. The number of bosons correspond to the number of fermions.

We evaluate the expectation value of the number operator respecting Eq. (3.29):

$$\langle \hat{c}_{i\sigma}^\dagger \hat{c}_{i\sigma} \rangle = p_\sigma^2 + D_i^2 + b_{xi}^2 + b_{yi}^2. \quad (3.36)$$

The left hand side of (3.36) is the density of  $\sigma$ -electrons at the lattice site  $i$ . If an  $\sigma$ -electron is situated at site  $i$  the lattice site can be either single occupied with spin  $\sigma$ , doubly occupied or even occupied by an electron pair. This relation is expressed by the right hand side of (3.36). The operator of a doubly occupied site can be expressed as [69]:

$$\langle \hat{n}_{i\uparrow} \hat{n}_{i\downarrow} \rangle = (D_i^2 + b_{xi}^2 + b_{yi}^2). \quad (3.37)$$

Additionally one finds constraints for the pair creation and annihilation operators:

$$\langle \hat{c}_{i\uparrow}^\dagger \hat{c}_{i\downarrow}^\dagger \rangle = (b_{xi} + ib_{yi})(D_i + E_i) \quad \text{and} \quad \langle \hat{c}_{i\downarrow} \hat{c}_{i\uparrow} \rangle = (b_{xi} - ib_{yi})(D_i + E_i), \quad (3.38)$$



combining the pairing terms with the mean field values of the bosons.

The unitary transformation (3.9) was introduced in order to transform the charge vector locally so that the expectation values of the  $x$ - and  $y$ -component of the charge vector vanish ( $\langle \hat{J}_i^x \rangle = 0$  and  $\langle \hat{J}_i^y \rangle = 0$ ) and the  $z$ -component transforms as  $\langle \tilde{J}_i^z \rangle = \frac{1}{\cos(\varphi_i)} \langle J_i^z \rangle$ . In this case the boson matrix  $\hat{\mathbf{B}}_i$  becomes diagonal in Eq. (3.33) if the boson field is mapped to the normal state. With the help of (3.35) and (3.36) one derives for the expectation values of the components of the pseudo charge vector  $\mathbf{J}_i$  in terms of the mean field values of the bosons:

$$J_i^x = b_{ix}(D_i + E_i), \quad J_i^y = b_{iy}(D_i + E_i), \quad J_i^z = \frac{1}{2}(D_i - E_i)(D_i + E_i). \quad (3.39)$$

In terms of the boson field that was originally introduced by Kotliar and Ruckenstein [55] the  $z$ -component reads:  $J_i^z = \frac{1}{2} \cos(\varphi_i)(d_i - e_i)(d_i + e_i)$ . We derive a set of equations that relates the 'originally' boson fields to the charge-rotational invariant bosons via the local angle  $\varphi_i$ :

$$\begin{aligned} D_i &= d_i \cos^2\left(\frac{\varphi_i}{2}\right) + e_i \sin^2\left(\frac{\varphi_i}{2}\right), & d_i &= \frac{D_i}{1 - \tan^2\left(\frac{\varphi_i}{2}\right)} + \frac{E_i}{1 - \cot^2\left(\frac{\varphi_i}{2}\right)}, \\ E_i &= d_i \sin^2\left(\frac{\varphi_i}{2}\right) + e_i \cos^2\left(\frac{\varphi_i}{2}\right), & e_i &= \frac{E_i}{1 - \tan^2\left(\frac{\varphi_i}{2}\right)} + \frac{D_i}{1 - \cot^2\left(\frac{\varphi_i}{2}\right)}. \end{aligned} \quad (3.40)$$

Given the values for the charge density  $n_{i\uparrow} = \rho_{ii}^{\uparrow\uparrow}$  and  $n_{i\downarrow} = \rho_{ii}^{\downarrow\downarrow}$  and the pair creation and annihilation operators  $J_i^+ = \rho_{ii}^{\uparrow\downarrow}$  and  $J_i^- = \rho_{ii}^{\downarrow\uparrow}$  we can derive the expectation values for boson fields.

We obtain for the  $z$ -component of the charge vector at the lattice site  $i$ :

$$J_i^z = \frac{1}{2}(n_{i\uparrow} + n_{i\downarrow} - 1). \quad (3.41)$$

The angle  $\varphi_i$  of the local rotation in charge space can be obtained using Eq. (3.16). We write down an expression for the double occupancy:

$$\langle \hat{n}_{i\uparrow} \hat{n}_{i\downarrow} \rangle = d_i^2 \cos^2\left(\frac{\varphi_i}{2}\right) + e_i^2 \sin^2\left(\frac{\varphi_i}{2}\right). \quad (3.42)$$

Further we make use of the auxiliary equations:

$$d_i = \sqrt{n_{i\uparrow}n_{i\downarrow} - \left(1 - \frac{1}{\cos(\varphi_i)}\right) J_i^z} \quad \text{and} \quad e_i = \sqrt{n_{i\uparrow}n_{i\downarrow} - \left(1 + \frac{1}{\cos(\varphi_i)}\right) J_i^z}.$$

With the help of Eqs. (3.36), (3.37) and (3.39) we derive:

$$\begin{aligned} b_{ix} &= \frac{(J_i^+ + J_i^-)}{2(D_i + E_i)}, & p_{i\uparrow} &= \sqrt{n_{i\uparrow} - n_{i\uparrow}n_{i\downarrow}}, \\ b_{iy} &= -i \frac{(J_i^+ - J_i^-)}{2(D_i + E_i)}, & p_{i\downarrow} &= \sqrt{n_{i\downarrow} - n_{i\uparrow}n_{i\downarrow}}, \end{aligned} \quad (3.43)$$

where we have respected  $J_i^x = \frac{1}{2}(J_i^+ + J_i^-)$  and  $J_i^y = -\frac{i}{2}(J_i^+ - J_i^-)$ . With Eq. (3.40) we obtain expressions for the expectation values of the six bosons for each lattice site. The generalized and normalized  $z$ -factors in (3.15) can be expressed in terms of the boson fields (3.40):

$$z_{i\uparrow} = \frac{e_i p_{i\uparrow} + d_i p_{i\downarrow}}{\sqrt{(e_i^2 + p_{i\downarrow}^2)(d_i^2 + p_{i\uparrow}^2)}} \quad \text{and} \quad z_{i\downarrow} = \frac{e_i p_{i\downarrow} + d_i p_{i\uparrow}}{\sqrt{(e_i^2 + p_{i\uparrow}^2)(d_i^2 + p_{i\downarrow}^2)}}. \quad (3.44)$$

With this set of equations we can calculate the expectation values of the bosons from the density matrix.

## 3.5 Gutzwiller Energy Functional and Lagrangian Multipliers

Now we can rewrite the Lagrange function in terms of the slave bosons including the constraints. Dropping the inter-site repulsion term that was discussed earlier we obtain:

$$\begin{aligned}
L^{GA} &= \sum_{ij} t_{ij} \langle \Psi_i^\dagger \mathbf{A}_i \tau_z \mathbf{A}_j \Psi_j \rangle + U \sum (D_i^2 + b_{xi}^2 + b_{yi}^2) \\
&+ \mu \sum_{\sigma} \left( \sum_i \rho_{ii}^{\sigma\sigma} - N_{\sigma} \right) \\
&+ \sum_i (\lambda_i^1 R_i^1 + \lambda_i^2 R_i^2 + \lambda_i^3 R_i^3 + \lambda_i^4 R_i^4 + \lambda_i^5 R_i^5)
\end{aligned} \tag{3.45}$$

where the double occupancy is expressed by using identity (3.37). We introduced the chemical potential  $\mu$  to conserve the electron numbers  $N_{\sigma}$ . The MFA matrix reads as:

$$\mathbf{A}_i = \frac{(z_{i\uparrow} + z_{i\downarrow})}{2} \begin{pmatrix} 1 & 0 \\ 0 & 1 \end{pmatrix} + \frac{(z_{i\uparrow} - z_{i\downarrow})}{2\beta_i} \begin{pmatrix} (D_i - E_i) & 2(b_{xi} - ib_{yi}) \\ 2(b_{xi} + ib_{yi}) & (E_i - D_i) \end{pmatrix}, \tag{3.46}$$

where  $\beta_i = \sqrt{(D_i - E_i)^2 + 4(b_{ix}^2 + b_{iy}^2)}$ . The local rotation angle  $\varphi_i$  is replaced by mean field values of the slave bosons. The MFA values are the variational parameters in this formulation.

The last terms in (3.45) include the sum of the bosonic constraints with the Lagrangian multipliers  $\lambda_i^{(j)}$  that read explicitly:

$$R_i^1 = \left( 2b_{xi}(D_i + E_i) - (\rho_{ii}^{\uparrow\downarrow} + \rho_{ii}^{\downarrow\uparrow}) \right), \tag{3.47}$$

$$R_i^2 = \left( 2b_{yi}(D_i + E_i) + i(\rho_{ii}^{\uparrow\downarrow} - \rho_{ii}^{\downarrow\uparrow}) \right), \tag{3.48}$$

$$R_i^3 = (D_i^2 + E_i^2 + 2(b_{ix}^2 + b_{iy}^2) + p_{i\uparrow}^2 + p_{i\downarrow}^2 - 1), \tag{3.49}$$

$$R_i^4 = (D_i^2 + (b_{ix}^2 + b_{iy}^2) + p_{i\uparrow}^2 - \rho_{ii}^{\uparrow\uparrow}), \tag{3.50}$$

$$R_i^5 = (D_i^2 + (b_{ix}^2 + b_{iy}^2) + p_{i\downarrow}^2 - \rho_{ii}^{\downarrow\downarrow}). \quad (3.51)$$

The constraints help to keep the solution in the physical part of the Hilbert space. Eq. (3.49) is the completeness condition where Eq. (3.47), Eq. (3.48), Eq. (3.50) and Eq. (3.51) guarantee the charge and spin conservation and the Pauli exclusion principle. We have to minimize (3.45) under the Slater condition ( $\rho = \rho^2$ ). From the saddle point condition we obtain a set of equations to derive the Lagrangian multipliers:

$$\frac{\partial E^{GA}}{\partial D_i} = 0, \quad \frac{\partial E^{GA}}{\partial E_i} = 0, \quad \frac{\partial E^{GA}}{\partial b_{ix}} = 0, \quad \frac{\partial E^{GA}}{\partial b_{iy}} = 0, \quad (3.52)$$

$$\frac{\partial E^{GA}}{\partial p_{i\uparrow}} = 0, \quad \frac{\partial E^{GA}}{\partial p_{i\downarrow}} = 0, \quad (3.53)$$

which yields the matrix equation:

$$\begin{pmatrix} 2b_{xi} & 2b_{yi} & 2D_i & 2D_i & 2D_i \\ 2b_{xi} & 2b_{yi} & 2E_i & 0 & 0 \\ 2(D_i + E_i) & 0 & 4b_{xi} & 2b_{xi} & 2b_{xi} \\ 0 & 2(D_i + E_i) & 4b_{yi} & 2b_{yi} & 2b_{yi} \\ 0 & 0 & 2p_{i\sigma} & 2p_{i\sigma} & 0 \end{pmatrix} \lambda_i = \begin{pmatrix} \partial_{D_i} T + U D_i \\ \partial_{E_i} T \\ \partial_{b_{xi}} T + 2U b_{xi} \\ \partial_{b_{yi}} T + 2U b_{yi} \\ \partial_{p_{i\sigma}} T \end{pmatrix}, \quad (3.54)$$

where we define the Lagrange parameter vector  $\lambda_i = (\lambda_i^1, \lambda_i^2, \lambda_i^3, \lambda_i^4, \lambda_i^5)$ . The expressions for the derivatives on the right hand side can be found in the appendix B.5.

## 3.6 Numerical Method

For the numerical calculation we combine the GA energy functional and the constraints from the unified slave boson study in one function. We present results for two dimensional square lattices of rectangular shape shown in Fig. (3.6). The cluster consists of  $N = N_x \times N_y$  lattice sites with the coordinates  $(i_x, i_y)$ . We refer to the lattice using the integer  $i$  counting the lattice sites line by line.

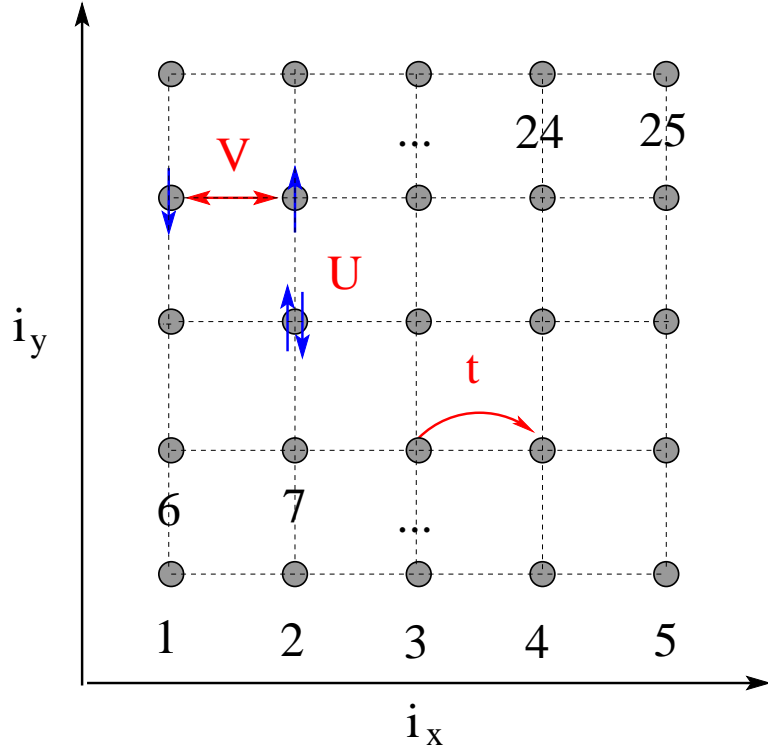


Figure 3.3: Lattice geometry for a 5x5 cluster.

We start with an orthogonal decomposition of the entries of the density matrix element

$\rho_{ij}^{\sigma\sigma'}$ :

$$\rho_{lm}^{\uparrow\uparrow} = \langle \hat{c}_{l\uparrow}^\dagger \hat{c}_{m\uparrow} \rangle = \sum_{k=1}^N X_l^{\alpha*}(k) X_m^\alpha(k) = \sum_{p=1}^N \phi_l^*(p) \phi_m(p) \quad (3.55)$$

$$\rho_{lm}^{\uparrow\downarrow} = \langle \hat{c}_{l\uparrow}^\dagger \hat{c}_{m\downarrow} \rangle = \sum_{k=1}^N X_l^{\alpha*}(k) Y_m^\alpha(k) = \sum_{p=1}^N \phi_l^*(p) \phi_{(m+N)}(p)$$

$$\rho_{lm}^{\downarrow\uparrow} = \langle \hat{c}_{l\downarrow} \hat{c}_{m\uparrow} \rangle = \sum_{k=1}^N Y_l^{\alpha*}(k) X_m^\alpha(k) = \sum_{p=1}^N \phi_{(l+N)}^*(p) \phi_m(p)$$

$$\rho_{lm}^{\downarrow\downarrow} = \langle \hat{c}_{l\downarrow} \hat{c}_{m\downarrow} \rangle = \sum_{k=1}^N X_l^\beta(k) X_m^{\beta*}(k) = \sum_{p=1}^N \phi_{(l+N)}(p+N) \phi_{m+N}^*(p+N),$$

The amplitudes in (3.55) are denoted as  $\phi_i(k)$  making up the set of variational parameters. We summarize the amplitudes of the diagonal representation as follows:

$$\mathbf{T} = \begin{pmatrix} X^\alpha & Y^\beta \\ Y^\alpha & X^\beta \end{pmatrix} = \begin{pmatrix} \phi_i(k) & \phi_i(k+N) \\ \phi_{(i+N)}(k) & \phi_{(i+N)}(k+N) \end{pmatrix}_{i,k=1,\dots,N}, \quad (3.56)$$

where  $\mathbf{T} \in \text{Mat}(2N \times 2N)$ . The amplitudes are complex and can be decomposed into real and imaginary part:

$$\phi_i(k) = \{x_i(k) + iy_i(k)\}, \quad (3.57)$$

where here the indices  $i$  and  $k$  run from 1 to  $2N$ . We collect the variational parameters in the real vector  $\mathbf{x}$ . It contains the entries of the matrix  $\mathbf{T}$  (3.56) column by column. The real and the imaginary part of the entries of the matrix in (3.56) build up a  $8N^2$  set of the components of  $\mathbf{x}$  with the  $4N^2$  real parts in the first section of  $\mathbf{x}$  and the  $4N^2$  imaginary parts in the second section.

The next subset of variational parameters collected in  $\mathbf{x}$  consists of the expectation values of the 6 boson fields ( $D_i, E_i, b_{xi}, b_{yi}, p_{i\uparrow}, p_{i\downarrow}$ ) of the dimension  $N$  for each boson. The vector  $\mathbf{x}$  is of dimension  $D = 8N^2 + 6N$  ( $\mathbf{x} \in \mathbb{R}^D$ ) and can be summarized as follows:

$$\mathbf{x} = \left( x_1(k)|_k \dots x_{2N}(k)|_k, y_1(k)|_k, \dots, y_{2N}(k)|_k, \{D_i, E_i, p_{i\uparrow}, p_{i\downarrow}, b_{xi}, b_{yi}\}_i \right), \quad (3.58)$$

where  $k$  runs over  $1 \dots 2N$  and the index  $i$  runs over the lattice sites  $\{1 \dots N\}$ . Now the energy functional ( $E := E(\mathbf{x})$ ) and the saddle point problem can be summarized symbolically:

$$E : \mathbb{R}^D \mapsto \mathbb{C}, \quad \text{Re}(E(\mathbf{x})) = \min!. \quad (3.59)$$

For the numerical calculation we add all Lagrangian constraints quadratically to the variational energy functional. This ensures that the function is minimized by force. We introduce the numerical parameters  $\Lambda_1, \dots, \Lambda_8$  that are large, positive numbers to

ensure that the constraints are fulfilled. Note that the numerical parameters  $\Lambda_i$  are not identical with the Lagrangian multipliers  $\lambda_i$ !

The final function reads:

$$\begin{aligned}
E = & \sum_{ij} t_{ij} \left[ (A_{11}^i A_{11}^j - A_{12}^i A_{21}^j) \rho_{ij}^{\uparrow\uparrow} + (A_{11}^i A_{12}^j - A_{12}^i A_{22}^j) \rho_{ij}^{\uparrow\downarrow} \right. \\
& \left. + (A_{21}^i A_{11}^j - A_{22}^i A_{21}^j) \rho_{ij}^{\downarrow\uparrow} + (A_{22}^i A_{22}^j - A_{21}^i A_{12}^j) \rho_{ij}^{\downarrow\downarrow} \right] \\
& + U \sum_i (D_i^2 + b_{xi}^2 + b_{yi}^2) \\
& + V \sum_{\langle ij \rangle} (\rho_{ii}^{\uparrow\uparrow} + \rho_{ii}^{\downarrow\downarrow}) (\rho_{jj}^{\uparrow\uparrow} + \rho_{jj}^{\downarrow\downarrow}) \\
& + V \sum_{\langle ij \rangle} \left[ (\rho_{ij}^{\uparrow\downarrow} \rho_{ji}^{\downarrow\uparrow} + \rho_{ij}^{\downarrow\uparrow} \rho_{ji}^{\uparrow\downarrow}) - (\rho_{ij}^{\uparrow\uparrow} \rho_{ji}^{\uparrow\uparrow} + \rho_{ij}^{\downarrow\downarrow} \rho_{ji}^{\downarrow\downarrow}) \right] \\
& + \sum_{j=1}^5 \Lambda_j \left( \sum_{i=1}^N (R_i^j)^2 \right) \\
& + \Lambda_6 \sum_{kq} \left( \sum_i \phi_i^*(k) \phi_i(q) - \delta_{kq} \right) \times \left( \sum_j \phi_j(k) \phi_j^*(q) - \delta_{kq} \right) \\
& + \Lambda_7 \left( \sum_i \rho_{ii}^{\uparrow\uparrow} - N_{\uparrow} \right)^2 + \Lambda_8 \left( \sum_i \rho_{ii}^{\downarrow\downarrow} - N_{\downarrow} \right)^2 .
\end{aligned} \tag{3.60}$$

where we have already included the inter-site interaction term. The parameter  $\Lambda_6$  ensures the orthogonality of the transformation matrix  $\phi_i(k)$  whereas  $\Lambda_7$  and  $\Lambda_8$  keep the particle numbers constant. Finally  $\Lambda_i$  ( $i = 1, \dots, 5$ ) couple the bosonic constraints to the function.

In order to find the saddle point solution of Eq. (3.60) with (3.59) we use an algorithm for minimization of unconstrained multivariate functions that was published and discussed in [91] and [92]. The algorithm minimizes an unconstrained nonlinear scalar valued function of a vector variable  $\mathbf{x}$  either by the Broyden-Fletcher-Goldfarb-Shanno (BFGS) variable metric algorithm or by a real conjugate gradient algorithm.

The method requires the knowledge of the gradient of the energy functional:  $\mathbf{G} =$

$(\frac{\partial E}{\partial x_l})_{l=1\dots D}$ . We calculate the derivatives with respect to the amplitudes  $i \in \{1 \dots 4N^2\}$  where we use the notation:

$$\frac{\partial E}{\partial x_i} = \sum_{lm,\sigma\sigma'} \frac{\partial E}{\partial \rho_{lm}^{\sigma\sigma'}} \sum_p \left( \frac{\partial \rho_{lm}^{\sigma\sigma'}}{\partial \phi_l^*(p)} \frac{\partial \phi_l^*(p)}{\partial x_i} + \frac{\partial \rho_{lm}^{\sigma\sigma'}}{\partial \phi_m(p)} \frac{\partial \phi_m(p)}{\partial x_i} \right). \quad (3.61)$$

The explicit expressions are given in the appendix B.5.

We start our calculation with an initialization of the density matrix. The distribution is defined by the density matrix  $\rho_{ii}^{\sigma\sigma}$  where the indices  $i$  and  $\sigma$  refer to the spatial position and to the electron spin. As a first step we need an orthogonal decomposition (3.56). For this reason we apply the HF diagonalization via the transformation (2.13) to obtain the initial set of amplitudes (3.57).

### 3.7 Characterization of the Solution

In our formulation we obtain possible solutions by minimizing the functional (3.60) with respect to all the constraints. The numerical output is the density matrix  $\rho_{ij}^{\sigma\sigma'}$  and the set of boson fields.

We classify the results into homogeneous and inhomogeneous solutions which either can be in the normal or in the superconducting state. In order to characterize the solution we calculate the on-site electron density and the expectation values of the charge vector. In the case of inhomogeneous solutions we derive an expression for the current density that can be separated into a normal current and a super current resulting from pair correlations.

The three components of  $\mathbf{J}_i$  are the expectation values of the local charge and superconducting order parameter for each lattice site.

$$J_i^x = \frac{1}{2} (\rho_{ii}^{\uparrow\downarrow} + \rho_{ii}^{\downarrow\uparrow}), \quad J_i^y = -\frac{i}{2} (\rho_{ii}^{\uparrow\downarrow} - \rho_{ii}^{\downarrow\uparrow}), \quad J_i^z = \frac{1}{2} (\rho_{ii}^{\uparrow\uparrow} + \rho_{ii}^{\downarrow\downarrow} - 1). \quad (3.62)$$

The charge state of each lattice site is represented by the three degrees of freedom of  $\mathbf{J}_i$ . The components are real where the  $z$ -component reflects the local charge density.



$J_i^x$  and  $J_i^y$  are the real and imaginary part of the expectation values of the local pair creation and annihilation. The length of the  $x$ - $y$ -projection (Fig. 3.1) can be taken as a local order parameter for the superconducting channel.

If one considers a homogeneous, half-filled superconductor with complex order parameter  $\Delta^{SC}$  it holds  $J_i^z = 0$  and  $J_i^x = \text{Re}(\Delta^{SC})$  and  $J_i^y = \text{Im}(\Delta^{SC})$ . Applying the attractive-repulsive transformation (see appendix Eq. (C.8)) the charge vector is transformed to the spin vector and one finds  $S_i^z = J_i^z$ ,  $S_i^x = (-1)^{i_x+i_y} J_i^x$  and  $S_i^y = (-1)^{i_x+i_y} J_i^y$ . Thus a homogeneous half filled superconductor in the attractive Hubbard model maps to an anti-ferromagnet in the repulsive model.

## The Current Density

For inhomogeneous solutions the charge and pair densities vary over the lattice. In order to derive the current density  $\mathbf{j}_i$  we start with the local charge density  $\rho_i$  and apply the continuity equation from classical electrodynamics:  $\nabla \cdot \mathbf{j}_i = -\dot{\rho}_i$ . We obtain the divergence of the local current density field on the left hand side. The time derivative of  $\rho$  follows from the Heisenberg equation of motion as:

$$\partial_t \hat{\rho}_i = i[\hat{H}, \hat{\rho}_i]_-, \quad (\hbar = 1). \quad (3.63)$$

The third component of the charge vector is proportional to the local charge density and we replace for  $\hat{\rho}_i$ :

$$\nabla \hat{\mathbf{j}}_i^z = i[\hat{H}, \hat{J}_i^z]_-. \quad (3.64)$$

We generalize the definition of the current density and we write down the commutators for all three components of the charge vector  $[\hat{H}, \hat{J}_i^\alpha]$  ( $\alpha = x, y, z$ ). We use the effective Hamiltonian  $\hat{H} = \hat{H}^{MFA} + \hat{W}$  and with the explicit expression from Eq. (B.1) and

Eq. (B.2) we obtain for the commutator with  $J_l^x$ :

$$\begin{aligned} \langle [\hat{H}, J_l^x] \rangle &= i\text{Im} \sum_{i \neq l} t_{il} \left\{ (A_{11}^i A_{11}^l - A_{12}^i A_{21}^l) \rho_{il}^{\uparrow\downarrow} + (A_{11}^i A_{12}^l - A_{12}^i A_{22}^l) \rho_{il}^{\uparrow\uparrow} \right. \\ &\quad - (A_{21}^i A_{11}^l - A_{22}^i A_{21}^l) \rho_{li}^{\downarrow\downarrow} + (A_{22}^i A_{22}^l - A_{21}^i A_{12}^l) \rho_{li}^{\uparrow\downarrow} \left. \right\} \\ &\quad + V [4n_i \rho_{il}^{\uparrow\downarrow} - (\rho_{li}^{\uparrow\uparrow} + \rho_{il}^{\downarrow\downarrow}) \rho_{il}^{\uparrow\downarrow} - (\rho_{il}^{\uparrow\uparrow} + \rho_{li}^{\downarrow\downarrow}) \rho_{li}^{\uparrow\downarrow}], \end{aligned} \quad (3.65)$$

the commutator with  $J^y$ :

$$\begin{aligned} \langle [\hat{H}, J_l^y] \rangle &= -i\text{Re} \sum_{i \neq l} t_{il} \left\{ (A_{11}^i A_{11}^l - A_{12}^i A_{21}^l) \rho_{il}^{\uparrow\downarrow} - (A_{11}^i A_{12}^l - A_{12}^i A_{22}^l) \rho_{il}^{\uparrow\uparrow} \right. \\ &\quad - (A_{21}^i A_{11}^l - A_{22}^i A_{21}^l) \rho_{li}^{\downarrow\downarrow} + (A_{22}^i A_{22}^l - A_{21}^i A_{12}^l) \rho_{li}^{\uparrow\downarrow} \left. \right\} \\ &\quad + V [4n_i \rho_{il}^{\uparrow\downarrow} - (\rho_{li}^{\uparrow\uparrow} + \rho_{il}^{\downarrow\downarrow}) \rho_{il}^{\uparrow\downarrow} - (\rho_{il}^{\uparrow\uparrow} + \rho_{li}^{\downarrow\downarrow}) \rho_{li}^{\uparrow\downarrow}], \end{aligned} \quad (3.66)$$

and finally the commutator with  $J^z$ :

$$\begin{aligned} \langle [\hat{H}, J_l^z] \rangle &= i\text{Im} \sum_{i \neq l} t_{il} \left\{ A_{11}^i A_{11}^l - A_{12}^i A_{21}^l \right\} \rho_{il}^{\uparrow\uparrow} - (A_{11}^i A_{12}^l - A_{12}^i A_{22}^l) \rho_{il}^{\uparrow\downarrow} \\ &\quad - (A_{11}^l A_{12}^i - A_{12}^l A_{22}^i) \rho_{li}^{\uparrow\downarrow} + (A_{22}^i A_{22}^l - A_{21}^i A_{12}^l) \rho_{il}^{\downarrow\downarrow} \left. \right\} \\ &\quad + V (\rho_{li}^{\uparrow\downarrow} \rho_{il}^{\downarrow\uparrow} + \rho_{il}^{\downarrow\uparrow} \rho_{li}^{\uparrow\downarrow}). \end{aligned} \quad (3.67)$$

The  $x$ - and  $y$ -part describe the pair current where the  $z$ -channel is the current density with respect to the normal charge carriers. In a two dimensional discrete lattice we approximate the divergence at the lattice site  $i$  as:

$$\nabla \mathbf{j}_i = (j_{i_x+1, i_y}^z - j_{i_x-1, i_y}^z) + (j_{i_x, i_y+1}^z - j_{i_x, i_y-1}^z), \quad (3.68)$$

where we have written the lattice site index  $i = (i_x, i_y)$  in Cartesian coordinates.

In the case of the commutator (3.67) we obtain for the normal current:

$$\begin{aligned}
\mathbf{j}_l^{(z)} = & i\text{Im} \sum_{i_x \neq l_x} \sum_{i_y} \left( t_{il} \left\{ A_{11}^i A_{11}^l - A_{12}^i A_{21}^l \right\} \rho_{il}^{\uparrow\uparrow} - (A_{11}^i A_{12}^l - A_{12}^i A_{22}^l) \rho_{il}^{\uparrow\downarrow} \right. \\
& - (A_{11}^l A_{12}^i - A_{12}^l A_{22}^i) \rho_{li}^{\uparrow\downarrow} + (A_{22}^i A_{22}^l - A_{21}^i A_{12}^l) \rho_{il}^{\downarrow\downarrow} \left. \right\} \\
& + V(\rho_{li}^{\uparrow\downarrow} \rho_{il}^{\downarrow\uparrow} + \rho_{il}^{\uparrow\downarrow} \rho_{li}^{\downarrow\uparrow}) \mathbf{e}_x \\
& + i\text{Im} \sum_{i_x} \sum_{i_y \neq l_y} \left( t_{il} \left\{ A_{11}^i A_{11}^l - A_{12}^i A_{21}^l \right\} \rho_{il}^{\uparrow\uparrow} - (A_{11}^i A_{12}^l - A_{12}^i A_{22}^l) \rho_{il}^{\uparrow\downarrow} \right. \\
& - (A_{11}^l A_{12}^i - A_{12}^l A_{22}^i) \rho_{li}^{\uparrow\downarrow} + (A_{22}^i A_{22}^l - A_{21}^i A_{12}^l) \rho_{il}^{\downarrow\downarrow} \left. \right\} \\
& + V(\rho_{li}^{\uparrow\downarrow} \rho_{il}^{\downarrow\uparrow} + \rho_{il}^{\uparrow\downarrow} \rho_{li}^{\downarrow\uparrow}) \mathbf{e}_y, \tag{3.69}
\end{aligned}$$

where  $\mathbf{e}_x$  and  $\mathbf{e}_y$  denote the Cartesian unity vectors.



# Chapter 4

## Homogeneous SC and CDW Solutions

In this chapter we apply the GA approach to charge and pair ordered solutions and compare the results with homogeneous SC results.

In the first section we discuss the stability of a homogeneous solution in infinite dimensions at half filling. We investigate the instability of the normal GA state towards superconductivity.

As the next step we show results for homogeneous SC and CDW states in finite systems. We compare the GA solutions qualitatively and quantitatively with the Hartree-Fock approximation of the Hubbard model.

Further we present a formulation of an effective GA-BCS Hamiltonian. With the help of the mean field values of the boson field we reformulate an effective one particle Hamiltonian. We present a Bardeen-Cooper-Schrieffer-like discussion and calculate the density of states for a homogeneous superconductor.

In the last part of this chapter we go a step beyond and we extend our discussion to non local pair correlation effects. Although this work is mainly based on the investigation

of s-wave SC, we apply the formalism to d-wave superconductivity in the *repulsive* Hubbard model ( $U > 0$ ).

## 4.1 Stability Analysis in Infinite Dimensions

The instability of a normal system towards SC order reflects in a divergent pair susceptibility. In order to approach the SC state from this point of view we apply the time dependent Gutzwiller approximation (TDGA) that was used earlier to calculate magnetic excitations in the repulsive Hubbard model [93–95]. We use this method to investigate the stability of a homogeneous paramagnetic saddle point solution obtained in the GA in the pair channel. We analyze our result in view to the phase transition from the normal to the superconducting phase.

Firstly we assume that an external field is applied. This external perturbation of the ground state causes a change in the free energy of the system:  $F = F_0 + \delta F$ . We denote  $F_0$  as the free energy of the GA ground state. The response to an external field induces small fluctuations of the generalized density matrix  $\rho = \rho_0 + \delta\rho$  and the double occupancy  $D = D_0 + \delta D$  where  $\rho_0$  and  $D_0$  refer to the saddle point solution of (3.14). We rewrite the standard GA functional (3.14) in the free energy formulation:

$$\begin{aligned}
 F^{GA} &= \sum_{i,j} t_{ij} \langle \Psi_i^+ \mathbf{A}_i \tau^z \mathbf{A}_j \Psi_j \rangle + U \sum_i \left[ D_i - J_i^z \sqrt{1 + \tan^2(\varphi_i)} \right] \\
 &- \mu \left( \sum_{i\sigma} \rho_{ii}^{\sigma\sigma} - N_e \right),
 \end{aligned} \tag{4.1}$$

where  $\mu$  is the chemical potential and  $N_e$  is the total number of electrons. We expand Eq.(4.1) up to second order in the generalized density matrix and double occupancy deviations.

We restrict our investigations to paramagnetic saddle point solutions in the normal conducting state  $\langle J_i^\pm \rangle_0 = 0$  so that the particle-particle (pp) and particle-hole (ph)

channel terms decouple. The free energy expansion in momentum space reads as:

$$F^{GA} \approx F_0^{GA} + \text{tr}\{h^0 \delta \rho\} + \delta F^{pp} + \delta F^{ph}. \quad (4.2)$$

The first term in Eq. (4.2) is the saddle-point free energy and  $\text{tr}\{h^0 \delta \rho\}$  contains the single-particle excitations on the GA level.

$F^{ph}$  contains the expansion with respect to the double occupancy and the part of the density matrix that commutes with the total particle number whereas  $F^{pp}$  contains the expansion with respect to the pair fluctuations  $\delta J_i^\pm$ . The deviation of the double occupancy parameter  $\delta D_i$  in the particle-hole term  $\delta F^{ph}$  can be eliminated by using the antiadiabaticity condition [93]:

$$\frac{\partial \delta F^{GA}[\rho, D]}{\partial \delta D_i} = 0. \quad (4.3)$$

Eq. (4.3) can be motivated from the assumption that the double occupancy is assumed to have a much faster dynamic as compared to the evolution of the density matrix.

In the homogeneous paramagnetic case the terms can be written in momentum representation:

$$\delta F^{pp} = \frac{1}{N} \sum_q V \delta J_q^+ \delta J_{-q}^-, \quad \delta F^{ph} = \frac{1}{N} \sum_q \begin{pmatrix} \delta \rho_q \\ \delta T_q \end{pmatrix} \begin{pmatrix} \mathbf{M}_q \end{pmatrix} \begin{pmatrix} \delta \rho_{-q} \\ \delta T_{-q} \end{pmatrix}. \quad (4.4)$$

The term  $\delta F^{ph}$  couples the local density fluctuations  $\delta \rho_q$  with the inter-site charge fluctuations of the form:

$$\delta T_q = \sum_{k\sigma} (\varepsilon_k^0 + \varepsilon_{k+q}) \delta \rho_{k+qk}^{\sigma\sigma} \quad \text{and} \quad \delta \rho_q = \sum_{k\sigma} \rho_{k+qk}^{\sigma\sigma}. \quad (4.5)$$

The particle-particle term  $\delta F^{pp}$  describes Gaussian fluctuations of the superconducting order parameter  $\delta J_q^\pm$ . The matrix elements of the interaction kernel  $\mathbf{M}_q$  include the derivatives of the entries of the MFA matrix  $\mathbf{A}_i$  and are given explicitly in appendix B.3.

For both channels the interaction kernels  $V(U)$  (in case of pp) and  $\mathbf{M}_q(U)$  (in case of ph) depend on the momentum  $q$  and the bare interaction  $U$ . Contrary the Hartree-Fock theory yields  $U$  in the pp- and  $U/2$  in the ph-channel.

Having proceeded so far we can now evaluate the ph- and pp-susceptibilities on the RPA level:

$$\chi_{ph}(\omega, q) = \begin{pmatrix} \langle\langle \hat{\rho}_q, \hat{\rho}_{-q} \rangle\rangle & \langle\langle \hat{T}_q, \hat{\rho}_{-q} \rangle\rangle \\ \langle\langle \hat{\rho}_q, \hat{T}_{-q} \rangle\rangle & \langle\langle \hat{T}_q, \hat{T}_{-q} \rangle\rangle \end{pmatrix}, \quad \chi_{pp}(\omega, q) = \langle\langle \hat{J}_q^+, \hat{J}_{-q}^- \rangle\rangle. \quad (4.6)$$

We apply the Dyson equation to obtain the full susceptibilities:

$$\begin{aligned} \chi_{ph}(\omega, q) &= [\mathbf{1} + \chi_{ph}^0(\omega, q)\mathbf{M}_q]^{-1}\chi_{ph}^0(\omega, q), \\ \chi_{pp}(\omega, q) &= [1 - \chi_{pp}^0(\omega, q)V]^{-1}\chi_{pp}^0(\omega, q), \end{aligned} \quad (4.7)$$

where  $\chi_{pp}^0$  and  $\chi_{ph}^0$  denote the non-interacting susceptibilities obtained within the GA.

## Results for the Hypercubic Lattice for $\delta = 0$

We now apply the approach developed above to the investigation of the pp- and ph-instabilities for an infinite dimensional (hyper cubic) lattice restricting to half filling  $n = 1$  ( $\delta = 0$ ). The density of states (DOS) is given by a Gaussian:

$$N(\omega) = \frac{1}{\sqrt{2\pi}B} \exp -\frac{\omega^2}{2B^2}. \quad (4.8)$$

where  $B$  is the band width. In the case of the ph-channel the charge density wave instability occurs at  $q = Q = [\pi, \pi, \dots]$  and only the  $[1, 1]$ -entry of the matrix  $\mathbf{M}_Q$  remains finite. We find that in this special case of particle-hole-symmetry the pp- and ph-effective interactions are related by  $2\mathbf{M}_{11Q} = V$  with:

$$V = -4e_0(u - 2)\frac{(1 + u)}{(1 - u)}, \quad u = \frac{U}{|8e_0|}, \quad (4.9)$$

which proves the consistency of our charge-rotational invariant TDGA. In Fig. (4.1) the  $U$ -dependence of  $\mathbf{M}_{11Q}$  and  $V$  at zero temperature is shown. For small attractions



the effective interaction approaches the limit of the HFA (dashed line). At a critical negative ratio  $U/B \approx -6.5$  one has a transition towards localized pairs at which the interactions vanish. In contrast one observes a divergence in  $M_{11Q}$  and  $V$  for  $U > 0$  at the Brinkman-Rice transition (see inset to Fig.(4.1)). Finally we calculate the

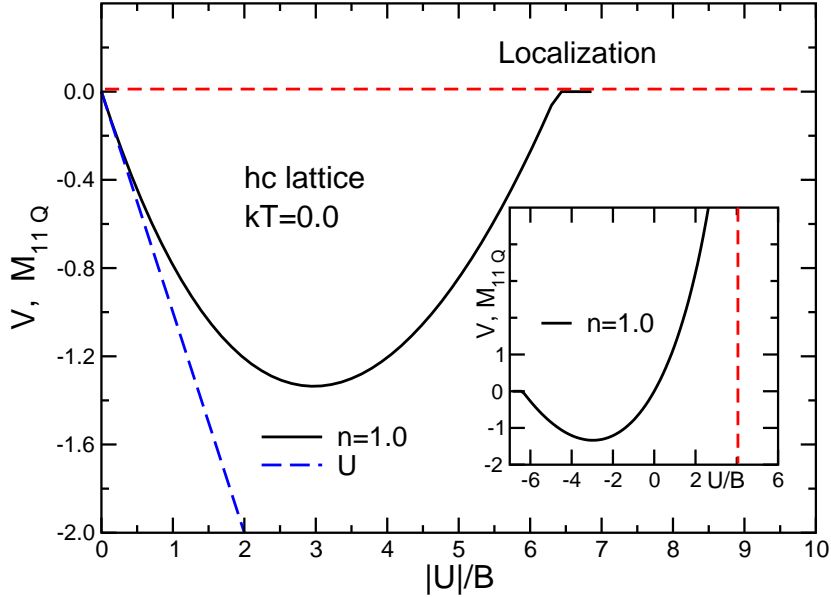


Figure 4.1: The effective ph/pp-interaction at zero temperature versus  $|U|/B$ .  $B$  is the bandwidth. The inset shows the complete range of the interaction for positive and negative  $U$  from localization to the Brinkman-Rice transition.

transition temperature for the phase transitions towards SC and CDW order from Eq. (4.7) again for a half filled hc-lattice. In Fig. (4.2) the resulting critical temperature as a function of  $|U|/B$  is shown and compared with results from BCS theory and Quantum-Monte-Carlo calculations (QMC) from [96].

The results show that the charge-rotational invariant TDGA can be used to calculate the stability of SC and CDW phases. Since the GA becomes exact in infinite dimensions we found a good agreement with the QMC data even for the order of magnitude of

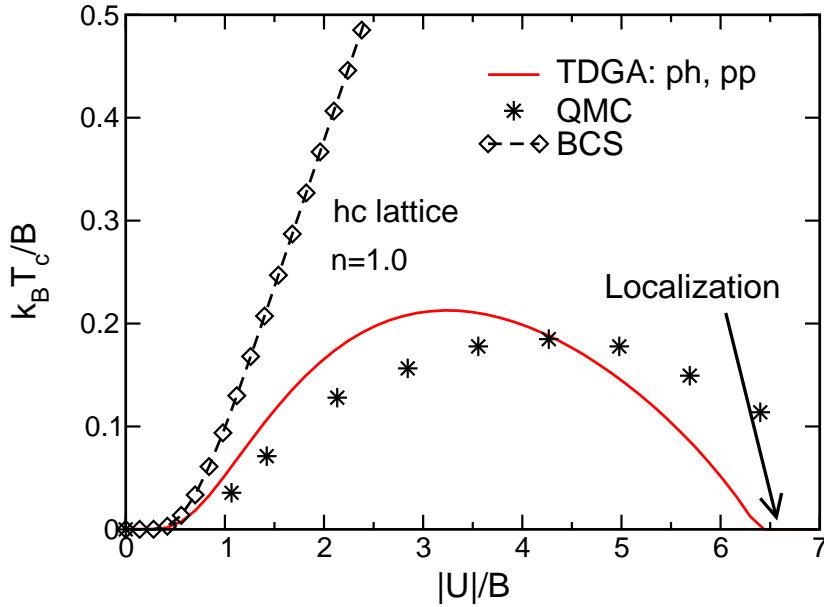


Figure 4.2: Critical temperature versus the on-site interaction  $|U|/B$ .  $B$  is the bandwidth. The  $k_B T_c$  to pp- and ph-instability lines are degenerated.

$T_c^{max}$ . It can be seen that in contrast to the BCS theory the charge-rotational TDGA can capture at least qualitatively the crossover from weak to strong coupling.

## 4.2 Solutions in the HFA and GA

We consider an  $8 \times 8$ -cluster where electron hopping is allowed between nearest neighbors only ( $t_{ij} = t$ ). We calculated the GA energy for a charge density wave and for a homogeneously charged ( $J_i^z = const$ ) superconductor. In Fig.(4.3) we present the saddle point energy for different doping rates  $\delta = N_h/L$  where  $N_h$  is the number of holes and  $L$  is the number of lattice sites. In the half filled case ( $\delta = 0$ ) the energy of the CDW and the SC are degenerate. We define the order parameter for the CDW

and for the SC as:

$$\Delta_{CDW} = \frac{1}{L} \sum_{i_x i_y} (-1)^{(i_x+i_y)} (\rho_{ii}^{\uparrow\uparrow} + \rho_{ii}^{\downarrow\downarrow}) \quad \text{and} \quad \Delta_{SC} = \frac{1}{L} \sum_{i_x i_y} \rho_{ii}^{\uparrow\downarrow}. \quad (4.10)$$

The inset of Fig. (4.3) shows the normalized order parameters corresponding to the doping rate. We calculated the order parameter with respect to the values at half filling:  $\bar{\Delta} = \Delta(\delta)/\Delta(\delta=0)$ . The saddle point solution at half filling can be compared

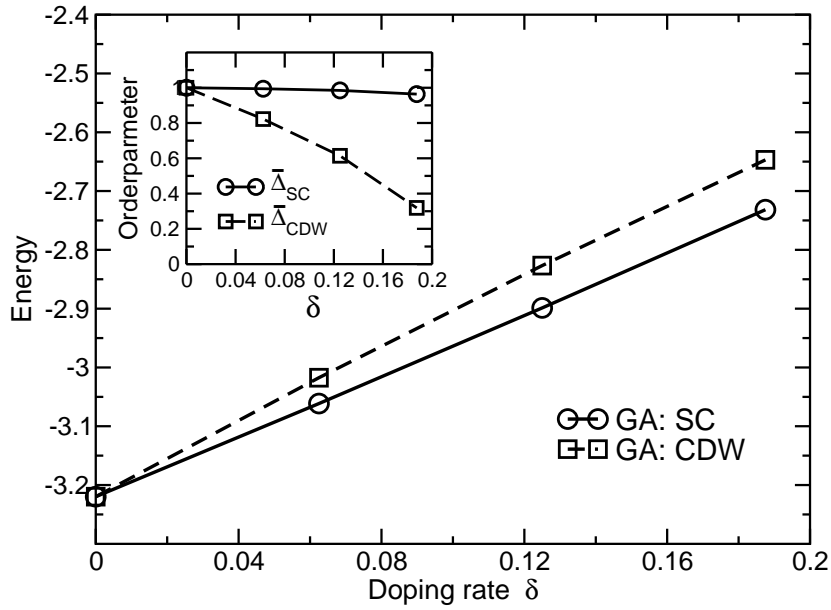


Figure 4.3: GA energy of homogeneous SC and CDW state as function of the doping rate. (Results are given for a  $8 \times 8$  cluster,  $U/t = -5$ ,  $V/t = 0$ ,  $t'/t = 0$ ). The inset shows the normalized CDW and SC order parameters  $\bar{\Delta}_{CDW}$  and  $\bar{\Delta}_{SC}$

with the results of the repulsive Hubbard model. If one applies the attraction-repulsion transformation the component  $J_i^z$  maps to the spin component  $S_i^z$ . The components  $J_i^x$  and  $J_i^y$  are transformed to  $(-1)^{(i_x+i_y)} S_i^{x/y}$ . Thus a CDW state is transformed to an anti-ferromagnet with the quantization along  $z$ . In the case of half filling a homogeneous SC maps to an anti-ferromagnet that is rotated into the  $S^x$ - $S^y$ -plane with equal energy.

As a next step we compare the GA saddle point solution and the Hartree-Fock approximation. In Fig. (4.4) we present the order parameters for a CDW at half filling as function of the interaction  $U/t$ . The CDW ordering in GA is weaker than in the HF.

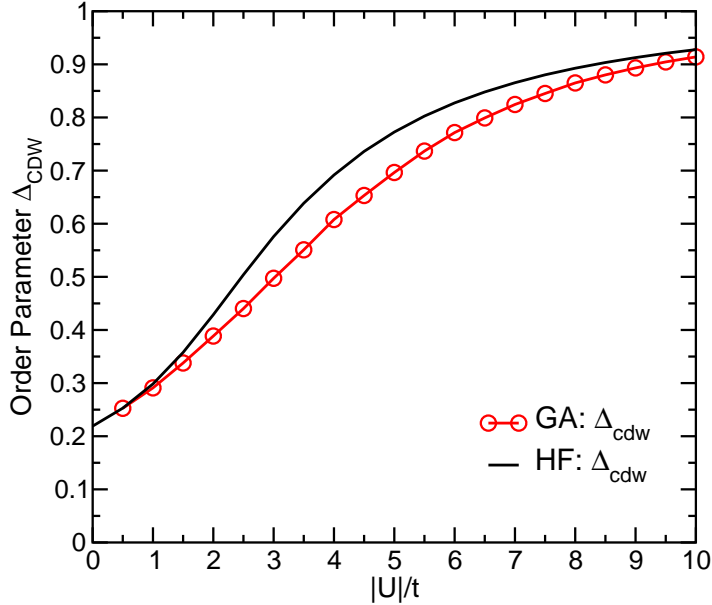


Figure 4.4: CDW order parameter for a homogeneous normal ground state (without SC).  $V/t = 0$  and  $t'/t = 0$ . HF and GA results for a  $8 \times 8$  cluster.

The most significant difference appears in the intermediate  $U$ -regime.

We find that the ground state energy of the GA is slightly below the HF ground state ( $\approx 1\%$ ). For example for  $U/t = -5$  we obtain the energy per lattice site (in units of the hopping parameter  $t$ ):  $e^{GA}/t = -3.220$  for the GA and  $e^{HFA}/t = -3.182$  for the HFA.

In Fig. (4.5) we compare GA and HF results for the kinetic energy for a normal CDW state as a function of the interaction parameter  $U/t$ . The elements of the MFA matrix  $\mathbf{A}_i$  renormalize the kinetic energy in the Gutzwiller energy functional. As an example we present the renormalization factor for the hopping amplitude  $\langle \hat{c}_{i\uparrow}^\dagger \hat{c}_{j\uparrow} \rangle$  in

Fig.(4.5). The absolute value of kinetic energy in total is larger in the GA than in the HF case. Translation processes are allowed between nearest neighbors only ( $t'/t = 0$ ). In the example in Fig.(4.5) we compare the kinetic energies for a CDW state. Two neighboring lattice sites are characterized by an energy difference. In the GA this gap is proportional to the Lagrange parameters  $\sim \lambda^{4,5}$ . (In the paramagnetic case it holds:  $\lambda^4 = \lambda^5$ .) It is larger than the gap in the HFA which is proportional to  $\sim Un$ .

If the ratio of  $U/t$  increases double occupancies are more preferred. This leads to an increase in the local charge concentration and thus to an increase of the CDW ordering. In the limit of large (negative)  $U$  the CDW order parameter saturates as shown in Fig. (4.4). In the small  $U$  regime ( $|U| > 0$ ) the GA approaches the HFA-limit.

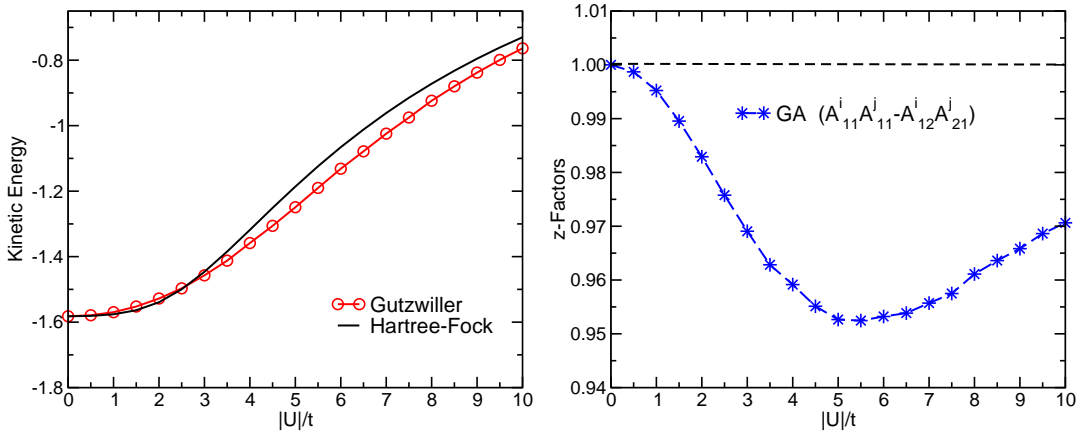


Figure 4.5: **Left:** Kinetic energy per lattice site versus the on-site attraction  $U$  for a CDW state on a half filled  $8 \times 8$  cluster. **Right:** Renormalization factor of the kinetic energy ( $\rho_{ij}^{\uparrow\uparrow}$ -part) in the GA case. (Results are given for  $t' = 0$  and  $V = 0$ .)

In the limit of  $U/t \rightarrow 0$  the CDW order parameter is finite. In the case of  $U/t = 0$  the model reduces to a free electron gas on a  $2d$ -lattice with the dispersion  $\varepsilon_{\mathbf{k}} = -2t[\cos(k_x) + \cos(k_y)]$ . In this case all one-particle states with  $\mathbf{k}$  and  $|\mathbf{k}| \leq k_F$  are occupied. If we restrict to nearest neighbor transitions the Fermi surface shows a nesting at half filling. At the Fermi edge there exist more possible  $k$ -states than electrons.

We can now construct different electron configurations in the first Brillouin zone (BZ) with equal energy. Because of the nesting these  $k$ -states on the Fermi edge are connected with the vector  $\mathbf{Q} = (\pi, \pi)$  (or  $\mathbf{q}^{(1|0)} = (\pi, 0)$ ,  $\mathbf{q}^{(0|1)} = (0, \pi)$ ). All possible configurations contribute to the ground-state wave function in the case of  $U/t = 0$ . The finite momentum vectors yield correlation to the expectation value of the charge element  $\Delta_q = 1/L \sum_{k\sigma} \langle \hat{c}_{k+q\sigma}^\dagger \hat{c}_{k\sigma} \rangle$  and thus a site dependent modulation of the local charge  $n_i = 1/L \sum_q \Delta_q \exp(i\mathbf{R}_i \mathbf{q}_i)$  that leads to a finite charge order parameter.

### 4.3 Transformation to an Effective GA-BCS Hamiltonian

In order to elucidate more clearly the difference between GA and HF we construct an effective Hamiltonian with the help of the saddle point solution that we obtain from the minimization of the GA energy functional (3.14). For this purpose we derive the Lagrange multipliers at the saddle point by the use of Eq. (3.54). We obtain the Hamiltonian from the derivative of the GA energy functional (3.14) with respect to the density matrix:

$$\{H^{MFA}\}_{ij}^{\sigma\sigma'} = \frac{\partial E^{GA}(\rho)}{\partial \rho_{ij}^{\sigma\sigma'}}, \quad (4.11)$$

where  $\rho = \{\rho_{ij}^{\sigma\sigma'}\}$  is the generalized density matrix. The explicit expressions are given in appendix A.1. If we re-derive the correct Gutzwiller energy at the saddle point from the expectation value of the effective Hamiltonian (4.11) we have to add a constant:  $E^{GA} = \langle \hat{H}^{MFA} \rangle + C$ . The constant  $C$  includes the mean field values of the boson fields. Finally we can rewrite an effective mean field Hamiltonian (MFA-Hamiltonian) that is given by Eq. (B.1) in the appendix.

In this section we assume a saddle point solution that is homogeneous and paramagnetic ( $A_{11}^i = A_{22}^i = z_0$  and  $A_i^{12} = A_i^{21} = 0$ ). In this case the effective Hamiltonian (B.1)

reduces to:

$$\begin{aligned} \hat{H}^{MFA} &= \sum_{i \neq j \sigma} z_0^2 t_{ij} \hat{c}_{i\sigma}^\dagger \hat{c}_{j\sigma} + \left[ \frac{U}{2} \left( 1 - \sqrt{1 + \frac{4|\Delta|^2}{(n-1)^2}} \right) - \tilde{\mu} \right] \sum_{i\sigma} \hat{c}_{i\sigma}^\dagger \hat{c}_{i\sigma} \\ &+ \Gamma \sum_i \hat{c}_{i\uparrow}^\dagger \hat{c}_{i\downarrow}^\dagger + \Gamma^* \sum_i \hat{c}_{i\downarrow} \hat{c}_{i\uparrow}. \end{aligned} \quad (4.12)$$

The Lagrange parameters do not depend on the lattice site index. We use the short hand notation:  $\Gamma = -(\lambda^1 - i\lambda^2)$  and  $\Gamma^* = -(\lambda^1 + i\lambda^2)$ . Since the solution is homogeneous and paramagnetic we use  $\lambda = \lambda^4 = \lambda^5$  so that this Lagrange parameter can be included in the chemical potential:  $\tilde{\mu} = \mu + \lambda$ . Further we replace the angle  $\varphi$  with help of Eq. (3.16) and the pair density using  $\Delta = \langle \hat{c}_{i\uparrow}^\dagger \hat{c}_{i\downarrow}^\dagger \rangle$  that we use as the superconducting order parameter. Now we transform (4.12) into  $k$ -space and obtain:

$$\begin{aligned} \hat{H}^{MFA} &= \sum_{k\sigma} \left\{ \varepsilon_k + \left[ \frac{U}{2} \left( 1 - \sqrt{1 + \frac{4|\Delta|^2}{(n-1)^2}} \right) - \tilde{\mu} \right] \right\} \hat{c}_{k\sigma}^\dagger \hat{c}_{k\sigma} \\ &+ \Gamma \sum_k \hat{c}_{k\uparrow}^\dagger \hat{c}_{-k\downarrow}^\dagger + \Gamma^* \sum_k \hat{c}_{-k\downarrow} \hat{c}_{k\uparrow}. \end{aligned} \quad (4.13)$$

The Fourier transformation of the hopping term reads:  $\varepsilon_k = z_0^2 \sum_j t_{ij} \exp(-i\mathbf{k}\mathbf{R}_{ij})$ . The order parameter for the superconducting phase transforms as:  $\Delta = \frac{1}{N} \sum_k \langle \hat{c}_{k\uparrow}^\dagger \hat{c}_{-k\downarrow}^\dagger \rangle$ . In order to diagonalize the Hamiltonian (4.13) we apply a Bogoliubov transformation where we introduce the new operators  $\hat{\gamma}_{k,0}$  and  $\hat{\gamma}_{k,1}$ :

$$\hat{c}_{k\uparrow} = u_k^* \hat{\gamma}_{k,0} + v_k \hat{\gamma}_{k,1}^\dagger \quad \text{and} \quad \hat{c}_{-k\downarrow}^\dagger = -v_k^* \hat{\gamma}_{k,0} + u_k \hat{\gamma}_{k,1}^\dagger. \quad (4.14)$$

The new operators fulfill the usual fermionic anti-commutation relations. The complex factors  $u_k$  and  $v_k$  obey:

$$u_k^2 = \frac{1}{2} \left( 1 + \frac{\tilde{\varepsilon}_k}{\sqrt{\tilde{\varepsilon}_k^2 + |\Gamma|^2}} \right) \quad \text{and} \quad v_k^2 = \frac{1}{2} \left( 1 - \frac{\tilde{\varepsilon}_k}{\sqrt{\tilde{\varepsilon}_k^2 + |\Gamma|^2}} \right). \quad (4.15)$$

We adopt the notation from BCS theory and define:

$$\tilde{E}_k = \sqrt{\tilde{\varepsilon}_k^2 + |\Gamma|^2} \quad \text{and} \quad \tilde{\varepsilon}_k = \varepsilon_k + \left[ \frac{U}{2} \left( 1 - \sqrt{1 + \frac{4|\Delta|^2}{(n-1)^2}} \right) - \tilde{\mu} \right]. \quad (4.16)$$

The transformed Hamiltonian has a single-particle form in terms of the new quasi particle operators:

$$\hat{H}^{eff} = \sum_k \tilde{E}_k \left( \hat{\gamma}_{k,0}^\dagger \hat{\gamma}_{k,0} + \hat{\gamma}_{k,1}^\dagger \hat{\gamma}_{k,1} \right) + \sum_k \left( \tilde{\varepsilon}_k - \tilde{E}_k \right). \quad (4.17)$$

With the help of (4.14) and (4.15) we can now derive an expression for the pair density  $\Delta = \frac{1}{N} \sum_k \langle \hat{c}_{k\uparrow}^\dagger \hat{c}_{-k\downarrow}^\dagger \rangle$ . We obtain an equation that relates the pair density and the Lagrange parameter:

$$\Delta = \frac{1}{2N} \sum_k \frac{\Gamma}{\sqrt{\tilde{\varepsilon}_k^2 + |\Gamma|^2}}. \quad (4.18)$$

If we insert the expression for  $\tilde{\varepsilon}_k$  in Eq. (4.18) we find that the right hand side includes also the superconducting order parameter  $\Delta$ .

On the other hand the HF method yields the standard gap equation from BCS theory:  $\Delta = 1/(2N) \sum_k (U\Delta) / \sqrt{(\varepsilon_k^{HF} - \mu)^2 + U^2|\Delta|^2}$ . Here the SC gap is proportional to the potential and reads  $2U|\Delta|$ .

In Eq. (4.18) the SC gap is twice the Lagrange parameter  $2|\Gamma|$ . Comparing the BCS result we find the correspondence  $|\Gamma| \leftrightarrow |U|\Delta$  so that  $|\Gamma|/\Delta$  can be interpreted as an effective pair potential. An analytical approach to the Lagrange parameter is discussed in section 3.5.

For a numerical study we calculate the density of states (DOS) for the homogeneous SC in the under doped regime. The density of states is defined as:

$$N(\omega) = 2 \sum_k \delta(\omega - E_k). \quad (4.19)$$

We take the mean field values of bosons at the saddle point and we obtain the Lagrange parameters with the help of Eq. (3.54). We formulate the effective Hamiltonian (B.1) that can be diagonalized numerically.

We obtain the energy spectrum  $\{E_k\}$  and thus we are able to calculate the DOS using Eq. (4.19). The results for an  $8 \times 8$ -cluster are shown in Fig. (4.6).



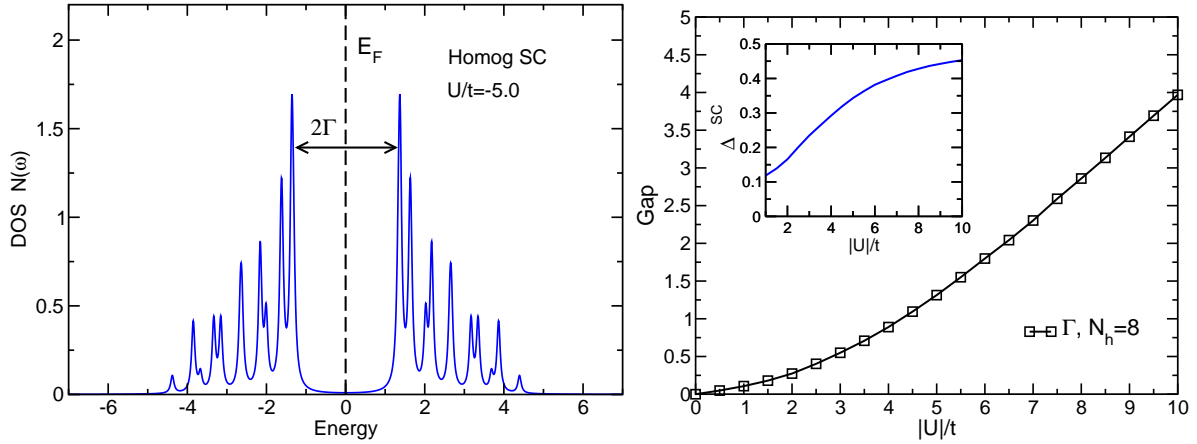


Figure 4.6: *Right:* Density of states for a homogeneous, under doped SC (Results for an  $8 \times 8$ -cluster and  $N_h = 8$ ). The dashed line the Fermi energy. *Left:* The gap  $2|\Gamma|$  versus the local interaction. The inset shows the pair density.

The Fermi energy is denoted  $E_F$ . We find a finite band gap at the Fermi energy that is given by the Lagrange parameters:  $2|\Gamma| = 2\sqrt{(\lambda^1)^2 + (\lambda^2)^2}$ . The  $U$ -dependence of the gap  $\Gamma$  is shown in the right graph. Additionally we show the results for the pair density  $\Delta$  versus the local interaction in inset in the right-hand-side graph of Fig. (4.6). The numerical results show that in the limit of  $U \rightarrow 0$  the order parameter  $\Delta$  approaches a finite value which can be explained as follows. In our results we obtain  $\Gamma$  and  $\Delta$  from the saddle point of Eq. (3.45). But in section 4.2 we argue that in the case of  $U/t = 0$  the system reduces to a free electron gas with the dispersion  $\epsilon_{\mathbf{k}} = -2t[\cos(k_x) + \cos(k_y)]$ . All one-particle states with  $\mathbf{k}$  and  $|\mathbf{k}| \leq k_F$  are occupied. Since we investigate a finite cluster we can construct different electron configuration at the Fermi edge in the first Brillouin zone (BZ). At the Fermi edge  $E_F$  there exists a set of possible discrete  $k$ -states with equal energy. All possible configurations contribute to the ground-state wave function in the case of  $U/t = 0$  which is not covered by the numerical minimization.

## 4.4 *d*-Wave Superconductivity

Although the main focus of this work is on *s*-wave superconductivity in the negative  $U$ -regime a strong motivation for the investigation of *d*-wave superconductivity in the repulsive model is obvious. As mentioned before experiments suggest that at low temperatures the HTSC have a  $\mathbf{k}$ -dependent energy gap  $\Delta(\mathbf{k})$  with *d*-wave symmetry [28, 29, 97].

Phase-sensitive symmetry tests, along with evidence from a number of non-phase-sensitive techniques have been combined to provide evidence in favor of predominantly *d*-wave pairing symmetry in a number of optimally doped cuprates. Exemplary we mention an early work [98] concerned with the study of YBCO-based SQUIDs<sup>1</sup>. From the measurements of the magnetic flux modulation one can determine the spatial anisotropy of the phase of the order parameter. The results give evidence for a phase shift of  $\pi$  that is predicted for the  $d_{x^2-y^2}$  pairing state. A detailed discussion of the results and an overview on experimental methods is given in [26].

Motivated by these works we focus on the question if *d*-wave pairing might be favored in strongly correlated systems with a repulsive, short range Coulomb interaction (positive  $U$ ). A study of dynamical pairing correlations for *s*- and *d*-wave symmetries based on a second order energy expansion on top of the GA energy functional was done in [99]. Possibly the phase transition to a *d*-wave symmetric ordered state - if it exists - is of first order in contrast to the transition to *s*-wave SC that is of second order. In contrast to our discussion the method in [99] is sensitive to second order phase transition.

In the following we present our investigation based on general arguments and the numerical study of the energies providing a direct approach to possible phase instabilities.

---

<sup>1</sup>SQUID: Superconducting QUantum Interference Device

### ***d*-Wave Order Parameter**

There exist considerable theoretical works [100, 101] based on the  $t$ - $t'$ - $J$ -model that study the possibility of  $d$ -wave pairing symmetry. Given both  $s$ -wave and  $d$ -wave pairing channels the conclusion of these studies is that the  $d$ -wave pairing depends on the band structure and doping rate. In the framework of the  $t$ - $J$ -model one derives for the gap:  $\Delta_k = -1/N \sum_{k'} V_{k-k'} \Delta_{k'} / (2E_{k'})$ , with a positive (antiferromagnetic) potential  $V_{k-k'}$ .  $E_k = \sqrt{\varepsilon_k^2 + \Delta_k^2}$  is the quasi particle energy in the superconducting state. If this potential is strongly peaked at  $\mathbf{Q} = \mathbf{k} - \mathbf{k}'$  (where  $\mathbf{Q} = (\pi, \pi)$  is the antiferromagnetic wave vector) and if we assume  $\Delta_{\mathbf{k}} > 0$  we derive  $\Delta_{\mathbf{k}} \approx -V_{\mathbf{Q}} \Delta_{\mathbf{k}-\mathbf{Q}} / (2N E_{\mathbf{k}-\mathbf{Q}})$  and thus we obtain:  $\Delta_{\mathbf{k}-\mathbf{Q}} < 0$ .

For a 2-dimensional lattice we introduce a nearest neighbor pair field operator in terms of the creation and annihilation operators:

$$\hat{\Delta}_{d_{x^2-y^2}} = \sum_{\langle ij \rangle} [\Delta_{ij} \hat{c}_{i\downarrow} \hat{c}_{j\uparrow} + \Delta_{ji}^* \hat{c}_{i\uparrow} \hat{c}_{j\downarrow}]. \quad (4.20)$$

In general the order parameter  $\Delta_{ij}$  depends on the spatial direction between the lattice sites  $i$  and  $j$ . Now we assume that the system is homogeneous and isotropic. Further on we assume that the order parameter is real and it depends only on the spatial distance of the nearest neighbors  $i$  and  $j$ :  $\Delta_{ij} = \Delta_{(i-j)}$ . Therefore we parameterize:

$$\begin{aligned} \Delta_{ij} = \Delta_0 \{ & [\delta(R_{ij}^x + 1) \delta(R_{ij}^y) + \delta(R_{ij}^x - 1) \delta(R_{ij}^y)] \\ & - [\delta(R_{ij}^x) \delta(R_{ij}^y + 1) + \delta(R_{ij}^x) \delta(R_{ij}^y - 1)] \}. \end{aligned} \quad (4.21)$$

with  $\mathbf{R}_{ij} = \mathbf{R}_i - \mathbf{R}_j$ . Thus the Fourier representation of the pair field operator (4.20) reads:

$$\Delta = \sum_{\mathbf{k}} \Delta_{\mathbf{k}}^{d_{x^2-y^2}} [\hat{c}_{k\downarrow}^\dagger \hat{c}_{-k\uparrow}^\dagger + \hat{c}_{-k\uparrow} \hat{c}_{k\downarrow}], \quad (4.22)$$

where the momentum structure of the order parameter yields:

$$\Delta_{\mathbf{k}}^{d_{x^2-y^2}} = 2\Delta_0 [\cos(k_x) - \cos(k_y)]. \quad (4.23)$$

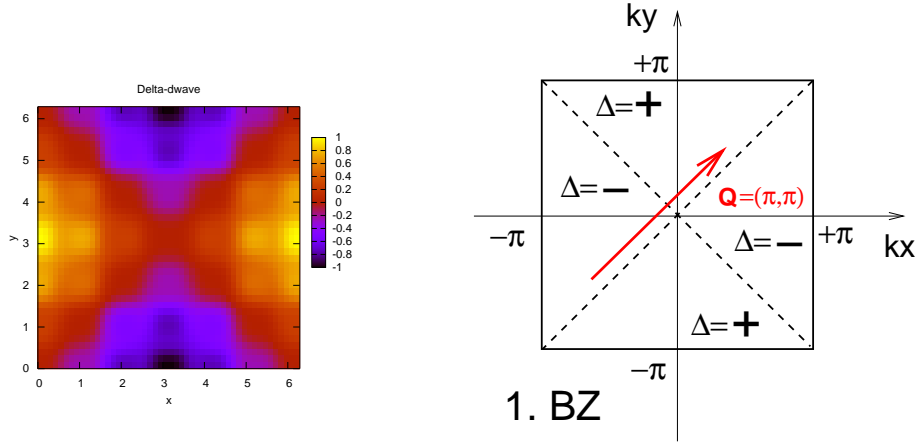


Figure 4.7: *Left:* density plot of the momentum structure of  $\Delta_{\mathbf{k}}^{d_{x^2-y^2}}$  in the first BZ. *Right:* Schematic plot in the first BZ. The momentum vector  $\mathbf{Q}$  connects states with positive and negative order parameter.

A schematic plot of the order parameter (4.23) is shown in Fig. (4.7). The antiferromagnetic wave vector  $\mathbf{Q} = (\pi, \pi)$  connects the section in the first Brillouin zone (BZ) including positive and negative values of the parameter ( $\Delta_{\mathbf{k}}^{d_{x^2-y^2}} = -\Delta_{(\mathbf{k}+\mathbf{Q})}^{d_{x^2-y^2}}$ ).

## Requirements to the Hamiltonian and Characterization of Possible Solutions

In the last section we discussed the nature of an effective Hamiltonian (B.1) that we derived from the GA results on the saddle point level. The kinetic part of this Hamiltonian includes non local pair correlations (e.g.  $\hat{c}_{i\uparrow}^\dagger \hat{c}_{j\downarrow}^\dagger$ ,  $i \neq j$ ).

In contrast the Hartree-Fock approximated Hubbard Hamiltonian (2.7) includes only on-site pair correlation. Thus a HF solution cannot support a possible  $d$ -wave ordering. As earlier mentioned we need a Hartree-Fock result for the initialization of the Gutzwiller variational approach. Therefore we add a new constraint to the HF

Hamiltonian that explicitly brings non-local pair correlation into the equation. The additional term reads:

$$\hat{H}_{d_{x^2-y^2}} = \sum_{i \neq j} \hat{c}_{i\uparrow}^\dagger \hat{c}_{j\downarrow}^\dagger \hat{c}_{i\downarrow} \hat{c}_{j\uparrow} \stackrel{HFA}{=} \sum_{i \neq j} [\Delta_{ij} \hat{c}_{i\downarrow} \hat{c}_{j\uparrow} + \Delta_{ji}^* \hat{c}_{i\uparrow}^\dagger \hat{c}_{j\downarrow}^\dagger] - \sum_{i \neq j} \Delta_{ij} \Delta_{ji}^*, \quad (4.24)$$

where we already applied the HFA. We use the short hand notation  $\Delta_{ij} = \langle \hat{c}_{i\uparrow}^\dagger \hat{c}_{j\downarrow}^\dagger \rangle$  and  $\Delta_{ij}^* = \langle \hat{c}_{i\downarrow} \hat{c}_{j\uparrow} \rangle$ . We assume a homogeneously charged system and we restrict to nearest-neighbor-correlations. Thus (4.24) reduces to:

$$\begin{aligned} \hat{H}_{d_{x^2-y^2}} = & \sum_i \Delta_0 \left[ c_{i\uparrow}^\dagger c_{i+x\downarrow}^\dagger + c_{i\uparrow}^\dagger c_{i-x\downarrow}^\dagger - c_{i\uparrow}^\dagger c_{i+y\downarrow}^\dagger - c_{i\uparrow}^\dagger c_{i-y\downarrow}^\dagger \right. \\ & \left. + c_{i\downarrow} c_{i+x\uparrow} + c_{i\downarrow} c_{i-x\uparrow} - c_{i\downarrow} c_{i+y\uparrow} - c_{i\downarrow} c_{i-y\uparrow} \right] - N^2 \Delta_0^2, \end{aligned} \quad (4.25)$$

with  $i \pm x$  for the nearest neighbors in  $x$ - and  $i \pm y$  for the nearest neighbors in  $y$ -direction.

We mentioned that we investigate the possibility of  $d$ -wave ordering in the framework of the effective Hamiltonian (B.1) that is based on the GA saddle point solution. We argue that from the structure of this Hamiltonian the existence of a  $d$ -wave state requires a local magnetization and  $s$ -wave superconductivity. In this case we obtain  $z_{i\uparrow} \neq z_{i\downarrow}$  and a local pair ordering  $J_i^\pm \neq 0$ . The off diagonal elements  $A_{12/21}^i = \frac{J_i^\pm}{2J_i^\pm} [z_{i\uparrow} - z_{i\downarrow}] \cos(\varphi_i)$  of the MFA matrix  $\mathbf{A}_i$  do not vanish. Thus the non local pair correlation  $\langle \hat{c}_{i\uparrow}^\dagger \hat{c}_{j\downarrow}^\dagger \rangle + h.c.$  contributes to the saddle point energy.

Under this condition we can assume  $(A_{11}^i A_{12}^j - A_{12}^i A_{22}^j) \neq 0$  and the effective Hamiltonian (B.1) reads:

$$\begin{aligned} \hat{H}^{MFA} = & \sum_{ij\sigma} T_{ij}^\sigma \hat{c}_{i\sigma}^\dagger \hat{c}_{j\sigma} + \sum_{ij} \left[ T_{ij}^+ \hat{c}_{i\uparrow}^\dagger \hat{c}_{j\downarrow}^\dagger + T_{ij}^- \hat{c}_{i\downarrow} \hat{c}_{j\uparrow} \right] \\ & + \sum_{i\sigma} \left[ \frac{U}{2} \left( 1 - \sqrt{1 + \tan^2(\varphi_i)} \right) - \mu - \lambda_i^{-\sigma} \right] \hat{c}_{i\sigma}^\dagger \hat{c}_{i\sigma} \\ & + \sum_i \left[ \Gamma_i^+ \hat{c}_{i\uparrow}^\dagger \hat{c}_{i\downarrow}^\dagger + \Gamma_i^- \hat{c}_{i\downarrow} \hat{c}_{i\uparrow} \right]. \end{aligned} \quad (4.26)$$

We combined the terms containing the entries of the matrix  $\mathbf{A}_i$  in  $T_{ij}^\sigma$  and  $T_{ij}^\pm$ :

$$\begin{aligned} T_{ij}^\uparrow &= t_{ij}(A_{11}^i A_{12}^j - A_{12}^i A_{22}^j) \quad \text{and} \quad T_{ij}^\downarrow = t_{ij}(A_{22}^i A_{22}^j - A_{21}^i A_{12}^j) \\ T_{ij}^+ &= t_{ij}(A_{11}^i A_{12}^j - A_{12}^i A_{22}^j) \quad \text{and} \quad T_{ij}^- = t_{ij}(A_{21}^i A_{11}^j - A_{22}^i A_{21}^j) \end{aligned} \quad (4.27)$$

Further we combined the Lagrange parameters  $\lambda_i^\uparrow = \lambda_i^4$  ( $\lambda_i^\downarrow = \lambda_i^5$ ) and  $\Gamma_i^\pm = -(\lambda_i^1 \mp \lambda_i^2)$ . After Fourier transformation of the Hamiltonian (4.26) we obtain:

$$\begin{aligned} \hat{H}^{MFA} &= \sum_{k\sigma} \tilde{\varepsilon}_k^\sigma \hat{c}_{k\sigma}^\dagger \hat{c}_{k\sigma} + \sum_{k,q} \Gamma_q^+ \hat{c}_{k\uparrow}^\dagger \hat{c}_{-k+q\downarrow}^\dagger + \sum_{k,q} \Gamma_q^- \hat{c}_{-k+q\downarrow} \hat{c}_{k\uparrow} \\ &+ \sum_k (\Delta_k^{d+} \hat{c}_{k\uparrow}^\dagger \hat{c}_{-k\downarrow}^\dagger + \Delta_k^{d-} \hat{c}_{-k\downarrow} \hat{c}_{k\uparrow}), \end{aligned} \quad (4.28)$$

where we used  $\Gamma_q^\pm = \frac{1}{N} \sum_i \Gamma_i^\pm \exp(\mp i \mathbf{R}_i \mathbf{q})$ . Now we require that the local contribution ( $s$ -wave part) to the SC order parameter is homogeneous and the non-local correlations depend only on the relative lattice spacing  $\mathbf{R}_{ij} = \mathbf{R}_i - \mathbf{R}_j$ . Thus we obtain for the non local part:

$$\Delta_k^{d\pm} = \sum_i T_{ij}^\pm \exp(\mp i \mathbf{k} \mathbf{R}_{ij}). \quad (4.29)$$

For the  $s$ -wave part we derive in this case:  $\Gamma_q^\pm = \Gamma^\pm \delta(q)$ . The explicit Fourier transform can be found in appendix B.2. As in the last section we eliminate the angle  $\varphi_i$  with help of Eq.(3.16) and the local pair density ( $s$ -wave part):  $\Delta^s = \frac{1}{N} \sum_i \langle \hat{c}_{i\uparrow}^\dagger \hat{c}_{i\downarrow}^\dagger \rangle$ . The effective single electron dispersion reads:

$$\tilde{\varepsilon}_k^\sigma = \sum_i \left\{ T_i^\sigma + \left[ \frac{U}{2} \left( 1 - \sqrt{1 + \frac{4|\Delta|^2}{(n-1)^2}} \right) - \tilde{\mu}_i^\sigma \right] \right\} \exp(-i \mathbf{R}_{ij} \mathbf{k}), \quad (4.30)$$

where we combined the chemical potential and the Lagrange parameter  $\tilde{\mu}_i^\sigma = \mu - \lambda_i^\sigma$ . In Eq. 4.30 we restrict to NN-hopping and we use the fact that the  $d$ -wave correlations depend only on the relative lattice spacing ( $T_{ij}^\sigma = T_i^\sigma$ ). Applying the Bogoliubov transformation (4.14) we transform to the new operators  $\hat{\gamma}_{k,0}$  and  $\hat{\gamma}_{k,1}$  and we obtain:

$$\hat{H}_{d_{x^2-y^2}}^{eff} = \sum_k \tilde{E}_k \left( \hat{\gamma}_{k,0}^\dagger \hat{\gamma}_{k,0} + \hat{\gamma}_{k,1}^\dagger \hat{\gamma}_{k,1} \right) + \sum_k \left( \tilde{\varepsilon}_k - \tilde{E}_k \right). \quad (4.31)$$

where we use the following definition:

$$\tilde{E}_k = \sqrt{\tilde{\varepsilon}_k^2 + |\Gamma^+ + \Delta_k^{d+}|^2}. \quad (4.32)$$

The local pair density  $\Delta^s$  can now be derived as discussed in section 4.3. We find an equation that relates the local pair density with the Lagrange order parameter  $\Gamma^+$  and the  $d$ -wave order parameter:

$$\Delta^s = \frac{1}{2N} \sum_k \frac{(\Gamma^+ + \Delta_k^{d+})}{\sqrt{\tilde{\varepsilon}_k^2 + |\Gamma^+ + \Delta_k^{d+}|^2}} \quad (4.33)$$

The equation shows that  $d$ -wave symmetric ordering coexists only with  $s$ -wave superconductivity. If we insert the expression (4.30) for  $\tilde{\varepsilon}_k$  in Eq. (4.33) we find that the right hand side includes also the local superconducting order parameter  $\Delta^s$ . If we require the local pair correlation to be zero ( $\Delta^s = 0$ ) it follows  $\Gamma^\pm = 0$  and  $T^\pm = 0$  and Eq. (4.33) can hold only if  $\Delta_k^{d+} = 0$  for all values of  $k$ . Comparing the results (4.33) with the standard gap equation from BCS theory where the SC gap is proportional to the potential we find correspondence  $|\Gamma^+ + \Delta_k^{d+}| \leftrightarrow |U|\Delta$  so that  $|\Gamma^+ + \Delta_k^{d+}|/\Delta$  can be interpreted as an effective  $k$ -dependent potential. From the numerical point of view we try to answer the question: Can a state including non local pair correlations be a possible solution in the GA approximated Hubbard model and does this correlation lower the energy? We assume a  $10 \times 10$  square lattice where we allow nearest neighbor hopping with the amplitude  $t$  and next nearest neighbor hoppings with the amplitude  $t'$ . The dispersion of non the interacting system reads:

$$\varepsilon_k = -2t(\cos(k_x) + \cos(k_y)) - 4t' \cos(k_x) \cos(k_y). \quad (4.34)$$

We introduce the spin order parameter:  $\Delta_{\mathbf{q}}^{spin} = \frac{1}{N} \sum_i (n_{i\uparrow} - n_{i\downarrow}) \exp(\mathbf{q}\mathbf{R}_i)$ , to classify the spin structures which may coexist with a  $d$ -wave state. We investigate two different structures namely: (1) Néel ordered states with  $\mathbf{q} = (\pi, \pi)$  and (2) collinear spin ordered states with  $\mathbf{q} = (\pi, 0)$ .

Motivated by the work [102,103] we assume  $t'/t \in [-0.5, 0.5]$  and  $|U|/|t| \gg 1$ . We work in the strongly correlated regime near half filling ( $n = 1 - \delta$ ) with  $\delta \ll 1$ . Both spin states fulfill the requirements that are necessary for the formation of  $d$ -wave ordering so that the entries of the matrix  $\mathbf{A}_i$  do not vanish. We studied the non-local pair correlation  $\langle \hat{c}_{i\uparrow}^\dagger \hat{c}_{j\downarrow}^\dagger \rangle$  which is given by the Fourier transform:

$$\Delta(\mathbf{k}, \mathbf{q} - \mathbf{k}) = \frac{1}{N} \sum_{i \neq j} \langle \hat{c}_{i\uparrow}^\dagger \hat{c}_{j\downarrow}^\dagger \rangle \exp [i(\mathbf{k}\mathbf{R}_{ij} + \mathbf{q}\mathbf{R}_j)]. \quad (4.35)$$

We evaluated (4.35) at  $\mathbf{q} = (0, 0)$  in the first Brillouin zone (BZ). In general we found for all structures and all choices of parameters  $\Delta(\mathbf{k}, -\mathbf{k}) \approx 0$ . A GA saddle point solution with a significant  $d$ -wave symmetric non-local pair ordering with a coexisting  $(\pi, \pi)$ - or  $(\pi, 0)$ -spin order does not exist. In both cases we found for the SC order parameter of the  $s$ -wave part very small values:  $\Delta^s \sim 10^{-4}$  to  $\Delta^s \sim 10^{-6}$ . In the positive  $U$  regime we found for zero and for finite ratios  $t'/t$  the standard spin ordered states that show a significant magnetization. As a consequence of the small local pair densities ( $s$ -wave part) the off-diagonal elements in the GA kinetic energy term ( $T_{ij}^+$  and  $T_{ij}^-$ ) in Eq. (3.18) are also small in the same order of magnitude. Due to the precision of our numerical method we did not find a significant contribution to the saddle point energy for all cases.

In accordance with Eq. (4.33) and the analytical argumentation we found that a zero local SC implies that the non-local pair-correlation vanishes. From our results we conclude that the  $d$ -wave symmetric state in the positive  $U$ -regime is not a solution of the Gutzwiller approximated Hubbard model.



# Chapter 5

## Inhomogeneous Solutions

The complex phase diagram for high- $T_c$  superconductors that was discussed earlier shows the competition between different ordered phases. In particular, the debate focusses on the nature of the pseudo-gap region and the question whether a real phase transition exists in that region.

As we outlined in chapter 1 the high- $T_c$  materials tend to the formation of inhomogeneous charge- and spin-structures. Among other experimental techniques surface sensitive methods give evidences for incommensurate spatial modulation of the electronic structure in high- $T_c$  materials.

In this chapter we investigate the GA solution of the Hubbard model that we prepared with stripe-shaped charge- and pair-ordered domains. We call a state a striped state if there exist spatially separated domains where the order parameter changes significantly [104]. On this basis we classify the inhomogeneities in the charge structure in the next section. We characterize the structure by the use of the pseudo charge vector field  $\mathbf{J}_i$  and the current density as discussed in section 3.7. We present stripe solutions of the attractive Hubbard model with and without nearest-neighbor-repulsion (parameter  $V$ ) and we discuss the stability of these solutions.

This chapter is organized as follows: First we present solutions where we set the inter-site repulsion to zero ( $V = 0$ ). We present solutions where the charge is arranged in form of stripes with a homogeneous charge and pair ordered structure within the stripes. We discuss the stability of a solution with  $N_h$  holes and with an energy  $E(N_h)$  by comparing this energy with a half filled homogeneous superconductor with the energy  $E_{SC}$ . We introduce then the binding energy per hole:

$$e_h = \frac{E(N_h) - E_{SC}}{N_h}. \quad (5.1)$$

We discuss this quantity with respect to the hole concentration in the stripes. A mathematical analysis allows a conclusion for an optimal doping or stripe filling [105] in view of the stripe formation.

In the next section we present results for  $V > 0$ . First we investigate the influence of a finite value of  $V$  without arranging the charge order in different domains. These stripeless solutions for nearest-neighbor-repulsion showed a new inhomogeneous structure. The CDW order parameter has constant phase over the cluster and the SC order parameter showed structure of a pair density wave.

In the third section we present stripe solutions for  $V > 0$ . The solutions are characterized by domains where the charge order parameter shows a phase shift. The domains are separated by superconducting domain walls.

In the last section of this chapter we investigate point-like charge and pair inhomogeneities. These are probably the simplest form of inhomogeneities. We show results for local charge inhomogeneities in small systems and in comprehension with the far-field-ordered charge structures. In this context we focus in the second part of the last section on polarons and bipolarons in comparison to vortices and anti-vortices. We also present our result in view of the interplay of these structures. An early comprehensive overview is given in [106].

## 5.1 Homogeneous Charged Stripes

As a first application we prepare structures under the condition of zero inter-site repulsion  $V = 0$ . The charge carriers are arranged in domains where the charge density is homogeneous within the domains. We consider a  $16 \times 4$ -cluster in the underdoped regime with 16 holes. In the upper panel of Fig. (5.1) we present the contour plot of the charge density  $\rho_{ii}$   $i = (i_x, i_y)$ . The holes are located in the four dark shaded domain walls separating regions of constant charge density. The lower panel shows the pair density  $\rho_{ii}^{\uparrow\downarrow} = \langle \hat{c}_{i\uparrow}^\dagger \hat{c}_{i\downarrow}^\dagger \rangle$ . The pair density corresponds to the charge structure. The SC order parameter changes its sign in the vertical stripes and varies from  $-0.4$  to  $+0.4$ . These regions are separated by domain walls where the SC order vanishes. The domain walls of the pair density correspond to the domain walls of the charge density.

In Fig. (5.2) we present the three graphs corresponding cuts along the physical  $x$ -axis. The graphs provide a quantitative picture of the charge density, the pair density and the double occupation. The charge density forms stripes where the electrons are evenly distributed in the SC domains. The holes prefer the walls where the SC order parameter vanishes.

Because normal charge and SC vanish the expectation value of the charge vector will take  $\langle \hat{\mathbf{J}}_i \rangle = (0, 0, -1)$  within the domain walls. In Fig. (5.3) we present the  $x$ - $y$ -projection of the vector  $\mathbf{J}_i$  for this example.

In a next step we like to compare the energy of a state with homogeneous charged stripes and the homogeneous SC. We find the energies of the striped state is on average 2.4% above the energy of a homogeneous SC (Tab. 5.1). We find that the difference in energies arises from the difference in the kinetic part of the energy. It increases whereas the potential part decreases with the formation of stripes. We found explicitly  $E_{kin}^{stripes} > E_{kin}^{SC}$  but in contrast  $E_{pot}^{stripes} < E_{pot}^{SC}$ .

In our investigation we could not find the stripe state to be the ground state. The

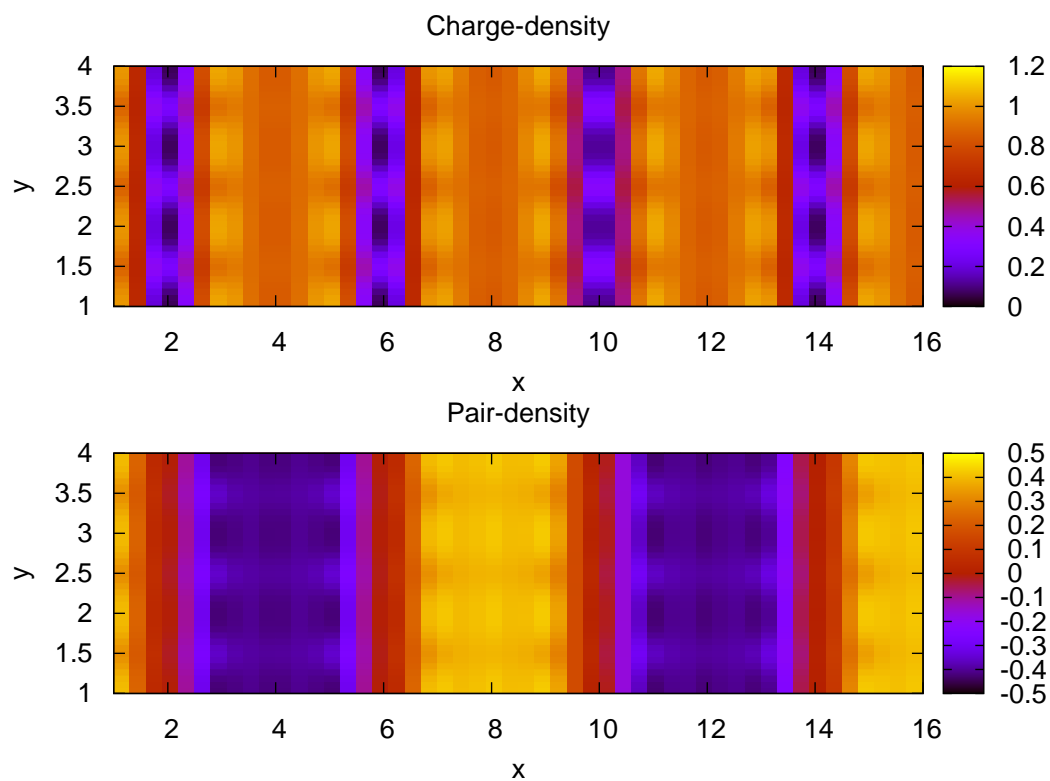


Figure 5.1: Contour plots of the charge- and pair-density for hole-doped  $16 \times 4$ -cluster with 4 plain stripes ( $N_h = 16$ ,  $t'/t = 0.0$  and  $U = -8$ )

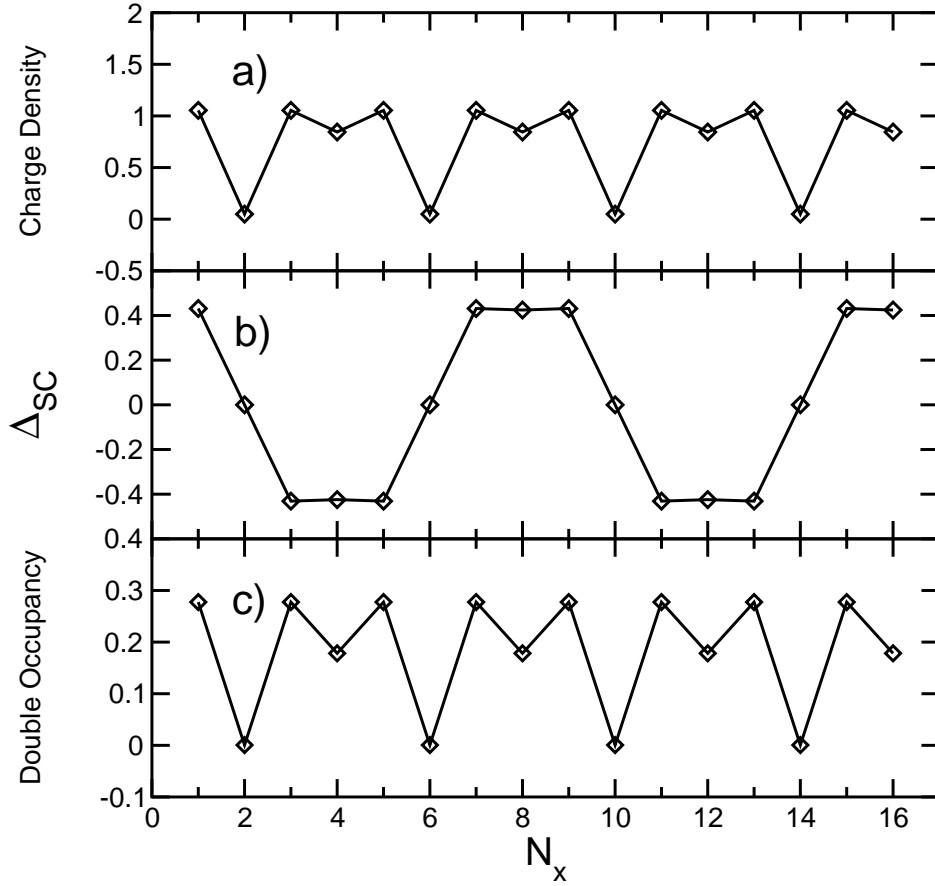


Figure 5.2: Cuts along the  $x$ -axis: (a) charge density, (b) SC order parameter, (c) double occupancy. ( $N_h = 16$ ,  $t'/t = 0.0$  and  $U = -8$ )

potential term seems to play an important role for the stripe formation. This motivates us to extend the potential interaction by the inter site repulsion term.

Additionally we mention that the discussed stripe arrangement of SC domains with different phases that are separated by normal conducting domain walls is a Josephson-like structure. For this reason we calculated the current density with the help of Eq. (3.69) but we found no current flowing through the domain walls.

| Doping<br>(holes) | Homogeneous SC<br>$e^{SC}/t$ | Stripes<br>$e^{Stripes}/t$ |
|-------------------|------------------------------|----------------------------|
| 0                 | -4.48                        | -4.37                      |
| 4                 | -4.23                        | -4.13                      |
| 8                 | -3.98                        | -3.88                      |

Table 5.1: Comparison of the energies per lattice site for homogeneous SC and a state with 4 charge stripes in units of the hopping parameter  $t$ . (Results are given for a  $16 \times 4$ -cluster with  $t/t' = 0$  and  $V/t = 0$ . Precision: 2nd position after decimal point).

## Stability and Optimal Stripe Filling

We like to give a statement in view to the stability of a structure as discussed above. We compare the energy of stripe solutions with the ground state energy of a half-filled homogeneous charged superconductor  $E_{SC}$ . At half filling the homogeneous SC and the CDW are energetically degenerate in the negative- $U$ -regime as discussed earlier. We consider  $16 \times 4$  four SC domains separated by hole doped domain walls with  $\Delta^{SC} = 0$ . In the density plot Fig. (5.1) and the charge vector field in Fig. (5.3) one finds stripes with a weak charge carrier concentration. The holes are located in the domain walls that are positioned at  $i_x \in \{2, 6, 10, 14\}$ . Because of symmetry reasons the holes are equally distributed over the stripes. We like to discuss the binding energy per hole (5.1) as function of the doping rate or the hole concentration in the stripe. Given the doping rate  $N_h$  we evaluate the hole density:

$$\nu = \frac{N_h}{n_s L_y} \quad (5.2)$$

where  $L_y$  is the number of lattice sites in the stripes along the  $y$ -direction and  $n_s$  is the number of stripes in the cluster.

In Fig. (5.4) we present the energy per hole versus  $\nu$ . We changed the doping rate,

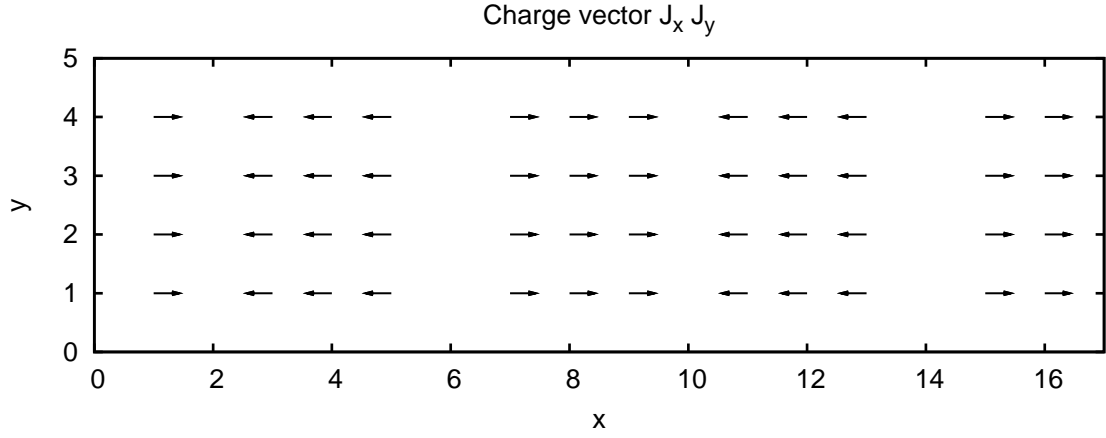


Figure 5.3: The  $x$ - $y$ -component of the charge vectors  $\vec{J}$ . There exist four domains where the vector field changes sign and it disappears in the  $x$ - $y$ -plane in the domain walls. ( $\Delta = 0$ )

system size and the stripe dimension. In this way we obtain a set of different values for the hole density in the stripes  $\nu$ . We investigate the influence of the next nearest neighbor (NNN) transitions for a finite parameter  $t'$ . In the diagram we present results for different ratios of the parameters  $t'/t$  as appropriate for cuprates. A negative ratio of  $t'$  and  $t$  favors the formation of partly filled metallic bands in the spin channel [105]. For a qualitative analysis and to guide the eye we fitted the results in Fig. (5.4). For this reason we expand the binding energy per  $y$ -length in a Taylor expansion up to second order in terms of  $\nu$ :

$$\frac{E_{\text{Stripes}}(N_h) - E_{\text{SC}}}{L_y n_s} \approx A + B\nu + C\nu^2. \quad (5.3)$$

With the help of (5.1) and (5.2) we obtain:

$$e_h \approx A \frac{1}{\nu} + B + C\nu. \quad (5.4)$$

This curve corresponds to the fits in Fig. (5.4). On the one hand we find that the system prefers hole filled stripes in the under doped regime. On the other hand we

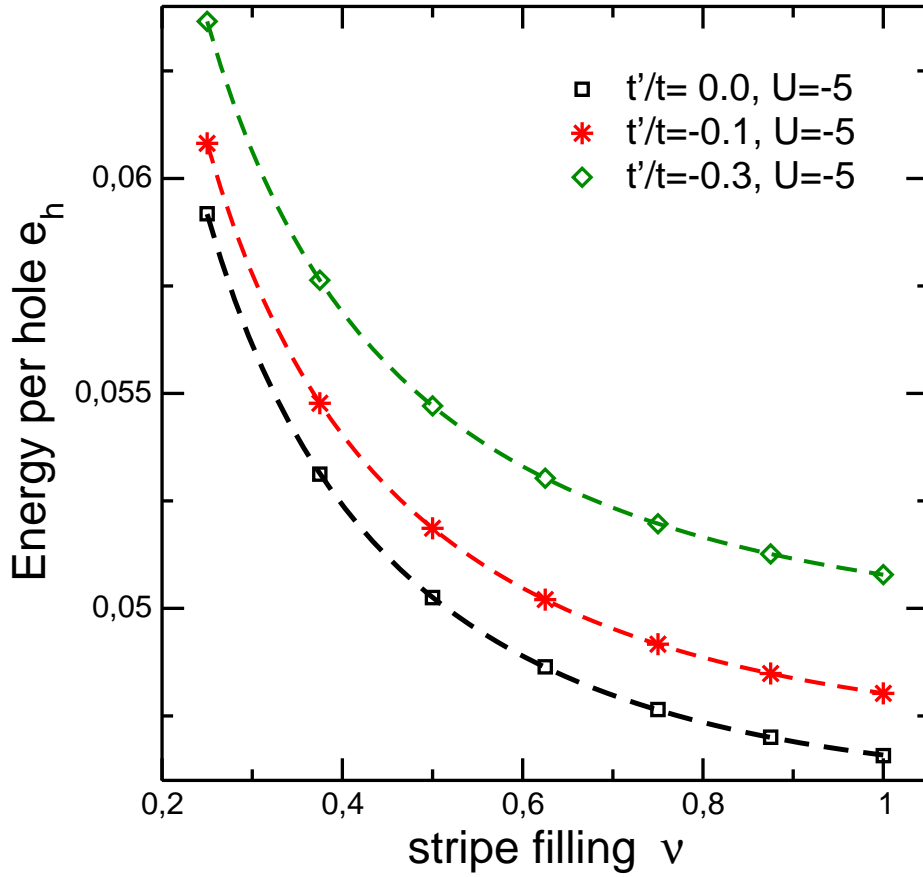


Figure 5.4: Binding energy per hole for stripes in  $y$ -direction as function of the stripe filling.  $\nu$  for different values of  $t'/t$ . The results were calculated for a  $16 \times 4$ -cluster and 4 domain walls. The dashed lines are the curve fits to guide the eye.

cannot find a local minimum in the energy per hole  $e_h$  for all choices of  $t'/t$ . This means also for the analytic minimum:  $\nu_{\min} \notin [0, 1]$ . From the local minimum of (5.4) at  $\nu_{\min} = \sqrt{A/C}$  we conclude  $A \geq C$ .

At this point we can summarize our results for the homogeneous stripes at  $V = 0$  as follows: Within the attractive Hubbard model (at  $V = 0$ ) we found no spontaneous symmetry breaking with regard to stripe formation. For all choices of parameters we



found the stripe solutions instable with respect to the homogeneous superconducting ground state.

In the next section we take into account the inter-site repulsion ( $V > 0$ ) in order to stabilize the stripe solution.

## 5.2 Stripe-less Solution for $V > 0$

In this chapter we focus on the influence of the inter-site repulsion term. It was proposed earlier [107] that the attractive Hubbard model with inter-site repulsion at half filling prefers the CDW ground state in view to the SC state. Our motivation was to influence the potential part of the energy and to stabilize the solution. We assume that solutions including anti-phase domains are preferred in view to homogeneous SC or CDW solutions. As we discussed in section 3.3 we add the term  $\hat{W} = V \sum_{\langle ij \rangle} (\hat{n}_{i\uparrow} + \hat{n}_{i\downarrow})(\hat{n}_{j\uparrow} + \hat{n}_{j\downarrow})$  to the Hubbard Hamiltonian. We decouple the term with the well-known HFA. The parameter  $V$  is a positive value representing the repulsion between fermions on adjacent lattice sites.

At first we discuss the influence of  $V$  without domain separations. We consider a  $16 \times 4$  cluster and present our results for  $V = 0$  at half filling ( $N_h = 0$ ). As shown in Fig. (5.6) we obtain a CDW state with a homogeneous superconductor characterized by a homogeneous pair density. The top panel shows the charge density  $n_i$  of the cluster. The lower panels show the  $z$ - $y$ - and the  $x$ - $y$ -projection of the vector  $\mathbf{J}_i$ . The alternating  $z$ -component represents the CDW structure of the normal charge. The  $x$ - $y$ -projection in the lower panel is the superconducting part of the charge vector, which represents a homogeneous SC. In a next step we compare the energy of the CDW ( $E^{CDW}$ ) and the energy of the homogeneous SC ( $E^{SC}$ ) by calculating the energy difference:

$$\Delta(E^{GA}) = E^{CDW} - E^{SC}. \quad (5.5)$$

The energy difference as function of the inter-site repulsion  $V/t$  is shown in Fig. (5.5).

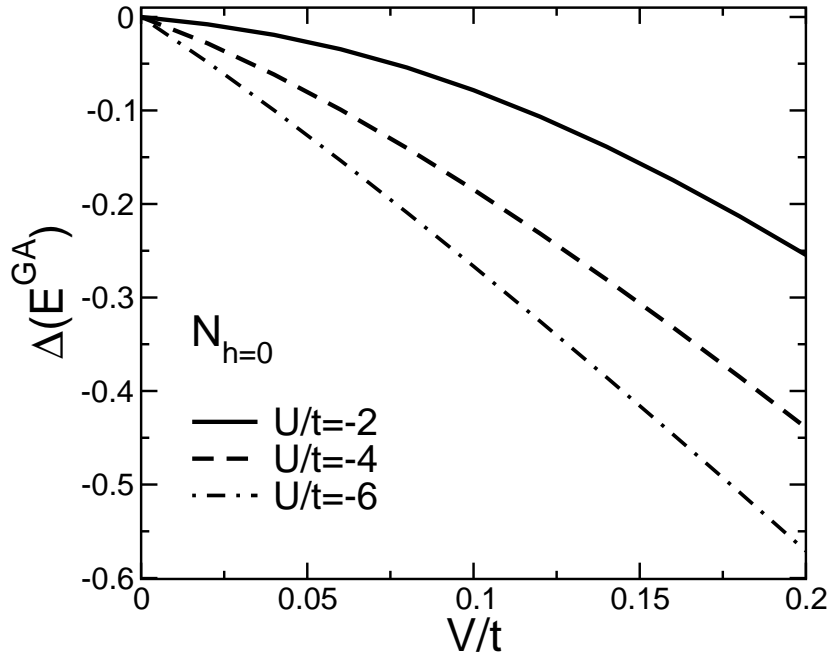


Figure 5.5: Energy difference  $\Delta(E^{GA})$  Eq. (5.5) at half filling ( $N_h = 0$ ).

As we see from the graphs a homogeneous SC and CDW order are degenerated ( $\Delta E^{GA} = 0$ ) if the inter-site repulsion vanishes ( $V = 0$ ). In the case  $V > 0$  the CDW state has lower energies. The inter-site repulsion favors the formation of CDW ordering. The homogeneous SC is a solution of the restricted charge rotational invariant GA-functional but it cannot be the ground state.

Now we focus on solutions in the *under doped regime with  $V > 0$* . Again we consider a  $16 \times 4$ -cluster which is doped with 8 holes (doping rate  $\delta = 0.875$ ). In the two upper panels of Fig. (5.7) we show the charge and the pair density. In the under doped regime we find that the CDW state is energetically preferred in the normal conducting channel. As we can see from the  $x$ - $y$ -projection of the vector  $\mathbf{J}_i$  the SC part has a checkerboard like density ( $\Delta_{i_x i_y} \sim \Delta_0 [1 + (-1)^{(i_x + i_y)}]$ ) which we refer to as pair density wave (PDW). In our investigation we found that the PDW is stable. It has the lowest

energy compared to the homogeneous charged SC and the homogeneous SC with CDW ordering.

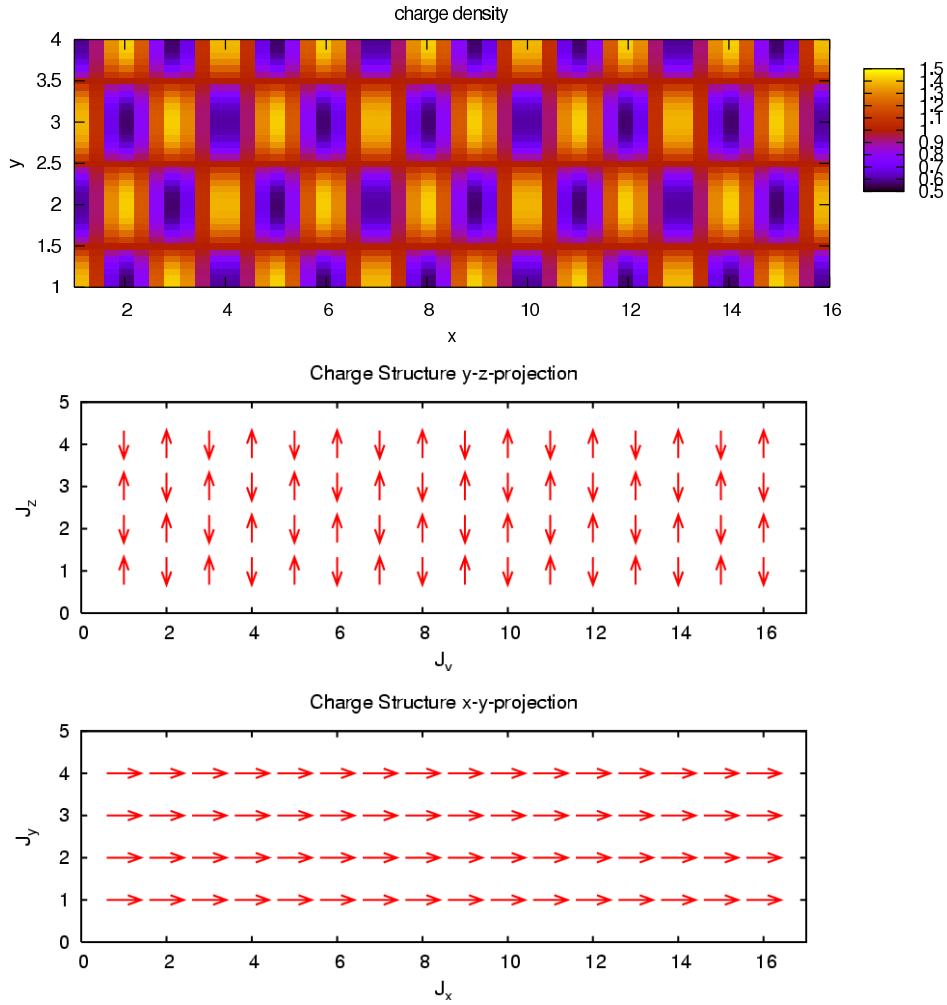


Figure 5.6: Charge structure for half filling. ( $N_h = 0$ ) *Top*: Charge density  $n_i$  (CDW). *Lower panels*:  $z$ - $y$  and  $x$ - $y$ -projection of the charge vector  $\mathbf{J}_i$ . (Results for:  $U/t = -6$ ,  $V/t = 0.02$ ,  $t'/t = 0$ .)

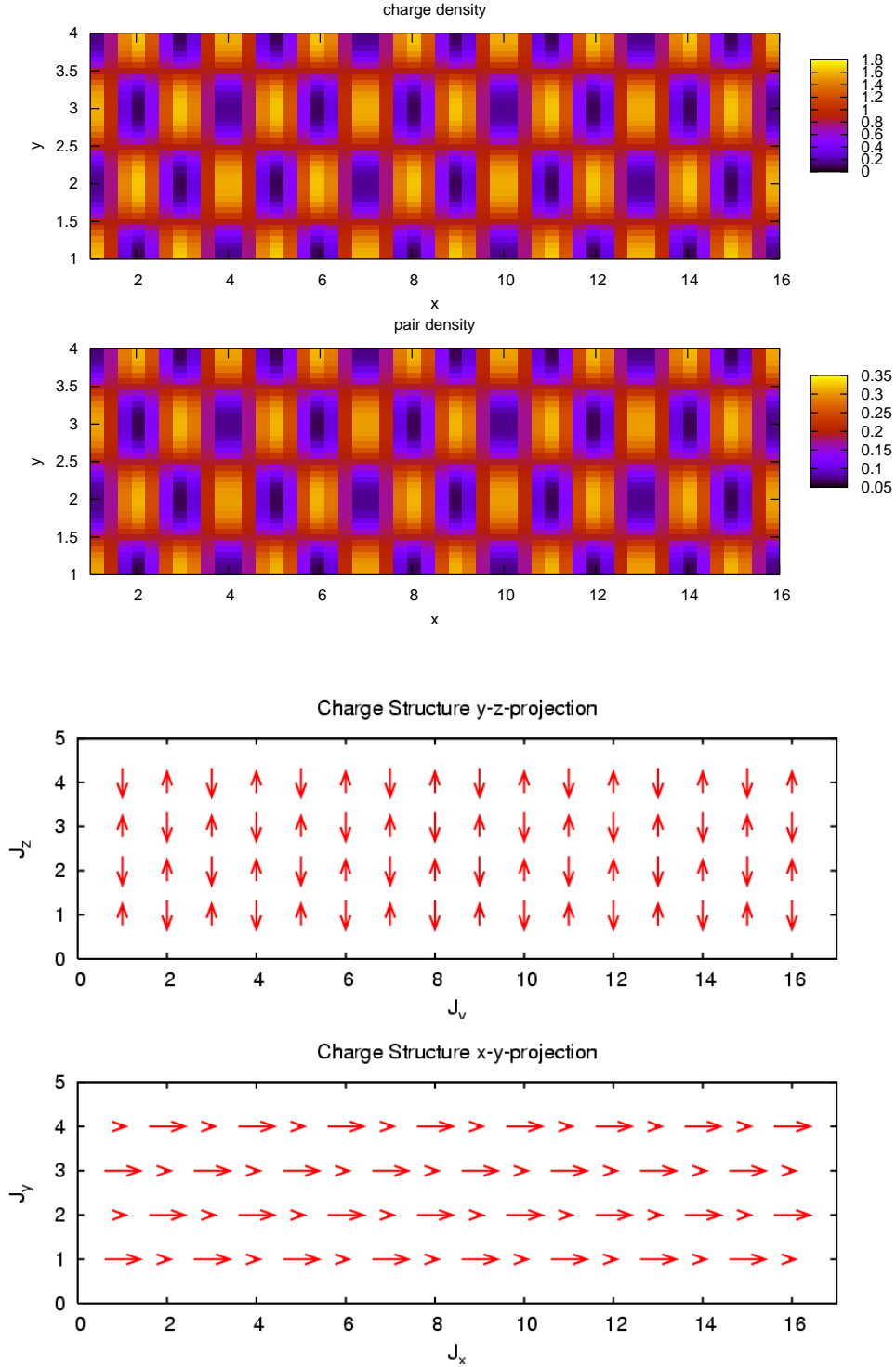


Figure 5.7: Charge structure for a PDW state in the hole doped regime ( $N_h = 8$ ). *Top panels:* Density plots of the charge  $n_i$  and pair-density  $\Delta_i$ . *Bottom panels:*  $y$ - $z$ - and  $x$ - $y$ -projection of the charge vector  $\mathbf{J}_i$ . (Results for:  $U/t = -10$ ,  $V/t=0.10$ ,  $t'/t = 0$ )

### 5.3 Stripes with $V > 0$

In this section we investigate the stripe formation and the interplay of the stripes for *under doped systems at  $V > 0$* . We consider a  $16 \times 4$ -cluster. The cluster is divided in 4 domains separated by domain walls at the lattice sites located at  $i_x \in \{2, 6, 10, 14\}$ . Within the domains the normal charge is arranged in form of a CDW.

The holes are located in the domain walls that are characterized by a small but homogeneous charge density. The pair density has a finite value and it is homogeneous in the domain walls. In the top panels of Fig. (5.8) we show the density plots of the local charge  $n_i$  and pair density  $\Delta_{i_x, i_y}^{SC} = \langle \hat{c}_{i\uparrow}^\dagger \hat{c}_{i\uparrow}^\dagger \rangle$ .

In the lower panels of Fig. (5.8) we present the projection of the charge vector field. The upper panel contains the normal charge while the lower panel contains the superconducting components of the vector  $\mathbf{J}_i$ . The field of the normal charge ( $J_z$ -component) changes its orientation from one domain to the other. The vector field rotates through the walls maximizing the superconducting order parameter  $\Delta_{i_x, i_y}^{SC}$ .

The charge ordered domains have a phase shift from one domain to the other. In order to give a quantitative state we introduce the local charge order parameter:

$$\Delta_{i_x, i_y}^{CDW} = (-1)^{(i_x + i_y)} [\langle \hat{n}_i \rangle - n_0], \quad (5.6)$$

where we used the average charge density  $n_0 = \frac{1}{N} \sum_i \langle \hat{n}_i \rangle$ . The local order parameter in Eq. (5.6) reflects the phase of the CDW with respect to the lattice site.

In Fig. (5.9) we present order parameters for the normal charge from Eq. (5.6) and for the pair density  $\Delta_{i_x, i_y}^{SC}$  along the  $x$ -axis for different ratios of  $V/t$ . The local values are averaged along the  $y$ -axis. The value for  $\Delta_{i_x, i_y}^{CDW}$  changes its sign from one charge ordered domain to the other and it vanishes for homogeneous charged domain walls. The pair density  $\Delta_{i_x, i_y}^{SC}$  has its maximum at the domain walls, where the superconducting order appears. An increasing inter-site repulsion favors the formation of the domains.

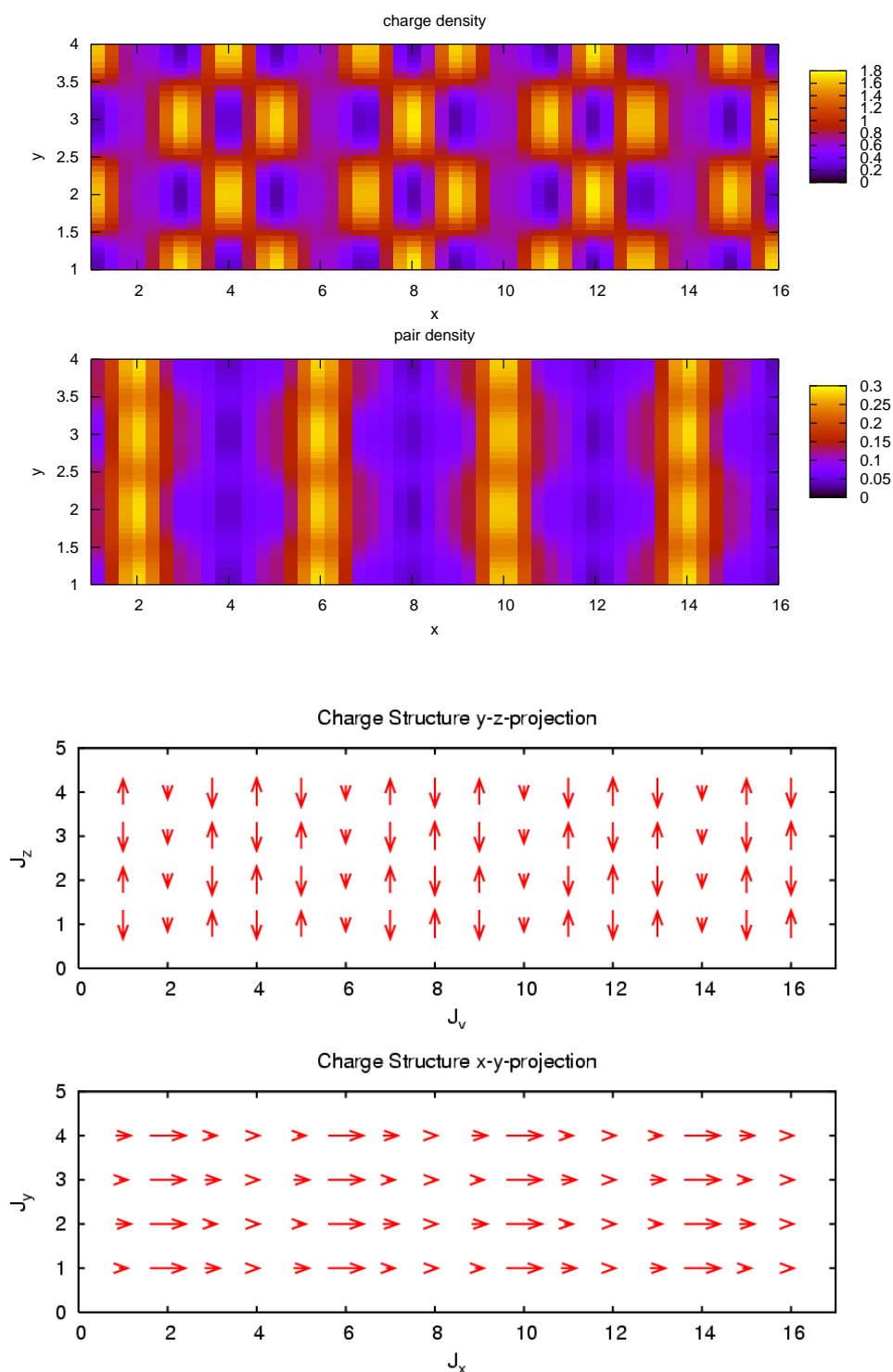


Figure 5.8: Phase shifted CDW domains: (*Top*: Charge- and pair-density. (*Bottom*: Vector field of charge vector. (Results for:  $N_h = 8$ ,  $U/t = -5$ ,  $t'/t = -0.3$ ,  $V/t = 0.1$ ).

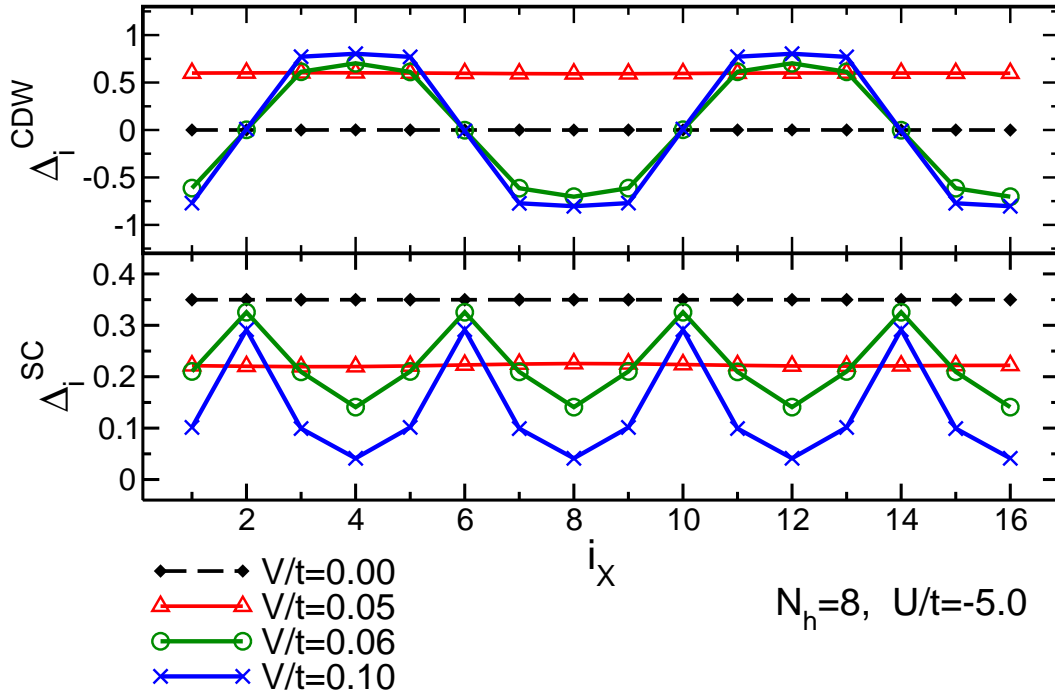


Figure 5.9: Influence of the ratio  $V/t$  to formation of anti-phase CDW domains: Order parameter along the physical  $x$ -axis for a  $16 \times 4$ -cluster in the under-doped regime (*Top*: CDW order parameter, *Bottom*: SC order parameter). Results are given for  $N_h = 8$ ,  $U/t = -5$ ,  $t'/t = -0.3$ ,  $V/t = 0.1$ .

At this point we compare the energies of the different structures that we have discussed in the last sections. In Fig. (5.10) we summarize the energy for the different structures versus the inter site repulsion in the under-doped regime. For an orientation we included the homogeneous charged SC (black solid line). We found that the most stable structure is a CDW state that overlaps a pair ordered superconductor (PDW) as discussed in section 5.2 and that is shown Fig. 5.7). These structures do not contain stripes. The dashed curves in Fig (5.10) represent the saddle point energies of structures that include charge ordered domains characterized by a phase shifted order parameter

as discussed above. For completeness we included graphs for these phase separated structures with two (triangle up) or four (triangle down) domains. We can conclude that the PDW is the ground state and it costs energy to create a phase separation from a PDW state.

Further we conclude that the negative Hubbard  $U$  favors doubly occupied sites and supports the formation of superconductivity in homogeneous and inhomogeneous states. Inhomogeneous, striped states lead to a local increase in superconducting correlations but a phase separation does not appear spontaneously. The inter-site repulsion  $V$  favors the stabilization of charge- and pair-density wave ordering.

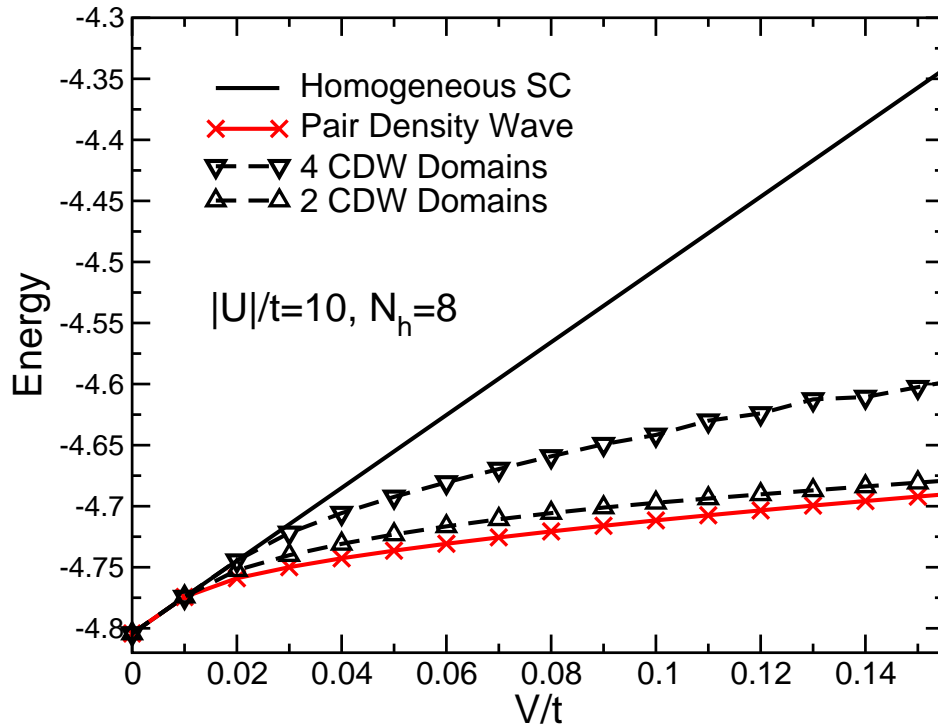


Figure 5.10: Comparison of the energy of homogeneous systems and stripe solutions versus the inter site repulsion  $V/t$ . *Black solid line*: Homogeneous SC. *Red line*: Pair density wave. *Dashed lines*: Domain separated structures.



## Stability Analysis of CDW Domains

Because we found that the holes prefer to be located in the domain walls we investigate the influence of the doping rate to the phase separation for different values of  $V > 0$ . Additionally we present examples where we included next nearest neighbor transitions. The kinetic part of the GA energy functional is modified by finite values of the parameter  $t'/t$ .

We calculate the energy per hole as introduced in Eq. (5.1) as a function of hole concentration in the domain walls.

In view to our previous discussion we have to choose an appropriate reference state to calculate the difference in energy in the case of doping. For this reason we take the PDW at half filling as reference energy  $E_{PDW}$  instead of the homogeneous superconductor. Thus we calculate the binding energy per hole as:  $e_h = (E_{Stripes}(N_h) - E_{PDW})/N_h$ . For different cluster dimensions we calculate the hole doping of the domain walls as:

$$\nu = 1 - \frac{1}{N_{DW}} \sum_{dw} n_i. \quad (5.7)$$

The sum goes over the lattice sites in domain walls.  $N_{DW}$  is the number of lattice sites in the domain walls.

In Fig. (5.11) we present results for different ratios of  $V/t$  and  $t'/t$  where we considered a  $10 \times 10$ -cluster divided into two CDW domains and two domain walls. As outlined in the previous discussion the domains are characterized by different phases of CDW order parameter. The domain walls have weakly but homogeneously charged lattice sites and a homogeneous superconducting order.

We conclude that the inter-site repulsion term favors the formation of domains (5.9). A growing ratio of  $V/t$  supports the stripe formation and the (hole) filling in the domain walls that is shown in the right panel of Fig. (5.11). In the case of  $V = 0$  no phase separation in the CDW channel takes place. A growing ratio of  $U/t$  supports the CDW formation but it acts against the phase separation in the cluster for larger values of  $U$ .

The NNN-interaction  $t'$  supports also the hole concentration in the domain walls. We found that a finite value of  $t'/t$  reduces the width of the domain walls in the small  $U/t$  and small  $V/t$  regime. In contrast to the results for the spin domains [105] we found no evidence for a local minimum of the energy per hole and thus we could not find an optimal stripe filling and doping rate.

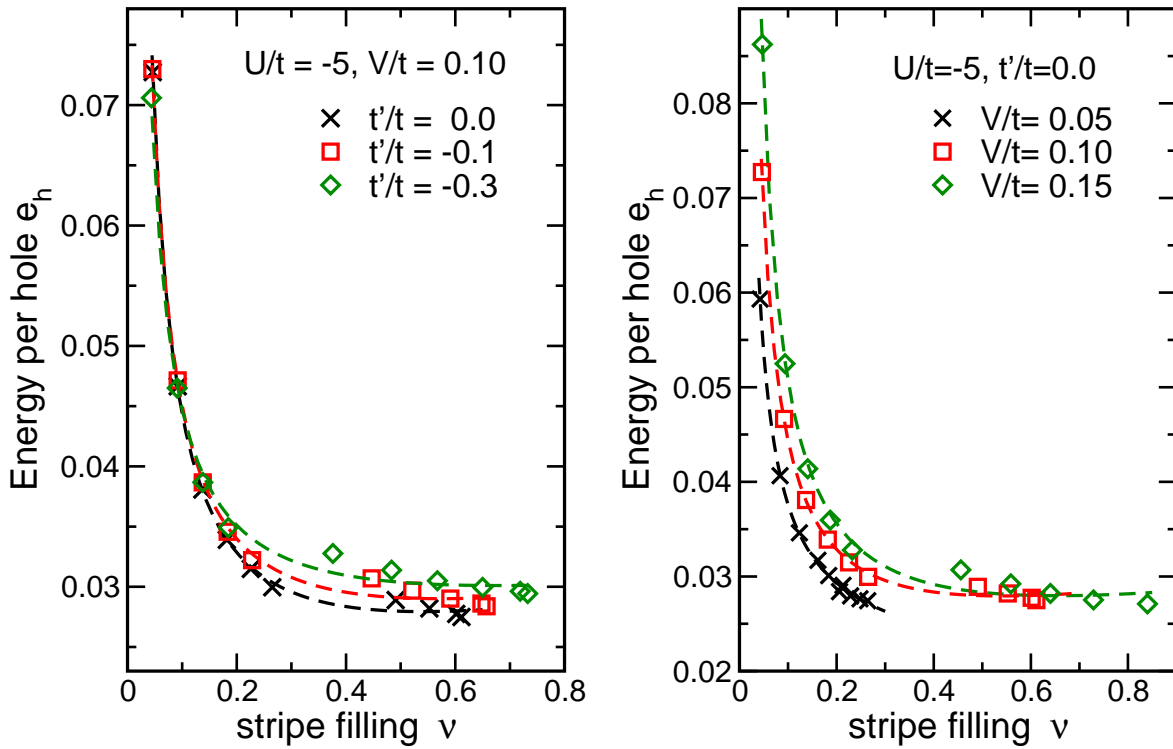


Figure 5.11: Binding energy per hole for stripes in  $y$ -dimension versus the stripe filling for various parameter sets. The dashed lines are the curve fits to guide the eye. The results are given for a  $10 \times 10$  cluster and two SC domain walls.

## 5.4 Vortices and Point-Like Inhomogeneities

Now we like to expand our investigation to point-like inhomogeneities and vortex structures in the framework of the Gutzwiller formalism of the Hubbard model.

The class of high- $T_c$  superconductors are strongly type II and, as such, their phenomenology is dominated by the presence of vortices over most of the phase diagram. The importance of this topic was realized early so that a comprehensive overview is given in [106]. Theoretical publications on the formation of coplanar, spin vortex phases in general have been published some years ago [108–111]. A study on the vortices, particular in framework of the Hubbard model, was done in [112], where the focus lies on vortices in magnetic textures. Motivated by these works we focus on the question if vortex structures play a role in the charge-rotational invariant GA of the Hubbard model.

### Self Trapped Polarons and Single Vortex States

As a first step we study the charge structure around a point-like inhomogeneity (single polarons). We consider a  $7 \times 7$ -cluster where we use open boundary conditions. We prepare a self-trapped polaron by adding an extra electron to a plain CDW state where the SC parameter is zero over the cluster. The density plots of the charge distribution and the  $x$ - $z$ -projection of the vector  $\mathbf{J}_i$  reflecting normal and SC charge is shown in Fig. (5.12). We consider a second structure that includes a single polaron on a CDW together with a local, point-like SC peak in the center of the lattice as shown in Fig. (5.13). At this point we define the SC order parameter locally as the length of the  $x$ - $y$ -projection of the expectation value of the vector  $\mathbf{J}_i$ :

$$\Delta_i^{SC} = \sqrt{\langle J_i^x \rangle^2 + \langle J_i^y \rangle^2}, \quad i = (i_x, i_y), \quad (5.8)$$

As a next step we consider a homogeneous, superconducting order on a homogeneously

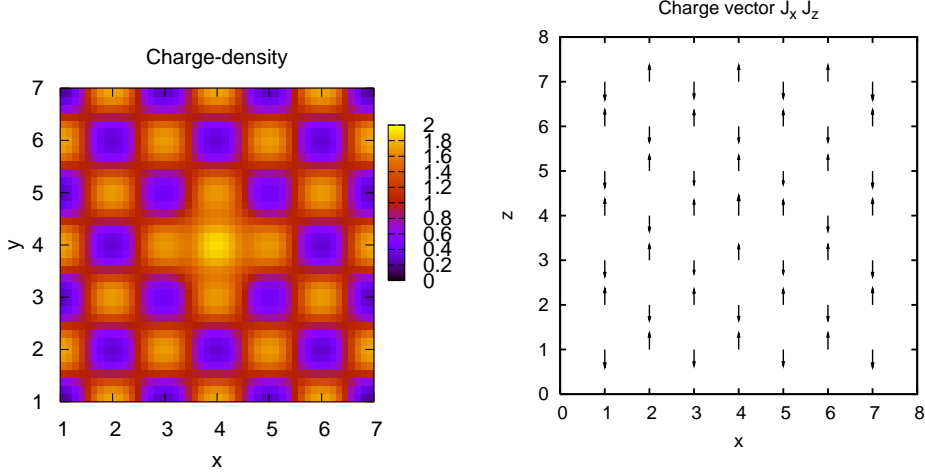


Figure 5.12: Charge density  $n_{i_x, i_y}$  and  $x$ - $z$ -projection of the charge vector  $J_i$  for a self-trapped polaron  $7 \times 7$ -cluster with zero SC. (Results are given for  $N_e = 50$ ,  $U/t = -5$ ,  $V/t = 0$ ,  $t'/t = 0$ .)

charged cluster. We disturb the system locally by adding an extra charge to the lattice where we respect the charge conservation within the whole cluster. In analogy to the magnetic vortices that are discussed in [111, 112] we prepare the structure of a possible vortex solution as follows. We consider a charge flow that rotates around the localized extra charge. At this point we classify two types of solutions namely vortex and anti-vortex configuration. In case of a vortex the current rotates anti-clockwise around the centered charge where in case of an anti-vortex the current rotates clockwise around the core. In Fig. (5.14) we show the  $x$ - $y$ -projection of the vector field  $\mathbf{J}_i$  for the vortex- (top) and the anti-vortex-solution (bottom) on a  $7 \times 7$ -cluster with a total number of electrons of  $N_e = 50$ . In the right-hand-side panels we show the normal current density corresponding to Eq. (3.69) namely  $\mathbf{j}_i^z \sim [\hat{H}, \hat{J}_i^z]$ . The charge density  $n_i$  and the SC order parameter for the vortex corresponding to Eq. (5.8) is shown in Fig. (5.15). Both order parameters approach a constant value in the far field of the vortex.

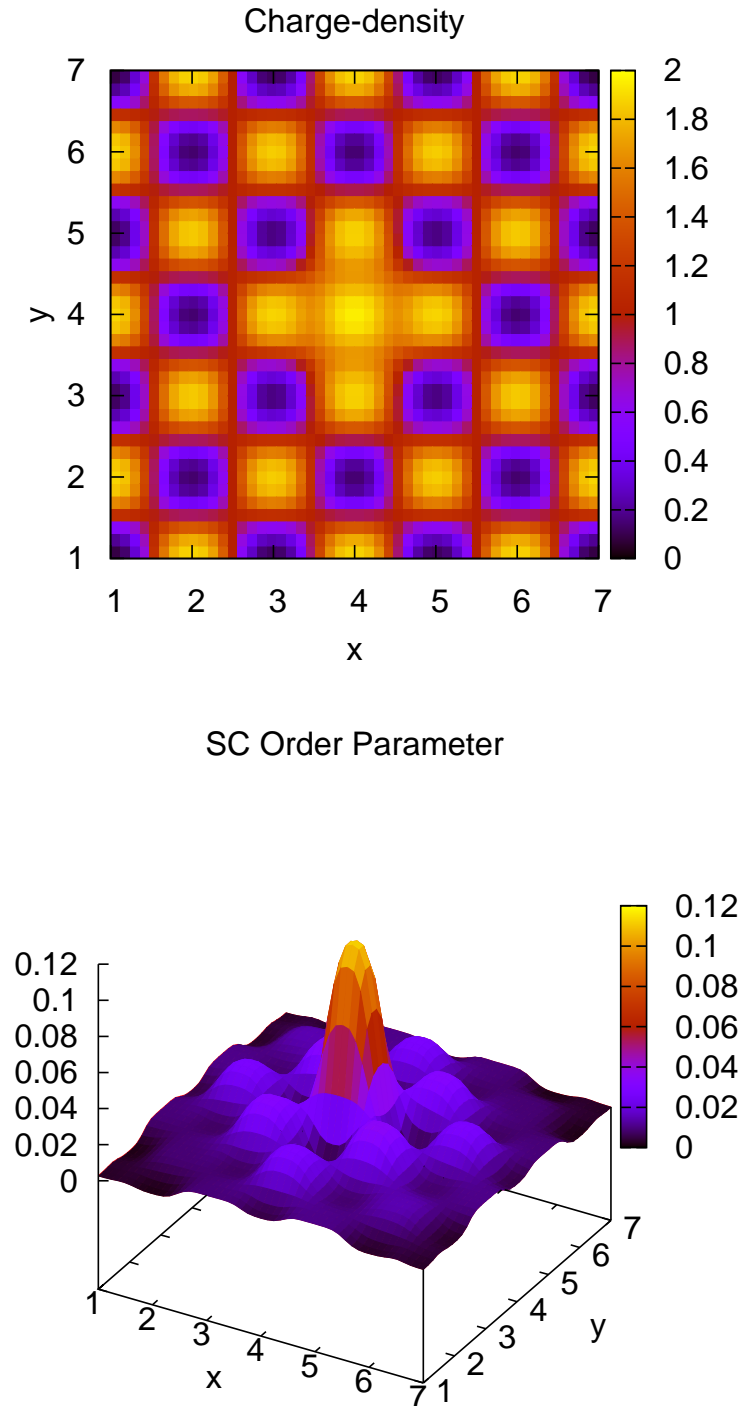


Figure 5.13: Charge structure of a single polaron with local SC. *Top*: charge density  $n_i$ . *Bottom*: local SC order parameter  $\Delta_i^{SC}$ . (Results are given for  $N_e = 50$ ,  $U/t = -10$ ,  $V/t = 0$ ,  $t'/t = 0$ .)

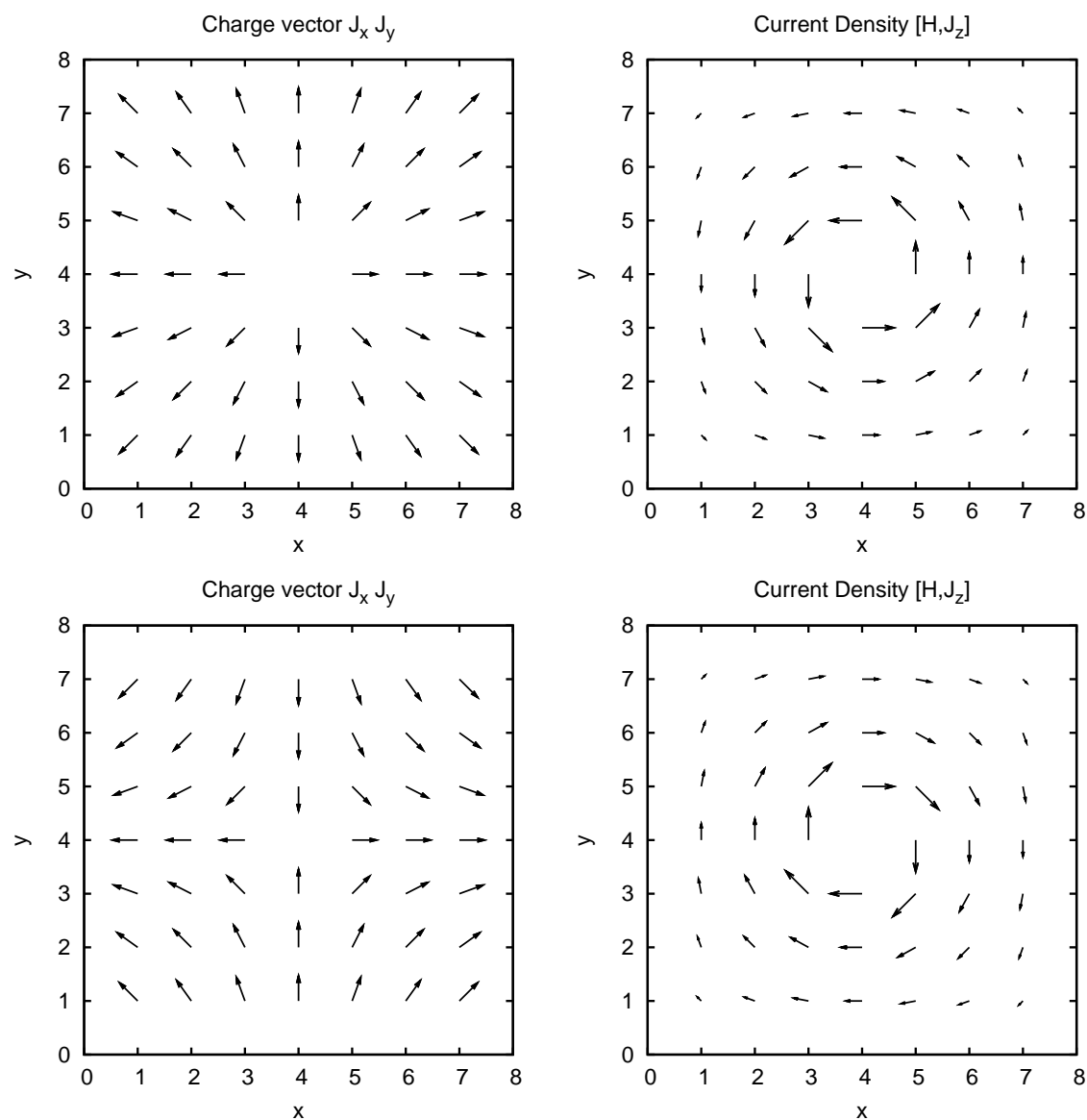


Figure 5.14: Charge and current structure for a vortex (*Top*) and anti-vortex (*Bottom*). *Left-hand-side panels:*  $x$ - $y$ -projection of the charge vector  $\mathbf{J}_i$ . *Right-hand-side panels:* normal current density  $\mathbf{j}^z \sim [H, J_z]$ . The SC order parameter is zero in the center of the (anti-)vortex core. The results are given for a single electron doped into the cluster. ( $U/t = -10$ ,  $N_e = 50$ ,  $V/t = 0$ ,  $t'/t = 0$ )

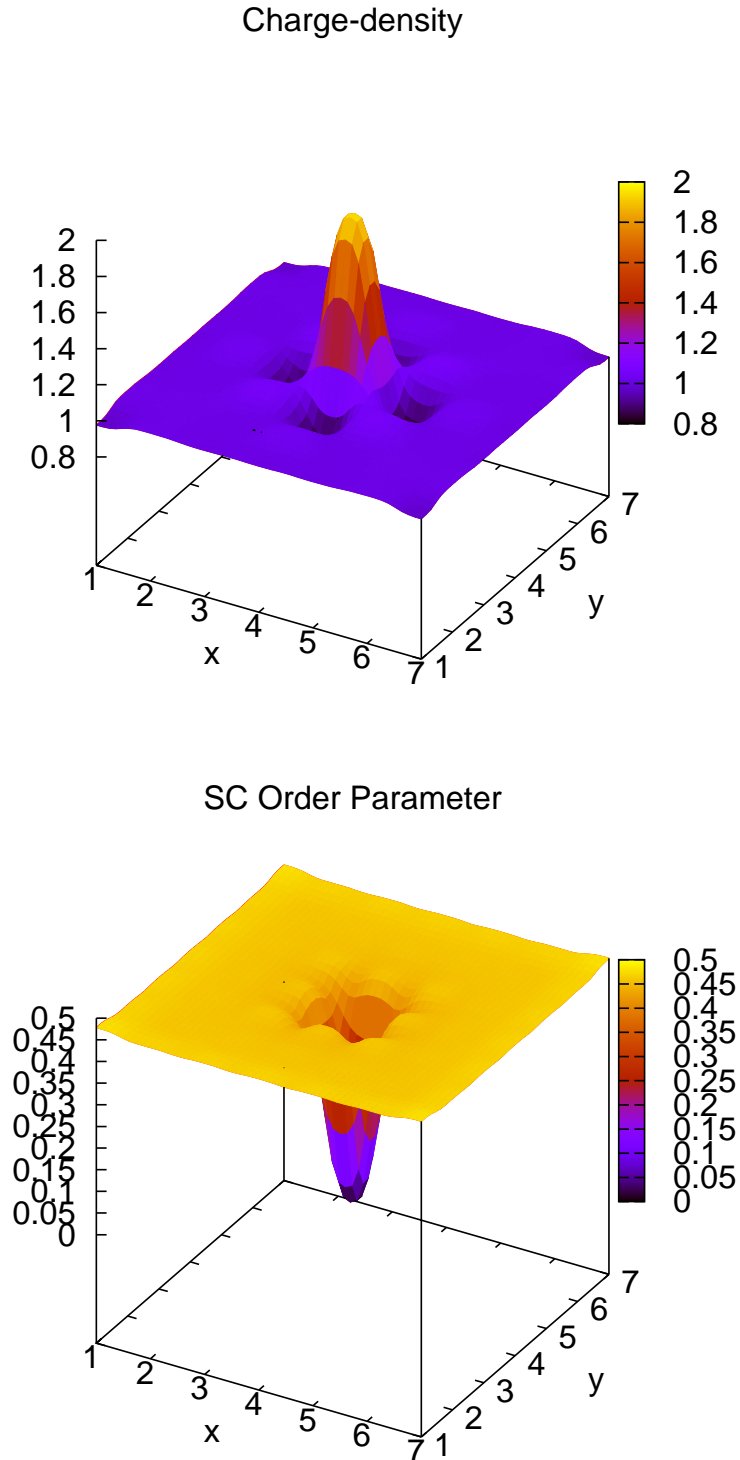


Figure 5.15: Charge structure of a (anti-)vortex state. *Top*: charge density. *Bottom*: local SC order parameter  $\Delta_{ixiy}^{SC}$ . (Results are given for  $N_e = 50$ ,  $U/t = -10$ ,  $V/t = 0$ ,  $t'/t = 0$ .)

## Energy of Vortices

In this section we like to compare the energies of the four different charge distributions that we have presented above. We summarize the total energies for various  $U/t$  in Tab. (5.2). The numerical precision of results is of order  $10^{-2}$ .

| Parameter   | Single Polaron | Single Polaron<br>and SC | Vortex         | Anti Vortex    |
|-------------|----------------|--------------------------|----------------|----------------|
| $U/t = -5$  | $E = -154.865$ | $E = -155.400$           | $E = -155.412$ | $E = -154.796$ |
| $U/t = -8$  | $E = -219.758$ | $E = -219.776$           | $E = -219.711$ | $E = -219.751$ |
| $U/t = -10$ | $E = -245.757$ | $E = -266.074$           | $E = -265.925$ | $E = -265.931$ |

Table 5.2: Comparison of the total energies in units of  $t$  for single a (anti-)vortex and a single polaron in an electron doped  $7 \times 7$ -cluster with  $N_e = 50$ ,  $t'/t$  and  $V/t = 0$ . The point charge is at position  $(4, 4)$ . The precision is to 2nd position after decimal point.

We see from the saddle point energies that the vortex and anti-vortex states are degenerate. For moderate ratios  $U/t$  the results show no significant differences in the energy to the CDW single polaron state. In the large- $U$ -regime (e.g.  $U = -10$ ) we find that the states with SC order are energetically preferred. It has been already discussed in literature that the energy of a single planar vortex has the well known logarithmic dependence on the radius  $R_s$  of the vortex [113]. This is given by the function:

$$e_V = C \ln \left( \frac{R_s}{r_a} \right), \quad (5.9)$$

where  $C$  is a parameter that depends on the charge.  $R_s$  is the radius of the vortex and  $r_a$  is a constant of order of the lattice spacing. This constant ensures that a cutoff appears if the radius becomes smaller than the unit cell.



On this basis we compare the influence of the system size on the energy per hole (electron). We investigate three different structures: In case of an electron doped system we prepare a CDW including a single polaron that is centered in the cluster. The second system is also a single electron doped state where we calculated the energy for a site-centered vortex state.

In case of hole doping we present results for an inter-site centered vortex. For all three structures we calculated the energy per lattice site  $e_d$ . We compare this result with the energy  $e_{SC}$  of a homogeneous charged superconductor at half filling. Finally we calculate the energy per dopant:

$$e_h = \frac{e_d - e_{SC}}{N_d}, \quad (5.10)$$

where  $N_d$  is the number of electrons  $N_e$  in case of electron doping or the number of holes  $N_h$  in case of hole doping.

We present the energy per electron (hole) in dependence of the lattice dimension  $N_x$  for the three different structures in Fig. (5.16). The energies for the electron-doped-single polaron and site-centered vortex structure is presented in the top graphs. The lower graph includes the energy per hole for the inter-site centered vortex. The graphs include curve fittings to guide the eye. In order to illustrate the fitting in our graphs we start with the logarithmic function for the energy per lattice site Eq. (5.9). Obviously the  $x$ -dimension of the cluster is proportional to the radius of the vortex where the lower limit is a system size of  $2 \times 2$ . In our case the minimum radius is  $r_a = 1$  which is the lattice constant. The lower energy limit is  $e_{r_a} \neq 0$ . From Eq. (5.9) we know  $e_V = 0$  for  $R_s = r_a$ . We cannot really identify the lattice dimensions with the vortex radius. For this reason we modify the Eq. (5.9) using  $N_x \sim 2R_s$ . Further we add a correction term  $e_{r_a}$  that ensures that the lower limit of the energy vortex is finite. The vortex energy reads:

$$e_V \sim C \ln \left( \frac{N_x}{2} \right) + e_{r_a}. \quad (5.11)$$

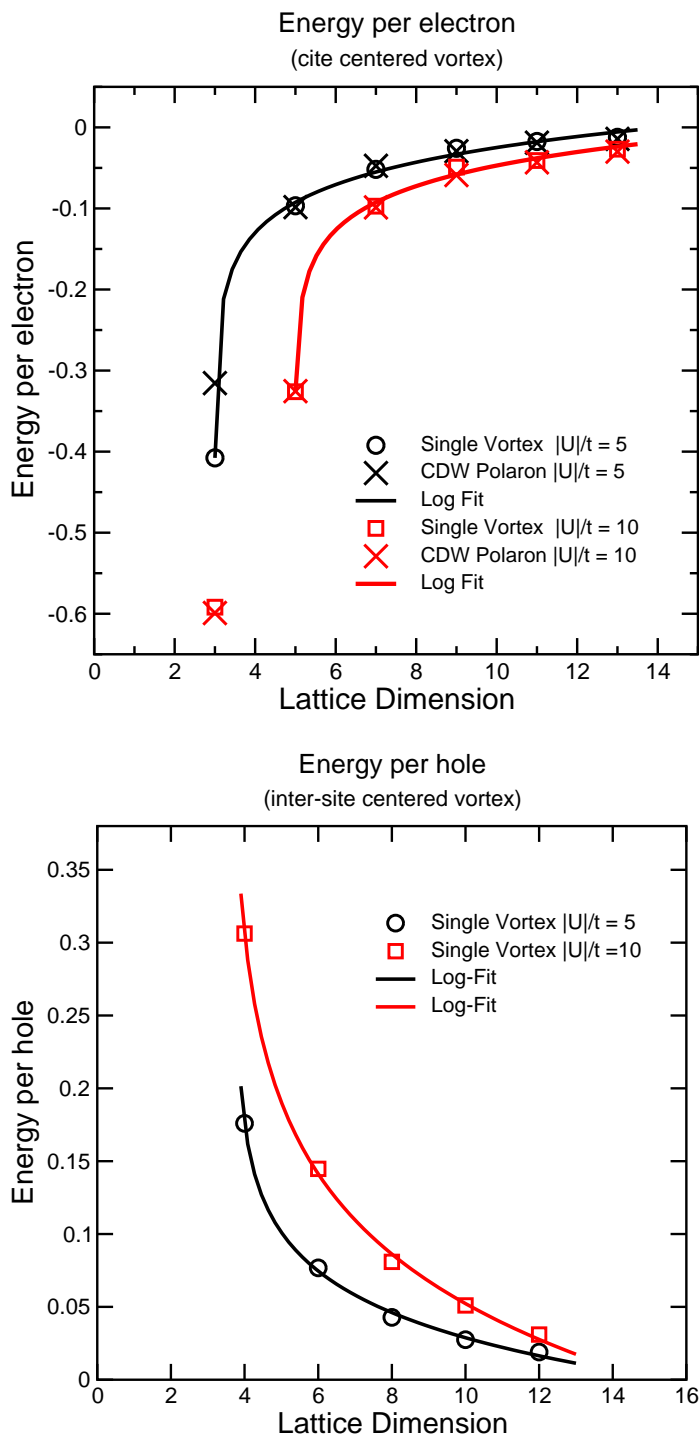


Figure 5.16: *Top*: Energy per electron for single electron doped *site-centered* vortex. *Bottom*: Energy per hole for an under doped *inter-site-centered* vortex ( $V/t = 0$ ,  $t'/t = 0$ ) Eq. (5.10). The lattice dimension is the number of sites  $N_x$  in  $x$ -direction.

In order to keep an equivalent structure of the equation (5.9) we rearrange the equation:

$$e_V = C \ln \left( \frac{1}{2} \exp \left( \frac{e_{r_a}}{C} \right) N_x \right). \quad (5.12)$$

We can now identify the vortex radius as  $R_s = \frac{1}{2} \exp \left( \frac{e_{r_a}}{C} \right) N_x$ .

## Bi-Polarons and Vortex-Anti-Vortex Pairs

In the next part we like to investigate the interplay between two point-like charges trapped in the CDW lattice (bi-polaron) in comparison with localized pairs of a vortex and anti-vortex (VAV-pairs). The interplay between VAV-pairs was discussed in the case of spin textures in [112] where the spin components in the  $x$ - $y$ -plane are given by  $\mathbf{S}_i = S_0 \exp(i\mathbf{Q}\mathbf{R}_i) [\cos(\phi_1 - \phi_2)\mathbf{e}_x - \sin(\phi_1 - \phi_2)\mathbf{e}_y] + S_z\mathbf{e}_z$ .  $\mathbf{Q}$  is the antiferromagnetic wave vector. If one applies the attraction-repulsion transformation (appendix C.2) one obtains the charge field  $\mathbf{J}_i$  of a VAV-pair structure:

$$\mathbf{J}_i = J_0 [\cos(\phi_1 - \phi_2)\mathbf{e}_x - \sin(\phi_1 - \phi_2)\mathbf{e}_y] + \frac{1}{2}(n_i - 1)\mathbf{e}_z, \quad (5.13)$$

where we added the  $z$ -component  $J_i^z = \frac{1}{2}(n_i - 1)$  for the normal charge.  $J^0$  is the length of the  $x$ - $y$ -projection of the charge vector. The parameters  $\phi_1$  and  $\phi_2$  refer to the angles between the  $x$ -axis and the vectors connecting vortex and anti-vortex core and the site  $\mathbf{R}_i$ . An overview of the charge vector field and the normal current is shown in Fig. (5.17) where the VAV-pair is localized at the lattice sites (2, 2) and (5, 5). The distance between the cores is  $\sqrt{18}$  lattice units.

As a next step we like to study the interplay between the vortex and the anti-vortex. We can conclude that an attractive or repulsive interaction exists if the energy of a VAV-pair varies with the relative distance. For this reason we calculated the total energy for VAV-pairs and bi-polarons on a  $6 \times 6$  and a  $10 \times 10$ -cluster in view to the relative distance of the cores in unit of the lattice constant. We summarized the results in Tabs. (5.3).

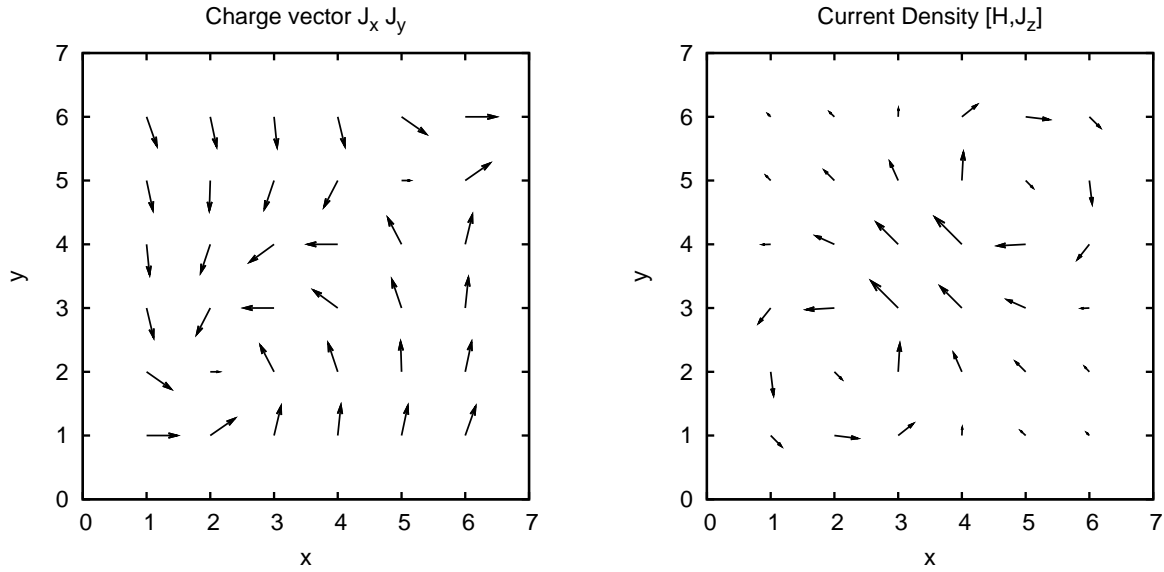


Figure 5.17: *Left:*  $x$ - $y$ -projection of the charge vector  $\mathbf{J}_i$  for a VAV-pair on a  $6 \times 6$ -cluster. *Right* normal current density  $j_i^z$  Eq. (3.69). The results are given for  $N_e = 38$ ,  $U/t = -12$ ,  $V/t = 0$ ,  $t'/t = 0$ .

The GA energies in Tabs. (5.3) are computed up to a precision of  $10^{-3}$ . From the results we can state that the VAV-pair has on average 2% lower energies than the polaron. We notice an increase in the energies with the increasing distance in the same order of magnitude. From our examples we can conclude that there is possibly a small vortex-anti-vortex attraction.

The results give only a very local picture because our numerical method is restricted to a relatively small cluster size of at most  $12 \times 12$  and open boundary conditions. In order to improve our results we now like to include the far field. For this reason we expand the cluster where we have already calculated the GA solution by a symmetric virtual cluster that continues the charge structure. We obtain the vector field  $\mathbf{J}_i$  with help of the analytic expression (5.13). From the discussion of the GA solution we assume that the SC order parameter in (5.8) is conserved in the far field. The far field limit of the

| Distance<br>$d/\sqrt{2}$ | Bi Polaron | VAV-Pair  | Distance<br>$d/\sqrt{2}$ | Bi Polaron | VAV-Pair |
|--------------------------|------------|-----------|--------------------------|------------|----------|
| 1                        | -236.7928  | -237.6420 | 1                        | -640.767   | -641.437 |
| 2                        | -236.8026  | -237.0183 | 2                        | -640.132   | -640.767 |
|                          |            |           | 3                        | -640.134   | -640.378 |
|                          |            |           | 4                        | -640.196   | -640.552 |

Table 5.3: Energies in unit of  $t$  for VAV-pairs and Bi-polarons in dependence of the relative distance in units of lattice spacing. *Left:*  $6 \times 6$ -cluster and  $N_e = 38$ . *Right:*  $10 \times 10$ -cluster and  $N_e = 102$ . (Results are given for:  $U/t = -12$ ,  $t'/t = 0$ ,  $V/t = 0$ . The precision is to the 2nd position after decimal point).

VAV-pair is a homogeneous SC whereas the field of the bi-polaron is continued as a plain CDW. In order to attach the far field continuously we take the value  $J_0$  from the SC order parameter  $\Delta_i^{SC}$  corresponding to Eq. (5.8) from the edge of the GA solution. The local charge density  $n_i$  is calculated continuously respecting the phase of the CDW structure. The energy of the virtual charge distribution is calculated by the classical two-dimensional anisotropic Heisenberg model [113]:

$$E^{Heis} = k \sum_{\langle ij \rangle} \mathbf{J}_i \mathbf{J}_j, \quad (5.14)$$

where  $k$  takes the value of  $4t^2/U$  and  $\mathbf{J}_i$  and  $\mathbf{J}_j$  are the classical values of the charge vector. The total energy per lattice site reads:

$$e = \frac{E^{GA} + E^{Heis}}{N^{tot}}, \quad (5.15)$$

where  $N^{tot}$  is the total number of lattice sites.

In Fig. (5.18) we present the energy per lattice site as a function of the lattice dimension in  $x$ -direction for a VAV-pair and a bi-polaron. The energies converge in both cases to

a constant.

The energies per lattice show that the VAV-solution is preferred in view to the bi-polaron. In the limit of the far field the bi-polaron structure approaches a CDW and the VAV-pair reaches the limit of a homogeneous SC. We derive the limits of the energy densities for the homogeneous SC and for the CDW with the help of the classical, lattice normalized Heisenberg energy  $e^{Heis} = E^{Heis}/N$ .

We use the SC order parameter  $\Delta^{SC}$ , the constant charge  $n$  and the phase of the CDW from our GA solution to continue the charge vectors. We obtain:

$$\mathbf{J}_i^{sc} = \frac{1}{2} \begin{pmatrix} \text{Re}(\Delta^{sc}) \\ \text{Im}(\Delta^{sc}) \\ \delta \end{pmatrix} \quad \text{and} \quad \mathbf{J}_i^{cdw} = \frac{1}{2} (\delta + (-1)^{(i_x+i_y)} \Delta^{ch}) \begin{pmatrix} 0 \\ 0 \\ 1 \end{pmatrix},$$

for the charge fields of the homogeneous SC and the plain CDW. We define  $\delta = \bar{n} - 1$  where  $\bar{n}$  is the average charge per lattice site and  $\Delta^{ch} \in [0, \bar{n}]$  is the charge difference between neighboring lattice sites. Restricting to the 4 nearest neighbors per site the Heisenberg limit of the energy density reads:

$$\begin{aligned} e^{sc} &= 4 \frac{k}{N} \sum_i \frac{1}{4} [(\Delta^{sc})^2 + \delta^2] = k[\delta^2 + (\Delta^{sc})^2] \\ e^{cdw} &= 4 \frac{k}{N} \sum_i \frac{1}{4} [\delta^2 - (\Delta^{ch})^2] = k[\delta^2 - (\Delta^{ch})^2] \end{aligned} \quad (5.16)$$

where  $k = \frac{4t^2}{U}$ . For the negative  $U$  regime we estimate  $e^{sc} < e^{cdw}$ . The energy densities of the Heisenberg system reach a limit with the increasing system size (dashed lines in Fig. (5.18).

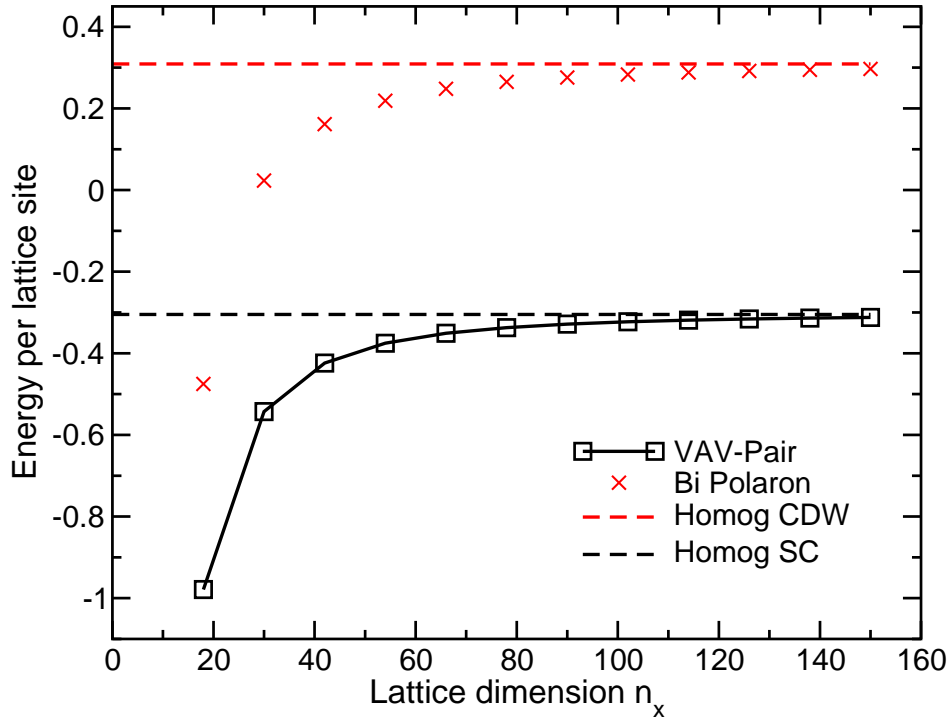


Figure 5.18: Energy per lattice site for the far field of a VAV-pair centered in a two electron doped quadratic cluster. The lattice dimension is the number of lattice sites in  $x$ -direction. (Results for  $U/t = -12$ ,  $V/t = 0$ ,  $t'/t = 0$ ). The dashed lines are the classical Heisenberg limits of a homogeneous CDW and a homogeneous SC state from Eq. (5.16).





## Chapter 6

# Gutzwiller Analysis of the Superfluid Stiffness

Now we like to discuss the response of the system to an external field. This allows to derive criteria whether our solution is metallic, superconducting or insulating. In this chapter we introduce the so-called *superfluid stiffness*  $D_S$ . The superfluid stiffness is comparable to the Drude weight  $D$  that is used to classify a metallic state. The Drude weight measures the ratio of density of mobile charge carriers to their mass whereas the superfluid stiffness measures the ratio of the *superfluid density*  $\rho_S$  to the mass. On the one hand the Drude weight can be derived from the penetration depth from the classical London theory. On the other hand both quantities can be derived in the framework of the linear response theory.

In this chapter we focus on the *superfluid density*  $\rho_S$  and we discuss our superconducting solution in view of this quantity.

## 6.1 Definition and Interpretation of the Superfluid Stiffness

If one discusses superconductivity one has to consider the Meissner-effect where an external magnetic field is repelled from the SC bulk. In the London theory one introduces the penetration depth  $\lambda$ . The inverse square of  $\lambda$  measures the superfluid density. Theoretically there are different ways to introduce this quantity. It can be derived as a constant of proportionality in the incremental free energy upon a twist of the order parameter [114]. Another possibility to derive the superfluid density is based on the linear response to twisted boundary conditions [115]. Yet another method uses certain limits of the current-current function [116, 117].

In the latter method an external vector potential  $\mathbf{A}(\mathbf{r}, t)$  is applied. In the presence of a vector potential the hopping term in the kinetic energy  $\hat{c}_{r+x\sigma}^\dagger \hat{c}_{r\sigma}$  is modified by the so called Peierls phase factors [118]. If the field is oriented along the  $x$ -axis the Peierls phase factors read:  $\sim \exp(iA_x(r))$ . In this case the increase of the ground state energy is proportional to the kinetic energy and the current in  $x$ -direction. In a next step the kinetic energy is expanded and one derives an expression for the paramagnetic current density in  $x$ -direction  $\hat{j}_x^P$ . Finally one calculates the full frequency dependent linear current response produced by the vector potential  $\mathbf{A}$  and one obtains:

$$\Lambda_{xx}(\mathbf{q}, i\omega) = \frac{1}{N} \int_0^\beta d\tau e^{i\omega\tau} \langle \hat{j}_x^P(\mathbf{q}, \tau) \hat{j}_x^P(-\mathbf{q}, 0) \rangle, \quad (6.1)$$

where  $\hat{j}_x^P(\mathbf{q}, \tau)$  is the Fourier transformed current density. One applies  $\omega \rightarrow \omega + i\delta$  as the usual analytic continuation.

The expressions for the so called *superfluid stiffness*  $D_S$  and *Drude weight*  $D$  can be obtained from the different limits of the double Fourier transform of the current-current correlation function  $\Lambda_{xx}$  [117]:

$$\frac{D}{\pi e^2} = -\langle k_x \rangle - \Lambda_{xx}(\mathbf{q} = 0, i\omega \rightarrow 0), \quad (6.2)$$

and a second limit:

$$\frac{D_s}{\pi e^2} = -\langle k_x \rangle - \Lambda_{xx}(q_x = x, q_y \rightarrow 0, i\omega = 0). \quad (6.3)$$

In order to derive this limit one supposes a uniform ( $\mathbf{q} = 0$ ) frequency dependent electric field. One now applies Faraday's and Ohm's law ( $\sigma \mathbf{e} = \mathbf{j}$ ) and thus the current response leads to the frequency dependent uniform conductivity  $\sigma_{xx}$ . For  $T = 0$  in the limit of  $\omega \rightarrow 0$  as in Eq. (6.2) the real part will take the form of a  $\delta$ -function:

$$\text{Re}(\sigma_{xx}) = D\delta(\omega), \quad (6.4)$$

where  $D$  is the Drude weight or charge stiffness [119].

If one requires a *static*, transverse gauge potential: ( $\mathbf{qA}(q, \omega = 0)$ ) the other limit of the current correlation function as in Eq. (6.3) leads to the superfluid stiffness  $D_S$ . In the limit of  $q \rightarrow 0$  the linear current response approaches the superfluid stiffness  $D_S$  [119].

The special requirement to the vector potential  $\nabla \mathbf{A} = \mathbf{qA} = 0$  is the so called London gauge. In the London theory it was shown that the Meissner effect follows if a static ( $\omega = 0$ ), long wave length  $q_y \rightarrow 0$  transverse vector potential is applied. The current density response of a superconductor takes the form  $j_x(q_y) = \frac{1}{4\pi} \frac{1}{\lambda^2} A_x q_y$ . In this case the magnetic field is expelled except for a penetration depth  $\lambda$ . The London equation only holds if one requires the London gauge for the vector potential [120]. The electrical field in the inner of a SC bulk vanishes but it exists a finite current density.

The knowledge of the limits  $D$  and  $D_S$  allows a better understanding of the nature of the solutions. The Drude weight  $D$  measures the ratio of the density of the mobile charge carriers to their mass, whereas the superfluid stiffness  $D_S$  measures the ratio of the superfluid density  $\rho_s$  to the mass. The crucial difference is the order in which the limits  $q \rightarrow 0$  and  $\omega \rightarrow 0$  approach zero. The character of the ground state is given by the values  $D$  and  $D_S$  in the bulk limit. For a superconductor at zero temperature and

disorder one expects finite values for  $D_S$ , and  $D$ . For a normal metal  $D_S = 0$  and  $D$  has to be finite. For an insulating state the superfluid density and the density of normal charge carriers goes to zero and one expects  $D_S = D = 0$  [121]. At finite temperatures this easy classification is not possible. In this case the  $\delta$ -function in Eq. (6.4) smears out and there is  $D = 0$  but  $\sigma_{xx}(\omega = 0)$  remains finite for a metallic system.

A non-zero superfluid stiffness corresponds not only to the Meissner effect it can also be used to estimate the critical temperature. Furthermore the Quantum-Monte-Carlo results [116] prove that  $D$  and  $D_S$  are equal if there is a gap in the system.

An alternative approach to define the superfluid stiffness is discussed in [122]. First, an expression for the *superfluid density*  $\rho_S$  is derived. The superfluid density  $\rho_S$  is related to the superfluid stiffness  $D_S$  via [117]:

$$\rho_S = \frac{D_S}{4\pi e^2}. \quad (6.5)$$

The external disturbance of the system induces a phase twist of the SC order parameter along the  $x$ -direction:  $\Delta(\mathbf{R}) = |\Delta| \exp(i\mathbf{q}\mathbf{R})$  and  $\mathbf{q} = (q_x, 0)$ .

The free energy per lattice site  $f$  depends on the phase twist and can be expanded around the undisturbed ground state in terms of the parameter  $q_x$ . The superfluid density  $\rho_S$  is defined as the second derivative of the free energy per site  $f$  with respect to a phase twist:

$$\rho_S = \frac{\partial^2}{\partial(q_x)^2} f(q_x) \quad (6.6)$$

Thus if the energy can be expressed as a function of  $q_x$  one can derive the superfluid stiffness. In the next section we follow this method in the framework of the GA and we compare our results with HF results presented in [122]. Further more we compare our solution for the superfluid stiffness with the results from the linear current response derived in the framework of the exact Gutzwiller-Monte-Carlo method [116, 117].

## 6.2 Superfluid Stiffness of the Gutzwiller Solution

In our approach we start with a homogeneous superconductor with the energy  $E_0$  that is represented by a homogeneous charge field  $\langle \mathbf{J}_i \rangle$ . We assume that an external field leads to a local twist of the vector field. We derive an analytic expression for the derivative of the energy in dependence of the twist. Further from the calculation we derive an expression for the superfluid density of a homogeneous charged superconductor.

The charge field can be represented by a set of Nambu vectors:

$$\Psi_i^\dagger = (c_{i\uparrow}^\dagger, c_{i\downarrow}^\dagger)^T \quad \text{and} \quad \Psi_i = (c_{i\uparrow}, c_{i\downarrow}). \quad (6.7)$$

We introduce the distortion of the vector field by a local rotation [117] that can be expressed by the unitary transformation:

$$U_i(\varphi_i) = \mathbf{1} \cos\left(\frac{\varphi_i}{2}\right) + i \sin\left(\frac{\varphi_i}{2}\right) \tau \eta. \quad (6.8)$$

The vector  $\eta = (\eta_x, \eta_y, \eta_z)$  is the rotation axis and  $\tau = (\tau_x, \tau_y, \tau_z)$  is an array of the Pauli matrices. We choose a rotation around the  $z$ -axis:  $\eta = e_z$ .

The transformed vector reads  $\Phi_i = U_i^\dagger \Psi_i$ . The choice of the rotation axis leaves the normal charge component  $J_i^z$  constant. The twist disturbs the SC order parameter and we obtain:

$$\tilde{J}_i^x = J_i^x \cos(\varphi_i) - J_i^y \sin(\varphi_i), \quad \tilde{J}_i^y = J_i^y \cos(\varphi_i) + J_i^x \sin(\varphi_i), \quad \tilde{J}_i^z = J_i^z. \quad (6.9)$$

We expand the transformation up to 2nd order:

$$U(\varphi_i) \approx \mathbf{1} + i \frac{\varphi_i}{2} \tau_z - \mathbf{1} \frac{\varphi_i^2}{8}, \quad (6.10)$$

which then is applied to the Hubbard Hamiltonian. The expectation value of the potential energy remains unchanged by the local transformation. The expression for

the kinetic energy reads:

$$T(\varphi) = T_0 + \sum_{ij\sigma} t_{ij} \left( -\frac{1}{8} \varphi_i^2 - \frac{1}{8} \varphi_j^2 + \frac{1}{4} \varphi_i \varphi_j \right) c_{i\sigma}^\dagger c_{j\sigma} - \frac{i}{2} \sum_{ij\sigma} t_{ij} (\varphi_i - \varphi_j) c_{i\sigma}^\dagger c_{j\sigma}. \quad (6.11)$$

We assume that the angular distortion increases by a constant value  $\varphi$  for a translation to nearest lattice site in positive  $x$ -direction:

$$\pm\varphi = \varphi_{i_x, i_y} - \varphi_{i_x \pm 1, i_y} \quad \text{and} \quad \varphi_{i_x, i_y} - \varphi_{i_x, i_y \pm 1} = 0. \quad (6.12)$$

We can now rewrite the kinetic energy in terms of the angular element  $\varphi$ :

$$T(\varphi) = T_0 - \frac{1}{8} \varphi^2 \underbrace{\sum_{i\sigma} \sum_{j=i\pm 1} t_{i,j} c_{i\sigma}^\dagger c_{j\sigma}}_{T_0^x} + \varphi \underbrace{\frac{i}{2} \sum_i \overbrace{\sum_{j=i\pm 1} \sum_{\sigma} t_{i,j} (c_{i\sigma}^\dagger c_{j\sigma} - c_{j\sigma}^\dagger c_{i\sigma})}^{J_{i,\alpha=x}^z}}_{J_{\alpha=x}^z}. \quad (6.13)$$

The expression  $T_0^x$  is the undisturbed kinetic energy in  $x$ -direction.  $J_{i,\alpha=x}^z$  is the current element of the normal charge flow between the lattice sites  $(i_x, i_y)$  and the two nearest neighbors in  $x$ -direction:  $(i_x \pm 1, i_y)$ . If charge transport is allowed along the nearest neighbors in  $x$ -direction the operator of the total current is  $J_{\alpha=x}^z$ . On the one hand the angular distortion of the charge vectors leads to a change in the ground state energy. On the other hand it leads to a normal current along the  $x$ -axis that acts backwards to the system. This current must be included in the final expression for the energy and this can be done by second order perturbation theory. Using the expression of the current operator along  $x$  from Eq. (6.13) one obtains for the energy:

$$E(\varphi) = E_0 - \frac{1}{8} \varphi^2 \langle T_0^x \rangle + \varphi \sum_i \langle J_i^z \rangle - \underbrace{\varphi^2 \sum_{\nu} \frac{\langle 0 | \sum_i J_{i,x}^z | \nu \rangle \langle \nu | \sum_i J_{i,x}^z | 0 \rangle}{E_{\nu} - E_0}}_{2nd\ order\ perturbation\ theory}. \quad (6.14)$$

We require that the total current in the system is zero. The first order perturbation theory does not contribute to the energy. Thus the total current vanishes and the third

term on the right hand side of Eq. (6.14) is zero. We have to evaluate the second order term from the perturbation theory with respect to the current element:

$$J_{i,x}^z = \frac{i}{2} \sum_{j=i\pm 1,\sigma} t_{ij} [c_{i\sigma}^\dagger c_{j\sigma} - c_{j\sigma}^\dagger c_{i\sigma}]. \quad (6.15)$$

If we use the definition of the superfluid density  $\rho_S$  from (6.6) we obtain:

$$\rho_S = -\frac{1}{2} \langle T_0^x \rangle - 2 \sum_{\nu} \frac{\langle 0 | \sum_i J_{x,i}^z | \nu \rangle \langle \nu | \sum_i J_{x,i}^z | 0 \rangle}{E_{\nu} - E_0}. \quad (6.16)$$

The expression for the second order perturbation theory can be evaluated within the time-dependent Gutzwiller approximation (TDGA). In the following we evaluate the superfluid density  $\rho_S$  by numerical methods in the framework of the GA with explicit additional constrains.

In the HF formalism without random-phase-approximation one obtains for the superfluid density:  $\rho_S^{HF} = -\frac{1}{2} \langle T_0^x \rangle$ . We compare our results with the HF results from [122] and exact results from the QMC [116, 117]. We start with a homogeneously charged superconductor on a  $8 \times 8$ -cluster with the homogeneous charge density  $n$ . The complex SC order parameter is defined by  $\Delta_0 = \langle J^x \rangle + i \langle J^y \rangle$ . We require a site-dependent distortion of the SC order parameter along the  $x$ -axis:

$$\Delta_i = |\Delta_0| \exp(i \mathbf{q}_k \mathbf{R}_i), \quad (6.17)$$

where we use the momentum vector:

$$\mathbf{q}_k = \left( \frac{2\pi}{L_x} k, 0 \right) \quad \text{and} \quad k \in \{0, 1, 2, \dots, N_x - 1\}. \quad (6.18)$$

$L_x = a \cdot N_x$  is the system length in  $x$ -direction and  $R_i^x = a \cdot i_x$  is the  $x$ -component of the lattice vector.  $a$  is the lattice constant and set to unity in the following. With the help of Euler's formula we find for the charge vector  $\mathbf{J}_i$  that is twisted along the positive  $x$ -axis:

$$J_i^x = |\Delta_0| \cos \left( \frac{2\pi}{N_x} k \cdot i_x \right), \quad J_i^y = |\Delta_0| \sin \left( \frac{2\pi}{N_x} k \cdot i_x \right), \quad J_i^z = \frac{1}{2}(n - 1). \quad (6.19)$$

The vector  $\mathbf{J}_i$  is rotated by an angular element  $q_k = \frac{2\pi}{N_x}k$  along nearest neighbor translation in  $x$ -direction. In order to fulfill periodic boundary conditions in  $x$ -direction the number of rotations of the vector  $\mathbf{J}_i$  along the lattice can only take integer values. Thus the angular element can only take discrete values. Now we are able to calculate the energy density as a function of the momentum vector  $e = e(k)$ .

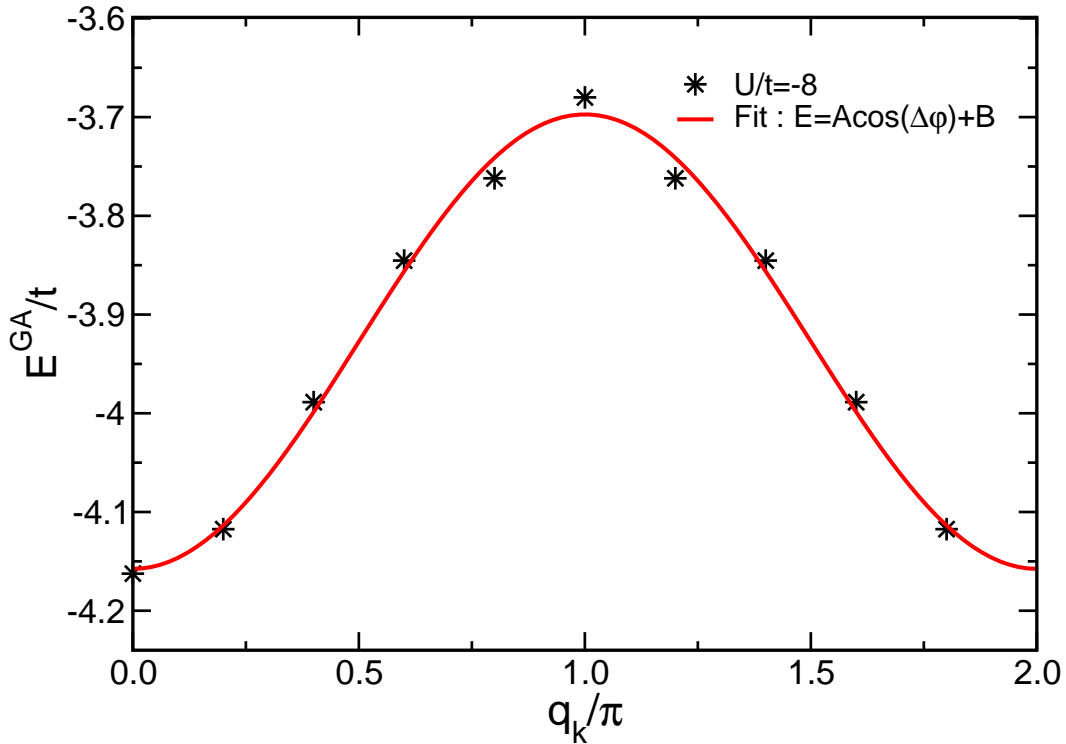


Figure 6.1: Total GA energy as function of local angular distortion  $q_k$  for a  $10 \times 10$ -cluster and  $U/t = -8$  and  $N_h = 8$ . The red curve fits the discrete values of  $q_k$ .

The graph of the energy versus the range of  $q_k$  in (6.18) shows a  $2\pi$ -periodicity of the energy (6.1). For  $q_k = 2\pi$  the vector  $\mathbf{J}_i$  is mapped onto itself by translation from  $i_x$  to  $i_x + 1$ . For  $q_k = \pi$  an alternating order parameter  $\Delta_{i_x, i_y} = (-1)^{i_x} \Delta_0$  is created and the increase in energy reaches a maximum.

We calculate the energy as a function of the twist for a  $8 \times 8$ -cluster. We obtain an



analytic expression for the second derivative of the energy with respect to the angle with the help of a quadratic curve fitting:

$$e(\varphi) = e_0 + \frac{1}{2}\rho_S\varphi^2, \quad (6.20)$$

where  $e_0$  is the energy per lattice site of the homogeneous SC where we use the first three values of  $\varphi$  in a row for the curve fit.

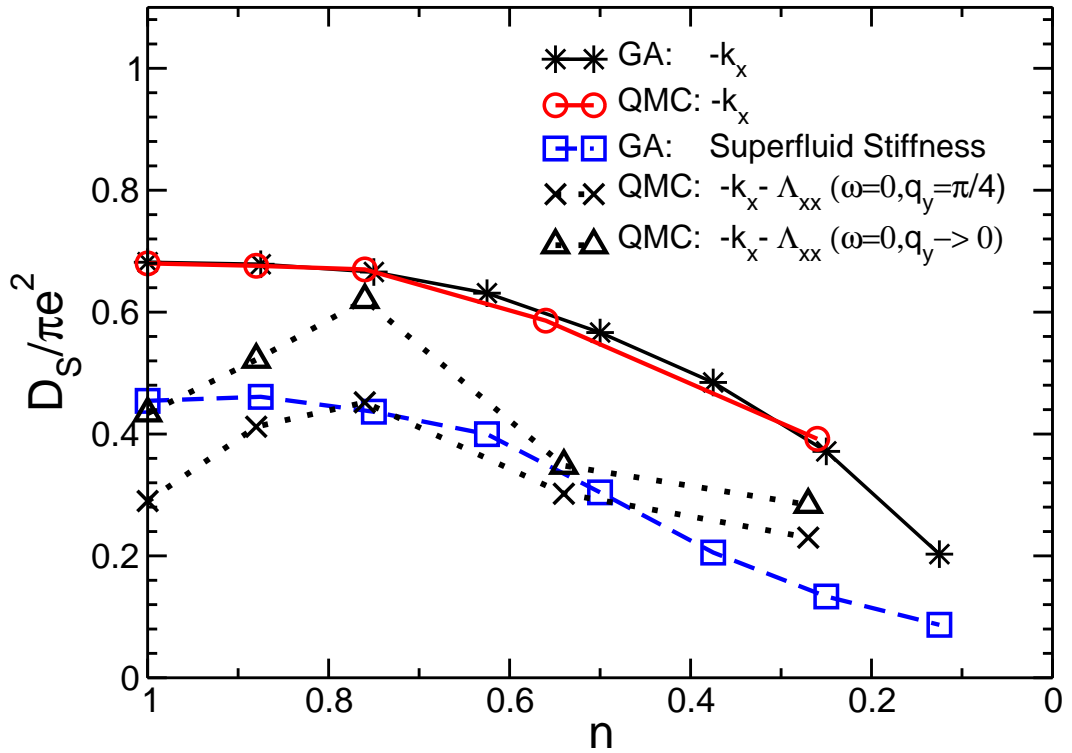


Figure 6.2: Kinetic energy and superfluid density. *Solid black and red line:* kinetic energy contribution to the superfluid density ( [116,117]). *Dashed black graphs:* QMC result for superfluid density (stiffness) using the numerical limits  $\omega = 0$  and  $q_y \rightarrow 0$  from Eq. (6.3). *Blue curve:* Superfluid stiffness of the GA solution using the definition Eq. (6.6). The results are given for  $U/t = -4$  and  $V/t = 0$ .

Alternatively we use the periodicity of the twisted system and fit the values via  $e(\varphi) = A_0 - \rho_S \cos(\varphi^2)$  with  $e_0 = A_0 - \rho_S$ .

In both cases we obtain a set of values for the superfluid density that are presented in Fig. (6.2). We compare the superfluid stiffness  $D_S$  with the QMC results from [116, 117]. *Note:* The superfluid stiffness  $D_S$  and the superfluid density  $\rho_S$  are related via:  $\rho_S = D_S/(4\pi e^2)$ . In Fig. (6.2) the value of  $2\rho_S = D_S/(2\pi e^2)$  is drawn versus the doping [122]. The solid lines show the kinetic part of the GA results from Eq. (6.14) and the QMC results from (6.3) which is one half the density of the kinetic energy in  $x$ -direction:  $\rho_S^{HF} = -\frac{1}{2N}\langle T_0^x \rangle$ . This is the result that one expects in the HF for the superfluid density.

The dotted lines show the QMC results for the full superfluid density where the  $(\omega, q_y \rightarrow 0)$ -limit corresponding to Eq. (6.3) was calculated numerically.

The blue dashed line is twice the value of the second derivative of the disturbed energy density. It corresponds to the superfluid density defined in Eq. (6.6).

The numerical results from the GA with additional constraints do not coincide with the QMC results. It shows that the full response corresponding to Eq. (6.16) has to be taken into account. We calculated the energy while the twisted charge field was fixed. The evaluation of the increase in energy by adding constraints to the system does not respect that the Lagrange multipliers  $\{\lambda_1^1, \dots, \lambda_i^5\}$  are not constant and depend on the distortion angle  $\varphi$ . This leads to a reduction of the numerical value of the superfluid stiffness which can be probably captured by the evaluation of the second order perturbation theory with respect to the current along the  $x$ -direction in Eq. (6.16).

### 6.3 Superfluid Stiffness and Sum Rules

In the next part we like to derive an expression for the superfluid density when the system is modulated by an angular distortion that is not translational invariant. We

express the local rotation angle by a Fourier series:

$$\varphi_i = \frac{1}{N} \sum_q e^{i\mathbf{R}_i \mathbf{q}} \varphi_q, \quad (6.21)$$

with the momentum vector  $\mathbf{q}$  and the angular difference:

$$\varphi_i - \varphi_j = \frac{1}{N} \sum_q (e^{iR_i q} - e^{iR_j q}) \varphi_q. \quad (6.22)$$

Now the local distortion depends on the coordinates and the angular increment is not translational invariant. We transform the creation and destruction operators into momentum representation using:

$$\hat{c}_{i\sigma}^\dagger = \frac{1}{\sqrt{N}} \sum_k e^{-iR_k k} \hat{c}_{k\sigma}^\dagger \quad \text{and} \quad \hat{c}_{i\sigma} = \frac{1}{\sqrt{N}} \sum_k e^{iR_k k} \hat{c}_{k\sigma}. \quad (6.23)$$

The energy Eq. (6.21) with angular perturbation reads in momentum representation:

$$\begin{aligned} E(\varphi) = E_0 &+ \frac{1}{8} \frac{1}{N^2} \sum_{kq\sigma} (\varepsilon_{k+q} + \varepsilon_{k-q} - 2\varepsilon_k) n_{k\sigma} \varphi_q \varphi_{-q} \\ &+ \frac{1}{N} \sum_q \langle \hat{j}_q^z \rangle \varphi_q \\ &- \frac{1}{N^2} \sum_{nq} \varphi_q \frac{\langle 0 | \hat{j}_q^z | n \rangle \langle n | \hat{j}_{-q}^z | 0 \rangle}{E_n - E_0} \varphi_{-q}. \end{aligned} \quad (6.24)$$

We respect the definition Eq. (6.6) for the superfluid density:

$$\rho_s(q) = \frac{1}{4N} \sum_{k\sigma} (\varepsilon_{k+q} + \varepsilon_{k-q} - 2\varepsilon_k) n_{k\sigma} - 2 \left( \frac{1}{N} \sum_n \frac{\langle 0 | \hat{j}_q^z | n \rangle \langle n | \hat{j}_{-q}^z | 0 \rangle}{E_n - E_0} \right), \quad (6.25)$$

where we used  $\varepsilon_k = \sum_j t_{ij} e^{-i(R_i - R_j)k}$ . The last term on the right hand side is the second order perturbation theory.

We transform the current operator  $\hat{j}_i^z = i\frac{1}{2} \sum_{j(i)} t_{ij} (\hat{c}_{i\sigma}^\dagger \hat{c}_{j\sigma} - \hat{c}_j^\dagger \hat{c}_{i\sigma})$  and the charge operator  $\hat{\rho}_i = \frac{1}{2} (\hat{c}_{i\uparrow}^\dagger \hat{c}_{i\uparrow} + \hat{c}_{i\downarrow}^\dagger \hat{c}_{i\downarrow})$  into the  $k$ -space:

$$\hat{j}_i^z = \frac{1}{\sqrt{N}} \sum_q \hat{j}_q^z e^{iR_i q} \quad \text{and} \quad \hat{\rho}_i = \frac{1}{\sqrt{N}} \sum_q \rho_q e^{iR_i q}, \quad (6.26)$$

where we used the short hand notations:

$$\begin{aligned}\hat{j}_q^z &= \frac{i}{2\sqrt{N}} \sum_{k\sigma} (\varepsilon_k - \varepsilon_{k+q}) \hat{c}_{k+q,\sigma}^\dagger \hat{c}_{k,\sigma}, \\ \hat{\rho}_q &= \frac{1}{2\sqrt{N}} \sum_k (\hat{c}_{k\uparrow}^\dagger \hat{c}_{k+q\uparrow} + \hat{c}_{k\downarrow}^\dagger \hat{c}_{k+q\downarrow}).\end{aligned}\quad (6.27)$$

The operators are related via the commutator relation  $[H, \hat{\rho}_q] = i\hat{j}_q^z$ . We find for the perturbation theory in second order:

$$\sum_n \frac{\langle 0 | \hat{j}_q^z | n \rangle \langle n | \hat{j}_{-q}^z | 0 \rangle}{E_0 - E_n} = \sum_n (E_n - E_0) \langle 0 | \hat{\rho}_q | n \rangle \langle n | \hat{S}_{\rho-q}^x | 0 \rangle. \quad (6.28)$$

where  $\hat{S}_{\rho-q}^x$  is the spectral density. An explicit example of the derivation is given in appendix C.3. The right hand side equals the first order spectral weight and can be replaced by:

$$\sum_n (E_n - E_0) \langle 0 | \hat{\rho}_q | n \rangle \langle n | \hat{S}_{\rho-q}^x | 0 \rangle = M_{\rho-q\rho_q}^{(1)} = \langle [\hat{\rho}_{-q}, [H, \hat{\rho}_q]] \rangle. \quad (6.29)$$

We can now use the *sum rules* to calculate the first order spectral weight by using the identity [123, 124]:

$$\frac{1}{\pi} \int d\omega \omega \text{Im}(\chi_{-qq}^z(\omega)) = -\langle [\rho_{-q}, [H, \rho_q]] \rangle, \quad (6.30)$$

where  $\chi_{-qq}^z(\omega)$  is the charge-charge-correlation function. A detailed derivation is given in appendix C.4. With the help of the Eqs. (6.28), (6.29) and (C.20) we obtain the expression:

$$\frac{1}{N} \sum_n \frac{\langle 0 | \sum_i \hat{j}_q^z | n \rangle \langle n | \sum_i \hat{j}_{-q}^z | 0 \rangle}{E_n - E_0} = \frac{1}{\pi} \int d\omega \omega \text{Im}(\chi_{-qq}^z(\omega)), \quad (6.31)$$

with the charge correlation function  $\chi_{-qq}^z(\omega)$  where we use  $[\rho_{-q}, [H, \rho_q]] = [[\rho_q, H], \rho_{-q}] = [[\rho_{-q}, H], \rho_q]$ .

As an example we apply the formula to the free system and we obtain for the susceptibility of the non-interacting system:

$$\begin{aligned}
\chi_{-qq}^{z0}(\omega) &= \langle\langle \hat{\rho}_{-q}; \hat{\rho}_q \rangle\rangle \\
&= \frac{1}{4N} \sum_{kk'\sigma\sigma'} \langle\langle c_{k\sigma}^\dagger c_{k-q\sigma}, c_{k\sigma'}^\dagger c_{k+q\sigma'} \rangle\rangle \\
&= \frac{1}{4N} \lim_{\delta \rightarrow 0} \sum_{k\sigma} \frac{(n_{k+q\sigma} - n_{k\sigma})}{\omega - (\varepsilon_k - \varepsilon_{k+q}) + i\delta}.
\end{aligned} \tag{6.32}$$

In the HF formulation one derives  $\chi_{-qq}^z(\omega) \sim \chi_{-qq}^{z0}(\omega)/[1 - U\chi_{-qq}^{z0}(\omega)]$  for the susceptibility of the interacting system. In the case of a free system we obtain for the imaginary part of (6.32):

$$\text{Im} \{ \chi_{-qq}^{z0}(\omega) \} = \frac{1}{4N} \lim_{\delta \rightarrow 0} \sum_{k\sigma} \frac{-\delta}{(\omega - (\varepsilon_k - \varepsilon_{k+q}))^2 + \delta^2} \times (n_{k+q\sigma} - n_{k\sigma}). \tag{6.33}$$

In order to solve the integral in the limit  $\delta \rightarrow 0$  we replace the  $\delta$ -function by the limit of the Lorentzian:

$$\lim_{\mu \rightarrow 0} \frac{\mu}{t^2 + \mu^2} = \pi \delta(t). \tag{6.34}$$

Finally we find with help of Eq. (6.33) for the integral over the imaginary part of the susceptibility:

$$\begin{aligned}
\frac{1}{\pi} \int d\omega \omega \text{Im}(\chi_{-qq}^{z0}(\omega)) &= \frac{1}{\pi} \frac{1}{4N} \sum_{k\sigma} \int d\omega \omega \text{Im} \left\{ \lim_{\delta \rightarrow 0} \left( \frac{(n_{k+q\sigma} - n_{k\sigma})}{\omega - \varepsilon_{k+q} + \varepsilon_k + i\delta} \right) \right\} \\
&= -\frac{1}{4N} \sum_{k\sigma} (n_{k+q\sigma} - n_{k\sigma}) \times \int d\omega \omega \delta(\omega - (\varepsilon_k - \varepsilon_{k+q})) \\
&= -\frac{1}{4N} \sum_{k\sigma} (2\varepsilon_k - \varepsilon_{k+q} - \varepsilon_{k-q}) n_{k\sigma}.
\end{aligned} \tag{6.35}$$

With the expression (6.25) we obtain for the superfluid density:

$$\rho_S(q) = \frac{1}{4N} \sum_{k\sigma} (2\varepsilon_k - \varepsilon_{k+q} - \varepsilon_{k-q}) n_{k\sigma}. \tag{6.36}$$

The superfluid density depends only on the dispersion  $\varepsilon_k$  which can be expanded in a Taylor series:

$$\varepsilon(\mathbf{k} \pm \mathbf{q}) = \varepsilon(\mathbf{k}) \pm \nabla \varepsilon(\mathbf{k}) \mathbf{q} + \frac{1}{2!} \sum_{\alpha\beta} \partial_\alpha \partial_\beta \varepsilon(\mathbf{k}) q_\alpha q_\beta \pm \dots \quad (6.37)$$

Now we assume a two dimensional lattice and we restrict to nearest neighbor hoppings with the dispersion:  $\varepsilon_k = -2t[\cos(k_x) + \cos(k_y)]$ . All non-diagonal derivative in the expansion vanish and we obtain:

$$\varepsilon(\mathbf{k} + \mathbf{q}) + \varepsilon(\mathbf{k} - \mathbf{q}) = 4t \cos(k_x) \sum_{m=0}^{\infty} \frac{q_x^{2m}}{(2m)!} + 4t \cos(k_y) \sum_{m=0}^{\infty} \frac{q_y^{2m}}{(2m)!}. \quad (6.38)$$

All odd derivatives vanish. We replace the power series of  $(q_x, q_y)$  by the cosine function. Now we can write for the superfluid density:

$$\begin{aligned} \rho_S^{NN}(q) &= -\frac{1}{2N} \sum_{k\sigma} \varepsilon_k n_{k\sigma} \\ &+ \frac{1}{2N} \cos(q_x) \sum_{k\sigma} 2t \cos(k_x) n_{k\sigma} + \frac{1}{2N} \cos(q_y) \sum_{k\sigma} 2t \cos(k_y) n_{k\sigma}, \end{aligned} \quad (6.39)$$

or in terms of the kinetic energy we finally obtain:

$$\rho_S^{NN}(q) = -\frac{1}{2N} \left[ T_0 - T_x \cos(q_x) - T_y \cos(q_y) \right], \quad (6.40)$$

where we use  $T_x = \sum_{k\sigma} 2t \cos(k_x) n_{k\sigma}$  and  $T_y = \sum_{k\sigma} 2t \cos(k_y) n_{k\sigma}$  for the free kinetic energies in  $x$ - and  $y$ -direction that are harmonically modulated by the vector  $\mathbf{q}$ .

## Summary and Conclusion

In this work we investigated a charge-rotationally invariant Gutzwiller approach to the Hubbard model. We derived the Gutzwiller variational energy functional and calculated various states from the saddle point solution in the attractive ( $U < 0$ ) regime. Motivated by different experimental findings that we discussed in chapter one we tried to answer the question whether pair correlations from broken symmetry states in the framework of the charge-rotational GA of the Hubbard model can be found.

As a first test we investigated the instability of a normal system towards SC in the framework of the time dependent Gutzwiller approximation (TDGA). From the expansion of the free energy functional we derived criteria for a phase transition from the normal to the superconducting phase in the paramagnetic regime. We calculated the critical temperature for an infinite dimensional lattice in good agreement with QMC data [96]. In contrast to the BCS theory our results showed that the charge-rotational TDGA can capture at least qualitatively the crossover from weak to strong coupling.

As a next step we investigated finite dimensional systems. We presented results for homogeneous superconducting and for charge-ordered states. We discussed the GA results in comparison with the HF approximation where we worked out the formal differences. The numerical investigations showed that the difference is mainly in the crossover from the weak to the strong coupling. In a next step we derived an effective Hamiltonian on top of the saddle point solution. We analyzed the effective Hamiltonian which has a BCS-like structure and we derived an expression for the gap in a self consistent formulation and we identified an effective potential. We verified the results by numerical calculations.

Motivated by different experimental works on  $d$ -wave symmetric  $k$ -dependent SC gaps we focussed on the question whether states including non-local pair correlations could be a solution of the GA and how does this correlation lower the energy. Restricting

to the positive- $U$  regime we discussed the formal requirements to the solution in view of a coexisting spin order and the interplay of local and non-local pair-order. Our numerical results showed that non-local pair correlations do not minimize the GA energy functional.

As a next step we prepared inhomogeneous solutions in the normal and in the extended Hubbard model including an additional inter-site interaction  $V$ . We presented inhomogeneous solutions that are characterized by stripe-shaped domains where the parameters for charge- and pair ordering change their phase or their amplitude. We found no spontaneous symmetry breaking with regard to stripe formation. The preparation of stripes costs energy and a stability analysis of the stripes based on the energy showed that the stripes are unstable with respect to a stripe-less ground state. In contrast to stripe formation in the spin ordered systems (for  $U > 0$ ) we could not calculate an energetically optimal doping rate or stripe filling.

In case of  $V > 0$  it turned out that a pair density wave (PDW) without stripes is the ground state.

In this work we presented also results on simple point like inhomogeneities namely polarons and (anti-)vortices on a finite cluster. We could determine a good agreement of our numerical results with the logarithmic dependence of the energy of the vortex state with respect to the vortex radius as well as possible attraction between vortex-anti-vortex pairs.

In the last chapter of this work we discussed the stability of solutions in view of superfluid stiffness. We gave a short overview on different analytical approaches to this quantity. We presented a derivation based on an expansion of the energy in view of an angular distortion of the charge vector field. The expression that we found includes terms from second order perturbation theory that can be evaluated within the time-dependent Gutzwiller approximation which is not covered by this work. Instead we presented results for the superfluid stiffness by numerical methods in the framework



of the GA with explicit additional constraints. In comparison with exact (QMC) results our approach turned out to be in good quantitative and qualitative agreement. A quantitative analysis of the superfluid stiffness in the framework of the TDGA will probably lead to better agreement with the exact results.

For an outlook we state that our investigation of phase instabilities are first results and can be taken as a motivation for more detailed studies. The TDGA method that we applied for the calculation of phase instabilities and critical temperatures in the hypercubic lattice can be applied to finite dimensional systems in the normal and extended Hubbard model. We mentioned that Gutzwiller analysis of the superfluid stiffness can also be proceeded in the framework of the TDGA.

The preparation of 'stripes' in the negative  $U$  regime was one of the main topics of this work. Interesting questions can rise from a combination of adjacent domains that are characterized by of positive and negative  $U$ .



# Appendix A

## A.1 Notation and Conventions

### Pauli Matrices

In 3.7 made use of the Pauli matrices to define the charge vector. The Pauli matrices hold explicitly:

$$\tau_x = \begin{pmatrix} 0 & 1 \\ 1 & 0 \end{pmatrix}, \quad \tau_y = i \begin{pmatrix} 0 & -1 \\ 1 & 0 \end{pmatrix}, \quad \tau_z = \begin{pmatrix} 1 & 0 \\ 0 & -1 \end{pmatrix}. \quad (\text{A.1})$$

### Frequently used Commutators

The fermionic field operators obey the following canonical anti-commutation relations:

$$[\hat{c}_{i\sigma}, \hat{c}_{j\sigma'}]_+ = 0, \quad [\hat{c}_{i\sigma}^\dagger, \hat{c}_{j\sigma'}^\dagger]_+ = 0 \quad \text{and} \quad [\hat{c}_{i\sigma}, \hat{c}_{j\sigma'}^\dagger]_+ = \delta_{ij}\delta_{\sigma\sigma'}, \quad (\text{A.2})$$

The resulting commutator relations read then:

$$\begin{aligned} [\hat{c}_{i\sigma}, \hat{c}_{j\sigma'}]_- &= 2\hat{c}_{i\sigma}\hat{c}_{j\sigma'} \\ [\hat{c}_{i\sigma}^\dagger, \hat{c}_{j\sigma'}^\dagger]_- &= 2\hat{c}_{i\sigma}^\dagger\hat{c}_{j\sigma'}^\dagger \\ [\hat{c}_{i\sigma}, \hat{c}_{j\sigma'}^\dagger]_- &= 2\hat{c}_{i\sigma}\hat{c}_{j\sigma'}^\dagger - \delta_{ij}\delta_{\sigma\sigma'}. \end{aligned} \quad (\text{A.3})$$

For composed operators we list a set of useful commutator relations:

$$\begin{aligned}
[\hat{c}_{i\sigma'}, \hat{c}_{l\sigma}^\dagger \hat{c}_{k\sigma}]_- &= \delta_{il} \delta_{\sigma\sigma'} \hat{c}_{k\sigma} & [\hat{c}_{i\sigma'}^\dagger, \hat{c}_{l\sigma}^\dagger \hat{c}_{k\sigma}]_- &= -\delta_{ik} \delta_{\sigma\sigma'} \hat{c}_{l\sigma}^\dagger & (A.4) \\
[\hat{c}_{i\sigma'}, \hat{c}_{l\sigma} \hat{c}_{k\sigma}^\dagger]_- &= -\delta_{ik} \delta_{\sigma\sigma'} \hat{c}_{l\sigma} & [\hat{c}_{i\sigma'}^\dagger, \hat{c}_{l\sigma} \hat{c}_{k\sigma}^\dagger]_- &= -\delta_{ik} \delta_{\sigma\sigma'} \hat{c}_{l\sigma} \\
[\hat{c}_{i\sigma'}, \hat{c}_{l\sigma} \hat{c}_{k\sigma}]_- &= 0 & [\hat{c}_{i\sigma'}, \hat{c}_{l\sigma}^\dagger \hat{c}_{k\sigma}^\dagger]_- &= \delta_{il} \delta_{\sigma\sigma'} \hat{c}_{k\sigma}^\dagger - \delta_{ik} \delta_{\sigma\sigma'} \hat{c}_{l\sigma}^\dagger \\
[\hat{c}_{i\sigma'}^\dagger, \hat{c}_{l\sigma}^\dagger \hat{c}_{k\sigma}^\dagger]_- &= 0 & [\hat{c}_{i\sigma'}^\dagger, \hat{c}_{l\sigma} \hat{c}_{k\sigma}]_- &= \delta_{il} \delta_{\sigma\sigma'} \hat{c}_{k\sigma} - \delta_{ik} \delta_{\sigma\sigma'} \hat{c}_{l\sigma}
\end{aligned}$$

In the case of  $l = k$  we obtain the commutators with number operator:

$$[\hat{c}_{i\sigma'}, \hat{n}_{k\sigma}]_- = \delta_{ik} \delta_{\sigma\sigma'} \hat{c}_{k\sigma}, \quad \text{and} \quad [\hat{c}_{i\sigma'}^\dagger, \hat{n}_{k\sigma}]_- = -\delta_{ik} \delta_{\sigma\sigma'} \hat{c}_{k\sigma}^\dagger. \quad (A.5)$$

For the commutation of pairs of fermionic operators we use the general formula:

$$[\hat{c}_{k_1\sigma_1}^\dagger \hat{c}_{k_2\sigma_2}, \hat{c}_{k_3\sigma_3}^\dagger \hat{c}_{k_4\sigma_4}]_- = \delta_{k_2k_3} \delta_{\sigma_2\sigma_3} \hat{c}_{k_1\sigma_1}^\dagger \hat{c}_{k_4\sigma_4} - \delta_{k_1k_4} \delta_{\sigma_1\sigma_4} \hat{c}_{k_3\sigma_3}^\dagger \hat{c}_{k_2\sigma_2}. \quad (A.6)$$

In terms of the number operators:  $\hat{n}_{l\uparrow} = \hat{c}_{l\uparrow}^\dagger \hat{c}_{l\uparrow}$  and  $\hat{n}_{l\downarrow} = \hat{c}_{l\downarrow}^\dagger \hat{c}_{l\downarrow}$  we obtain explicitly:

$$\begin{aligned}
[\hat{c}_{i\uparrow}^\dagger \hat{c}_{j\uparrow}, \hat{n}_{l\uparrow}]_- &= \delta_{lj} \hat{c}_{i\uparrow}^\dagger \hat{c}_{l\uparrow} & [\hat{c}_{i\uparrow}^\dagger \hat{c}_{j\uparrow}, \hat{n}_{l\downarrow}]_- &= -\delta_{li} \hat{c}_{i\uparrow}^\dagger \hat{c}_{j\uparrow} & (A.7) \\
[\hat{c}_{i\downarrow}^\dagger \hat{c}_{j\downarrow}, \hat{n}_{l\uparrow}]_- &= \delta_{lj} \hat{c}_{i\downarrow}^\dagger \hat{c}_{l\downarrow} & [\hat{c}_{i\downarrow}^\dagger \hat{c}_{j\downarrow}, \hat{n}_{l\downarrow}]_- &= -\delta_{li} \hat{c}_{i\downarrow}^\dagger \hat{c}_{j\downarrow} \\
[\hat{c}_{i\uparrow}^\dagger \hat{c}_{j\downarrow}^\dagger, \hat{n}_{l\uparrow}]_- &= -\delta_{li} \hat{c}_{i\uparrow}^\dagger \hat{c}_{j\downarrow}^\dagger & [\hat{c}_{i\uparrow}^\dagger \hat{c}_{j\downarrow}^\dagger, \hat{n}_{l\downarrow}]_- &= -\delta_{lj} \hat{c}_{i\uparrow}^\dagger \hat{c}_{l\downarrow}^\dagger \\
[\hat{c}_{i\downarrow}^\dagger \hat{c}_{j\uparrow}^\dagger, \hat{n}_{l\uparrow}]_- &= \delta_{lj} \hat{c}_{i\downarrow}^\dagger \hat{c}_{l\uparrow}^\dagger & [\hat{c}_{i\downarrow}^\dagger \hat{c}_{j\uparrow}^\dagger, \hat{n}_{l\downarrow}]_- &= \delta_{li} \hat{c}_{i\downarrow}^\dagger \hat{c}_{l\uparrow}^\dagger
\end{aligned}$$

In terms of the ladder operators:  $\hat{J}_l^+ = \hat{c}_{l\uparrow}^\dagger \hat{c}_{l\downarrow}^\dagger$  and  $\hat{J}_l^- = \hat{c}_{l\downarrow} \hat{c}_{l\uparrow}$  we obtain explicitly:

$$\begin{aligned}
[\hat{c}_{i\uparrow}^\dagger \hat{c}_{j\uparrow}, \hat{J}_l^+]_- &= \delta_{lj} \hat{c}_{i\uparrow}^\dagger \hat{c}_{l\downarrow}^\dagger & [\hat{c}_{i\uparrow}^\dagger \hat{c}_{j\uparrow}, \hat{J}_l^-]_- &= -\delta_{li} \hat{c}_{i\downarrow} \hat{c}_{j\uparrow} & (A.8) \\
[\hat{c}_{i\downarrow}^\dagger \hat{c}_{j\downarrow}, \hat{J}_l^+]_- &= \delta_{lj} \hat{c}_{i\uparrow}^\dagger \hat{c}_{i\downarrow}^\dagger & [\hat{c}_{i\downarrow}^\dagger \hat{c}_{j\downarrow}, \hat{J}_l^-]_- &= -\delta_{li} \hat{c}_{j\downarrow} \hat{c}_{l\uparrow} \\
[\hat{c}_{i\uparrow}^\dagger \hat{c}_{j\downarrow}^\dagger, \hat{J}_l^+]_- &= 0 & [\hat{c}_{i\uparrow}^\dagger \hat{c}_{j\downarrow}^\dagger, \hat{J}_l^-]_- &= \delta_{lj} \hat{c}_{i\uparrow}^\dagger \hat{c}_{l\uparrow} - \delta_{li} \hat{c}_{i\downarrow} \hat{c}_{j\downarrow}^\dagger \\
[\hat{c}_{i\downarrow}^\dagger \hat{c}_{j\uparrow}^\dagger, \hat{J}_l^+]_- &= \delta_{lj} \hat{c}_{i\downarrow} \hat{c}_{l\downarrow}^\dagger - \delta_{li} \hat{c}_{i\uparrow}^\dagger \hat{c}_{j\uparrow} & [\hat{c}_{i\downarrow}^\dagger \hat{c}_{j\uparrow}^\dagger, \hat{J}_l^-]_- &= 0.
\end{aligned}$$

The commutators of the spin operators  $\hat{S}_l^+ = \hat{c}_{l\uparrow}^\dagger \hat{c}_{l\downarrow}$  and  $\hat{S}_l^- = \hat{c}_{l\downarrow}^\dagger \hat{c}_{l\uparrow}$  and the double occupancy operator  $\hat{n}_{i\uparrow} \hat{n}_{i\downarrow} = \hat{c}_{i\uparrow}^\dagger \hat{c}_{i\uparrow} \hat{c}_{i\downarrow}^\dagger \hat{c}_{i\downarrow}$  must vanish because:

$$\begin{aligned} [\hat{n}_{i\uparrow} \hat{n}_{i\downarrow}, \hat{S}_l^+]_- &= \delta_{il} (\hat{c}_{l\uparrow}^\dagger \hat{c}_{l\uparrow}^\dagger \hat{c}_{l\downarrow} \hat{c}_{l\uparrow} - \hat{c}_{l\downarrow}^\dagger \hat{c}_{l\uparrow}^\dagger \hat{c}_{l\downarrow} \hat{c}_{l\downarrow}) \\ [\hat{n}_{i\uparrow} \hat{n}_{i\downarrow}, \hat{S}_l^-]_- &= \delta_{il} (\hat{c}_{l\downarrow}^\dagger \hat{c}_{l\downarrow}^\dagger \hat{c}_{l\uparrow} \hat{c}_{l\downarrow} - \hat{c}_{l\uparrow}^\dagger \hat{c}_{l\downarrow}^\dagger \hat{c}_{l\uparrow} \hat{c}_{l\uparrow}). \end{aligned} \quad (\text{A.9})$$

Because the operator products  $\hat{c}_{l\sigma}^\dagger \hat{c}_{l\sigma}^\dagger$  and  $\hat{c}_{l\sigma} \hat{c}_{l\sigma}$  violate the Pauli law the commutators (A.9) project any state onto 0.

## Density Matrix

Define the density matrix operator:

$$\hat{B} = \sum_i [\Delta_i (\hat{c}_{i\uparrow}^\dagger \hat{c}_{i\downarrow}^\dagger - \hat{c}_{i\downarrow}^\dagger \hat{c}_{i\uparrow}^\dagger) + \Delta_i^* (\hat{c}_{i\downarrow} \hat{c}_{i\uparrow} - \hat{c}_{i\uparrow} \hat{c}_{i\downarrow})] + \sum_{i\sigma} n_{i\sigma} (\hat{c}_{i\sigma}^\dagger \hat{c}_{i\sigma} - \hat{c}_{i\sigma} \hat{c}_{i\sigma}^\dagger). \quad (\text{A.10})$$

If we wish to distinguish between operators and expectation values explicitly we use the symbol  $\rho$ : for the density matrix:

$$\begin{aligned} \rho_{ij}^{\uparrow\uparrow} &= \langle \hat{c}_{i\uparrow}^\dagger \hat{c}_{j\uparrow} \rangle, & \rho_{ij}^{\downarrow\downarrow} &= \langle \hat{c}_{i\downarrow}^\dagger \hat{c}_{j\downarrow} \rangle, \\ \rho_{ij}^{\uparrow\downarrow} &= \langle \hat{c}_{i\uparrow}^\dagger \hat{c}_{j\downarrow} \rangle, & \rho_{ij}^{\downarrow\uparrow} &= \langle \hat{c}_{i\downarrow}^\dagger \hat{c}_{j\uparrow} \rangle, \end{aligned} \quad (\text{A.11})$$

For the off diagonal entries we note the following relation explicitly:

$$\rho_{ij}^{\uparrow\downarrow} = \langle \hat{c}_{i\uparrow}^\dagger \hat{c}_{j\downarrow} \rangle = \langle \hat{c}_{j\downarrow} \hat{c}_{i\uparrow} \rangle^* = (\rho_{ji}^{\downarrow\uparrow})^*. \quad (\text{A.12})$$



# Appendix B

## B.1 Effective Mean Field Hubbard Hamiltonian

Applying the mean-field approximation the next step replaces the boson fields by its expectation values. This leads to the following effective MFA Hamiltonian:

$$\begin{aligned}
\hat{H}^{MFA} = & \sum_{i \neq j} t_{ij} \left[ (A_{11}^i A_{11}^j - A_{12}^i A_{21}^j) \hat{c}_{i\uparrow}^\dagger \hat{c}_{j\uparrow} + (A_{11}^i A_{12}^j - A_{12}^i A_{22}^j) \hat{c}_{i\uparrow}^\dagger \hat{c}_{j\downarrow} \right. \\
& \left. + (A_{21}^i A_{11}^j - A_{22}^i A_{21}^j) \hat{c}_{i\downarrow} \hat{c}_{j\uparrow} + (A_{22}^i A_{22}^j - A_{21}^i A_{12}^j) \hat{c}_{i\downarrow} \hat{c}_{j\downarrow} \right] \\
& + U \sum_i \left[ D_i^2 - \frac{1}{2} (\hat{c}_{i\uparrow}^\dagger \hat{c}_{i\uparrow} - \hat{c}_{i\downarrow}^\dagger \hat{c}_{i\downarrow} - 1) \left( \sqrt{1 + \tan^2(\varphi_i)} - 1 \right) \right] \\
& - \mu \sum_{i\sigma} \hat{c}_{i\sigma}^\dagger \hat{c}_{i\sigma} \\
& + \sum_i \lambda_i^1 \left( 2b_{xi}(D_i + E_i) - (\hat{c}_{i\uparrow}^\dagger \hat{c}_{i\downarrow}^\dagger + \hat{c}_{i\downarrow} \hat{c}_{i\uparrow}) \right) \\
& + \sum_i \lambda_i^2 \left( 2b_{yi}(D_i + E_i) + i(\hat{c}_{i\uparrow}^\dagger \hat{c}_{i\downarrow}^\dagger - \hat{c}_{i\downarrow} \hat{c}_{i\uparrow}) \right) \\
& + \sum_i \lambda_i^4 (D_i^2 + (b_{ix}^2 + b_{iy}^2) + p_{i\uparrow}^2 - \hat{c}_{i\uparrow}^\dagger \hat{c}_{i\uparrow}) \\
& + \sum_i \lambda_i^5 (D_i^2 + (b_{ix}^2 + b_{iy}^2) + p_{i\downarrow}^2 - \hat{c}_{i\downarrow}^\dagger \hat{c}_{i\downarrow}) \\
& + \sum_i \lambda_i^3 (D_i^2 + E_i^2 + 2(b_{ix}^2 + b_{iy}^2) + p_{i\uparrow}^2 + p_{i\downarrow}^2 - 1).
\end{aligned} \tag{B.1}$$

## Hartree-Fock-Decoupled Inter-Site-Repulsion

The Hartree-Fock terms of the inter site repulsion read:

$$\begin{aligned} \hat{W}_{HF} = & + V \sum_{\langle ij \rangle} \left\{ \sum_{\sigma\sigma'} \left[ \langle \hat{c}_{i\sigma}^\dagger \hat{c}_{i\sigma} \rangle \hat{c}_{j\sigma'}^\dagger \hat{c}_{j\sigma'} + \langle \hat{c}_{j\sigma'}^\dagger \hat{c}_{j\sigma'} \rangle \hat{c}_{i\sigma}^\dagger \hat{c}_{i\sigma} \right] \right. \\ & - \sum_{\sigma} \left[ \langle \hat{c}_{i\sigma}^\dagger \hat{c}_{j\sigma} \rangle \hat{c}_{j\sigma}^\dagger \hat{c}_{i\sigma} + \langle \hat{c}_{j\sigma}^\dagger \hat{c}_{i\sigma} \rangle \hat{c}_{i\sigma}^\dagger \hat{c}_{j\sigma} \right] \\ & \left. + \sum_{\sigma} \left[ \langle \hat{c}_{i\sigma}^\dagger \hat{c}_{j-\sigma}^\dagger \rangle \hat{c}_{j-\sigma} \hat{c}_{i\sigma} + \langle \hat{c}_{i\sigma}^\dagger \hat{c}_{j-\sigma} \rangle \hat{c}_{j-\sigma}^\dagger \hat{c}_{i\sigma}^\dagger \right] \right\}, \end{aligned} \quad (\text{B.2})$$

## B.2 Fourier Transformation of the $d$ -wave Interaction Term

With the short hand writing  $\Delta_{ij}^{d+} = T_{ij}^+ + \lambda_{ij}^{d+}$ :

$$\begin{aligned} \sum_{ij} \Delta_{ij}^{d+} \hat{c}_{i\uparrow}^\dagger \hat{c}_{j\downarrow}^\dagger &= \sum_{\langle ij \rangle} \Delta_i^{d+} \hat{c}_{i\uparrow}^\dagger \hat{c}_{j\downarrow}^\dagger \quad (\text{B.3}) \\ &= \frac{1}{N} \sum_{\langle ij \rangle} \sum_{k_1 k_2} \Delta_i^{d+} \hat{c}_{k_1\uparrow}^\dagger \hat{c}_{k_2\downarrow}^\dagger \exp\left(-iR_i k_1 - iR_j k_2\right) \\ &= \frac{1}{N} \sum_{\langle ij \rangle} \sum_{kq} \Delta_i^{d+} \hat{c}_{k\uparrow}^\dagger \hat{c}_{-k+q\downarrow}^\dagger \exp\left(-i(R_i - R_j)k\right) \exp\left(-iR_j q\right) \\ &= \frac{1}{N} \sum_i \sum_{kq} \Delta_i^{d+} \hat{c}_{k\uparrow}^\dagger \hat{c}_{-k+q\downarrow}^\dagger \\ &\times \left\{ \exp\left(-ik_x\right) \exp\left(-iR_{(i+x)}q\right) + \exp\left(ik_x\right) \exp\left(-iR_{(i-x)}q\right) \right. \\ &\left. + \exp\left(-ik_y\right) \exp\left(-iR_{(i+y)}q\right) + \exp\left(ik_y\right) \exp\left(-iR_{(i-y)}q\right) \right\} \\ &= \sum_{kq} 2\Delta^{d+} \hat{c}_{k\uparrow}^\dagger \hat{c}_{-k+q\downarrow}^\dagger \left\{ \cos(k_x) + \cos(k_y) \right\} \delta(q) \\ &= \sum_k 2\Delta^{d+} \hat{c}_{k\uparrow}^\dagger \hat{c}_{-k\downarrow}^\dagger \left\{ \cos(k_x) + \cos(k_y) \right\} \end{aligned}$$

where we used homogeneity and isotropy arguments.



### B.3 Interaction Kernel of the ph-Channel in the Free Energy Expansion of the GA Functional

The interaction matrix of the ph channel in the free energy expansion reads as:

$$\mathbf{M}_q = \begin{pmatrix} A_q & B_q \\ B_q & C_q \end{pmatrix} \quad (\text{B.4})$$

$$\begin{aligned} A_q &= V_q - \frac{L_q^2}{4M_q} \\ B_q &= \frac{1}{4} \left( z_0 z'_D \frac{L_q}{M_q} + z_0 (z' + z_{+-}) \right) \\ C_q &= -\frac{1}{4} \frac{1}{M_q} (z_0 z'_D)^2 \end{aligned} \quad (\text{B.5})$$

and

$$\begin{aligned} V_q &= \frac{1}{8} (z' + z_{+-})^2 \frac{1}{N} \sum_{k\sigma} (\varepsilon_{k+q} + \varepsilon_{k-q}) n_{k\sigma} + \frac{1}{4} z_0 (z''_{++} + 2z''_{+-} + z''_{--}) e_0 \\ L_q &= \frac{1}{2} z'_D (z' + z_{+-}) \frac{1}{N} \sum_{k\sigma} (\varepsilon_{k+q} + \varepsilon_{k-q}) n_{k\sigma} + z_0 (z''_{\sigma D} + z''_{-\sigma D}) e_0 \\ M_q &= \frac{1}{2} (z'_D)^2 \frac{1}{N} \sum_{k\sigma} (\varepsilon_{k+q} + \varepsilon_{k-q}) n_{k\sigma} + z_0 z'_D e_0 \end{aligned} \quad (\text{B.6})$$

with  $e_0 = \frac{1}{N} \sum_{k\sigma} \varepsilon_k n_{k\sigma}$  and the abbreviations homogeneous solution:

$$\begin{aligned} z' &= \frac{\partial z_{i\sigma}}{\partial n_{i\sigma}} & z'_{+-} &= \frac{\partial z_{i\sigma}}{\partial n_{i-\sigma}} & z'_D &= \frac{\partial z_{i\sigma}}{\partial D_i} \\ z''_{\sigma D} &= \frac{\partial^2 z_{i\sigma}}{\partial n_{i\sigma} \partial D_i} & z''_{-\sigma D} &= \frac{\partial^2 z_{i\sigma}}{\partial n_{i-\sigma} \partial D_i} & z''_{++} &= \frac{\partial^2 z_{i\sigma}}{\partial n_{i\sigma}^2} \\ z''_{\sigma D} &= \frac{\partial z_{i\sigma}}{\partial D_i^2} & z''_{+-} &= \frac{\partial^2 z_{i\sigma}}{\partial n_{i-\sigma} n_{i\sigma}} & z''_{--} &= \frac{\partial^2 z_{i\sigma}}{\partial n_{i-\sigma} n_{i-\sigma}} \end{aligned} \quad (\text{B.7})$$

## B.4 The Constrained GA Energy Functional

This is the GA energy functional without the inter site repulsion:

$$\begin{aligned}
E = & \sum_{ij} t_{ij} \left[ (A_{11}^i A_{11}^j - A_{12}^i A_{21}^j) \rho_{ij}^{\uparrow\uparrow} + (A_{11}^i A_{12}^j - A_{12}^i A_{22}^j) \rho_{ij}^{\uparrow\downarrow} \right. \\
& \left. + (A_{21}^i A_{11}^j - A_{22}^i A_{21}^j) \rho_{ij}^{\downarrow\uparrow} + (A_{22}^i A_{22}^j - A_{21}^i A_{12}^j) \rho_{ij}^{\downarrow\downarrow} \right] \\
& + U \sum_i (D_i^2 + b_{xi}^2 + b_{yi}^2) \\
& + V \sum_{\langle ij \rangle} (\rho_{ii}^{\uparrow\uparrow} + \rho_{ii}^{\downarrow\downarrow}) (\rho_{jj}^{\uparrow\uparrow} + \rho_{jj}^{\downarrow\downarrow}) \\
& + V \sum_{\langle ij \rangle} \left[ (\rho_{ij}^{\uparrow\downarrow} \rho_{ji}^{\downarrow\uparrow} + \rho_{ij}^{\downarrow\uparrow} \rho_{ji}^{\uparrow\downarrow}) - (\rho_{ij}^{\uparrow\uparrow} \rho_{ji}^{\uparrow\uparrow} + \rho_{ij}^{\downarrow\downarrow} \rho_{ji}^{\downarrow\downarrow}) \right] \\
& + \Lambda_1 \sum_{kq} \left( \sum_i \phi_i^*(k) \phi_i(q) - \delta_{kq} \right) \left( \sum_j \phi_j(k) \phi_j^*(q) - \delta_{kq} \right) \\
& + \Lambda_2 \left( \sum_i \rho_{ii}^{\uparrow\uparrow} - N_{\uparrow} \right)^2 \\
& + \Lambda_3 \left( \sum_i \rho_{ii}^{\downarrow\downarrow} - N_{\downarrow} \right)^2 \\
& + \Lambda_4 \sum_i \left( 2b_{xi}(D_i + E_i) - (\rho_{ii}^{\uparrow\downarrow} + \rho_{ii}^{\downarrow\uparrow}) \right)^2 \\
& + \Lambda_5 \sum_i \left( 2b_{yi}(D_i + E_i) + i(\rho_{ii}^{\uparrow\downarrow} - \rho_{ii}^{\downarrow\uparrow}) \right)^2 \\
& + \Lambda_6 \sum_i (D_i^2 + E_i^2 + 2(b_{ix}^2 + b_{iy}^2) + p_{i\uparrow}^2 + p_{i\downarrow}^2 - 1)^2 \\
& + \Lambda_7 \sum_i (D_i^2 + (b_{ix}^2 + b_{iy}^2) + p_{i\uparrow}^2 - \rho_{ii}^{\uparrow\uparrow})^2 \\
& + \Lambda_8 \sum_i (D_i^2 + (b_{ix}^2 + b_{iy}^2) + p_{i\downarrow}^2 - \rho_{ii}^{\downarrow\downarrow})^2.
\end{aligned} \tag{B.8}$$

## B.5 Derivatives of the GA-functional

The energy functional depend and the densities  $\rho_{ij}^{\sigma\sigma'}$  that depend again on the complex amplitudes  $\phi_i(k)$ . We split the complex amplitudes from the  $k$ -space decomposition of the densities into a real and imaginary part:  $\phi_i(k) = x_i(k) + iy_i(k)$  and  $\phi_i^*(k) = x_i(k) - iy_i(k)$ . We treat real and imaginary part as independent variables reducing the GA-energy functional as a real function including a complex variable  $i$ . Additionally the functional depend on  $6 \times N$  expectation values of the slave bosons from the charge rational invariant formulation.

### Derivatives of the Densities $\rho_{ij}^{\sigma\sigma'}$ with respect to the Amplitudes $\phi_i(k)$ and $\phi_i^*(k)$

We write down the derivative of the  $k$ -space decomposition of Eq. (3.55).

$$\begin{aligned} \frac{\partial \rho_{lm}^{\sigma\sigma'}}{\partial x_i(k)} &= (\delta_{mi}\phi_l^*(k) + \delta_{li}\phi_m(k)) \\ \frac{\partial \rho_{lm}^{\sigma\sigma'}}{\partial y_i(k)} &= i(\delta_{mi}\phi_l^*(k) - \delta_{li}\phi_m(k)). \end{aligned} \quad (\text{B.9})$$

We applying a case differentiation with respect to the indices  $i$  and  $k$  and we evaluate the expressions (B.9):

In the case  $k \in [1, N]$  and  $i \in [1, N]$ :

$$\begin{aligned} \frac{\partial \rho_{lm}^{\uparrow\uparrow}}{\partial \phi_i(k)} &= \delta_{li}\phi_m(k) + \delta_{m,i}\phi_l(k), & \frac{\partial \rho_{lm}^{\uparrow\downarrow}}{\partial \phi_i(k)} &= \delta_{li}\phi_{(m+N)}(k) \\ \frac{\partial \rho_{lm}^{\downarrow\uparrow}}{\partial \phi_i(k)} &= \delta_{mi}\phi_{(l+N)}(k), & \frac{\partial \rho_{lm}^{\downarrow\downarrow}}{\partial \phi_i(k)} &= 0. \end{aligned} \quad (\text{B.10})$$

In the case  $k \in [N + 1, 2N]$  and  $i \in [N + 1, 2N]$  :

$$\begin{aligned} \frac{\partial \rho_{lm}^{\uparrow\uparrow}}{\partial \phi_i(k)} &= 0, & \frac{\partial \rho_{lm}^{\uparrow\downarrow}}{\partial \phi_i(k)} &= 0, \\ \frac{\partial \rho_{lm}^{\downarrow\uparrow}}{\partial \phi_i(k)} &= 0, & \frac{\partial \rho_{lm}^{\downarrow\downarrow}}{\partial \phi_i(k)} &= \delta_{l+N} \phi_m(k) + \delta_{m+N} \phi_l(k). \end{aligned} \quad (\text{B.11})$$

In the case  $k \in [N + 1, 2N]$  and  $i \in [1, N]$  :

$$\begin{aligned} \frac{\partial \rho_{lm}^{\uparrow\uparrow}}{\partial \phi_i(k)} &= 0, & \frac{\partial \rho_{lm}^{\uparrow\downarrow}}{\partial \phi_i(k)} &= 0, \\ \frac{\partial \rho_{lm}^{\downarrow\uparrow}}{\partial \phi_i(k)} &= 0, & \frac{\partial \rho_{lm}^{\downarrow\downarrow}}{\partial \phi_i(k)} &= 0. \end{aligned} \quad (\text{B.12})$$

In the case  $k \in [1, N]$  and  $i \in [N + 1, 2N]$ :

$$\begin{aligned} \frac{\partial \rho_{lm}^{\uparrow\uparrow}}{\partial \phi_i(k)} &= 0, & \frac{\partial \rho_{lm}^{\uparrow\downarrow}}{\partial \phi_i(k)} &= \delta_{m+N} \phi_l(k), \\ \frac{\partial \rho_{lm}^{\downarrow\uparrow}}{\partial \phi_i(k)} &= \delta_{l+N} \phi_m(k), & \frac{\partial \rho_{lm}^{\downarrow\downarrow}}{\partial \phi_i(k)} &= 0. \end{aligned} \quad (\text{B.13})$$

**Derivatives of  $E^{GA}$  with respect to the Real Part of  $\phi_i(k)$  and  $\phi_i^*(k)$**

$$\begin{aligned}
\frac{\partial E}{\partial x_i(k)} &= \sum_m^N t_{im}(A_{11}^i A_{11}^m - A_{12}^i A_{21}^m) \phi_m(k) \theta(N-k) \\
&+ \sum_l^N t_{li}(A_{11}^l A_{11}^i - A_{12}^l A_{21}^i) \phi_l^*(k) \theta(N-k) \\
&+ \sum_m^N t_{i-Nm}(A_{21}^{i-N} A_{12}^m - A_{22}^{i-N} A_{22}^m) \phi_{m+N}(k) \theta(k-N) \\
&+ \sum_l^N t_{i-Nm}(A_{21}^l A_{12}^{i-N} - A_{22}^l A_{22}^{i-N}) \phi_{l+N}^*(k) \theta(k-N) \\
&+ \sum_m^N t_{im}(A_{11}^i A_{12}^m - A_{12}^i A_{22}^m) \phi_{m+N}(k) \theta(N-k) \\
&+ \sum_l^N t_{li-N}(A_{11}^l A_{12}^{i-N} - A_{12}^l A_{22}^{i-N}) \phi_l^*(k) \theta(N-k) \\
&+ \sum_l^N t_{li}(A_{21}^l A_{11}^i - A_{22}^l A_{21}^i) \phi_{l+N}^*(k) \theta(N-k) \\
&+ \sum_m^N t_{i-Nm}(A_{21}^{i-N} A_{11}^m - A_{22}^{i-N} A_{21}^m) \phi_m(k) \theta(N-k) \\
&+ \Lambda_{ik} \\
&+ 4\Lambda_2 \left( \sum_j \rho_{jj}^{\uparrow\uparrow} - N_{\uparrow} \right) \text{Re}(\phi_i(k)) \theta(N-k) \quad i \leq N \\
&+ 4\Lambda_3 \left( \sum_j \rho_{jj}^{\downarrow\downarrow} - N_{\downarrow} \right) \text{Re}(\phi_i(k)) \theta(k-N) \quad i > N \\
&+ 4\Lambda_4 \left( 2b_{xi}(D_i + E_i) - (\rho_{ii}^{\downarrow\downarrow} + \rho_{ii}^{\uparrow\uparrow}) \right) \begin{cases} -\text{Re}(\phi_{i+N}(k)) \theta(N-k), & i \leq N \\ -\text{Re}(\phi_{i-N}(k)) \theta(N-k), & i > N \end{cases} \\
&+ 4\Lambda_5 \left( 2b_{yi}(D_i + E_i) + i(\rho_{ii}^{\uparrow\downarrow} - \rho_{ii}^{\downarrow\uparrow}) \right) \begin{cases} -\text{Im}(\phi_{i+N}(k)) \theta(N-k), & i \leq N \\ +\text{Im}(\phi_{i-N}(k)) \theta(N-k), & i > N \end{cases} \\
&+ 4\Lambda_7 (D_i^2 + (b_{xk}^2 + b_{yk}^2) + p_{i\uparrow}^2 - \rho_{ii}^{\uparrow\uparrow}) \text{Re}(\phi_i(k)) \theta(N-k), \quad i \leq N \\
&+ 4\Lambda_8 (D_i^2 + (b_{xk}^2 + b_{yk}^2) + p_{i\downarrow}^2 - \rho_{ii}^{\downarrow\downarrow}) \text{Re}(\phi_i(k)) \theta(k-N), \quad i > N
\end{aligned} \tag{B.14}$$

**Derivatives of  $E^{GA}$  with respect to the imaginary Part  
of  $\phi_i(k)$  and  $\phi_i^*(k)$**

$$\begin{aligned}
\frac{\partial E}{\partial y_i(k)} = & - i \sum_m^N t_{im} (A_{11}^i A_{11}^m - A_{12}^i A_{21}^m) \phi_m(k) \theta(N-k) \\
& + i \sum_l^N t_{li} (A_{11}^l A_{11}^i - A_{12}^l A_{21}^i) \phi_l^*(k) \theta(N-k) \\
& + - i \sum_m^N t_{i-Nm} (A_{21}^{i-N} A_{12}^m - A_{22}^{i-N} A_{22}^m) \phi_{m+N}(k) \theta(k-N) \\
& + i \sum_l^N t_{i-Nm} (A_{21}^l A_{12}^{i-N} - A_{22}^l A_{22}^{i-N}) \phi_{l+N}^*(k) \theta(k-N) \\
& - i \sum_m^N t_{im} (A_{11}^i A_{12}^m - A_{12}^i A_{22}^m) \phi_{m+N}(k) \theta(N-k) \\
& + i \sum_l^N t_{li-N} (A_{11}^l A_{12}^{i-N} - A_{12}^l A_{22}^{i-N}) \phi_l^*(k) \theta(N-k) \\
& + i \sum_l^N t_{li} (A_{21}^l A_{11}^i - A_{22}^l A_{21}^i) \phi_{l+N}^*(k) \theta(N-k) \\
& - i \sum_m^N t_{i-Nm} (A_{21}^{i-N} A_{11}^m - A_{22}^{i-N} A_{21}^m) \phi_m(k) \theta(N-k) \\
& + \Gamma_{ik} \\
& + 4\Lambda_2 \left( \sum_j \rho_{jj}^{\uparrow\uparrow} - N_{\uparrow} \right) \text{Im}(\phi_i(k)) \theta(N-k) \quad i \leq N \\
& + 4\Lambda_3 \left( \sum_j \rho_{jj}^{\downarrow\downarrow} - N_{\downarrow} \right) \text{Im}(\phi_i(k)) \theta(k-N) \quad i > N \\
& + 4\Lambda_4 \left( 2b_{xi}(D_i + E_i) - (\rho_{ii}^{\uparrow\downarrow} + \rho_{ii}^{\downarrow\uparrow}) \right) \begin{cases} +\text{Im}(\phi_{i+N}(k)) \theta(N-k), & i \leq N \\ +\text{Im}(\phi_{i-N}(k)) \theta(N-k), & i > N \end{cases} \\
& + 4\Lambda_5 \left( 2b_{yi}(D_i + E_i) + i(\rho_{ii}^{\uparrow\downarrow} - \rho_{ii}^{\downarrow\uparrow}) \right) \begin{cases} +\text{Re}(\phi_{i+N}(k)) \theta(N-k), & i \leq N \\ -\text{Re}(\phi_{i-N}(k)) \theta(N-k), & i > N \end{cases} \\
& + 4\Lambda_7 (D_i^2 + (b_{xk}^2 + b_{yk}^2) + p_{i\uparrow}^2 - \rho_{ii}^{\uparrow\uparrow}) \text{Im}(\phi_i(k)) \theta(N-k), \quad i \leq N \\
& + 4\Lambda_8 (D_i^2 + (b_{xk}^2 + b_{yk}^2) + p_{i\downarrow}^2 - \rho_{ii}^{\downarrow\downarrow}) \text{Im}(\phi_i(k)) \theta(k-N), \quad i > N.
\end{aligned} \tag{B.15}$$

### Case Differentiation with respect to the Indices

The given general can be simplified by apply the case differentiation of the set of indices. One obtains the for Eq. (B.14):

In the case of  $i \leq N$ :

$$\begin{aligned}
\frac{\partial E}{\partial x_i(k)} &= 2 \sum_m^N t_{im} (A_{11}^i A_{11}^m - A_{12}^i A_{21}^m) \text{Re}(\phi_m(k)) \theta(N-k) \\
&+ 2 \sum_m^N t_{im} \text{Re}((A_{11}^i A_{12}^m - A_{12}^i A_{22}^m) \phi_{m+N}(k)) \theta(N-k) \\
&+ \Lambda_{ik} \\
&+ 4\Lambda_2 \left( \sum_j \rho_{jj}^{\uparrow\uparrow} - N_{\uparrow} \right) \text{Re}(\phi_i(k)) \theta(N-k) \quad i \leq N \\
&+ 4\Lambda_4 \left( 2b_{xi}(D_i + E_i) - (\rho_{ii}^{\uparrow\downarrow} + \rho_{ii}^{\downarrow\uparrow}) \right) (-\text{Re}(\phi_{i+N}(k)) \theta(N-k)) \\
&+ 4\Lambda_5 \left( 2b_{yi}(D_i + E_i) + i(\rho_{ii}^{\uparrow\downarrow} - \rho_{ii}^{\downarrow\uparrow}) \right) (-\text{Im}(\phi_{i+N}(k)) \theta(N-k)) \\
&+ 4\Lambda_7 (D_i^2 + (b_{xk}^2 + b_{yk}^2) + p_{i\uparrow}^2 - \rho_{ii}^{\uparrow\uparrow}) \text{Re}(\phi_i(k)) \theta(N-k).
\end{aligned} \tag{B.16}$$

In the case of  $i > N$ :

$$\begin{aligned}
\frac{\partial E}{\partial x_i(k)} &= 2 \sum_m^N t_{i-Nm} (A_{21}^{i-N} A_{12}^m - A_{22}^{i-N} A_{22}^m) \text{Re}(\phi_{m+N}(k)) \theta(k-N) \\
&+ 2 \sum_m^N t_{i-Nm} \text{Re}((A_{21}^{i-N} A_{11}^m - A_{22}^{i-N} A_{21}^m) \phi_m(k)) \theta(N-k) \\
&+ \Lambda_{ik} \\
&+ 4\Lambda_3 \left( \sum_j \rho_{jj}^{\downarrow\downarrow} - N_{\downarrow} \right) \text{Re}(\phi_i(k)) \theta(k-N) \\
&+ 4\Lambda_4 \left( 2b_{xi}(D_i + E_i) - (\rho_{ii}^{\uparrow\downarrow} + \rho_{ii}^{\downarrow\uparrow}) \right) (-\text{Re}(\phi_{i-N}(k)) \theta(N-k)) \\
&+ 4\Lambda_5 \left( 2b_{yi}(D_i + E_i) + i(\rho_{ii}^{\uparrow\downarrow} - \rho_{ii}^{\downarrow\uparrow}) \right) (\text{Im}(\phi_{i-N}(k)) \theta(N-k)) \\
&+ 4\Lambda_8 (D_i^2 + (b_{xk}^2 + b_{yk}^2) + p_{i\downarrow}^2 - \rho_{ii}^{\downarrow\downarrow}) \text{Re}(\phi_i(k)) \theta(k-N).
\end{aligned} \tag{B.17}$$

One obtains the for Eq. (B.15):

In the case of  $i \leq N$ :

$$\begin{aligned}
\frac{\partial E}{\partial y_i(k)} &= 2 \sum_m^N t_{im} (A_{11}^i A_{11}^m - A_{12}^i A_{21}^m) \text{Im}(\phi_m(k)) \theta(N-k) \\
&+ 2 \sum_m^N t_{im} \text{Im}((A_{11}^i A_{12}^m - A_{12}^i A_{22}^m) \phi_{m+N}(k)) \theta(N-k) \\
&+ \Gamma_{ik} \\
&+ 4\Lambda_2 \left( \sum_j \rho_{jj}^{\uparrow\uparrow} - N_{\uparrow} \right) \cdot \text{Im}(\phi_i(k)) \theta(N-k) \\
&+ 4\Lambda_4 \left( 2b_{xi}(D_i + E_i) - (\rho_{ii}^{\uparrow\downarrow} + \rho_{ii}^{\downarrow\uparrow}) \right) \cdot \text{Im}(\phi_{i+N}(k)) \theta(N-k) \\
&+ 4\Lambda_5 \left( 2b_{yi}(D_i + E_i) + i(\rho_{ii}^{\uparrow\downarrow} - \rho_{ii}^{\downarrow\uparrow}) \right) \cdot \text{Re}(\phi_{i+N}(k)) \theta(N-k) \\
&+ 4\Lambda_7 (D_i^2 + (b_{xk}^2 + b_{yk}^2) + p_{i\uparrow}^2 - \rho_{ii}^{\uparrow\uparrow}) \cdot \text{Im}(\phi_i(k)) \theta(N-k).
\end{aligned} \tag{B.18}$$

In the case of  $i > N$ :

$$\begin{aligned}
\frac{\partial E}{\partial y_i(k)} &= 2 \sum_m^N t_{i-Nm} (A_{21}^{i-N} A_{12}^m - A_{22}^{i-N} A_{22}^m) \text{Im}(\phi_{m+N}(k)) \theta(k-N) \\
&+ 2 \sum_l^N t_{l i-N} \text{Im}((A_{11}^l A_{12}^{i-N} - A_{12}^l A_{22}^{i-N}) \phi_l(k)) \theta(N-k) \\
&+ \Gamma_{ik} \\
&+ 4\Lambda_3 \left( \sum_j \rho_{jj}^{\downarrow\downarrow} - N_{\downarrow} \right) \cdot \text{Im}(\phi_i(k)) \theta(k-N) \\
&+ 4\Lambda_4 \left( 2b_{xi}(D_i + E_i) - (\rho_{ii}^{\uparrow\downarrow} + \rho_{ii}^{\downarrow\uparrow}) \right) \cdot \text{Im}(\phi_{i-N}(k)) \theta(N-k) \\
&+ 4\Lambda_5 \left( 2b_{yi}(D_i + E_i) + i(\rho_{ii}^{\uparrow\downarrow} - \rho_{ii}^{\downarrow\uparrow}) \right) \cdot (-\text{Re}(\phi_{i-N}(k))) \theta(N-k) \\
&+ 4\Lambda_8 (D_i^2 + (b_{xk}^2 + b_{yk}^2) + p_{i\downarrow}^2 - \rho_{ii}^{\downarrow\downarrow}) \cdot \text{Im}(\phi_i(k)) \theta(k-N).
\end{aligned} \tag{B.19}$$



## Derivatives with respect to the Boson Fields

$$\begin{aligned}
\frac{\partial E}{\partial D_k} = & \sum_i t_{ki} \left[ \left( 2 \frac{\partial A_{11}^k}{\partial D_k} A_{11}^i - \frac{\partial A_{12}^k}{\partial D_k} A_{21}^i - \frac{\partial A_{21}^k}{\partial D_k} A_{12}^i \right) \rho_{ki}^{\uparrow\uparrow} \right. \\
& \left. \left( 2 \frac{\partial A_{22}^k}{\partial D_k} A_{22}^i - \frac{\partial A_{21}^k}{\partial D_k} A_{12}^i - \frac{\partial A_{12}^k}{\partial D_k} A_{21}^i \right) \rho_{ki}^{\downarrow\downarrow} \right] \\
& + \left( \frac{\partial A_{11}^k}{\partial D_k} A_{12}^i + \frac{\partial A_{12}^k}{\partial D_k} A_{11}^i - \frac{\partial A_{12}^k}{\partial D_k} A_{22}^i - \frac{\partial A_{22}^k}{\partial D_k} A_{12}^i \right) \rho_{ki}^{\uparrow\downarrow} \\
& + \left( \frac{\partial A_{21}^k}{\partial D_k} A_{11}^i + \frac{\partial A_{11}^k}{\partial D_k} A_{21}^i - \frac{\partial A_{21}^k}{\partial D_k} A_{22}^i - \frac{\partial A_{22}^k}{\partial D_k} A_{21}^i \right) \rho_{ij}^{\downarrow\uparrow} \\
& + 2UD_k \\
& + 4\Lambda_4 b_{xk} \left( 2b_{xk}(D_k + E_k) - (\rho_{kk}^{\uparrow\downarrow} + \rho_{kk}^{\downarrow\uparrow}) \right) \\
& + 4\Lambda_5 b_{yk} \left( 2b_{yk}(D_k + E_k) + i(\rho_{kk}^{\uparrow\downarrow} - \rho_{kk}^{\downarrow\uparrow}) \right) \\
& + 4\Lambda_6 D_k (D_k^2 + E_k^2 + 2(b_{kx}^2 + b_{ky}^2) + p_{k\uparrow}^2 + p_{k\downarrow}^2 - 1) \\
& + 4\Lambda_7 D_k (D_k^2 + (b_{kx}^2 + b_{ky}^2) + p_{k\uparrow}^2 - \rho_{kk}^{\uparrow\uparrow}) \\
& + 4\Lambda_8 D_k (D_k^2 + (b_{kx}^2 + b_{ky}^2) + p_{k\downarrow}^2 - \rho_{kk}^{\downarrow\downarrow})
\end{aligned} \tag{B.20}$$

$$\begin{aligned}
\frac{\partial E}{\partial E_k} = & \sum_i t_{ki} \left[ \left( 2 \frac{\partial A_{11}^k}{\partial E_k} A_{11}^i - \frac{\partial A_{12}^k}{\partial E_k} A_{21}^i - \frac{\partial A_{21}^k}{\partial E_k} A_{12}^i \right) \rho_{ki}^{\uparrow\uparrow} \right. \\
& \left. \left( 2 \frac{\partial A_{22}^k}{\partial E_k} A_{22}^i - \frac{\partial A_{21}^k}{\partial E_k} A_{12}^i - \frac{\partial A_{12}^k}{\partial E_k} A_{21}^i \right) \rho_{ki}^{\downarrow\downarrow} \right] \\
& + \left( \frac{\partial A_{11}^k}{\partial E_k} A_{12}^i + \frac{\partial A_{12}^k}{\partial E_k} A_{11}^i - \frac{\partial A_{21}^k}{\partial E_k} A_{22}^i - \frac{\partial A_{22}^k}{\partial E_k} A_{21}^i \right) \rho_{ki}^{\uparrow\downarrow} \\
& + \left( \frac{\partial A_{21}^k}{\partial E_k} A_{11}^i + \frac{\partial A_{11}^k}{\partial E_k} A_{21}^i - \frac{\partial A_{12}^k}{\partial E_k} A_{22}^i - \frac{\partial A_{22}^k}{\partial E_k} A_{12}^i \right) \rho_{ij}^{\downarrow\uparrow} \\
& + 4\Lambda_4 b_{xk} \left( 2b_{xk}(D_k + E_k) - (\rho_{kk}^{\uparrow\downarrow} + \rho_{kk}^{\downarrow\uparrow}) \right) \\
& + 4\Lambda_5 b_{yk} \left( 2b_{yk}(D_k + E_k) + i(\rho_{kk}^{\uparrow\downarrow} - \rho_{kk}^{\downarrow\uparrow}) \right) \\
& + 4\Lambda_6 E_k (D_k^2 + E_k^2 + 2(b_{kx}^2 + b_{ky}^2) + p_{k\uparrow}^2 + p_{k\downarrow}^2 - 1)
\end{aligned} \tag{B.21}$$

$$\begin{aligned}
\frac{\partial E}{\partial b_{xk}} &= \sum_i t_{ki} \left[ \left( 2 \frac{\partial A_{11}^k}{\partial b_{xk}} A_{11}^i - \frac{\partial A_{12}^k}{\partial b_{xk}} A_{21}^i - \frac{\partial A_{21}^k}{\partial b_{xk}} A_{12}^i \right) \rho_{ki}^{\uparrow\uparrow} \right. \\
&\quad \left. \left( 2 \frac{\partial A_{22}^k}{\partial b_{xk}} A_{22}^i - \frac{\partial A_{21}^k}{\partial b_{xk}} A_{12}^i - \frac{\partial A_{12}^k}{\partial b_{xk}} A_{21}^i \right) \rho_{ki}^{\downarrow\downarrow} \right] \\
&\quad + \left( \frac{\partial A_{11}^k}{\partial b_{xk}} A_{12}^i + \frac{\partial A_{12}^k}{\partial b_{xk}} A_{11}^i - \frac{\partial A_{12}^k}{\partial b_{xk}} A_{22}^i - \frac{\partial A_{22}^k}{\partial b_{xk}} A_{12}^i \right) \rho_{ki}^{\uparrow\downarrow} \\
&\quad + \left( \frac{\partial A_{21}^k}{\partial b_{xk}} A_{11}^i + \frac{\partial A_{11}^k}{\partial b_{xk}} A_{21}^i - \frac{\partial A_{21}^k}{\partial b_{xk}} A_{22}^i - \frac{\partial A_{22}^k}{\partial b_{xk}} A_{21}^i \right) \rho_{ij}^{\downarrow\uparrow} \\
&+ 2U b_{xk} \\
&+ 4\Lambda_4 (D_k + E_k) \left( 2b_{xk} (D_k + E_k) - (\rho_{kk}^{\uparrow\downarrow} + \rho_{kk}^{\downarrow\uparrow}) \right) \\
&+ 8\Lambda_6 b_{xk} (D_k^2 + E_k^2 + 2(b_{xk}^2 + b_{yk}^2) + p_{k\uparrow}^2 + p_{k\downarrow}^2 - 1) \\
&+ 4\Lambda_7 b_{xk} (D_k^2 + (b_{xk}^2 + b_{yk}^2) + p_{k\uparrow}^2 - \rho_{kk}^{\uparrow\uparrow}) \\
&+ 4\Lambda_8 b_{xk} (D_k^2 + (b_{xk}^2 + b_{yk}^2) + p_{k\downarrow}^2 - \rho_{kk}^{\downarrow\downarrow})
\end{aligned} \tag{B.22}$$

$$\begin{aligned}
\frac{\partial E}{\partial b_{yk}} &= \sum_i t_{ki} \left[ \left( 2 \frac{\partial A_{11}^k}{\partial b_{yk}} A_{11}^i - \frac{\partial A_{12}^k}{\partial b_{yk}} A_{21}^i - \frac{\partial A_{21}^k}{\partial b_{yk}} A_{12}^i \right) \rho_{ki}^{\uparrow\uparrow} \right. \\
&\quad \left. \left( 2 \frac{\partial A_{22}^k}{\partial b_{yk}} A_{22}^i - \frac{\partial A_{21}^k}{\partial b_{yk}} A_{12}^i - \frac{\partial A_{12}^k}{\partial b_{yk}} A_{21}^i \right) \rho_{ki}^{\downarrow\downarrow} \right] \\
&\quad + \left( \frac{\partial A_{11}^k}{\partial b_{yk}} A_{12}^i + \frac{\partial A_{12}^k}{\partial b_{yk}} A_{11}^i - \frac{\partial A_{12}^k}{\partial b_{yk}} A_{22}^i - \frac{\partial A_{22}^k}{\partial b_{yk}} A_{12}^i \right) \rho_{ki}^{\uparrow\downarrow} \\
&\quad + \left( \frac{\partial A_{21}^k}{\partial b_{yk}} A_{11}^i + \frac{\partial A_{11}^k}{\partial b_{yk}} A_{21}^i - \frac{\partial A_{21}^k}{\partial b_{yk}} A_{22}^i - \frac{\partial A_{22}^k}{\partial b_{yk}} A_{21}^i \right) \rho_{ij}^{\downarrow\uparrow} \\
&+ 2U b_{yk} \\
&+ 4\Lambda_5 (D_k + E_k) \left( 2b_{yk} (D_k + E_k) + i(\rho_{kk}^{\uparrow\downarrow} - \rho_{kk}^{\downarrow\uparrow}) \right) \\
&+ 8\Lambda_6 b_{yk} (D_k^2 + E_k^2 + 2(b_{xk}^2 + b_{yk}^2) + p_{k\uparrow}^2 + p_{k\downarrow}^2 - 1) \\
&+ 4\Lambda_7 b_{yk} (D_k^2 + (b_{xk}^2 + b_{yk}^2) + p_{k\uparrow}^2 - \rho_{kk}^{\uparrow\uparrow}) \\
&+ 4\Lambda_8 b_{yk} (D_k^2 + (b_{xk}^2 + b_{yk}^2) + p_{k\downarrow}^2 - \rho_{kk}^{\downarrow\downarrow})
\end{aligned} \tag{B.23}$$

$$\begin{aligned}
\frac{\partial E}{\partial p_{k\uparrow}} &= \sum_i t_{ki} \left[ \left( 2 \frac{\partial A_{11}^k}{\partial p_{k\uparrow}} A_{11}^i - \frac{\partial A_{12}^k}{\partial p_{k\uparrow}} A_{21}^i - \frac{\partial A_{21}^k}{\partial p_{k\uparrow}} A_{12}^i \right) \rho_{ki}^{\uparrow\uparrow} \right. \\
&\quad \left. \left( 2 \frac{\partial A_{22}^k}{\partial p_{k\uparrow}} A_{22}^i - \frac{\partial A_{21}^k}{\partial p_{k\uparrow}} A_{12}^i - \frac{\partial A_{12}^k}{\partial p_{k\uparrow}} A_{21}^i \right) \rho_{ki}^{\downarrow\downarrow} \right] \\
&\quad + \left( \frac{\partial A_{11}^k}{\partial p_{k\uparrow}} A_{12}^i + \frac{\partial A_{12}^k}{\partial p_{k\uparrow}} A_{11}^i - \frac{\partial A_{12}^k}{\partial p_{k\uparrow}} A_{22}^i - \frac{\partial A_{22}^k}{\partial p_{k\uparrow}} A_{12}^i \right) \rho_{ki}^{\uparrow\downarrow} \\
&\quad + \left( \frac{\partial A_{21}^k}{\partial p_{k\uparrow}} A_{11}^i + \frac{\partial A_{11}^k}{\partial p_{k\uparrow}} A_{21}^i - \frac{\partial A_{21}^k}{\partial p_{k\uparrow}} A_{22}^i - \frac{\partial A_{22}^k}{\partial p_{k\uparrow}} A_{21}^i \right) \rho_{ij}^{\downarrow\uparrow} \\
&\quad + 4\Lambda_6 p_{k\uparrow} (D_k^2 + E_k^2 + 2(b_{xk}^2 + b_{yk}^2) + p_{k\uparrow}^2 + p_{k\downarrow}^2 - 1) \\
&\quad + 4\Lambda_7 p_{k\uparrow} (D_k^2 + (b_{xk}^2 + b_{yk}^2) + p_{k\uparrow}^2 - \rho_{kk}^{\uparrow\uparrow})
\end{aligned} \tag{B.24}$$

$$\begin{aligned}
\frac{\partial E}{\partial p_{k\downarrow}} &= \sum_i t_{ki} \left[ \left( 2 \frac{\partial A_{11}^k}{\partial p_{k\downarrow}} A_{11}^i - \frac{\partial A_{12}^k}{\partial p_{k\downarrow}} A_{21}^i - \frac{\partial A_{21}^k}{\partial p_{k\downarrow}} A_{12}^i \right) \rho_{ki}^{\uparrow\uparrow} \right. \\
&\quad \left. \left( 2 \frac{\partial A_{22}^k}{\partial p_{k\downarrow}} A_{22}^i - \frac{\partial A_{21}^k}{\partial p_{k\downarrow}} A_{12}^i - \frac{\partial A_{12}^k}{\partial p_{k\downarrow}} A_{21}^i \right) \rho_{ki}^{\downarrow\downarrow} \right] \\
&\quad + \left( \frac{\partial A_{11}^k}{\partial p_{k\downarrow}} A_{12}^i + \frac{\partial A_{12}^k}{\partial p_{k\downarrow}} A_{11}^i - \frac{\partial A_{12}^k}{\partial p_{k\downarrow}} A_{22}^i - \frac{\partial A_{22}^k}{\partial p_{k\downarrow}} A_{12}^i \right) \rho_{ki}^{\uparrow\downarrow} \\
&\quad + \left( \frac{\partial A_{21}^k}{\partial p_{k\downarrow}} A_{11}^i + \frac{\partial A_{11}^k}{\partial p_{k\downarrow}} A_{21}^i - \frac{\partial A_{21}^k}{\partial p_{k\downarrow}} A_{22}^i - \frac{\partial A_{22}^k}{\partial p_{k\downarrow}} A_{21}^i \right) \rho_{ij}^{\downarrow\uparrow} \\
&\quad + 4\Lambda_6 p_{k\downarrow} (D_k^2 + E_k^2 + 2(b_{xk}^2 + b_{yk}^2) + p_{k\uparrow}^2 + p_{k\downarrow}^2 - 1) \\
&\quad + 4\Lambda_8 p_{k\downarrow} (D_k^2 + (b_{xk}^2 + b_{yk}^2) + p_{k\downarrow}^2 - \rho_{kk}^{\downarrow\downarrow})
\end{aligned} \tag{B.25}$$

## B.6 Derivatives of the z-Factors

The z-factors read in the non-rational invariant formulation [55]:

$$z_{i\uparrow} = \frac{e_i p_{i\uparrow} + d_i p_{i\downarrow}}{\sqrt{(e_i^2 + p_{i\downarrow}^2)(d_i^2 + p_{i\uparrow}^2)}} \quad \text{and} \quad z_{i\downarrow} = \frac{e_i p_{i\downarrow} + d_i p_{i\uparrow}}{\sqrt{(e_i^2 + p_{i\uparrow}^2)(d_i^2 + p_{i\downarrow}^2)}}. \quad (\text{B.26})$$

In order to calculate the derivatives with respect to the mean field values of charge rotational invariant bosons we apply the chain rule e.g.:

$$\frac{\partial z_{i\sigma}}{\partial D_i} = \left[ \frac{\partial z_{i\sigma}}{\partial d_i} \frac{\partial d_i}{\partial D_i} + \frac{\partial z_{i\sigma}}{\partial e_i} \frac{\partial e_i}{\partial D_i} \right]. \quad (\text{B.27})$$

We calculate the derivatives of the functions (B.26) with respect to the expectation values of the non-rotational slave bosons and we obtain for the z-factor ( $\uparrow$ ):

$$\begin{aligned} \frac{\partial z_{i\uparrow}}{\partial p_{i\uparrow}} &= \frac{1}{\sqrt{(e_i^2 + p_{i\downarrow}^2)(d_i^2 + p_{i\uparrow}^2)}} \left[ e_i - \frac{(e_i p_{i\uparrow} + d_i p_{i\downarrow}) p_{i\uparrow}}{d_i^2 + p_{i\uparrow}^2} \right], \\ \frac{\partial z_{i\uparrow}}{\partial p_{i\downarrow}} &= \frac{1}{\sqrt{(e_i^2 + p_{i\downarrow}^2)(d_i^2 + p_{i\uparrow}^2)}} \left[ d_i - \frac{(e_i p_{i\uparrow} + d_i p_{i\downarrow}) p_{i\downarrow}}{e_i^2 + p_{i\downarrow}^2} \right], \\ \frac{\partial z_{i\uparrow}}{\partial e_i} &= \frac{1}{\sqrt{(e_i^2 + p_{i\downarrow}^2)(d_i^2 + p_{i\uparrow}^2)}} \left[ p_{i\uparrow} - \frac{(e_i p_{i\uparrow} + d_i p_{i\downarrow}) e_i}{e_i^2 + p_{i\downarrow}^2} \right], \\ \frac{\partial z_{i\uparrow}}{\partial d_i} &= \frac{1}{\sqrt{(e_i^2 + p_{i\downarrow}^2)(d_i^2 + p_{i\uparrow}^2)}} \left[ p_{i\downarrow} - \frac{(e_i p_{i\uparrow} + d_i p_{i\downarrow}) d_i}{d_i^2 + p_{i\uparrow}^2} \right]. \end{aligned} \quad (\text{B.28})$$

For the z-factor ( $\downarrow$ ):

$$\begin{aligned}
\frac{\partial z_{i\downarrow}}{\partial p_{i\uparrow}} &= \frac{1}{\sqrt{(e_i^2 + p_{i\uparrow}^2)(d_i^2 + p_{i\downarrow}^2)}} \left[ d_i - \frac{(e_i p_{i\downarrow} + d_i p_{i\uparrow}) p_{i\uparrow}}{e_i^2 + p_{i\uparrow}^2} \right], \\
\frac{\partial z_{i\downarrow}}{\partial p_{i\downarrow}} &= \frac{1}{\sqrt{(e_i^2 + p_{i\uparrow}^2)(d_i^2 + p_{i\downarrow}^2)}} \left[ e_i - \frac{(e_i p_{i\downarrow} + d_i p_{i\uparrow}) p_{i\downarrow}}{d_i^2 + p_{i\downarrow}^2} \right], \\
\frac{\partial z_{i\downarrow}}{\partial e_i} &= \frac{1}{\sqrt{(e_i^2 + p_{i\uparrow}^2)(d_i^2 + p_{i\downarrow}^2)}} \left[ p_{i\downarrow} - \frac{(e_i p_{i\downarrow} + d_i p_{i\uparrow}) e_i}{e_i^2 + p_{i\uparrow}^2} \right], \\
\frac{\partial z_{i\downarrow}}{\partial d_i} &= \frac{1}{\sqrt{(e_i^2 + p_{i\uparrow}^2)(d_i^2 + p_{i\downarrow}^2)}} \left[ p_{i\uparrow} - \frac{(e_i p_{i\downarrow} + d_i p_{i\uparrow}) d_i}{d_i^2 + p_{i\downarrow}^2} \right].
\end{aligned} \tag{B.29}$$

We calculate the derivatives in the charge rotational invariant formulation: (with respect to  $D_i$ ,  $E_i$ ,  $b_{ix}$ ,  $b_{iy}$ ):

$$\begin{aligned}
d_i &= \frac{1}{2} \left[ D_i + E_i + \sqrt{(D_i - E_i)^2 + 4(b_{ix}^2 + b_{iy}^2)} \right] \\
e_i &= \frac{1}{2} \left[ D_i + E_i - \sqrt{(D_i - E_i)^2 + 4(b_{ix}^2 + b_{iy}^2)} \right],
\end{aligned} \tag{B.30}$$

The set of the derivatives reads than:

$$\begin{aligned}
\frac{\partial d_i}{\partial D_i} &= \frac{1}{2} \left( 1 + \frac{D_i - E_i}{\sqrt{(D_i - E_i)^2 + 4(b_{ix}^2 + b_{iy}^2)}} \right), \\
\frac{\partial d_i}{\partial E_i} &= \frac{1}{2} \left( 1 - \frac{D_i - E_i}{\sqrt{(D_i - E_i)^2 + 4(b_{ix}^2 + b_{iy}^2)}} \right), \\
\frac{\partial d_i}{\partial b_{xi}} &= \frac{2b_{ix}}{\sqrt{(D_i - E_i)^2 + 4(b_{ix}^2 + b_{iy}^2)}}, \\
\frac{\partial d_i}{\partial b_{yi}} &= \frac{2b_{iy}}{\sqrt{(D_i - E_i)^2 + 4(b_{ix}^2 + b_{iy}^2)}}.
\end{aligned} \tag{B.31}$$

and

$$\begin{aligned}
\frac{\partial e_i}{\partial D_i} &= \frac{1}{2} \left( 1 - \frac{D_i - E_i}{\sqrt{(D_i - E_i)^2 + 4(b_{ix}^2 + b_{iy}^2)}} \right), \\
\frac{\partial e_i}{\partial E_i} &= \frac{1}{2} \left( 1 + \frac{D_i - E_i}{\sqrt{(D_i - E_i)^2 + 4(b_{ix}^2 + b_{iy}^2)}} \right), \\
\frac{\partial e_i}{\partial b_{xi}} &= \frac{-2b_{ix}}{\sqrt{(D_i - E_i)^2 + 4(b_{ix}^2 + b_{iy}^2)}}, \\
\frac{\partial e_i}{\partial b_{yi}} &= \frac{-2b_{iy}}{\sqrt{(D_i - E_i)^2 + 4(b_{ix}^2 + b_{iy}^2)}}.
\end{aligned} \tag{B.32}$$

We end up with a complete set the final simplified derivatives for the z-factors in the charge rotational invariant formulation:

$$\begin{aligned}
\frac{\partial z_{i\uparrow}}{\partial D_i} &= \frac{1}{2\sqrt{(e_i^2 + p_{i\downarrow}^2)(d_i^2 + p_{i\uparrow}^2)}} \\
&\times \left[ \left( p_{i\downarrow} - \frac{(e_i p_{i\uparrow} + d_i p_{i\downarrow}) d_i}{d_i^2 + p_{i\uparrow}^2} \right) \left( 1 + \frac{D_i - E_i}{\sqrt{(D_i - E_i)^2 + 4(b_{ix}^2 + b_{iy}^2)}} \right) \right. \\
&\quad \left. + \left( p_{i\uparrow} - \frac{(e_i p_{i\uparrow} + d_i p_{i\downarrow}) e_i}{e_i^2 + p_{i\downarrow}^2} \right) \left( 1 - \frac{D_i - E_i}{\sqrt{(D_i - E_i)^2 + 4(b_{ix}^2 + b_{iy}^2)}} \right) \right],
\end{aligned} \tag{B.33}$$

$$\begin{aligned}
\frac{\partial z_{i\uparrow}}{\partial E_i} &= \frac{1}{2\sqrt{(e_i^2 + p_{i\downarrow}^2)(d_i^2 + p_{i\uparrow}^2)}} \\
&\times \left[ \left( p_{i\downarrow} - \frac{(e_i p_{i\uparrow} + d_i p_{i\downarrow}) d_i}{d_i^2 + p_{i\uparrow}^2} \right) \left( 1 - \frac{D_i - E_i}{\sqrt{(D_i - E_i)^2 + 4(b_{ix}^2 + b_{iy}^2)}} \right) \right. \\
&\quad \left. + \left( p_{i\uparrow} - \frac{(e_i p_{i\uparrow} + d_i p_{i\downarrow}) e_i}{e_i^2 + p_{i\downarrow}^2} \right) \left( 1 + \frac{D_i - E_i}{\sqrt{(D_i - E_i)^2 + 4(b_{ix}^2 + b_{iy}^2)}} \right) \right],
\end{aligned} \tag{B.34}$$

$$\begin{aligned} \frac{\partial z_{i\uparrow}}{\partial b_{xi}} &= \frac{2b_{ix}}{\sqrt{(D_i - E_i)^2 + 4(b_{ix}^2 + b_{iy}^2)}} \frac{1}{\sqrt{(e_i^2 + p_{i\downarrow}^2)(d_i^2 + p_{i\uparrow}^2)}} \\ &\times \left[ \left( p_{i\downarrow} - \frac{(e_i p_{i\uparrow} + d_i p_{i\downarrow}) d_i}{d_i^2 + p_{i\uparrow}^2} \right) - \left( p_{i\uparrow} - \frac{(e_i p_{i\uparrow} + d_i p_{i\downarrow}) e_i}{e_i^2 + p_{i\downarrow}^2} \right) \right], \end{aligned} \quad (\text{B.35})$$

$$\begin{aligned} \frac{\partial z_{i\uparrow}}{\partial b_{yi}} &= \frac{2b_{iy}}{\sqrt{(D_i - E_i)^2 + 4(b_{ix}^2 + b_{iy}^2)}} \frac{1}{\sqrt{(e_i^2 + p_{i\downarrow}^2)(d_i^2 + p_{i\uparrow}^2)}} \\ &\times \left[ \left( p_{i\downarrow} - \frac{(e_i p_{i\uparrow} + d_i p_{i\downarrow}) d_i}{d_i^2 + p_{i\uparrow}^2} \right) - \left( p_{i\uparrow} - \frac{(e_i p_{i\uparrow} + d_i p_{i\downarrow}) e_i}{e_i^2 + p_{i\downarrow}^2} \right) \right], \end{aligned} \quad (\text{B.36})$$

$$\begin{aligned} \frac{\partial z_{i\downarrow}}{\partial D_i} &= \frac{1}{2\sqrt{(e_i^2 + p_{i\uparrow}^2)(d_i^2 + p_{i\downarrow}^2)}} \\ &\times \left[ \left( p_{i\uparrow} - \frac{(e_i p_{i\downarrow} + d_i p_{i\uparrow}) d_i}{d_i^2 + p_{i\downarrow}^2} \right) \left( 1 + \frac{D_i - E_i}{\sqrt{(D_i - E_i)^2 + 4(b_{ix}^2 + b_{iy}^2)}} \right) \right. \\ &\left. + \left( p_{i\downarrow} - \frac{(e_i p_{i\downarrow} + d_i p_{i\uparrow}) e_i}{e_i^2 + p_{i\uparrow}^2} \right) \left( 1 - \frac{D_i - E_i}{\sqrt{(D_i - E_i)^2 + 4(b_{ix}^2 + b_{iy}^2)}} \right) \right], \end{aligned} \quad (\text{B.37})$$

$$\begin{aligned} \frac{\partial z_{i\downarrow}}{\partial E_i} &= \frac{1}{2\sqrt{(e_i^2 + p_{i\uparrow}^2)(d_i^2 + p_{i\downarrow}^2)}} \\ &\times \left[ \left( p_{i\uparrow} - \frac{(e_i p_{i\downarrow} + d_i p_{i\uparrow}) d_i}{d_i^2 + p_{i\downarrow}^2} \right) \left( 1 - \frac{D_i - E_i}{\sqrt{(D_i - E_i)^2 + 4(b_{ix}^2 + b_{iy}^2)}} \right) \right. \\ &\left. + \left( p_{i\downarrow} - \frac{(e_i p_{i\downarrow} + d_i p_{i\uparrow}) e_i}{e_i^2 + p_{i\uparrow}^2} \right) \left( 1 + \frac{D_i - E_i}{\sqrt{(D_i - E_i)^2 + 4(b_{ix}^2 + b_{iy}^2)}} \right) \right], \end{aligned} \quad (\text{B.38})$$

$$\begin{aligned} \frac{\partial z_{i\downarrow}}{\partial b_{xi}} &= \frac{2b_{ix}}{\sqrt{(D_i - E_i)^2 + 4(b_{ix}^2 + b_{iy}^2)}} \frac{1}{2\sqrt{(e_i^2 + p_{i\uparrow}^2)(d_i^2 + p_{i\downarrow}^2)}} \\ &\times \left[ \left( p_{i\uparrow} - \frac{(e_i p_{i\downarrow} + d_i p_{i\uparrow}) d_i}{d_i^2 + p_{i\downarrow}^2} \right) - \left( p_{i\downarrow} - \frac{(e_i p_{i\downarrow} + d_i p_{i\uparrow}) e_i}{e_i^2 + p_{i\uparrow}^2} \right) \right], \end{aligned} \quad (\text{B.39})$$

$$\begin{aligned} \frac{\partial z_{i\downarrow}}{\partial b_{yi}} &= \frac{2b_{iy}}{\sqrt{(D_i - E_i)^2 + 4(b_{ix}^2 + b_{iy}^2)}} \frac{1}{2\sqrt{(e_i^2 + p_{i\uparrow}^2)(d_i^2 + p_{i\downarrow}^2)}} \\ &\times \left[ \left( p_{i\uparrow} - \frac{(e_i p_{i\downarrow} + d_i p_{i\uparrow}) d_i}{d_i^2 + p_{i\downarrow}^2} \right) - \left( p_{i\downarrow} - \frac{(e_i p_{i\downarrow} + d_i p_{i\uparrow}) e_i}{e_i^2 + p_{i\uparrow}^2} \right) \right]. \end{aligned} \quad (\text{B.40})$$

## B.7 Derivatives of the MFA Matrix $\mathbf{A}^i$

The MFA matrix  $\mathbf{A}^i$ , that includes the local rotation and the mean field values of the boson fields is a function of the z-factors in the charge rotational invariant formulation:

$$\begin{aligned} A_{11}^i &= (z_{i\uparrow} \cos^2(\frac{\varphi_i}{2}) + z_{i\downarrow} \sin^2(\frac{\varphi_i}{2})) \\ A_{22}^i &= (z_{i\uparrow} \sin^2(\frac{\varphi_i}{2}) + z_{i\downarrow} \cos^2(\frac{\varphi_i}{2})) \\ A_{12}^i &= \frac{b_{xi} - ib_{yi}}{D_i - E_i} (z_{i\uparrow} - z_{i\downarrow}) \cos(\varphi_i) \\ A_{21}^i &= \frac{b_{xi} + ib_{yi}}{D_i - E_i} (z_{i\uparrow} - z_{i\downarrow}) \cos(\varphi_i) \end{aligned} \quad (\text{B.41})$$

The rotation angle  $\varphi_i$  can be written in terms of the slave bosons:

$$\begin{aligned} \cos^2(\frac{\varphi_i}{2}) &= \frac{1}{2}(1 + \cos(\varphi_i)) = \frac{1}{2} \left( 1 + \frac{D_i - E_i}{\sqrt{(D_i - E_i)^2 - 4(b_{ix}^2 + b_{iy}^2)}} \right) \\ \sin^2(\frac{\varphi_i}{2}) &= \frac{1}{2}(1 - \cos(\varphi_i)) = \frac{1}{2} \left( 1 - \frac{D_i - E_i}{\sqrt{(D_i - E_i)^2 - 4(b_{ix}^2 + b_{iy}^2)}} \right) \end{aligned} \quad (\text{B.42})$$



Summarizing formulae (B.41) and (B.42) the components of MFA matrix reads as:

$$\begin{aligned}
A_{11}^i &= \frac{1}{2} \left( (z_{i\uparrow} + z_{i\downarrow}) + (z_{i\uparrow} - z_{i\downarrow}) \frac{D_i - E_i}{\sqrt{(D_i - E_i)^2 + 4(b_{ix}^2 + b_{iy}^2)}} \right) \\
A_{22}^i &= \frac{1}{2} \left( (z_{i\uparrow} + z_{i\downarrow}) - (z_{i\uparrow} - z_{i\downarrow}) \frac{D_i - E_i}{\sqrt{(D_i - E_i)^2 + 4(b_{ix}^2 + b_{iy}^2)}} \right) \\
A_{12}^i &= (z_{i\uparrow} - z_{i\downarrow}) \frac{b_{xi} - ib_{yi}}{\sqrt{(D_i - E_i)^2 + 4(b_{ix}^2 + b_{iy}^2)}} \\
A_{21}^i &= (z_{i\uparrow} - z_{i\downarrow}) \frac{b_{xi} + ib_{yi}}{\sqrt{(D_i - E_i)^2 + 4(b_{ix}^2 + b_{iy}^2)}}
\end{aligned} \tag{B.43}$$

We the final expression for the derivatives of the 4 components of the MFA matrix  $\mathbf{A}^i$  with respect to the 6 charge rotational slave bosons:

$$\begin{aligned}
\frac{\partial A_{11}^i}{\partial D_i} &= \frac{1}{2} \left[ \left( \frac{\partial z_{i\uparrow}}{\partial D_i} + \frac{\partial z_{i\downarrow}}{\partial D_i} \right) \right. \\
&\quad + \left( \frac{\partial z_{i\uparrow}}{\partial D_i} - \frac{\partial z_{i\downarrow}}{\partial D_i} \right) \frac{D_i - E_i}{\sqrt{(D_i - E_i)^2 - 4(b_{ix}^2 + b_{iy}^2)}} \\
&\quad \left. + (z_{i\uparrow} - z_{i\downarrow}) \left( \frac{1}{\sqrt{(D_i - E_i)^2 - 4(b_{ix}^2 + b_{iy}^2)}} - \frac{(D_i - E_i)^2}{\left( \sqrt{(D_i - E_i)^2 - 4(b_{ix}^2 + b_{iy}^2)} \right)^3} \right) \right],
\end{aligned} \tag{B.44}$$

$$\begin{aligned}
\frac{\partial A_{11}^i}{\partial E_i} &= \frac{1}{2} \left[ \left( \frac{\partial z_{i\uparrow}}{\partial E_i} + \frac{\partial z_{i\downarrow}}{\partial E_i} \right) \right. \\
&\quad + \left( \frac{\partial z_{i\uparrow}}{\partial E_i} - \frac{\partial z_{i\downarrow}}{\partial E_i} \right) \frac{D_i - E_i}{\sqrt{(D_i - E_i)^2 + 4(b_{ix}^2 + b_{iy}^2)}} \\
&\quad \left. - (z_{i\uparrow} - z_{i\downarrow}) \left( \frac{1}{\sqrt{(D_i - E_i)^2 - 4(b_{ix}^2 + b_{iy}^2)}} - \frac{(D_i - E_i)^2}{\left( \sqrt{(D_i - E_i)^2 - 4(b_{ix}^2 + b_{iy}^2)} \right)^3} \right) \right],
\end{aligned} \tag{B.45}$$

$$\begin{aligned} \frac{\partial A_{11}^i}{\partial p_{i\uparrow}} &= \frac{1}{2} \left[ \left( \frac{\partial z_{i\uparrow}}{\partial p_{i\uparrow}} + \frac{\partial z_{i\downarrow}}{\partial p_{i\uparrow}} \right) \right. \\ &\quad \left. + \left( \frac{\partial z_{i\uparrow}}{\partial p_{i\uparrow}} - \frac{\partial z_{i\downarrow}}{\partial p_{i\uparrow}} \right) \frac{D_i - E_i}{\sqrt{(D_i - E_i)^2 + 4(b_{ix}^2 + b_{iy}^2)}} \right], \end{aligned} \quad (\text{B.46})$$

$$\begin{aligned} \frac{\partial A_{11}^i}{\partial p_{i\downarrow}} &= \frac{1}{2} \left[ \left( \frac{\partial z_{i\uparrow}}{\partial p_{i\downarrow}} + \frac{\partial z_{i\downarrow}}{\partial p_{i\downarrow}} \right) \right. \\ &\quad \left. + \left( \frac{\partial z_{i\uparrow}}{\partial p_{i\downarrow}} - \frac{\partial z_{i\downarrow}}{\partial p_{i\downarrow}} \right) \frac{D_i - E_i}{\sqrt{(D_i - E_i)^2 + 4(b_{ix}^2 + b_{iy}^2)}} \right], \end{aligned} \quad (\text{B.47})$$

$$\begin{aligned} \frac{\partial A_{11}^i}{\partial b_{ix}} &= \frac{1}{2} \left[ \left( \frac{\partial z_{i\uparrow}}{\partial b_{ix}} + \frac{\partial z_{i\downarrow}}{\partial b_{ix}} \right) \right. \\ &\quad + \left( \frac{\partial z_{i\uparrow}}{\partial b_{ix}} - \frac{\partial z_{i\downarrow}}{\partial b_{ix}} \right) \frac{D_i - E_i}{\sqrt{(D_i - E_i)^2 + 4(b_{ix}^2 + b_{iy}^2)}} \\ &\quad \left. - (z_{i\uparrow} - z_{i\downarrow}) \frac{4b_{ix}(D_i - E_i)}{\left( \sqrt{(D_i - E_i)^2 + 4(b_{ix}^2 + b_{iy}^2)} \right)^3} \right], \end{aligned} \quad (\text{B.48})$$

$$\begin{aligned} \frac{\partial A_{11}^i}{\partial b_{iy}} &= \frac{1}{2} \left[ \left( \frac{\partial z_{i\uparrow}}{\partial b_{iy}} + \frac{\partial z_{i\downarrow}}{\partial b_{iy}} \right) \right. \\ &\quad + \left( \frac{\partial z_{i\uparrow}}{\partial b_{iy}} - \frac{\partial z_{i\downarrow}}{\partial b_{iy}} \right) \frac{D_i - E_i}{\sqrt{(D_i - E_i)^2 + 4(b_{ix}^2 + b_{iy}^2)}} \\ &\quad \left. - (z_{i\uparrow} - z_{i\downarrow}) \frac{4b_{iy}(D_i - E_i)}{\left( \sqrt{(D_i - E_i)^2 + 4(b_{ix}^2 + b_{iy}^2)} \right)^3} \right] \end{aligned} \quad (\text{B.49})$$

$$\begin{aligned}
\frac{\partial A_{22}^i}{\partial D_i} &= \frac{1}{2} \left[ \left( \frac{\partial z_{i\uparrow}}{\partial D_i} + \frac{\partial z_{i\downarrow}}{\partial D_i} \right) \right. \\
&\quad - \left( \frac{\partial z_{i\uparrow}}{\partial D_i} - \frac{\partial z_{i\downarrow}}{\partial D_i} \right) \frac{D_i - E_i}{\sqrt{(D_i - E_i)^2 + 4(b_{ix}^2 + b_{iy}^2)}} \\
&\quad \left. - (z_{i\uparrow} - z_{i\downarrow}) \left( \frac{1}{\sqrt{(D_i - E_i)^2 - 4(b_{ix}^2 + b_{iy}^2)}} - \frac{(D_i - E_i)^2}{\left( \sqrt{(D_i - E_i)^2 - 4(b_{ix}^2 + b_{iy}^2)} \right)^3} \right) \right], \tag{B.50}
\end{aligned}$$

$$\begin{aligned}
\frac{\partial A_{22}^i}{\partial E_i} &= \frac{1}{2} \left[ \left( \frac{\partial z_{i\uparrow}}{\partial E_i} + \frac{\partial z_{i\downarrow}}{\partial E_i} \right) \right. \\
&\quad - \left( \frac{\partial z_{i\uparrow}}{\partial E_i} - \frac{\partial z_{i\downarrow}}{\partial E_i} \right) \frac{D_i - E_i}{\sqrt{(D_i - E_i)^2 + 4(b_{ix}^2 + b_{iy}^2)}} \\
&\quad \left. + (z_{i\uparrow} - z_{i\downarrow}) \left( \frac{1}{\sqrt{(D_i - E_i)^2 - 4(b_{ix}^2 + b_{iy}^2)}} - \frac{(D_i - E_i)^2}{\left( \sqrt{(D_i - E_i)^2 - 4(b_{ix}^2 + b_{iy}^2)} \right)^3} \right) \right], \tag{B.51}
\end{aligned}$$

$$\begin{aligned}
\frac{\partial A_{22}^i}{\partial p_{i\uparrow}} &= \frac{1}{2} \left[ \left( \frac{\partial z_{i\uparrow}}{\partial p_{i\uparrow}} + \frac{\partial z_{i\downarrow}}{\partial p_{i\uparrow}} \right) \right. \\
&\quad \left. - \left( \frac{\partial z_{i\uparrow}}{\partial p_{i\uparrow}} - \frac{\partial z_{i\downarrow}}{\partial p_{i\uparrow}} \right) \frac{D_i - E_i}{\sqrt{(D_i - E_i)^2 + 4(b_{ix}^2 + b_{iy}^2)}} \right], \tag{B.52}
\end{aligned}$$

$$\begin{aligned}
\frac{\partial A_{22}^i}{\partial p_{i\downarrow}} &= \frac{1}{2} \left[ \left( \frac{\partial z_{i\uparrow}}{\partial p_{i\downarrow}} + \frac{\partial z_{i\downarrow}}{\partial p_{i\downarrow}} \right) \right. \\
&\quad \left. - \left( \frac{\partial z_{i\uparrow}}{\partial p_{i\downarrow}} - \frac{\partial z_{i\downarrow}}{\partial p_{i\downarrow}} \right) \frac{D_i - E_i}{\sqrt{(D_i - E_i)^2 + 4(b_{ix}^2 + b_{iy}^2)}} \right], \tag{B.53}
\end{aligned}$$

$$\begin{aligned} \frac{\partial A_{22}^i}{\partial b_{ix}} &= \frac{1}{2} \left[ \left( \frac{\partial z_{i\uparrow}}{\partial b_{ix}} + \frac{\partial z_{i\downarrow}}{\partial b_{ix}} \right) \right. \\ &\quad - \left( \frac{\partial z_{i\uparrow}}{\partial b_{ix}} - \frac{\partial z_{i\downarrow}}{\partial b_{ix}} \right) \frac{D_i - E_i}{\sqrt{(D_i - E_i)^2 + 4(b_{ix}^2 + b_{iy}^2)}} \\ &\quad \left. + (z_{i\uparrow} - z_{i\downarrow}) \frac{4b_{ix}(D_i - E_i)}{\left( \sqrt{(D_i - E_i)^2 + 4(b_{ix}^2 + b_{iy}^2)} \right)^3} \right], \end{aligned} \quad (\text{B.54})$$

$$\begin{aligned} \frac{\partial A_{22}^i}{\partial b_{iy}} &= \frac{1}{2} \left[ \left( \frac{\partial z_{i\uparrow}}{\partial b_{iy}} + \frac{\partial z_{i\downarrow}}{\partial b_{iy}} \right) \right. \\ &\quad - \left( \frac{\partial z_{i\uparrow}}{\partial b_{iy}} - \frac{\partial z_{i\downarrow}}{\partial b_{iy}} \right) \frac{D_i - E_i}{\sqrt{(D_i - E_i)^2 + 4(b_{ix}^2 + b_{iy}^2)}} \\ &\quad \left. + (z_{i\uparrow} - z_{i\downarrow}) \frac{4b_{iy}(D_i - E_i)}{\left( \sqrt{(D_i - E_i)^2 + 4(b_{ix}^2 + b_{iy}^2)} \right)^3} \right], \end{aligned} \quad (\text{B.55})$$

$$\begin{aligned} \frac{\partial A_{12}^i}{\partial D_i} &= \left( \frac{\partial z_{i\uparrow}}{\partial D_i} - \frac{\partial z_{i\downarrow}}{\partial D_i} \right) \frac{(b_{ix} - ib_{iy})}{\sqrt{(D_i - E_i)^2 + 4(b_{ix}^2 + b_{iy}^2)}} \\ &\quad - (z_{i\uparrow} - z_{i\downarrow}) \frac{(b_{ix} - ib_{iy})(D_i - E_i)}{\left( \sqrt{(D_i - E_i)^2 + 4(b_{ix}^2 + b_{iy}^2)} \right)^3} \end{aligned} \quad (\text{B.56})$$

$$\begin{aligned} \frac{\partial A_{12}^i}{\partial E_i} &= \left( \frac{\partial z_{i\uparrow}}{\partial E_i} - \frac{\partial z_{i\downarrow}}{\partial E_i} \right) \frac{(b_{ix} - ib_{iy})}{\sqrt{(D_i - E_i)^2 + 4(b_{ix}^2 + b_{iy}^2)}} \\ &\quad + (z_{i\uparrow} - z_{i\downarrow}) \frac{(b_{ix} - ib_{iy})(D_i - E_i)}{\left( \sqrt{(D_i - E_i)^2 + 4(b_{ix}^2 + b_{iy}^2)} \right)^3}, \end{aligned} \quad (\text{B.57})$$

$$\frac{\partial A_{12}^i}{\partial p_{i\uparrow}} = \left( \frac{\partial z_{i\uparrow}}{\partial p_{i\uparrow}} - \frac{\partial z_{i\downarrow}}{\partial p_{i\uparrow}} \right) \frac{(b_{ix} - ib_{iy})}{\sqrt{(D_i - E_i)^2 + 4(b_{ix}^2 + b_{iy}^2)}}, \quad (\text{B.58})$$

$$\frac{\partial A_{12}^i}{\partial p_{i\downarrow}} = \left( \frac{\partial z_{i\uparrow}}{\partial p_{i\downarrow}} - \frac{\partial z_{i\downarrow}}{\partial p_{i\downarrow}} \right) \frac{(b_{ix} - ib_{iy})}{\sqrt{(D_i - E_i)^2 + 4(b_{ix}^2 + b_{iy}^2)}}, \quad (\text{B.59})$$

$$\begin{aligned} \frac{\partial A_{12}^i}{\partial b_{ix}} &= \left( \frac{\partial z_{i\uparrow}}{\partial b_{ix}} - \frac{\partial z_{i\downarrow}}{\partial b_{ix}} \right) \frac{(b_{ix} - ib_{iy})}{\sqrt{(D_i - E_i)^2 + 4(b_{ix}^2 + b_{iy}^2)}} \\ &+ (z_{i\uparrow} - z_{i\downarrow}) \left( \frac{1}{\sqrt{(D_i - E_i)^2 + 4(b_{ix}^2 + b_{iy}^2)}} - \frac{4b_{ix}(b_{ix} - ib_{iy})}{\left(\sqrt{(D_i - E_i)^2 + 4(b_{ix}^2 + b_{iy}^2)}\right)^3} \right), \end{aligned} \quad (\text{B.60})$$

$$\begin{aligned} \frac{\partial A_{12}^i}{\partial b_{iy}} &= \left( \frac{\partial z_{i\uparrow}}{\partial b_{iy}} - \frac{\partial z_{i\downarrow}}{\partial b_{iy}} \right) \frac{(b_{ix} - ib_{iy})}{\sqrt{(D_i - E_i)^2 + 4(b_{ix}^2 + b_{iy}^2)}} \\ &+ (z_{i\uparrow} - z_{i\downarrow}) \left( \frac{-i}{\sqrt{(D_i - E_i)^2 + 4(b_{ix}^2 + b_{iy}^2)}} - \frac{4b_{iy}(b_{ix} - ib_{iy})}{\left(\sqrt{(D_i - E_i)^2 + 4(b_{ix}^2 + b_{iy}^2)}\right)^3} \right), \end{aligned} \quad (\text{B.61})$$

$$\begin{aligned} \frac{\partial A_{21}^i}{\partial D_i} &= \left( \frac{\partial z_{i\uparrow}}{\partial D_i} - \frac{\partial z_{i\downarrow}}{\partial D_i} \right) \frac{(b_{ix} + ib_{iy})}{\sqrt{(D_i - E_i)^2 + 4(b_{ix}^2 + b_{iy}^2)}} \\ &- (z_{i\uparrow} - z_{i\downarrow}) \frac{(b_{ix} + ib_{iy})(D_i - E_i)}{\left(\sqrt{(D_i - E_i)^2 + 4(b_{ix}^2 + b_{iy}^2)}\right)^3}, \end{aligned} \quad (\text{B.62})$$

$$\begin{aligned} \frac{\partial A_{21}^i}{\partial E_i} &= \left( \frac{\partial z_{i\uparrow}}{\partial E_i} - \frac{\partial z_{i\downarrow}}{\partial E_i} \right) \frac{(b_{ix} + ib_{iy})}{\sqrt{(D_i - E_i)^2 + 4(b_{ix}^2 + b_{iy}^2)}} \\ &+ (z_{i\uparrow} - z_{i\downarrow}) \frac{(b_{ix} + ib_{iy})(D_i - E_i)}{\left(\sqrt{(D_i - E_i)^2 + 4(b_{ix}^2 + b_{iy}^2)}\right)^3}, \end{aligned} \quad (\text{B.63})$$

$$\frac{\partial A_{21}^i}{\partial p_{i\uparrow}} = \left( \frac{\partial z_{i\uparrow}}{\partial p_{i\uparrow}} - \frac{\partial z_{i\downarrow}}{\partial p_{i\uparrow}} \right) \frac{(b_{ix} + ib_{iy})}{\sqrt{(D_i - E_i)^2 + 4(b_{ix}^2 + b_{iy}^2)}}, \quad (\text{B.64})$$

$$\frac{\partial A_{21}^i}{\partial p_{i\downarrow}} = \left( \frac{\partial z_{i\uparrow}}{\partial p_{i\downarrow}} - \frac{\partial z_{i\downarrow}}{\partial p_{i\downarrow}} \right) \frac{(b_{ix} + ib_{iy})}{\sqrt{(D_i - E_i)^2 + 4(b_{ix}^2 + b_{iy}^2)}}, \quad (\text{B.65})$$

$$\begin{aligned} \frac{\partial A_{21}^i}{\partial b_{ix}} &= \left( \frac{\partial z_{i\uparrow}}{\partial b_{ix}} - \frac{\partial z_{i\downarrow}}{\partial b_{ix}} \right) \frac{(b_{ix} + ib_{iy})}{\sqrt{(D_i - E_i)^2 + 4(b_{ix}^2 + b_{iy}^2)}} \\ &+ (z_{i\uparrow} - z_{i\downarrow}) \left( \frac{1}{\sqrt{(D_i - E_i)^2 + 4(b_{ix}^2 + b_{iy}^2)}} - \frac{4b_{ix}(b_{ix} + ib_{iy})}{\left(\sqrt{(D_i - E_i)^2 + 4(b_{ix}^2 + b_{iy}^2)}\right)^3} \right), \end{aligned} \quad (\text{B.66})$$

$$\begin{aligned} \frac{\partial A_{21}^i}{\partial b_{iy}} &= \left( \frac{\partial z_{i\uparrow}}{\partial b_{iy}} - \frac{\partial z_{i\downarrow}}{\partial b_{iy}} \right) \frac{(b_{ix} + ib_{iy})}{\sqrt{(D_i - E_i)^2 + 4(b_{ix}^2 + b_{iy}^2)}} \\ &+ (z_{i\uparrow} - z_{i\downarrow}) \left( \frac{i}{\sqrt{(D_i - E_i)^2 + 4(b_{ix}^2 + b_{iy}^2)}} - \frac{4b_{iy}(b_{ix} + ib_{iy})}{\left(\sqrt{(D_i - E_i)^2 + 4(b_{ix}^2 + b_{iy}^2)}\right)^3} \right). \end{aligned} \quad (\text{B.67})$$

## B.8 Derivatives of the Inter Site Repulsion Term

The expectation value of the inter site repulsion term reads:

$$\begin{aligned} \langle \hat{H}_{HF}^R \rangle &= V \sum_{\langle ij \rangle} [ \langle \hat{c}_{i\uparrow}^\dagger \hat{c}_{i\uparrow} \rangle \langle \hat{c}_{j\uparrow}^\dagger \hat{c}_{j\uparrow} \rangle + \langle \hat{c}_{i\uparrow}^\dagger \hat{c}_{i\uparrow} \rangle \langle \hat{c}_{j\downarrow}^\dagger \hat{c}_{j\downarrow} \rangle \\ &+ \langle \hat{c}_{i\downarrow}^\dagger \hat{c}_{i\downarrow} \rangle \langle \hat{c}_{j\uparrow}^\dagger \hat{c}_{j\uparrow} \rangle + \langle \hat{c}_{i\downarrow}^\dagger \hat{c}_{i\downarrow} \rangle \langle \hat{c}_{j\downarrow}^\dagger \hat{c}_{j\downarrow} \rangle \\ &- \langle \hat{c}_{i\uparrow}^\dagger \hat{c}_{j\uparrow} \rangle \langle \hat{c}_{i\uparrow}^\dagger \hat{c}_{j\uparrow} \rangle - \langle \hat{c}_{i\downarrow}^\dagger \hat{c}_{j\downarrow} \rangle \langle \hat{c}_{i\downarrow}^\dagger \hat{c}_{j\downarrow} \rangle \\ &+ \langle \hat{c}_{i\uparrow}^\dagger \hat{c}_{j\downarrow} \rangle \langle \hat{c}_{j\downarrow}^\dagger \hat{c}_{i\uparrow} \rangle + \langle \hat{c}_{j\uparrow}^\dagger \hat{c}_{i\downarrow} \rangle \langle \hat{c}_{i\downarrow}^\dagger \hat{c}_{j\uparrow} \rangle ]. \end{aligned} \quad (\text{B.68})$$

We write down the partial derivatives (B.68) with respect to the amplitudes of the Bogolioubov transformation.

In the case of  $m \leq N$  and  $k \leq N$  one obtains:

$$\begin{aligned} \frac{\partial}{\partial x_m(k)} H^R &= 4x_m(k) \sum_{j(m)} (\rho_{jj}^{\uparrow\uparrow} + \rho_{jj}^{\downarrow\downarrow}) \\ &- 4 \sum_{j(m)} \left[ \operatorname{Re}(\rho_{mj}^{\uparrow\uparrow}) x_j(k) - \operatorname{Im}(\rho_{mj}^{\uparrow\uparrow}) y_j(k) \right] \\ &+ 4 \sum_{j(m)} \left[ \operatorname{Re}(\rho_{mj}^{\downarrow\downarrow}) x_{j+N}(k) + \operatorname{Im}(\rho_{mj}^{\downarrow\downarrow}) y_{j+N}(k) \right], \end{aligned} \quad (\text{B.69})$$

and

$$\begin{aligned} \frac{\partial}{\partial y_m(k)} H^R &= 4y_m(k) \sum_{j(m)} (\rho_{jj}^{\uparrow\uparrow} + \rho_{jj}^{\downarrow\downarrow}) \\ &- 4 \sum_{j(m)} \left[ \operatorname{Re}(\rho_{mj}^{\uparrow\uparrow}) y_j(k) + \operatorname{Im}(\rho_{mj}^{\uparrow\uparrow}) x_j(k) \right] \\ &+ 4 \sum_{j(m)} \left[ \operatorname{Re}(\rho_{mj}^{\downarrow\downarrow}) y_{j+N}(k) - \operatorname{Im}(\rho_{mj}^{\downarrow\downarrow}) x_{j+N}(k) \right]. \end{aligned} \quad (\text{B.70})$$

In the case of  $m > N$  and  $k \leq N$  one obtains:

$$\frac{\partial}{\partial x_m(k)} H^R = 4 \sum_{j(m)} \left[ \operatorname{Re}(\rho_{(m-N)j}^{\downarrow\uparrow}) x_j(k) + \operatorname{Im}(\rho_{(m-N)j}^{\downarrow\uparrow}) y_j(k) \right], \quad (\text{B.71})$$

and

$$\frac{\partial}{\partial y_m(k)} H^R = 4 \sum_{j(m-N)} \left[ \operatorname{Re}(\rho_{(m-N)j}^{\downarrow\uparrow}) y_j(k) - \operatorname{Im}(\rho_{(m-N)j}^{\downarrow\uparrow}) x_j(k) \right]. \quad (\text{B.72})$$

In the case of  $m > N$  and  $k > N$  one obtains:

$$\begin{aligned} \frac{\partial}{\partial x_m(k)} H^R &= 4x_m(k) \sum_{j(m-N)} (\rho_{jj}^{\uparrow\uparrow} + \rho_{jj}^{\downarrow\downarrow}) \\ &- 4 \sum_{j(m-N)} \left[ \operatorname{Re}(\rho_{(m-N)j}^{\downarrow\downarrow}) x_{j+N}(k) + \operatorname{Im}(\rho_{(m-N)j}^{\downarrow\downarrow}) y_{j+N}(k) \right], \end{aligned} \quad (\text{B.73})$$

and

$$\begin{aligned} \frac{\partial}{\partial x_m(k)} H^{\text{R}} &= 4y_m(k) \sum_{j(m-N)} (\rho_{jj}^{\uparrow\uparrow} + \rho_{jj}^{\downarrow\downarrow}) \\ &- 4 \sum_{j(m-N)} \left[ \text{Re}(\rho_{(m-N)j}^{\downarrow\downarrow}) y_{j+N}(k) - \text{Im}(\rho_{(m-N)j}^{\downarrow\downarrow}) x_{j+N}(k) \right]. \end{aligned} \quad (\text{B.74})$$



# Appendix C

## C.1 The Bardeen-Cooper-Schrieffer Theory

We start with the BCS Hamiltonian operator reads in the free energy formulation:

$$H = \sum_{k\sigma} (\varepsilon_k - \mu) \hat{c}_{k\sigma}^\dagger \hat{c}_{k\sigma} - U \sum_{kk'} \hat{c}_{k'\uparrow}^\dagger \hat{c}_{-k'\downarrow}^\dagger \hat{c}_{-k\downarrow} \hat{c}_{k\uparrow}. \quad (\text{C.1})$$

The kinetic energy describes s-wave-like electron system an potential term includes the phonon mediated attractive electron interaction where two electron corresponds to an other with opposite momentum and spin. We follow the derivation in [125] but we add the Fermi energy  $\mu$  in order to work in the canonical ensemble.

In the first step we perform the mean-field approximation where we use a HF-like decoupling where we respect the anomalous pair correlations yielding the effective Hamiltonian:

$$\begin{aligned} H^{eff} &= \sum_{k\sigma} (\varepsilon_k - \mu) \hat{c}_{k\sigma}^\dagger \hat{c}_{k\sigma} - U \sum_{kk'} \langle \hat{c}_{k'\uparrow}^\dagger \hat{c}_{-k'\downarrow}^\dagger \rangle \hat{c}_{-k\downarrow} \hat{c}_{k\uparrow} - U \sum_{kk'} \langle \hat{c}_{-k\downarrow} \hat{c}_{k\uparrow} \rangle \hat{c}_{k'\uparrow}^\dagger \hat{c}_{-k'\downarrow}^\dagger \\ &+ U \sum_{kk'} \langle \hat{c}_{k'\uparrow}^\dagger \hat{c}_{-k'\downarrow}^\dagger \rangle \langle \hat{c}_{-k\downarrow} \hat{c}_{k\uparrow} \rangle. \end{aligned} \quad (\text{C.2})$$

New order parameters can be defined:  $\Delta = \sum_k \langle \hat{c}_{-k\downarrow} \hat{c}_{k\uparrow} \rangle$  and  $\Delta^* = \sum_k \langle \hat{c}_{k\uparrow}^\dagger \hat{c}_{-k\downarrow}^\dagger \rangle$  measuring the average pair density. This Hamiltonian has a unusual form since two creation

and destruction operators follow in one term. In order to bring this Hamiltonian in the one particle formulation one uses the Bogoliubov-Transformation:

$$\begin{aligned}\hat{\alpha}_k &= u_k \hat{c}_{k\uparrow} - v_k \hat{c}_{-k\downarrow}^\dagger, & \hat{\alpha}_k^\dagger &= u_k^* \hat{c}_{k\uparrow}^\dagger - v_k^* \hat{c}_{-k\downarrow} \\ \hat{\beta}_k &= u_k \hat{c}_{-k\downarrow} + v_k \hat{c}_{k\uparrow}^\dagger, & \hat{\beta}_k^\dagger &= u_k^* \hat{c}_{-k\downarrow}^\dagger + v_k^* \hat{c}_{k\uparrow}\end{aligned}\quad (\text{C.3})$$

where the new operators obey the fermionic anti commutator relations:

$$\begin{aligned}\left[\hat{\alpha}_k, \hat{\beta}_{k'}\right]_+ &= 0, & \left[\hat{\alpha}_k^\dagger, \hat{\beta}_{k'}^\dagger\right]_+ &= 0, & \left[\hat{\alpha}_k, \hat{\beta}_{k'}^\dagger\right]_+ &= 0, \\ \left[\hat{\alpha}_k, \hat{\alpha}_{k'}^\dagger\right]_+ &= \left[\hat{\beta}_k, \hat{\beta}_{k'}^\dagger\right]_+ & &= (|u_k|^2 + |v_k|^2) \delta_{kk'}.\end{aligned}\quad (\text{C.4})$$

For normalization reasons the transformation must hold:  $|u_k|^2 + |v_k|^2 = 1$ . The  $u_k$  and  $v_k$  have to be calculated with respect to the effective Hamiltonian  $H^{eff}$ . The Hamiltonian has to be diagonal and bilinear in the new operator vectors  $(\hat{\alpha}_k^\dagger, \hat{\beta}_k)$  and  $(\hat{\alpha}_k, \hat{\beta}_k^\dagger)$ :

$$|u_k|^2 = \frac{1}{2} \left(1 + \frac{\varepsilon_k - \mu}{E_k}\right) \quad \text{and} \quad |v_k|^2 = \frac{1}{2} \left(1 - \frac{\varepsilon_k - \mu}{E_k}\right), \quad (\text{C.5})$$

and the definition:

$$E_k = \sqrt{(\varepsilon_k - \mu)^2 + U^2 \Delta^2}. \quad (\text{C.6})$$

The effective Hamiltonian than takes the form:

$$H^{eff} = \sum_{k\sigma} E_k (\hat{\alpha}_k^\dagger \hat{\alpha}_k + \hat{\beta}_k^\dagger \hat{\beta}_k) + \sum_k (\varepsilon_k - \mu - E_k) + U |\Delta|^2$$

If one expresses the order parameter with respect to the effective Hamiltonian  $\Delta = \sum_k \langle \hat{c}_{-k\downarrow} \hat{c}_{k\uparrow} \rangle_{H^{eff}}$  respecting (C.3) and (C.5) one derives the simplified self consistency equation (provided  $\Delta \neq 0$ ):

$$1 = \frac{U}{2} \sum_k \frac{1}{\sqrt{(\varepsilon_k - \mu)^2 + U^2 |\Delta|^2}} \quad (\text{C.7})$$

This equation allows the calculation of the order parameter  $\Delta$ .

## C.2 Attraction-Repulsion Transformation

The attractive Hubbard model can be transferred to the repulsive (normal) Hubbard model with an inter-atomic Ising exchange with an additional external field [48, 50, 107]:

$$\begin{aligned}\hat{c}_{i\uparrow} &= \hat{g}_{i\uparrow}, & \hat{c}_{i\downarrow} &= (-1)^{i_x+i_y} \hat{g}_{i\downarrow}^\dagger, \\ \hat{c}_{i\uparrow}^\dagger &= \hat{g}_{i\uparrow}^\dagger, & \hat{c}_{i\downarrow}^\dagger &= (-1)^{i_x+i_y} \hat{g}_{i\downarrow}.\end{aligned}\quad (\text{C.8})$$

Respecting the anti commutation  $[\hat{g}_{i\sigma}^\dagger, \hat{g}_{j\sigma}]_+ = \delta_{ij}$  we obtain for the Hubbard Hamiltonian for NN transitions:

$$\begin{aligned}\hat{H} &= \sum_{\langle ij \rangle \sigma} t_{ij} \hat{c}_{i\sigma}^\dagger \hat{c}_{j\sigma} + U \sum_i \hat{c}_{i\uparrow}^\dagger \hat{c}_{i\uparrow} \hat{c}_{i\downarrow}^\dagger \hat{c}_{i\downarrow} \\ &= \sum_{\langle ij \rangle \sigma} t_{ij} \hat{g}_{i\sigma}^\dagger \hat{g}_{j\sigma} + U \sum_i (-1)^{2(i_x+i_y)} \hat{g}_{i\uparrow}^\dagger \hat{g}_{i\uparrow} \hat{g}_{i\downarrow} \hat{g}_{i\downarrow}^\dagger \\ &= \sum_{\langle ij \rangle \sigma} t_{ij} \hat{g}_{i\sigma}^\dagger \hat{g}_{j\sigma} - U \sum_i \hat{g}_{i\uparrow}^\dagger \hat{g}_{i\uparrow} \hat{g}_{i\downarrow}^\dagger \hat{g}_{i\downarrow} + U \sum_i \hat{g}_{i\uparrow}^\dagger \hat{g}_{i\uparrow}\end{aligned}\quad (\text{C.9})$$

where the kinetic energy commutes for the summation over NN and NNN explicitly:

$$\begin{aligned}\hat{T}_\downarrow &= \sum_{ij} t_{ij} (-1)^{(i_x+i_y+j_x+j_y)} \hat{g}_{i\downarrow} \hat{g}_{j\downarrow}^\dagger \\ &= \sum_i \left\{ \sum_{l=\pm 1} t \left[ (-1)^{(2i_x+l+2i_y)} \hat{g}_{i\downarrow} \hat{g}_{j\downarrow}^\dagger + (-1)^{(2i_x+2i_y+l)} \hat{g}_{i\downarrow} \hat{g}_{j\downarrow}^\dagger \right] + \sum_{n,m=\pm 1} t' (-1)^{i_x+n+i_y+m} \hat{g}_{i\downarrow} \hat{g}_{j\downarrow}^\dagger \right\} \\ &= \sum_{ij}^{NN} t_{ij} (-1) \hat{g}_{i\downarrow} \hat{g}_{j\downarrow}^\dagger + \sum_{ij}^{NNN} t'_{ij} \hat{g}_{i\downarrow} \hat{g}_{j\downarrow}^\dagger \\ &= \sum_{ij}^{NN} t_{ij} \hat{g}_{i\downarrow}^\dagger \hat{g}_{j\downarrow} + \sum_{ij}^{NNN} \tilde{t}'_{ij} \hat{g}_{i\downarrow}^\dagger \hat{g}_{j\downarrow}\end{aligned}\quad (\text{C.10})$$

where we use the short hand notation  $j = (j_x, j_y)$ . We used the anti commutator relation for  $j \neq j = 0$  and the symmetry relations  $t_{ij} = t_{ji}$  and we replaced  $\tilde{t}'_{ij} = -t'_{ij}$ . The attractive-repulsive-transformation changes the sign of the NNN hopping parameter.

The charge vector  $\hat{\mathbf{J}}$  transforms to the Spin vector  $\hat{\mathbf{S}}$ . The components read:

$$\begin{aligned}\hat{J}_i^x &= \frac{1}{2} \left[ \hat{c}_{i\uparrow}^\dagger \hat{c}_{i\downarrow}^\dagger + \hat{c}_{i\downarrow} \hat{c}_{i\uparrow} \right] \\ &= \frac{1}{2} (-1)^{(i_x+i_y)} \left[ \hat{g}_{i\uparrow}^\dagger \hat{g}_{i\downarrow} + \hat{g}_{i\downarrow}^\dagger \hat{g}_{i\uparrow} \right] \\ &= (-1)^{(i_x+i_y)} \hat{S}_i^x\end{aligned}\tag{C.11}$$

and in analogy we derive  $\hat{J}_i^y = (-1)^{(i_x+i_y)} S_i^y$  and  $\hat{J}_i^z = \hat{S}_i^z$ . For the ladder operators we obtain:  $\hat{J}_i^\pm \iff (-1)^{i_x+i_y} \hat{S}_i^\pm$  and for the order parameters:

$$n_i \iff \tilde{m}_i + 1 \quad \text{and} \quad m_i \iff \tilde{n}_i - 1,\tag{C.12}$$

where we used the definition  $n_i = (n_{i\uparrow} + n_{i\downarrow})$  and  $m_i = (n_{i\uparrow} - n_{i\downarrow})$ . With the help of this formulae one can transform a homogeneous charged superconductor to an anti-ferromagnet.

### C.3 Second Order Perturbation Theory

We assume arbitrary local charge density  $\rho_i = \frac{1}{2}(c_{i\uparrow}^\dagger c_{i\uparrow} + c_{i\downarrow}^\dagger c_{i\downarrow})$ . Applying the continuity equation we use  $[H, \rho_i] = iJ_i^z$  with the local charge density we derive an expression for the total current flow at lattice site  $i$ :

$$[\hat{H}, \hat{\rho}_i] = \sum_m \hat{J}_{i,m}^z\tag{C.13}$$

where  $\hat{H}$  is the Hubbard Hamiltonian Eq. (2.1) and the sum goes over all lattice sites where transition processes are allowed by the matrix element  $t_{ij}$ . In order to find an expression for the 2nd order perturbation theory the transform Hilbert vectors and

operators into the Heisenberg picture:

$$\begin{aligned}
\langle 0 | \sum_{im} \hat{J}_{i,m}^z | \nu \rangle &= \langle 0 | \exp \left( -\frac{i}{\hbar} \hat{H} t \right) \exp \left( \frac{i}{\hbar} \hat{H} t \right) \sum_{im} \hat{J}_{i,m}^z \exp \left( -\frac{i}{\hbar} \hat{H} t \right) \exp \left( \frac{i}{\hbar} \hat{H} t \right) | \nu \rangle \\
&= \langle 0 |_H [\hat{H}, \hat{\rho}^H] | \nu \rangle_H \\
&= (-i\hbar) \langle 0 |_H \frac{d}{dt} \hat{\rho}^H | \nu \rangle_H \\
&= (-i\hbar) \langle 0 |_H \frac{d}{dt} \left( e^{i\frac{\hat{H}}{\hbar} t} \hat{\rho}^S e^{-i\frac{\hat{H}}{\hbar} t} \right) | \nu \rangle_H \\
&= \langle 0 |_H \hat{H} e^{i\frac{\hat{H}}{\hbar} t} \hat{\rho}^S e^{-i\frac{\hat{H}}{\hbar} t} - e^{i\frac{\hat{H}}{\hbar} t} \hat{\rho}^S e^{-i\frac{\hat{H}}{\hbar} t} \hat{H} | \nu \rangle_H \\
&= (E_0 - E_\nu) \langle 0 | \hat{\rho} | \nu \rangle
\end{aligned} \tag{C.14}$$

where  $\sum_{im}$  include all directions. We solve the second order perturbation theory:

$$\sum_{\nu} \frac{\langle 0 | \sum_{im} \hat{J}_{i,m}^z | \nu \rangle \langle \nu | \sum_{im} \hat{J}_{i,m}^z | 0 \rangle}{E_\nu - E_0} = \sum_{\nu} (E_\nu - E_0) |\langle 0 | \hat{\rho} | \nu \rangle|^2 \tag{C.15}$$

We obtain the first moment of the spectral density on the right hand site, that can be solved by using the sum rule.

$$\sum_{\nu} (E_\nu - E_0) |\langle 0 | \hat{\rho} | \nu \rangle|^2 = \langle [\hat{\rho}, [\hat{H}, \hat{\rho}]] \rangle \tag{C.16}$$

Since the total charge commutes with the Hamiltonian the 2nd order perturbation theory vanishes.

## C.4 Green's Function and Sum Rule

We like to derive the identity (6.30) from section 6.3. The general form is written as:

$$M_{AB}^{(n)} = \int_{-\infty}^{\infty} A_{AB}(\omega) \omega^n d\omega. \tag{C.17}$$

where  $A_{AB}$  is the spectral density between the operators  $A$  and  $B$  and  $M_{AB}^{(n)}$  is the spectral weight of order  $n$  and the spectral density is declared as:

$$\begin{aligned}
A_{AB}(\omega) &= \lim_{\delta \rightarrow 0^+} \frac{i}{2\pi} \left( G_{AB}(\omega + i\delta) - G_{AB}(\omega - i\delta) \right) \\
&= \lim_{\delta \rightarrow 0^+} \frac{i}{2\pi} \left( G_{AB}^{\text{ret}}(\omega) - G_{AB}^{\text{av}}(\omega) \right) \\
&= \lim_{\delta \rightarrow 0^+} \frac{i}{2\pi} \left( \frac{X}{Y + i\delta} - \frac{X}{Y - i\delta} \right) \\
&= \lim_{\delta \rightarrow 0^+} \frac{1}{\pi} \frac{X\delta}{Y^2 - \delta^2}.
\end{aligned} \tag{C.18}$$

with the retarded and advanced Green functions. The last line in Eq. (C.18) can be written as:

$$A_{AB}(\omega) = - \lim_{\delta \rightarrow 0^+} \left\{ \frac{1}{\pi} \text{Im} \left( G_{AB}(\omega + i\delta) \right) \right\}. \tag{C.19}$$

In the case of  $n = 1$  and  $M_{AB}^{(1)} = \langle [[A, H], B] \rangle$  this leads to the to:

$$\frac{1}{\pi} \int d\omega \omega \text{Im} \left( G_{AB}^{\text{ret}}(\omega) \right) = - \langle [[A, H], B] \rangle \tag{C.20}$$

where we use the continuity of the retarded Green function in the upper complex plane:

$$G_{AB}^{\text{ret}}(\omega) = \lim_{\delta \rightarrow 0^+} G_{AB}(\omega + i\delta). \tag{C.21}$$

This argumentation is a consequence from the sum rule.

# Bibliography

- [1] Bednorz, J. and Müller, K. A. (1986) *Z. Phys. B* **64**, 189–193.
- [2] Batlogg, B., Hwang, H. Y., Takagi, H., Cava, R. J., Kao, H. L., and Kwo, J. (1994) *Physica C: Superconductivity* **235-240(Part 1)**, 130 – 133.
- [3] Timusk, T. and Statt, B. (1999) *Rep. Prog. Phys.* **62**, 61.
- [4] Emery, V. J. and Kivelson, S. A. (1995) *Nature* **374**, 434–437.
- [5] Lee, P. A., Nagaosa, N., and Wen, X.-G. Jan 2006 *Rev. Mod. Phys.* **78(1)**, 17–85.
- [6] Tranquada, J. M., Buttrey, D. J., Sachan, V., and Lorenzo, J. E. Aug 1994 *Phys. Rev. Lett.* **73(7)**, 1003–1006.
- [7] Sachan, V., Buttrey, D. J., Tranquada, J. M., Lorenzo, J. E., and Shirane, G. May 1995 *Phys. Rev. B* **51(18)**, 12742–12746.
- [8] Tranquada, J. M., Kong, Y., Lorenzo, J. E., Buttrey, D. J., Rice, D. E., and Sachan, V. Sep 1994 *Phys. Rev. B* **50(9)**, 6340–6351.
- [9] Tranquada, J. M. (1998) , Kluwer, Dordrecht, The Netherlands, .
- [10] Tranquada, J. M., Lorenzo, J. E., Buttrey, D. J., and Sachan, V. Aug 1995 *Phys. Rev. B* **52(5)**, 3581–3595.

- [11] Fujita, M., Goka, H., Yamada, K., Tranquada, J. M., and Regnault, L. P. Sep 2004 *Phys. Rev. B* **70(10)**, 104517.
- [12] Tranquada, J. M., Sternlieb, B. J., Axe, J. D., Nakumara, Y., and Uchida, S. (1995) *Nature* **375**, 561.
- [13] Ichikawa, N., Uchida, S., Tranquada, J. M., Niemöller, T., Gehring, P. M., Lee, S.-H., and Schneider, J. R. Aug 2000 *Phys. Rev. Lett.* **85(8)**, 1738–1741.
- [14] Moodenbaugh, A. R., Xu, Y., Suenaga, M., Folkerts, T. J., and Shelton, R. N. Sep 1988 *Phys. Rev. B* **38(7)**, 4596–4600.
- [15] Tranquada, J. M., Axe, J. D., Ichikawa, N., Moodenbaugh, A. R., Nakamura, Y., and Uchida, S. Jan 1997 *Phys. Rev. Lett.* **78(2)**, 338–341.
- [16] Grafe, H.-J., Curro, N. J., Hucker, M., and Buchner, B. (2006) *Phys. Rev. Lett.* **96(1)**, 017002.
- [17] Yamada, K., Lee, C. H., Kurahashi, K., Wada, J., Wakimoto, S., Ueki, S., Kimura, H., Endoh, Y., Hosoya, S., Shirane, G., Birgeneau, R. J., Greven, M., Kastner, M. A., and Kim, Y. J. Mar 1998 *Phys. Rev. B* **57(10)**, 6165–6172.
- [18] Fujita, M., Yamada, K., Hiraka, H., Gehring, P. M., Lee, S. H., Wakimoto, S., and Shirane, G. Jan 2002 *Phys. Rev. B* **65(6)**, 064505.
- [19] Mook, H. A., Dai, P., and Doğan, F. Feb 2002 *Phys. Rev. Lett.* **88(9)**, 097004.
- [20] Arai, M., Nishijima, T., Endoh, Y., Egami, T., Tajima, S., Tomimoto, K., Shiohara, Y., Takahashi, M., Garrett, A., and Bennington, S. M. Jul 1999 *Phys. Rev. Lett.* **83(3)**, 608–611.
- [21] Dai, P., Mook, H. A., Hunt, R. D., and Doğan, F. Jan 2001 *Phys. Rev. B* **63(5)**, 054525.



- [22] Tranquada, J. M. (2005) *cond-mat/0512115*.
- [23] Krämer, S. and Mehring, M. Jul 1999 *Phys. Rev. Lett.* **83(2)**, 396–399.
- [24] Singer, P. M., Hunt, A. W., and Imai, T. Jan 2002 *Phys. Rev. Lett.* **88(4)**, 047602.
- [25] Haase, J., Slichter, C. P., and Milling, C. T. (2002) *J. Supercond.* **15(4)**, 339.
- [26] Tsuei, C. C. and Kirtley, J. R. Oct 2000 *Rev. Mod. Phys.* **72(4)**, 969.
- [27] Hoffman, J. E., McElroy, K., Lee, D.-H., Lang, K. M., Eisaki, H., Uchida, S., and Davis, J. C. (2002) *Science* **297(5584)**, 1148–1151.
- [28] McElroy, K., Lee, D.-H., Hoffman, J. E., Lang, K. M., Lee, J., Hudson, E. W., Eisaki, H., Uchida, S., and Davis, J. C. May 2005 *Phys. Rev. Lett.* **94(19)**, 197005.
- [29] Hashimoto, A., Momono, N., Oda, M., and Ido, M. Aug 2006 *Phys. Rev. B* **74(6)**, 064508.
- [30] Howald, C., Eisaki, H., Kaneko, N., Greven, M., and Kapitulnik, A. Jan 2003 *Phys. Rev. B* **67(1)**, 014533.
- [31] Wang, Q.-H. and Lee, D.-H. Jan 2003 *Phys. Rev. B* **67(2)**, 020511.
- [32] Kohsaka, Y., Taylor, C. and Wahl, P., Schmidt, A., Lee, J., Fujita, K., Alldredge, J. W., McElroy, K., Lee, J., Eisaki, H., Uchida, S., Lee, D.-H., and Davis, J. C. (2008) *Nature* **454**, 1072–1078.
- [33] Hanaguri, T., Kohsaka, Y., Davis, J. C., Lupien, C., Yamada, I., Azuma, M., Takano, M., Ohishi, K., Ono, M., and Takagi, H. (2007) *NATURE PHYS.* **3**, 865.

- [34] Mattheiss, L. F., Gyorgy, E. M., and Johnson, D. W. Mar 1988 *Phys. Rev. B* **37(7)**, 3745–3746.
- [35] Kamihara, Y., Watanabe, T., Hirano, M., and Hosono, H. (2008) *Journal of the American Chemical Society* **130**, 3296–3297.
- [36] Emery, V. J. Jun 1987 *Phys. Rev. Lett.* **58(26)**, 2794–2797.
- [37] Varma, C. M., Schmitt-Rink, S., and Abrahams, E. (1987) *Solid State Communications* **62(10)**, 681 – 685.
- [38] Schadschneider, A. Vorlesung Theoretische Festkörperphysik II (2002).
- [39] Hybertsen, M. S., Schlüter, M., and Christensen, N. E. May 1989 *Phys. Rev. B* **39(13)**, 9028–9041.
- [40] Zhang, F. C. and Rice, T. M. Mar 1988 *Phys. Rev. B* **37(7)**, 3759–3761.
- [41] Anderson, P. W. (1987) *Science* **235(4793)**, 1196–1198.
- [42] Lieb, E. H. and Wu, F. Y. (1968) *Phys. Rev. Lett.* **20**, 1445.
- [43] Gutzwiller, M. C. (1963) *Phys. Rev. Lett.* **10(5)**, 159–161.
- [44] Hubbard, J. (1963) *Proc. R. Soc. Lond. A* **276**, 238.
- [45] Hubbard, J. (1964) *Proc. R. Soc. Lond. A* **277**, 237.
- [46] Kanamori, J. (1963) *Prog. Theor. Phys.* **30**, 275.
- [47] Anderson, P. W. Jul 1959 *Phys. Rev.* **115(1)**, 2.
- [48] Robaszkiewicz, S., Micnas, R., C. (1981) *Phys. Rev. B* **23**, 1447.

- [49] Robaszkiewicz, S., Micnas, R., and Chao, K. A. Aug 1981 *Phys. Rev. B* **24(3)**, 1579–1582.
- [50] Shiba, H. (1981) *Prog. Theor. Phys.* **48**, 2171.
- [51] Gutzwiller, M. C. Mar 1965 *Phys. Rev.* **137(6A)**, A1726–A1735.
- [52] Metzner, W. and Vollhardt, D. Jan 1989 *Phys. Rev. Lett.* **62(3)**, 324–327.
- [53] Barnes, S. (1977) *J. Phys.* **F7**, 2637–2647.
- [54] Coleman, P. Mar 1984 *Phys. Rev. B* **29(6)**, 3035–3044.
- [55] Kotliar, Gabriel and Ruckenstein, Andrei E. (1986) *Phys. Rev. Lett.* **57(11)**, 1362–1365.
- [56] Fresard, R. and Wölfle, D. (1992) *Int. J. Mod. Phys. B* **6**, 685–704.
- [57] Metzner, W. and Vollhardt, D. Jul 1987 *Phys. Rev. Lett.* **59(1)**, 121–124.
- [58] Metzner, W. and Vollhardt, D. May 1988 *Phys. Rev. B* **37(13)**, 7382–7399.
- [59] Gutzwiller, M. C. May 1964 *Phys. Rev.* **134(4A)**, A923–A941.
- [60] Gebhard, F. May 1990 *Phys. Rev. B* **41(13)**, 9452–9473.
- [61] Brinkman, W. F. and Rice, T. M. Nov 1970 *Phys. Rev. B* **2(10)**, 4302–4304.
- [62] van Dongen, P. G. J., Gebhard, F., and Vollhardt, D. (1989) *Zeitschrift für Physik B Condensed Matter* **76(2)**, 199–210.
- [63] Anderson, P. W. Dec 1958 *Phys. Rev.* **112(6)**, 1900–1916.
- [64] Edegger, B., Muthukumar, V. N., and Gros, C. (2007) *Advances in Physics* **56**, 927–1033.

- [65] Vollhardt, D. Jan 1984 *Rev. Mod. Phys.* **56**(1), 99.
- [66] Bünemann, J., Gebhard, F., Radnoczi, K., and Fazekas, P. (2005) *J. Phys. Condens. Matter* **17**(25), 3807–3814.
- [67] Bąk, M. and Micnas, R. (1998) *J. Phys. Condens. Matter* **10**(40), 9029–9054.
- [68] Bulka, B. R. (1993) *Phys. Status Solidi B* **180**(2), 401–409.
- [69] Bulka, B. R. and Robaszkiewicz, S. Nov 1996 *Phys. Rev. B* **54**(18), 13138–13151.
- [70] Sofo, J. O. and Balseiro, C. A. Jan 1992 *Phys. Rev. B* **45**(1), 377–382.
- [71] Anderson, P. W. Apr 1975 *Phys. Rev. Lett.* **34**(15), 953–955.
- [72] Anderson, P. W. (1979) *Ill-Condensed Matter, Les Houches Session XXXI* p. 161.
- [73] Ginzburg, V. L. (1964) *Zh. Eksp. Teor. Fiz.* **47**, 2318.
- [74] Ginzburg, V. L. (1976) *Usp. Fiz. Nauk* **118**, 315.
- [75] Little, W. A. (1964) *Phys. Rev.* **A134**, 1416.
- [76] Little, W. A. (1981) *Int. J. Quantum Chem.* **15**, 545–54 Quantum Chemistry Symposium.
- [77] Ionova, G., Makarov, E., and Ionov, S. June 1977 *Phys. Status Solidi B* **81**(2), 671–679.
- [78] Ionov, S. P., Ionova, G. V., Maiybaev, A. I. and Manakova, L. A., and Semin, G. K. (1981) *Izv. Akad. Nauk SSSR* **45**, 589.
- [79] Ionov, S. P. (1985) *Izv. Akad. Nauk, Seriya Fizicheskaya* **49**(2), 310–25.

- [80] Moizhes, B. and Drabkin, I. July 1983 *Fizika Tverdogo Tela* **25(7)**, 1974–1982.
- [81] Alexandrov, A. and Ranninger, J. Aug 1981 *Phys. Rev. B* **24(3)**, 1164–1169.
- [82] Alexandrov, A. S., Ranninger, J., and Robaszkiewicz, S. Apr 1986 *Phys. Rev. B* **33(7)**, 4526–4542.
- [83] Micnas, R., Ranninger, J., and Robaszkiewicz, S. (1987) *Journal of Magnetism and Magnetic Materials* **63-64**, 420 – 422.
- [84] Ionov, S., Lubimov, V., Ionova, G., and Markarov, E. (1975) *Phys. Status Solidi B* **71(1)**, 11–57.
- [85] Robaszkiewicz, S. (1979) *Acta Phys. Pol. A* **45**, 75.
- [86] Shiba, H. (1972) *Prog. Theor. Phys.* **48(6)**, 2171–2186.
- [87] Krivnov, V. and Ovchinnikov, A. (1974) *Zhurnal Eksperimental'noi i Teoreticheskoi Fiziki* **67(4)**, 1568–1581.
- [88] Bahder, T. B. and Woynarovich, F. Feb 1986 *Phys. Rev. B* **33(4)**, 2114–2121.
- [89] Gusmão, M. A. Feb 1987 *Phys. Rev. B* **35(4)**, 1682–1686.
- [90] Scalettar, R. T., Loh, E. Y., Gubernatis, J. E., Moreo, A., White, S. R., Scalapino, D. J., Sugar, R. L., and Dagotto, E. Mar 1989 *Phys. Rev. Lett.* **62(12)**, 1407–1410.
- [91] Shanno, D. F. and Phua, K. H. (1976) *ACM Trans. Math. Softw.* **2(1)**, 87–94.
- [92] Shanno, D. F. and Phua, K. H. (1980) *ACM Trans. Math. Softw.* **6(4)**, 618–622.
- [93] Seibold, G. and Lorenzana, J. Mar 2001 *Phys. Rev. Lett.* **86(12)**, 2605–2608.

- [94] Seibold, G., Becca, F., and Lorenzana, J. Feb 2003 *Phys. Rev. B* **67(8)**, 085108.
- [95] Seibold, G., Becca, F., Rubin, P., and Lorenzana, J. (2004) *Phys. Rev. B* **69(15)**, 1551XX(12).
- [96] Jarrell, M. Jul 1992 *Phys. Rev. Lett.* **69(1)**, 168–171.
- [97] Wise, W. D., Boyer, M. C., Chatterjee, K., Kondo, T., Takeuchi, T., Ikuta, H., Wang, Y., and Hudson, E. W. (2008) *Nat Phys* **4**, 696–699.
- [98] Wollman, D. A., Van Harlingen, D. J., Lee, W. C., Ginsberg, D. M., and Leggett, A. J. Sep 1993 *Phys. Rev. Lett.* **71(13)**, 2134–2137.
- [99] Seibold, G., Becca, F., and Lorenzana, J. (2008) *Phys. Rev. B* **78(4)**, 045114.
- [100] O'Donovan, C. and Carbotte, J. P. (1995) *Physica C: Superconductivity* **252(1-2)**, 87 – 99.
- [101] Wheatley, J. and Xiang, T. (1993) *Solid State Communications* **88(8)**, 593 – 595.
- [102] Tocchio, L. F., Becca, F., Parola, A., and Sorella, S. (2008) *Phys. Rev. B* **78(4)**, 041101.
- [103] Paramekanti, A., Randeria, M., and Trivedi, N. Nov 2001 *Phys. Rev. Lett.* **87(21)**, 217002.
- [104] Salkola, M. I. and Schrieffer, J. R. Jun 1998 *Phys. Rev. B* **57(22)**, 14433–14439.
- [105] Seibold, G. and Lorenzana, J. (2004) *Phys. Rev. B* **69**, 134513.
- [106] Blatter, G., Feigel'man, M. V., Geshkenbein, V. B., Larkin, A. I., and Vinokur, V. M. Oct 1994 *Rev. Mod. Phys.* **66(4)**, 1125–1388.

- [107] Micnas, R., Ranninger, J., and Robaszkiewicz, S. (1990) *Rev. Mod. Phys.* **62**, 113.
- [108] Berciu, M. and John, S. Jun 1999 *Phys. Rev. B* **59(23)**, 15143–15159.
- [109] Timm, C. and Bennemann, K. Nov 1999 *J. Low Temp. Phys.* **117(3-4)**, 205–209.
- [110] Timm, C. and Bennemann, K. H. May 2000 *Phys. Rev. Lett.* **84(21)**, 4994–4997.
- [111] Vergés, J. A., Louis, E., Lomdahl, P. S., Guinea, F., and Bishop, A. R. Mar 1991 *Phys. Rev. B* **43(7)**, 6099–6108.
- [112] Seibold, G. Dec 1998 *Phys. Rev. B* **58(23)**, 15520–15527.
- [113] Gouva, M. E., Wysin, G. M., Bishop, A. R., and Mertens, F. G. Jun 1989 *Phys. Rev. B* **39(16)**, 11840–11849.
- [114] Fisher, M. E., Barber, M. N., and Jasnow, D. Aug 1973 *Phys. Rev. A* **8(2)**, 1111–1124.
- [115] Shastry, B. S. and Sutherland, B. Jul 1990 *Phys. Rev. Lett.* **65(2)**, 243–246.
- [116] Scalapino, D. J., White, S. R., and Zhang, S. Apr 1993 *Phys. Rev. B* **47(13)**, 7995–8007.
- [117] Scalapino, D. J., White, S. R., and Zhang, S. C. May 1992 *Phys. Rev. Lett.* **68(18)**, 2830–2833.
- [118] Peierls, R. November 1933 *Z. Phys.* **80(11-12)**, 763–791.
- [119] Kopietz, P. Apr 1998 *Phys. Rev. B* **57(13)**, 7829–7834.
- [120] Tinkham, M. (1980) *Introduction to Superconductivity*, Robert E. Krieger Publishing Company, INC., Malabar, Florida, USA.

- [121] Kohn, W. Jan 1964 *Phys. Rev.* **133(1A)**, A171–A181.
- [122] Denteneer, P. J. H. Mar 1994 *Phys. Rev. B* **49(9)**, 6364–6367.
- [123] Elk, K. and Gasser, W. (1979) Die Methode der Greenschen Funktionen in der Festkörperphysik, Akademie-Verlag Berlin, Chapter (3.5) 'Summenregeln', p. 47: Eqs. (3.5.43) and (3.5.45).
- [124] Nolting, W. (2001) Viel-Teilchentheorie, volume **7**, of Grundkurs Theoretische Physik Springer-Verlag, fifth edition.
- [125] Czycholl, G. (2000) Theoretische Festkörperphysik, Vieweg, .



# Danksagung

An dieser Stelle möchte ich allen danken, die mich beim Anfertigen dieser Arbeit unterstützt haben:

Herrn Prof. Dr. Götz Seibold danke ich für die freundschaftliche Aufnahme am Institut, für seinen fachlichen Rat und seine Geduld bei der Betreuung dieser Arbeit.

Herrn Prof. Dr. V. Hizhnykov, Univ. Tartu sowie Herrn Prof. Dr. M. Grilli, Univ. La Sapienza, Rom danke ich für die freundliche Übernahme der Zweitgutachten.

Ich bedanke mich bei Herrn Dr. Domnic Merkt und Herrn Dipl.-Phys. Ernst von Oelsen für ihren guten Rat in allen praktischen Fragen sowie für ihre Mühe beim Korrekturlesen der Dissertationsschrift.

Ich danke allen Mitgliedern des Instituts für die gute Zusammenarbeit und die Schaffung einer angenehmen, entspannten Arbeitsatmosphäre, die beim Anfertigen dieser Arbeit von wesentlicher Bedeutung war.

Ich danke meinen vielen ungenannten Freunden und Wegbegleitern, die mir mit Schwert und Schild und Pfeil und Bogen - ob hoch zu Ross oder im Sand der Arena - den Rücken frei gehalten haben.

Nicht zuletzt geht mein Dank an meine Eltern, die mich in den schwersten Zeiten immer wieder Kraft schöpfen ließen und auf deren Unterstützung ich mich immer verlassen konnte.

Mein ganz besonderer Dank gilt meiner lieben Sabine, die mich in der letzten, schweren Phase der Promotion nicht nur tapfer ertrug, sondern die mich ermutigte, pflegte und mich mit all ihren Kräften unterstützte.